INFORMATION TO USERS

University of Alberta

Gas-Solid Mass Transfer in a Rotary Drum

by

© Ritika Jauhari

A thesis submitted to the Faculty of Graduate Studies and Research in partial fulfillment of

the requirements for the degree of

Master of Science

Department of Chemical and Materials Engineering

Edmonton, Alberta

Spring 1997

The author has granted a non-exclusive licence allowing the National Library of Canada to reproduce, loan, distribute or sell copies of his/her thesis by any means and in any form or format, making this thesis available to interested persons.

The author retains ownership of the copyright in his/her thesis. Neither the thesis nor substantial extracts from it may be printed or otherwise reproduced with the author's permission.

L'auteur a accordé une licence non exclusive permettant à la Bibliothèque nationale du Canada de reproduire, prêter, distribuer ou vendre des copies de sa thèse de quelque manière et sous quelque forme que ce soit pour mettre des exemplaires de cette thèse à la disposition des personnes intéressées.

L'auteur conserve la propriété du droit d'auteur qui protège sa thèse. Ni la thèse ni des extraits substantiels de celle-ci ne doivent être imprimés ou autrement reproduits sans son autorisation.

0-612-21176-2

Canadä

University of Alberta

Library Release Form

Name of Author: Ritika Jauhari

Title of Thesis: Gas-Solid Mass Transfer in a Rotary Drum

Degree: Master of Science

Year this Degree Granted: 1997

Ritika Jauhari

811 Erin Place
Edmonton, Alberta
T5T 1M6
Canada

January 28, 1997.
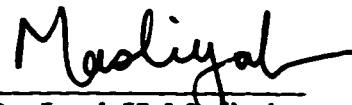
University of Alberta

Faculty of Graduate Studies and Research

The undersigned certify that they have read, and recommend to the Faculty of Graduate Studies and Research for acceptance, a thesis entitled Gas-Solid Mass Transfer in a Rotary Drum submitted by Ritika Jauhari in partial fulfillment of the requirements for the degree of Master of Science.

Dr. Murray R. Gray
(Supervisor)

Dr. Jacob H. Masliyah
(Co-Supervisor)

Dr. A. Paul Watkinson

January 27, 1997

Dr. Hani Henein

This thesis is dedicated to my parents Mrs. Asha Johri and Mr. Mohan Jauhari for their

endless love and encouragement.

ABSTRACT

Rotating drums are widely used in a variety of processes such as solids mixing, drying and gas-solid reaction with heat and mass transfer. Heat transfer to solids in rotary kilns has been studied extensively. Gas-solid mass transfer has not been studied and it is important in some ceramic manufacture and solid-state fermentation processes.

Gas-solid volumetric mass transfer coefficients, $k_s A$ in a rotary drum were measured by evaporation of n-decane into dry air from the surface of porous solids, where k_s is the gas-solid mass transfer coefficient and A is the total mass transfer area. The effects of varying parameters (drum rotational speed, N, solids volume fraction, η and the presence of baffles) on $k_s A$ were measured. The operating ranges were: N varied from 0.09 to 2.0 rpm and η varied from 0.043 to 0.25.

The value of $k_s A$ increased with increasing drum rotational speed in the presence and absence of baffles (solids in rolling mode). The value of $k_s A$ in the mass transfer experiments ranged from 6.35 L/min to 67.35 L/min. The $k_s A$ values obtained for the rolling bed were lower than those obtained in the presence of baffles. In the presence of baffles, $k_s A$ was independent of η although the solids motion in the drum was different. For the rolling bed case, $k_s A$ increased with increasing solids volume fraction. Mass transfer in the rolling bed was modeled based on the particle motion. Experimental results of the present study compared well with the literature studies on heat or mass transfer in rotary kilns, moving beds and single spheres.

ACKNOWLEDGEMENTS

TABLE OF CONTENTS

LIST OF TABLES

LIST OF FIGURES

NOMENCLATURE

A	total mass transfer area, m^2
A_c	cross-sectional area of empty dryer, m^2
a	ratio of the total mass transfer area to the volume occupied by the liquid, in case of liquid fermentation, m^2/m^3 OR ratio of the total mass transfer area to the volume occupied by the solids, in case of gas solid mass transfer, m^2/m^3
B	contact surface area, Equation (2-38), m^2
b	intercept, Equation (3-8), 1/Torr
$C(t)$	drum tracer concentration, mol/L
C_i	initial tracer concentration in the drum before the step change, mol/L or mol/m^3
C_{inlet}	inlet gas phase concentration of the diffusing substance, mol/L or mol/m^3
CF	correction factor, Equation (2-36)
C_f	steady-state tracer concentration in drum, mol/L or mol/m^3
C_p	specific heat, J/kg.K
C^{sat}	gas phase saturation concentration of the diffusing substance, mol/L or mol/m^3
C^{ss}	steady-state gas phase concentration of the diffusing substance, mol/L or mol/m^3
D	drum diameter, m
D_{AB}	diffusivity, m^2/s
D_e	equivalent diameter, m
D_p	particle diameter, m
$E(t)$	Residence Time Distribution function E(t), 1/min

e	constant, Equation (2-32)
F_E	ratio of the mass of hydrocarbon evaporated to the initial mass of hydrocarbon
F_E^{max}	maximum value of F_E , Equation (4-1)
Fr	Froude number
g	acceleration due to gravity, m/s^2
h	total bed depth, m
h_a	active-layer thickness, m
h_{gs}	gas-solid heat transfer coefficient, W/m^2.K
J	Equation (2-33), 1/m
$k_L a$	gas-liquid mass transfer coefficient as defined in fermentation, min^{-1}
k_s	gas- particle mass transfer coefficient, m/s or m/min or L/min.m^2
k_s'	gas-solid normalized mass transfer coefficient, s^{-1}
$k_s A$	gas-solid volumetric mass transfer coefficient, L/min
$k_s a$	gas-solid mass transfer coefficient as defined in fermentation, min^{-1}
L	length of drum, m
L_v	vertical length of fall, m
L_s	chord length, m
M	material feed rate, m^3/s
m	slope, Equation (3-8), min/L.Torr
N	rotational speed, rev/min or rpm
N_A	molar flux of diffusing substance per unit mass transfer area, mol/m^2.s
N_c	critical rotational speed, rpm

N_e effective number of falling particles

Nu Nusselt number

Nu_{gs} Nusselt number, Equation (2-26)

Pr Prandtl number

Q gas flow rate, L/min

Q_{top} volumetric flow rate of solids to active layer region of the rolling bed, m^3/s

Q_{bulk} volumetric flow rate of solids to the bulk region of rolling bed, m^3/s

R radius of the drum, m

RE relative error, %

Re Reynolds number

Re_g gas phase Reynolds number, Equation (2-27)

Re_p Reynolds number for a single particle, Equation (2-21)

Re_ω transverse Reynolds number, Equation (2-28)

$S(t)$ tracer signal, Torr

S_A cross-sectional area of the active bed, m^2

S_f steady-state tracer signal, Torr

S_i initial tracer signal before step change, Torr

S^{sat} gas phase saturation signal of the diffusing substance, Torr

S^{ss} gas phase steady-state signal of the diffusing substance, Torr

Sc Schmidt number

Sh Sherwood number

t time, min

t_f time of fall of particle, s

t_{top} average residence time in top plane, s

t_{bot} average residence time for rotation, s

Ua volumetric heat transfer coefficient, $W/m^3.K$

U_o relative velocity, m/s

u gas velocity, m/s

V drum volume, L or m^3

$V_a(z)$ velocity profile in active region of rolling bed, m/s

$V_b(z')$ velocity profile in the bulk flow region of rolling bed, m/s

V_m mean velocity of a particle on the top plane, m/s

V_p falling velocity of particle, m/s

V_s surface particle velocity, m/s

V_W drum wall velocity, m/s

X decane content (dry basis), g dec/g VD solids

y logarithmic mean fraction of inert non-diffusing component in a mixture

Z constant, Equation (2-32)

z depth scale, m

z' depth scale, m

Greek

α slope of dryer, degree

β central angle, rad

ε void fraction

ε_f void fraction of fluidized bed

η solids volume fraction or percent fill

θ dynamic angle of repose, degree

θ_{init} initial discharge angle, rad

λ thermal conductivity, W/m.K

μ viscosity, kg/m.s

ρ gas density, kg/m^3

ρ_p particle density, kg/m^3

τ average residence time, min

τ_{pred} predicted average residence time, min

ϕ angle particles in flight make with horizontal, degree

ω angular velocity, rad/s

Subscripts

1   first steady-state

2   second steady-state

1. INTRODUCTION

Rotary drums are most widely used industrial process equipment for processing of granular materials in a variety of applications such as drying, incineration, mixing, heating, humidification, calcining, reducing, sintering, and gas-solid reactions. Rotating drums are easy to operate and are flexible for handling difficult solid feeds having a wide range of particle size distribution. Rotary drums can be used in both batch and continuous operations. The design of a rotary drum can vary greatly. The simplest construction is having the drum without any flights or lifters. Drums may also contain flights or lifters which are spaced evenly about the circumference and extend along the length of the drum. These flights or lifters shower the particles into the gas stream and are suitable for gas-solid contacting to increase heat and mass transfer (Sherritt et al., 1996). Drums may be horizontal or slightly inclined and are operated less than half full. For continuous operations, gas flow may be cocurrent or countercurrent to the solids flow.

A rotary drum is used for contacting gases and solids and the most common use is in drying and cooling solids such as wood chips, coal, grains, fertilizer pellets, and ores (Sherritt et al., 1996). Another common use of a rotary drum is for incinerating organic wastes like toluene in solids or sludges (Owens et al., 1992). Rotary kilns also have a long history of use in metallurgical and chemical processes such as reduction of iron oxide pellets, calcination of petroleum coke and manufacture of cement (Brimacombe and Watkinson, 1978a,b). Rotating drums are also used for blending of particulate solids in some ceramic and pharmaceutical applications (Rao et al., 1991).

Most of the chemical and metallurgical processes are high temperature processes, hence the main functions of the rotary kiln are to heat the solids to the reaction temperature and provide heat for endothermic reactions. Usually the solid material passes first through a low temperature drying zone. Then the solid material moves into the heating zone where the solids are heated to the reaction temperature. Finally the solids move into the reaction zone where heat and mass transfer with chemical reaction takes place. In the drying and reaction zones, heat transfer may be the rate limiting process, therefore literature studies have concentrated on the various modes of heat transfer (Barr et al., 1989a,b).

Mixing of solids plays an important role in the performance of rotary drums. In a rotary kiln, good heat transfer between gases and solids is mainly due to efficient mixing of the solids (Rao et al., 1991). In rotary drum mixers, improper mixing can result in products of fluctuating quality which has a severe impact in applications such as pharmaceuticals. Due to the importance of mixing in rotary drum mixers, there are several studies in the literature which deal with mixing of granular materials (Rutgers, 1965). During processes like gasification of coal char with carbon-dioxide (Mehrotra and Brimacombe, 1990), the transverse bed motion undergoes a change from rolling to sliding/slumping modes during the course of the reaction. As a result, the heat and/or mass transfer to and within the bed of char particles is reduced which significantly affects the overall gasification kinetics. Consequently studies were conducted on transverse particle

motion which influences heat transfer from the gas and walls to the bulk of the particles in the rotary kiln (Lehmberg et al., 1977).

As rotary drums are largely used in applications where heat transfer is the limiting step, heat transfer, mixing and particle motion in rotary drums have been studied quite extensively. However, there are some other rotary drum applications where gas-solid mass transfer is important. These applications are in some ceramic (Wei, 1983) and solid-state fermentation (SSF) processes.

Solid-state fermentation is the growth of microorganisms on solid materials without the presence of free liquid. Presence of moisture is essential in solid-state fermentation but it exists in an absorbed or complexed form within the solid matrix (Cannel and Moo-Young, 1980a). Due to the low amounts of water present in the substrate, commonly fungi are used in SSF processes. There are three traditional SSF processes which are still in use today: oriental food fermentations, mould-ripened cheese and composting. SSF are also useful systems for production of protein, biomass, enzymes and other valuable metabolites (Nigam and Singh, 1994). Disposal of pesticide waste using SSF techniques may be an economically feasible alternative compared to other methods (Berry et al., 1993).

Another major area where SSF is used is in agricultural applications for fungal spore production and legume inoculant production. Fungal spores are needed in agricultural applications such as inorganic phosphate solubilization by fungi in soil to

increase the wheat yield (Asea et al, 1988). Similarly, legume inoculants ensure that symbiotic nitrogen-fixing bacteria colonize legumes such as soya beans, thereby providing nitrogen to the plants (Smith, 1992).

Fungal spores are produced by SSF in fixed-bed column reactors (Larroche and Gros, 1989) and legume inoculants are normally produced in bags (Somasegaran, 1985). Most SSF systems are aerobic in nature, therefore, adequate oxygen is required for maximal growth and survival of the microorganisms. The limiting mass transfer step in SSF can be oxygen transfer to the microorganisms growing on the substrate (Cannel and Moo-Young, 1980b). The transfer of oxygen is achieved by mixing and aeration. Static fermentors such as fixed-bed column reactors, tray reactors and bags may provide inadequate mixing resulting in less oxygen transfer, which in turn causes a decline in the microbial growth.

An attractive alternative to the above mentioned reactors is a rotary drum fermentor. The drum rotation enhances mixing and exposure of substrate particles to the gas (Lonsane et al., 1985). Since the oxygen transfer occurs directly from the gas phase, the enhanced mixing increases the oxygen availability to the microorganisms. Microbial growth in drum fermentors is found to be rapid and uniform. The performance of rotary drums has been improved by including internals like baffles which further enhance the mixing and hence improves the oxygen transfer (Fung and Mitchell, 1995). Thus gas-solid mass transfer is important for solid-state fermentation systems. Information about oxygen

transfer or gas-solid mass transfer in rotary drums is unavailable in the literature. Research on mass transfer is required to optimize the performance of rotating drum bioreactors.

The objective of this project is to study the effect of drum rotational speed, solids volume fraction, and baffles on the volumetric gas-solid mass transfer coefficient, k_sA. The experimental mass transfer data will be compared with data from analogous heat and mass transfer studies in the literature. Mass transfer in a rotating drum is modeled based on the particle motion.

2.   LITERATURE REVIEW

2.1   Particle motion and mixing

Particle motion is important in rotary kiln processes because it influences heat and mass transfer. As a result particle motion and mixing in drums have been studied extensively. In this section some of the relevant rotating drum literature will be reviewed and the effect of particle motion on heat or mass transfer will be emphasized. Any information that relates particle motion/mixing to heat transfer should be useful due to analogy between heat and mass transfer. Particle motion in some simpler cases such as fluidized beds will also be described for comparison sake.

The simplest situation where there is no particle motion is that for flow around a stationary sphere. Kunii and Levenspiel (1977) have mentioned particle motion in unrestrained fixed beds and fluidized beds. In an unrestrained fixed bed, the gas is at a low flow rate and it percolates through the void space between the stationary particles. With an increase in gas flow rate, the particles move apart and vibrate. At a still higher velocity, the particles in the expanded bed remain suspended in the flowing gas. This is referred to as minimum fluidization. For gas-solid systems an increase in gas flow rate or velocity beyond minimum fluidization results in vigorous solids movement.

Sherritt et al.(1993) have described the particle motion for a rotating drum fitted with a number of lifters or flights spaced about the circumference and extending along the drum length. As the flighted drum rotates, the flights lift and cascade or shower the particles into the gas stream. The cascading particles form sheets or curtains which traverse the drum below the flights. The selection of the number and shape of flights depends on the flow characteristics of the solids. For sticky materials, straight flights normal to the drum wall are used whereas two-sided or other complex shapes are used for free-flowing materials.

There are different degrees of loading of a flighted drum as shown in Figure 2-1. Depending on the angle of rotation at which the flights begin to discharge (i.e. initial discharge angle, θ_{init}), the flights could be underloaded, overloaded with no buried flights or overloaded with at least one buried flight. In an underloaded drum, the initial discharge angle is in the upper half of the drum and in an overloaded drum the initial discharge angle is in the lower half of the drum. For a discharging flight, the particles emerge at the solids bed surface, slide down the bed surface and discharge over the flight top. If the drum is horizontal, the sliding particles move on a plane perpendicular to the drum axis and are not axially displaced. When the drum is angled, the particles are displaced down the axis each time they are lifted by a flight and dropped.

θ_{init}

(a) Underloaded

(b) Overloaded with
no buried flights

θ_{init}

(c) Overloaded with at
least one buried flight

θ_{init}
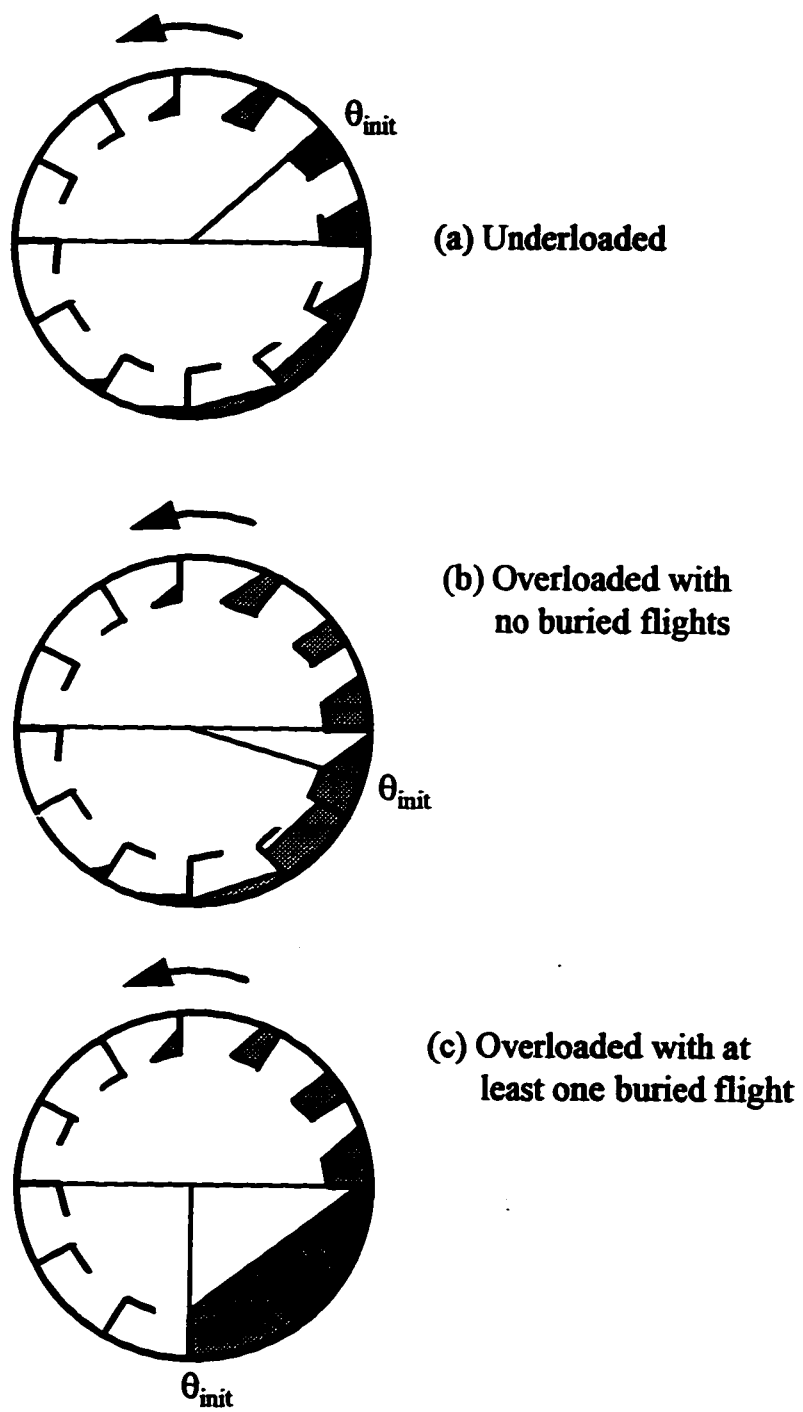
Figure 2-1. Degrees of loading of a flighted drum.

Numerous studies of particle motion and mixing in rotating drums without baffles can be found in the literature. Oyama (1980) used photography to study motion of particles in a horizontal rotating drum. The motion of particles was influenced by not only the drum rotational speed and drum diameter but also by physical characteristics of the solids such as moisture content. Oyama had studied particle motion at higher rotational speeds (> 20 rpm).

Hogg and Fuerstenau (1972) studied transverse mixing in rotating drums. They showed that transverse mixing (mixing of solid particles in the plane perpendicular to the horizontal axis of rotation) was a combination of diffusion and convection. Diffusion of particles was considered only in the radial direction and convection only in the angular direction. A model was developed that related the rate of mixing to the percent fill of solids in the drum. As the percent fill was increased, the mixing time had drastically increased. Therefore more number of revolutions were required to achieve the same amount of mixing when the fill was increased.

Extensive studies on solids motion in drums without lifters or flights was conducted by Henein et al.(1983a,b). The different forms of transverse bed motion that can take place as a kiln rotates on its axis are: slipping, slumping, rolling, cascading, cataracting and centrifuging. These modes of transverse bed motion are shown in Figure 2-2. Depending on the operating variables such as rotational speed, drum diameter,

(a) Slipping

(b) Slumping

(c) Rolling

(d) Cascading

(e) Cataracting

(f) Centrifuging
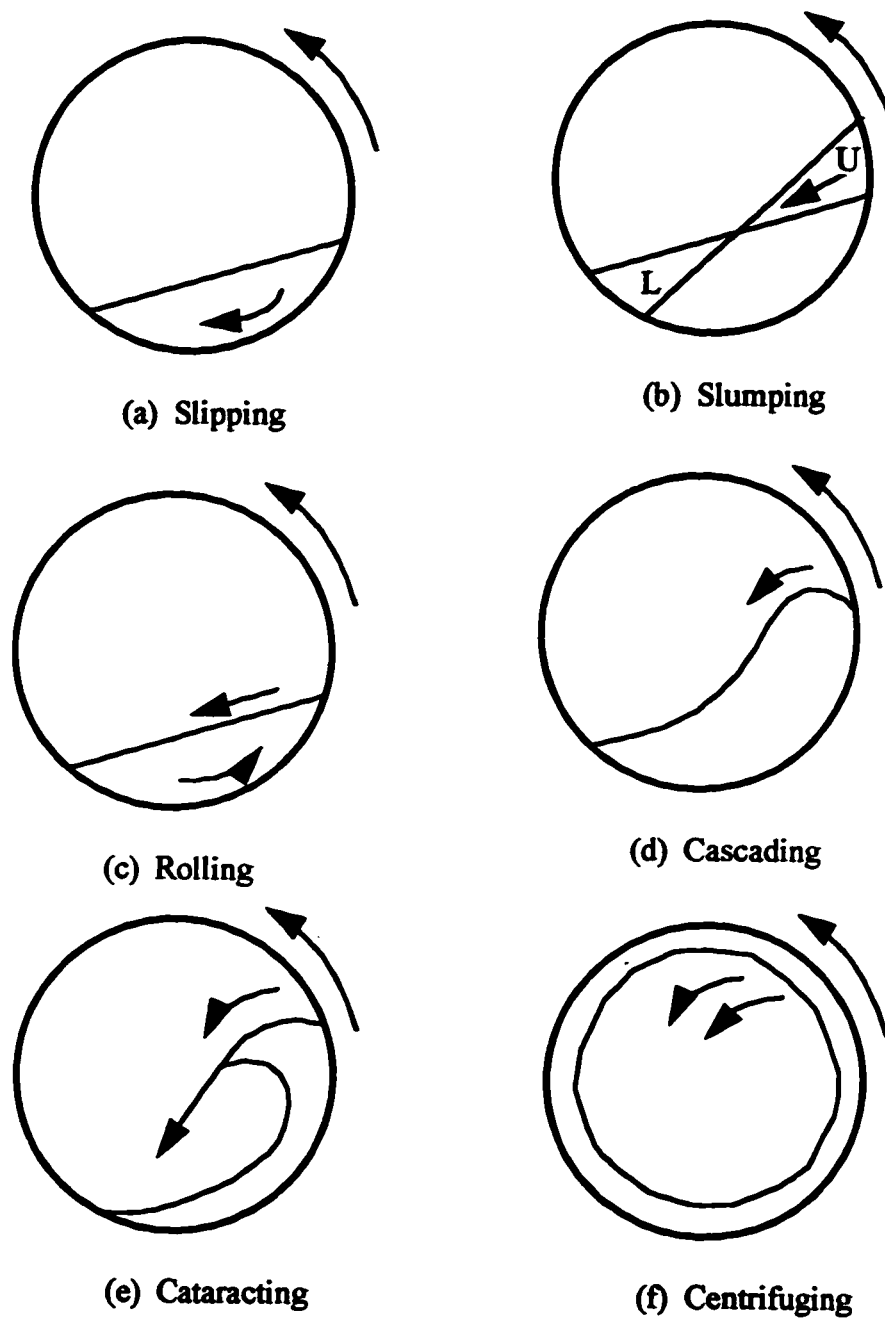
Figure 2-2. Modes of transverse bed motion in a rotating drum with increasing rotational speed.

percent fill, bed/wall friction and solid particle characteristics any of the aforementioned bed motions can be achieved. In the slipping mode, the bed slides against the inside surface of the drum so that the solids bed is poorly mixed resulting in poor heat transfer characteristics. In the slumping mode, the bed rotates upward with the drum wall until a segment of the bed in the upper part (U) detaches and slumps towards the lower extremity of the bed surface (L). The slump occurs periodically. At higher rotational speeds, an active layer of solids continuously moves over the bed surface resulting in a rolling bed appearance. At even higher speeds, the cascading mode occurs. It is characterized by a crescent or kidney shaped bed cross-section which results from the solids in the upper corner of the bed riding high up the wall before detaching. During the cataracting mode, a significant portion of the solids bed is projected into the free space of the drum, followed by showering back to the solids bed at the bottom of the drum. Centrifuging occurs when the drum rotational speed is above the critical rotational speed which is defined as (Henein et al., 1983b):

$$N_c = \frac{30}{\pi} \sqrt{\frac{2g}{D}} \qquad (2\text{-}1)$$

During the centrifuging mode, the solids bed centrifuges at the drum wall. Cataracting and centrifuging are not found in normal rotary kiln operations.

A literature review of transverse rolling bed motion studies indicated that early investigators assumed an infinitely thin active layer, h_a at the bed surface in which the particles moved downwards (Figure 2-3a).
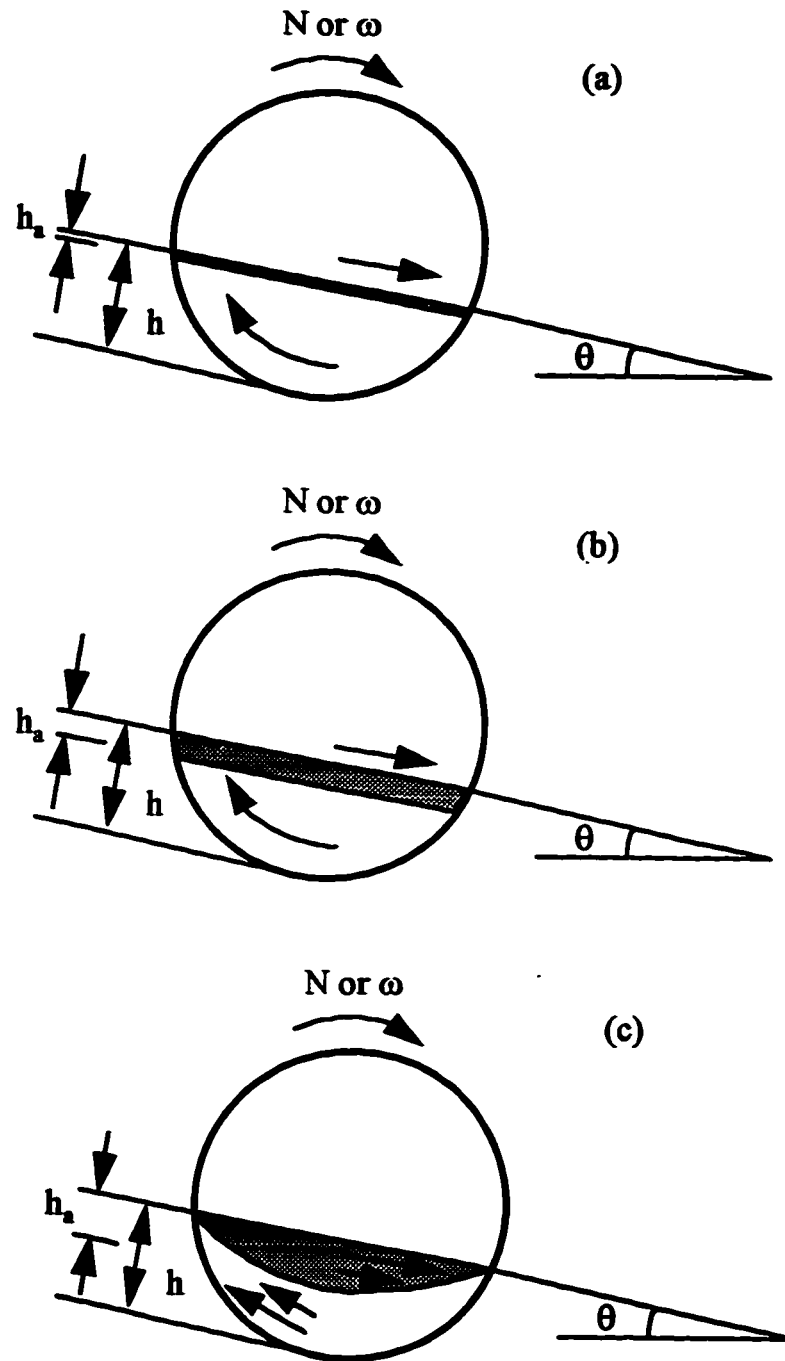
Figure 2-3. Transverse motion in rolling beds (a) very thin active layer (b) active layer of finite thickness (c) active layer of crescent shape.

The remainder of the bed formed a lower zone in which the material rotated upward in a plug flow movement. Such was the case with Saeman (1951) and Carley-Macauly and Donald (1962). Then Rutgers (1965) assumed the active upper zone to have a finite thickness, h_s where the solids moved downward, while the lower zone motion was upward in plug flow movement (Figure 2-3b). Recent investigators assumed the active upper zone to be crescent-shaped having an active layer thickness, h_s . The lower zone is also crescent-shaped and the motion was upward in plug flow movement (Figure 2-3c), as observed by Henein et al. (1983a).

Wes et al. (1976) studied solids mixing as a function of the drum rotational speed, number and height of strips on the drum wall and the degree of filling. From their experimental study they found that the transverse mixing increased with the number of strips until sufficient strips were provided to ensure a non-moving layer against the wall i.e. bed was in rolling mode. Also the transverse mixing increased with increasing rotational speed of the drum and with increasing normal height of the strips. However the transverse mixing decreased with an increase in the degree of fill.

A study of particle motion and mixing in slipping and rolling beds was also done by Woodle and Munro (1993). For slipping mode studies, the drum wall was smooth and for the rolling mode, thin strips were attached to the cylinder inner wall to increase the friction between the particles and the wall. Particle mixing was more rapid in the rolling mode than during the slipping mode. In the rolling mode, the active layer was of finite uniform

thickness (Figure 2-3b). This layer was fast moving and was well mixed, but there was a relatively slow moving and slow mixing zone in the center of the bed. The active layer thickness increased with increased solids loading but not as rapidly as the solids loading. As a result, the particles mixed less rapidly at higher solids loading levels. In the rolling mode, rate of mixing decreased with increased loading. But the increase in mixing time was not linearly related to the increase in loading. The rate of mixing was dependent on the number of revolutions rather than the rotational speed if operating within a particular mode of bed motion. Therefore doubling the rotational speed halves the mixing time. However, if increase in rotational speed changed the bed motion from slipping to rolling, then the rate of mixing would change more significantly than the change in rotational speed. Particle type (based on size, shape) had an effect on mixing time. An empirical equation was developed to predict mixing times of various particle types if the rate of mixing of any one particle type was known. The empirical equation required the ratio of the coefficient of particle/particle friction to the coefficient of particle/wall friction for the particle type whose mixing time is known and also of the particle type whose mixing time is not known.

Henein et al. (1983a) conducted an experimental study of the effect of rotational speed, bed depth, drum diameter, particle size and particle shape on bed motion. They delineated the different types of bed motion on a bed behavior diagram, which is a plot of bed depth, h (or percent fill, η) versus rotational speed, N. From their literature review of particle motion and from their experimental data, important qualitative and quantitative

observations were made. Results for rolling beds are presented here as this type of bed motion is the most common one in rotary kiln operations.

For rolling beds, continuous motion of a layer of solids occurs over the bed surface. This rolling zone is fed continuously with solids from the bulk of the bed, which reach the upper part of the bed as the kiln rotates. The rolling bed at low rotational speeds has a constant angle of inclination and a flat planar surface. The inclination of the rolling bed is assumed to be the dynamic angle of repose. Henein et al. (1983a) found that spherical particles showed rolling behavior at low rotational speeds when compared with irregular shaped particles. Rolling beds are favored by high percent filling. The dynamic angle of repose is not affected by the bed depth or rotational speed. For spherical particles of 4.9mm diameter, they obtained a dynamic angle of repose, θ of 30.2 °. Rolling beds are also characterized by active layer depth, h_a. Figure 2-3c shows a schematic of the rolling bed with crescent-shaped active layer of depth, h_a.

At constant bed depth, the active layer was found to be thinner for smaller sized particles. Increasing bed depth (or percent fill) and rotational speed, increased the active layer thickness, h_a. At rotational speeds larger than 2 rpm, spherical particles of size 4.3 mm, had an active layer thickness of 10 mm at a bed depth of 65 mm. For shallow beds at rotational speeds less than 2 rpm, the active layer may occupy upto one-third of the bed depth. But for deeper beds ($h/D_p > 50$) where h is the total bed depth and D_p is the particle diameter, the fraction declined to about 8 percent. The importance of the active layer for

convective heat and mass transfer was emphasized because the greater the fraction of bed occupied by the active layer, the more time the particles will be exposed to the gases in the freeboard relative to the time spent in the lower or passive region. Increasing the active layer enhances mixing of particles and may increase heat transfer from the gas to the solids bed.

Perron and Bui (1992) proposed a method for predicting the transverse rolling motion of a granular bed based on modeling the particle bed as a pseudoplastic non-Newtonian fluid. The bed velocity profiles in the downward moving active zone and in the upward moving lower zone can be predicted from this model. They found that the model succeeded in predicting the overall velocity profile when compared with the experimentally measured velocity profile obtained from the literature. The velocity profile in the upper zone indicated that velocity was maximum at the bed surface and then it decreased rapidly as the bed depth increased. In the lower zone, the velocity profile was flat, indicating that the bulk motion observed experimentally was in plug flow, due to rotation of the drum.

Perron and Bui (1990) developed a semi-experimental model for predicting the axial velocity of granular beds in rotating drums. In their model, the apparent viscosity of the bed needs to be determined. The expression derived for obtaining the viscosity depends on the bed depth, h_*, dynamic friction angle, θ, fill angle, β and the drum angular velocity, ω. The model can predict the axial velocity as a function of central angle, β and dynamic angle of repose, θ.

Boateng and Barr (1996) developed a mathematical model for predicting gas-solid heat transfer in a rolling bed. In this model, they used a granular flow model for the bed which was used to determine the particle velocity profiles within the bed. The velocity profile in the active layer region was assumed to be parabolic. They studied the rolling bed mode because this mode of bed motion is characterized by improved mixing of particles and faster surface renewal. These characteristics promote good heat transfer from the gas to the solids bed. They assumed the active layer to be crescent shaped (Figure 2-3c) where vigorous mixing of solids occurred. The flow model allowed prediction of the velocity profile in the transverse plane of the active layer. They did some experiments which indicated that the active-layer was thin and was typically 4 % of the chord length, L_x. For a 0.41 m diameter drum operating at 2.0 rpm and 12% solids fill, the velocity profile in the active layer region was predicted using the model. Particle velocity at the bed surface was highest and then it decreased rapidly with bed depth, reaching minimum value of zero at an active layer depth of approximately 2.25 cm. When the drum rotational speed was varied in the range: 1.5 to 5.0 rpm, the particle velocity at the bed surface increased and the bed depth at which the velocity approached zero (i.e. h_a) also increased.

Tscheng (1978) conducted an experimental study of convective heat transfer to a rolling bed. The active layer region was assumed to be of finite thickness, h_a and the velocity profile in the active layer region was assumed to be linear (Figure 2-4). They derived an expression for the rate of particles emerging from the plug flow region to the active surface region by integrating the velocity of the particles normal to the bed surface.

From the assumption of linear velocity profile, another expression for the rate of particles rolling on the surface was derived. Equating the two rate expressions, they obtained the following equation to predict the surface particle velocity, V_s in the active layer region:

$$V_s = \frac{\pi N}{120 h_a} \left[L_s^2 - 8R h_a \cos\left(\frac{\beta}{2}\right) \right] \tag{2-2}$$

where h_a is the active layer thickness, N is the rotational speed, L_s is the chord length, R is the radius and β is the central angle.
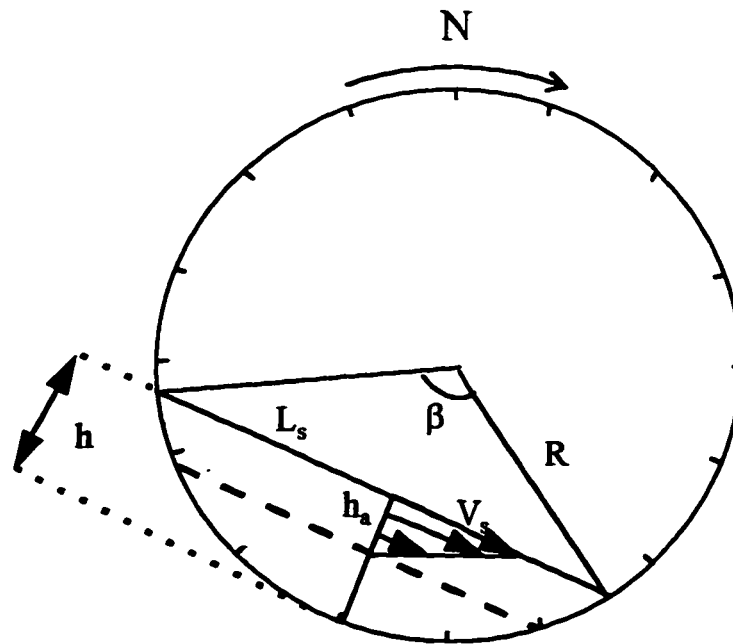
Figure 2-4. Particle velocity profile in active layer, Tscheng (1978).

Lebas et al.(1995) conducted experiments in a pilot scale rotary kiln with coal and coke particles to study the mean residence time, bed depth profile and the time spent by the particles on the surface of the rolling bed. The surface particle velocity, V_s in the active

layer was also measured photographically for coal particles at 18% fill and uniform bed depth. The kiln slope was 1° and rotational speed was varied from 2 to 4 rpm. Their results are shown in Figure 2-5. Linear regression of their data on a logarithmic plot gave the following regression line:

$$V_s = 0.163N^{0.674} \qquad (2\text{-}3)$$
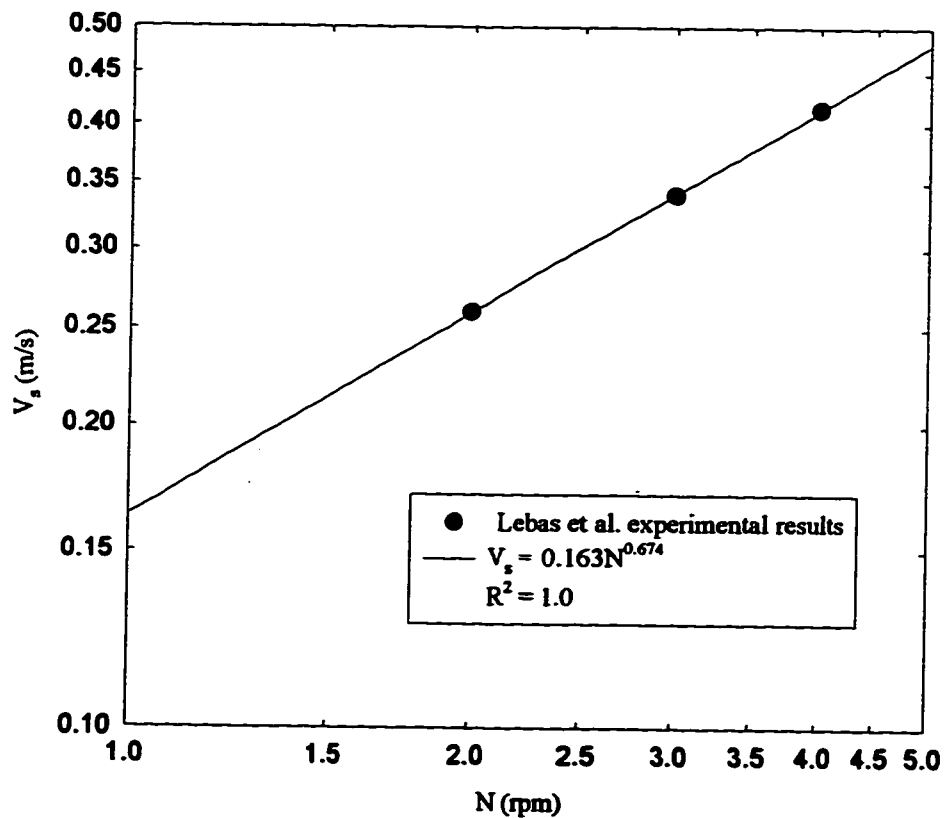
Figure 2-5. Surface particle velocity as a function of rotational speed. Lebas et al.(1995) results.

Mu and Perlmutter (1980a) developed a model to predict solids mixing and material transport in a continuous flow rotary dryer. In modeling the rolling bed, the active layer thickness was assumed to be finite (Figure 2-3b). Based on the particle trajectories in the active layer region, an expression was developed for obtaining the average velocity along the active layer surface. Mu and Perlmutter (1980b) used this model equation and computed the average surface particle velocity, V_s. The results from this model prediction at low rotational speeds (0.5-2 rpm) are shown in Figure 2-6.
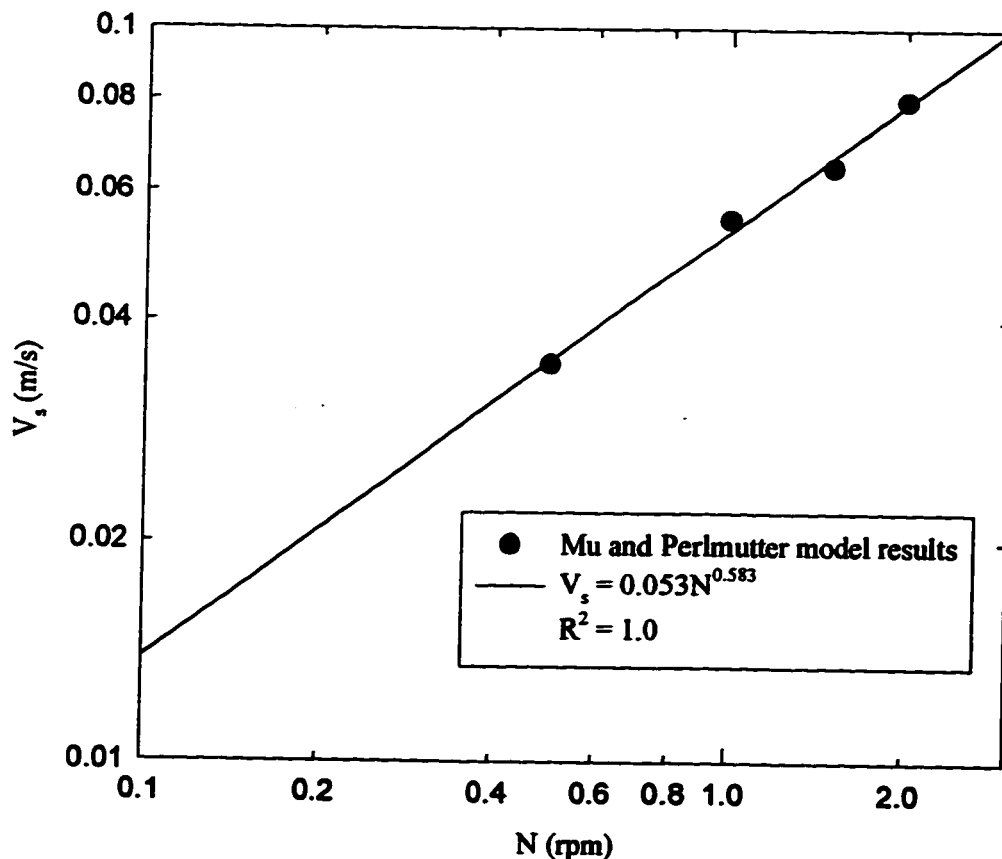
Figure 2-6. Surface particle velocity as a function of rotational speed. Mu and Perlmutter (1980 b) results.

Linear regression of Mu and Perlmutter (1980) results on a logarithmic plot gave the following regression line:

$$V_s = 0.053N^{0.583}$$

(2-4)

Ferron and Singh (1991) derived expressions for the various particulate transport processes that occur in a rolling bed. The top planar surface of the rolling bed is the active region for particulate mixing. The individual particles are relatively free of the surrounding particles and move randomly which permits the dispersion of particles of different composition. The packing in the bottom or the bulk of the solid is dense enough to cause the particulate mass to respond to rotation as an almost complete rigid body. The solids volumetric flow rate to the top plane, Q_{top} is given by:

$$Q_{top} = \frac{\pi L_s RLN}{120} \sin\left(\frac{\beta}{2}\right)$$

(2-5)

where L_s is the chord length, R is the drum radius, L is the drum length, N is the rotational speed and β is the central angle. The mean speed of a particle on the top plane, V_m is given by the following equation for a sparsely populated top plane:

$$V_m = 1.6186\left[g\frac{L_s}{2}\sin\theta\right]^{\frac{1}{2}}$$

(2-6)

where g is the acceleration due to gravity and θ is the angle of repose of the solids. Note that the mean speed of a particle has no dependence on the drum rotational speed.

A particle makes several excursions over the top plane and through the bulk during each revolution of the drum. The average residence time for the top plane, t_{top} and for rotation, t_{rot} are respectively given by:

$$t_{top} = \frac{2L_s}{3V_m} \tag{2-7}$$

$$t_{rot} = \frac{240\eta R^2}{L_s^2 N} - \frac{2L_s}{3V_m} \tag{2-8}$$

where η is the solids volume fraction in the drum. The time spent on the top plane is much smaller than required for rotation.

2.2 Gas-solid mass transfer in packed and fluidized beds

Many studies on gas-solid mass transfer coefficients in fixed and fluidized beds can be found in the literature. These studies span different ranges of gas velocities, voidages and Reynolds number. Kumar and Sublette (1993), Wakao and Funazkri (1978) and Dwivedi and Upadhyay (1977) have reviewed some of the literature on fixed and fluidized beds. Kunii and Levenspiel (1977) have mentioned studies on heat and mass transfer in fixed and fluidized beds. They concluded that heat and mass transfer rates

between gas and particles are higher for fluidized beds when compared with other modes of contacting such as fixed and moving beds.

Richardson and Szekely (1961) measured mass transfer coefficients in fluidized beds by unsteady-state adsorption of carbon tetrachloride vapors from the fluidizing gas on to the surface of porous catalysts. Under the assumptions of complete mixing of solids and plug flow of the gas phase, the following correlations were obtained:

$$Sh = 0.374 Re^{1.18} \qquad (0.1 < Re < 15) \qquad (2\text{-}9)$$

$$Sh = 2.01 Re^{0.5} \qquad (15 < Re < 250)$$

The dimensionless numbers (Sherwood number, Sh and Reynolds number, Re) are defined as:

$$Sh = \frac{k_s D_p}{D_{AB}} \qquad (2\text{-}10)$$

$$Re = \frac{u \rho D_p}{\mu} \qquad (2\text{-}11)$$

where k_s is the mass transfer coefficient, D_p is the particle diameter, D_{AB} is the gas phase diffusivity, u is the gas velocity, ρ is the gas density and μ is the gas viscosity. At Reynolds number below 5, the Sherwood number has a value less than the theoretical minimum value of two. This was due to back-mixing of the gas and was corrected by taking

longitudinal diffusivity into account. The re-calculated results showed that Sherwood number increases from a value of 2 at low Reynolds number and approaches the value found at Reynolds number greater than 15 (Equation 2-9).

Yoon and Thodos (1972) measured mass transfer coefficients in shallow fluidized beds by evaporation of n-decane from the surface of porous Celite particles ranging from 1.8 mm to 3.1 mm in diameter. Their correlation was of the following form:

$$Sh = \frac{1}{\varepsilon_f} 0.947 Re^{0.5} Sc^{0.33} \qquad (\ 100 < Re < 450\ ) \qquad (2\text{-}12)$$

where ε_f is the void fraction of fluidized bed. The Schmidt number, Sc is defined as follows:

$$Sc = \frac{\mu}{\rho D_{AB}} \qquad (2\text{-}13)$$

For packed beds, mass transfer in the low Reynolds number regime was studied by Petrovic and Thodos (1968). Mass transfer coefficients were measured by vaporization of water and heavy hydrocarbons from the surface of porous spheres. After accounting for axial mixing, the following correlation was established:

$$Sh = \frac{1}{\varepsilon} 0.357 Re^{0.641} Sc^{0.33} \qquad (\ 3 < Re < 230\ ) \qquad (2\text{-}14)$$

where ε is the void fraction of the packed bed.

Mass transfer studies of packed beds with coarse solids can be summarized by the following correlation (Kunii and Levenspiel, 1969):

$$y \cdot Sh = \quad 2.0 + 1.8 \, Re^{0.5} \, Sc^{0.33} \qquad Re > 80 \qquad (2\text{-}15)$$

where y is the logarithmic mean fraction of inert non-diffusing component in a mixture.

2.3   Gas-solid heat transfer in moving beds

Akiyama et al. (1993) experimentally obtained convective gas-solid heat transfer coefficients at high temperatures in a counter-current moving bed. The following correlation was obtained to predict the heat transfer coefficients:

$$Nu = \quad 2.0 + 0.39 \, Re^{0.5} \, Pr^{0.33} \qquad (\, 250 < Re < 650) \qquad (2\text{-}16)$$

The Nusselt number, Nu and Prandtl number, Pr are defined as follows:

$$Nu = \frac{h_{gs} D_p}{\lambda} \qquad (2\text{-}17)$$

$$Pr = \frac{C_p \mu}{\lambda} \qquad (2\text{-}18)$$

where h_{gs} is the gas-solid heat transfer coefficient, λ is the thermal conductivity and C_p is the specific heat of the gas.

Another study on convective heat transfer in a counter-current moving bed was conducted by Sissom and Jackson (1967). They found that Nusselt number, Nu was proportional to the Reynolds number, Re in the following form:

$$Nu \propto Re^{1.3} \qquad\qquad (10 < Re < 50) \qquad\qquad (2\text{-}19)$$

2.4   Gas-solid mass and heat transfer for a single sphere

Sherwood et al.(1975) have reviewed literature on mass transfer between a fluid and single sphere. If the fluid around the sphere is also stagnant then mass transfer only occurs by diffusion. Increasing the gas velocity or turbulence has an appreciable effect on mass transfer. The mass transfer can also be enhanced by vibrating or rotating the sphere.

For a single sphere moving through a fluid, the mass transfer at the surface is given by (Kunii and Levenspiel, 1969):

$$y \cdot Sh = \ \ 2.0 + 0.6 Re_p^{0.5} Sc^{0.33} \qquad\qquad (2\text{-}20)$$

In this case the Reynolds number for a single particle, Re_p is defined as:

$$Re_p = \ \frac{D_p \rho U_o}{\mu} \qquad\qquad (2\text{-}21)$$

where U_o is the relative velocity of the sphere through the fluid.

Ranz and Marshall (1952) conducted experiments on evaporation of water drops from which they estimated the convective mass transfer and heat transfer coefficients. Dry air at room temperature was used to evaporate water drops and the following empirical equations were obtained:

$$Sh = 2.0 + Re_p^{0.5} Sc^{0.33} \qquad (2\text{-}22)$$

$$Nu = 2.0 + Re_p^{0.5} Pr^{0.33} \qquad (2\text{-}23)$$

2.5   Heat and mass transfer in rotary kilns, dryers and coolers

Many studies of heat transfer in kilns and dryers are found in the literature because heat transfer and mixing are usually the rate limiting steps in rotary kiln operations. In the following sections, trends/correlations in literature that aid in predicting heat transfer coefficient, h_{gs}, volumetric heat transfer coefficient, Ua and contact surface area for heat transfer are presented.

2.5.1   Studies of heat transfer coefficient, h_{gs} in rotary kilns

Saeman and Mitchell (1954) investigated the primary factors which determine the rate of heat transfer in a rotating kiln. The first factor is the material cascade rate which depends on the size and number of flights, the holdup and the rotation rate. The second factor is the air-material entrainment ratio which depends on flight size and slightly

on rotation rate. They showed that primary variables like diameter, speed, size and number of flights, slope, particle size, air rate and feed rate affect the heat transfer rate mainly insofar as these variables affect the cascade rate. The heat transfer coefficient was found to be proportional to the material cascade rate over a wide range of primary variables. The ratio of heat transfer to the cascade rate for fully loaded flights varied most strongly with flight size. Variation with rotational rate and size and type of material was less significant.

An experimental heat transfer study in a direct-fired rotary kiln was conducted by Brimacombe and Watkinson (1978a,b). Their study focused on measurement of heat transfer rates from gas to wall and gas to solids. The objective was to relate heat transfer and bed mixing to kiln operating parameters such as rotational speed, percent fill and solids flow rate. The operating variables were in the following range: rotational speed, N (0.25 to 2.0 rpm), percent fill, η (5 to 14%), solids feed rate (4.6 to 37.8 g/s) and gas rate (19.4 to 30.0 g/s). The kiln was inclined at a slope of 2.4 ° and was 5.5 m long with an internal diameter of 0.406m. The mean diameter of the solids used in their study was 0.58 mm.

From their experimental studies, Brimacombe and Watkinson found that gas to solids heat flux is up to ten fold greater than the heat flux between the gas and wall. Also gas-solids heat flux was found to be a function of solids feed rate at low throughput but it was constant at high throughputs. At low feed rates, corresponding to low rotational speeds, the bed was in the slumping mode. Due to the poor mixing, the heat flux to the

solids was governed by mixing in the bed. On the other hand, at higher feed rates and rotational speeds, the bed was in rolling mode and heat transfer control had changed to the gas side. Assuming that bed mixing is crudely related to N, then solids mixing should control heat transfer at the lowest speeds and gas-solid transfer controls heat transfer at the highest speeds. Thus, increasing rotational speed should increase the dependence of gas to solids heat flux on gas temperatures. The above assumption was verified as they observed that effect of gas temperature increased with increasing rotational speed.

Brimacombe and Watkinson (1978a,b) also investigated the relationship between the bed motion and heat transfer characteristics by observing the particle motion. Three types of motion were observed in the experiments: slumping, rolling and transitional (only part of bed surface is characterized by rolling and remainder shows slumping behavior). From the particle motion studies they produced a plot of bed depth and rotational speed with the different regions of bed behavior delineated. Slumping was observed at N<0.4 rpm and at very low bed depths. These results were in agreement with the effect of solids feed rate on the gas to solids heat flux. At feed rates below 9 g/s and rotational speed below 0.4 rpm, the bed was in the slumping mode resulting in low gas to solids heat flux. Similarly, at feed rates greater than 20 g/s the bed was in the rolling mode and gas-solid heat transfer was high.

The literature reviewed by Brimacombe and Watkinson (1978 a,b) suggested that heat transfer to the solids occurs in two stages- (i) heat transfer to a thin layer of particles

at the surface and (ii) heat transfer by mixing of this top layer into the bed. Depending on the particle motion, either of the two stages could control heat transfer. They considered the two heat flow regimes corresponding to rolling bed and slumping bed separately. The gas-side convective coefficient for the rolling bed and burden-side coefficient for the slumping bed were calculated. The burden-side coefficient was calculated from heat transfer data with feed rates less than 9 g/s. In this calculation, the surface particle temperature and the solids bed temperature were used. Thus burden-side coefficients are heat transfer coefficients due to bed mixing. For the calculation of the gas-side convective coefficients, the average gas temperature and solids bed temperature were used.

Under rolling bed conditions, heat flux to the solids was found to be independent of rotational speed, percent fill and solids throughput. This insensitivity was because the rate of mixing of particles was high and resistance to heat flow in bed was at minimum. The convective heat transfer coefficient, h_{gs}, was calculated based on chord length of the bed. They expected h_{gs} to vary with the freeboard gas throughput but could not verify this hypothesis because their data at high solids feed rate were for essentially constant fuel and air rates. The convective side coefficients, h_{gs} from this study were in the range 120 to 240 W/m²K. The burden-side heat transfer coefficient had values ranging from 700 to 1200 W/m²K.

Tscheng and Watkinson (1979) conducted an experimental study of convective heat transfer from hot air to sand in a counter-current, non-fired rotary kiln (2.5m X

0.19m ID). They measured the gas-solid convective heat transfer coefficient, h_{gs}, as a function of rotational speed (0.4-6.0 rpm), percent fill (6.5-17%) and gas throughput (650-3300 $kg/m^2.h$). Gas to wall heat transfer coefficients were also measured. The interior surface of the kiln was roughened so that the solids motion in the drum was in the rolling mode except at 0.4 rpm.

Due to the rolling motion of the solids there was effective radial mixing which resulted in uniformity of radial bed temperatures. For calculation of h_{gs}, the gas-solid heat transfer coefficient, the bed surface was assumed to be planar and heat transfer area was taken equal to chord length times the kiln length. Tscheng and Watkinson (1979) found that increasing the gas flow rate increased the gas-solid heat transfer coefficient. If heat transfer resistance from gas to bed consists of two resistances in series, one in the gas phase and one within the solids bed, then the strong dependence of h_{gs} on the gas flow rate suggested that the major resistance of heat flow from the gas to the rolling bed was on the gas side. They also noted a slight positive effect of increasing the drum rotational speed on h_{gs}, because when the kiln rotated at low speeds, the bed was in the slumping mode. Under slumping conditions, bed mixing probably controls the heat transfer, therefore h_{gs} increased substantially with rotating speed until rolling started. Once rolling started, the effect of increasing rotational speed was lower than under slumping conditions. Some tests with a lucite kiln and polystyrene particles (3 mm diameter) showed that the velocity of the particles on the surface was proportional to the square root of the rotational speed.

Increasing the degree of fill had a slight negative effect on h_{gs}. Tscheng and Watkinson suggested that this was due to reduction in the bed surface to volume ratio. This ratio is important in heat transfer as heat is first transferred to the particles that roll down the surface and mix with the particles of other surface layers before returning into the bed. The heated mixed particles then remain in the bed before they emerge back on the bed surface. It was found that the gas-solid heat transfer coefficient was roughly an order of magnitude higher than that from gas to wall. This was probably due to the under estimation of the true surface area and the effect of the transverse velocity of particles down the surface.

From the experimental data Tscheng and Watkinson (1979) obtained the following dimensionless form for the Nusselt number (based on equivalent diameter, D_e):

$$Nu_{gs} = 0.46 Re_g^{0.535} Re_\omega^{0.104} \eta^{-0.341} \qquad 1600 < Re_g < 8000 \qquad (2\text{-}24)$$

where η is the solids volume fraction. The equivalent diameter, D_e, and dimensionless numbers (Nusselt number, Nu_{gs}, axial gas phase Reynolds number, Re_g and transverse Reynolds number, Re_ω) are defined as follows:

$$D_e = \frac{0.5D(2\pi - \beta + \sin\beta)}{(\pi - \frac{\beta}{2} + \sin\frac{\beta}{2})} \qquad (2\text{-}25)$$

$$Nu_{gs} = \frac{h_{gs}D_e}{k} \qquad (2\text{-}26)$$

$$Re_g = \frac{u\rho D_e}{\mu} \tag{2-27}$$

$$Re_\omega = \frac{D_e^2 \omega \rho}{\mu} \tag{2-28}$$

where D is the drum diameter, β is the central angle, u is the superficial gas velocity and ω is the angular velocity of the drum.

Mu and Perlmutter (1981) developed a model to describe the performance of rotary reactors, which included a detailed description of particle motion and heat transfer coefficients. In the model, they used the following correlation to evaluate the gas-solid convective heat transfer coefficient, h_{gs}:

$$h_{gs} = 0.023 \left[\frac{\rho\lambda}{\mu} \right]^{0.8} \left[\frac{\lambda}{D_e} \right]^{0.2} \left[u^2 + V_s^2 \right]^{0.4} \tag{2-29}$$

where D_e is the equivalent diameter of kiln, ρ is the gas density, μ is the gas viscosity, λ is the gas thermal conductivity, u is the gas velocity and V_s is the surface particle velocity.

Boateng and Barr (1996) developed a mathematical model for predicting gas-solid heat transfer in a rolling bed. This thermal model incorporates a two-dimensional model of the transverse bed into a one-dimensional plug flow model for rotary kilns. The model can be used to predict the temperature distribution within the solids bed at any axial position of the kiln. For model validation, they did pilot kiln experiments for a rolling bed of approximately 2.25 mm diameter spherical particles. The solids fill, η was varied from 12

% to 27 % and rotational speed, N was varied from 1.5 to 2.0 rpm. They found good
agreement between the model predictions and the experimental data. After verifying the
validity of the thermal model, they did model predictions to study the effect of granular
material on the temperature distribution in the bed. The model predicted that for a rolling
bed at a low rotational speed of 1.5 rpm, a slight temperature gradient was established
between the active layer and the rest of the bed. When the drum rotational speed was
increased upto 5.0 rpm, the temperature gradient reduced and isothermal conditions were
reached in the bed. They concluded that for a rolling bed with uniform particle size, the
velocity profile enhanced the thermal conductivity of the bed and facilitated temperature
uniformity in the bed.

2.5.2 Studies of volumetric heat transfer coefficient, Ua in rotary dryers and coolers

Friedman and Marshall (1949) measured volumetric heat transfer
coefficients in a rotary dryer as a function of air rate, feed rate, rotation rate, slope and
number of flights. Experiments were conducted in a 1.82 m long by 0.305 m diameter
dryer. Both co-current and counter-current flows were studied. Flights used in this study
were 1" long with 3/8 " long lip (at an angle of 135 ° from the normal to the drum wall).

They found that at fixed rotational speed (10 rpm) and number of flights (8), the
volumetric heat transfer coefficient, Ua increased with increasing air velocity. Also Ua
slightly increased with increasing percent fill which was achieved by increasing the solids

flow rate. The rotation rate, N had no effect on Ua because rotation rate changed rate of showering and holdup such that the amount of material suspended in the air was the same.

By decreasing the slope of the dryer, the holdup of solids was increased. The volumetric heat transfer coefficient, Ua increased with decreasing slope until critical holdup of 3% was reached. Further decrease in slope did not change Ua as the solids holdup in the drum was above the critical holdup of 3%. As holdup in the dryer increased, flights became fully loaded until finally a point was reached where any increase in holdup caused no further increase in flight loading and a bed of material formed at the bottom of the dryer. This bed did not effectively contact the air. Friedman and Marshall expected this critical holdup to change with dryer size or flight design, however, did not conduct any experiments to verify their hypothesis.

The volumetric heat transfer coefficient, Ua increased from zero flights to two flights but after that as the number of flights were increased to four and eight, Ua did not increase rapidly, indicating only a small increase in contacting area was achieved with additional flights. In the absence of flights, material received heat by convection to the surface of the solids bed and by conduction from the shell.

Hirosue and Shinohara (1976) developed a semi-theoretical equation for evaluating the volumetric heat transfer coefficient, Ua in rotary dryers and coolers. The two parameters involved in the predictive equation were determined from literature data.

An attempt was also made to explain the relationship between operating variables (holdup, particle diameter) and the heat transfer coefficient.

For predicting the heat transfer coefficient Hirosue and Shinohara assumed that heat transfer between particle and air occurs only when the particles are falling. They assumed that the volumetric heat transfer coefficient is equal to the product of the effective number of falling particles per unit volume, surface area of a spherical particle and h_{gs} obtained from the Ranz-Marshall (1952 a,b) equation. They obtained the following equation from the above assumptions:

$$Ua = h_{gs}\pi D_p^2 \left[\frac{N_e}{A_c L}\right] \tag{2-30}$$

where N_e is the effective number of falling particles, A_c is the cross-sectional area of dryer, L is the length of the dryer. The convective gas-solid heat transfer coefficient, h_{gs} is given

by: $$h_{gs} = \frac{\lambda}{D_p}\left[2.0 + 0.6 Re_p^{0.5} Pr^{0.33}\right] \tag{2-31}$$

where Prandtl number, Pr is defined as Equation (2-18) and Reynolds number, Re_p is defined as Equation (2-21) where $U_o = \sqrt{V_p^2 + u^2}$. Here u is the gas velocity and V_p is the falling velocity of particle. From their previous work they obtained the following expressions for obtaining N_e/L :

$$\frac{N_e}{L} = ZJ^e \tag{2-32}$$

$$J = \frac{\eta^{1.37}Fr^{0.41}A_c}{D_p^3} \tag{2-33}$$

$$Fr = \frac{\pi D N^2}{3600 \cdot g} \tag{2-34}$$

where η is the solids holdup (%), D is the drum diameter, g is acceleration due to gravity and Fr is the Froude number. Hirosue (1989) used literature data to compute values of $\frac{UaA_c}{h_{gs}\pi D_p^2}$ and J which were plotted to obtain the constants: Z and e. Hirosue obtained the following equations from correlating the literature data:

$$Ua = \frac{0.536 h_{gs} \eta^{1.005} D^{0.3075} N^{0.615}}{D_p^{0.25} g^{0.3075} A_c^{0.25}} \qquad 3\times10^5 \leq J \leq 1.5\times10^8 \tag{2-35}$$

$$Ua = \frac{53.2 h_{gs} \eta^{1.005} D^{0.205} N^{0.41} D_p^{0.25}}{g^{0.205} A_c^{0.5}} \qquad 1.5\times10^8 \leq J \leq 2\times10^{10}$$

To account for the influence of falling particles surrounding a single falling particle, Hirosue(1989) introduced a correction factor, CF that was close to unity when the average number of particles falling was relatively small. The correction factor is less than unity as the average number of falling particles is increased because of insufficient contact between the particles and the air. The semi-theoretical equation for evaluating volumetric heat transfer coefficient, Ua was given by:

$$Ua = CF h_{gs} \pi D_p^2 \frac{N_e}{A_c L} \tag{2-36}$$

For the two ranges of J as shown in Equation (2-35), the values of CF are:

$$CF = 37.5 J^{-1/4} \qquad 3\times10^5 \leq J \leq 1.5\times10^8$$

$$CF = 4190 J^{-1/2} \qquad 1.5\times10^8 \leq J \leq 2\times10^{10}$$

The various trends in heat transfer coefficient, h_{gs} and volumetric heat transfer coefficient, Ua that were mentioned in sections 2.5.1 and 2.5.2 are summarized in Table 2-1.

Table 2-1. Trends in heat transfer coefficient and heat flux for the different parameters.

Reference	Apparatus	Bed Motion	Parameters				h_{gs}	Ua	Gas-solid heat flux
			N	u	T_e	η			
Saeman and Mitchell (1954)	Rotary dryer, flights		*↑				*↑		
Brimacombe and Watkinson (1978a,b)	Direct-fired rotary kiln, no baffles	Rolling mode at high N and high η	↑		↑	↑	NE ↑		NE
Tscheng and Watkinson (1979)	Non-fired rotary kiln, no baffles	Rolling mode	↑	↑		↑	↑ ↑ ↓		
Mu and Perlmutter (1981)	none (used model)	Rolling bed		↑	.		↑		
Friedman and Marshall (1949)	Rotary dryer and cooler, flights		↑ or ↓	↑		↑ changes with N		↑ ↑ NE	
Hirosue and Shinohara (1976)	Rotary dryer and cooler, flights		↑	↑		↑	↑	↑ ↑ ↑	

NE= no effect

* Arrows indicate change in heat transfer with changes in operating parameters, for example, an increase in rotational speed (N) resulted in an increase in the heat transfer coefficient (h_{gs}).

2.5.3 Study of heat and mass transfer coefficients in a rotary kiln (transverse aeration)

Chang (1994) measured heat and mass transfer coefficients between gas and solid particles in the transverse bed of a transversely aerated rotary kiln incinerator. Transverse aeration was provided by passing the aeration gas from nozzles in the drum wall through the particle bed. This mode of aeration was made possible by valves that rotated with the drum. The heat and mass transfer coefficients were measured for 30% fill and rotational speed in the range of 0.5 and 10 rpm. The kiln used in the experiments was 0.1 m long with 0.3 m diameter and was not inclined. The aeration rate was in the range of 0.002-0.01 m^3/s. Chang found that both heat and mass transfer coefficients were sensitive to aeration rate or the superficial gas velocity and not the rotational speed. Also transverse bed temperature distribution was uniform which indicated good transverse mixing in the drum. The following correlation was obtained to predict the mass transfer coefficient:

$$Sh = 0.0122 \, Re^{1.372} \qquad (10 < Re < 100) \qquad (2\text{-}37)$$

where Sherwood number, Sh is defined as Equation (2-10) and Reynolds number, Re is defined as Equation (2-11).

2.5.4 Estimation of contact surface area for heat transfer

The contact surface area for heat transfer in rolling beds was assumed by Brimacombe and Watkinson (1978a,b) and Tscheng and Watkinson (1979) to be equal to chord length times the kiln length. The true contact area between the gas and solids would be much larger as stated by Tscheng and Watkinson (1979) because even in a static bed, the actual contact area can be double the planar surface depending on the particle arrangement. Therefore with rolling particles the contact area would be even greater.

In a flighted drum, Friedman and Marshall (1949) believed that there was an increase in the contact area when additional flights were added to the drum. They did not make any contact area measurements but had come to this conclusion based on the measurements of the volumetric heat transfer coefficient, Ua.

Hirosue and Shinohara (1976) had assumed that in a flighted drum, the contact area was related to the number of falling particles and the surface area of a spherical particle (Section 2.5.2). Later Hirosue (1989) introduced a correction factor in the heat transfer coefficient correlation which accounted for the decrease in the contact area between a particle and air when the number of falling particles increased.

Schofield and Gilkin (1962) suggested that the heat transfer coefficient can be evaluated in terms of total surface area of material exposed to air. They correlated the rate

of cascading flow to surface area and proposed the following equation to calculate surface area in contact with air, B:

$$B = \frac{6MLt_f}{\left[D_p \rho_p L_v \sin\alpha - \frac{1.5\phi \rho^2 u^2 U_o D_p L_v}{g\mu} \right]}$$

(2-38)

where M is the material feed rate, t_f is the time of fall of particle, L is the length of the dryer, α is the slope of dryer, L_v is the vertical length of fall, ϕ is the angle particles in flight make with the horizontal, D_p is the particle diameter, U_o is the relative velocity, g is the acceleration due to gravity, μ is the gas viscosity, ρ is the gas density, ρ_p is the particle density and u is the gas velocity.

3.0   THEORY

3.1   Development of expressions for evaluation of volumetric mass transfer coefficient, k_sA

3.1.1   Steady-state piecewise method

For a substance diffusing into the gas phase, the molar flux per unit mass transfer area is given by Treybal (1980) as:

$$N_A = k_s(C^{sat} - C^{ss})$$

(3-1)

where k_s is the mass transfer coefficient, C^{sat} is the gas phase saturation concentration of the diffusing substance and C^{ss} is the gas phase steady-state concentration of the diffusing substance.

Performing a steady-state mole balance (for the diffusing substance) on a system shown in Figure 3-1, the following expression is obtained:

$$k_sA(C^{sat} - C^{ss}) = QC^{ss}$$

(3-2)

where A is the area available for mass transfer and Q is the volumetric flow rate of the gas.
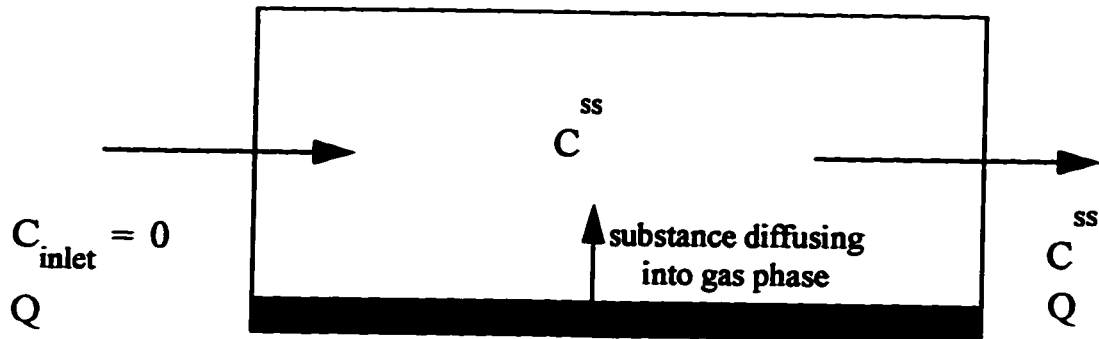
Figure 3-1. Schematic diagram of the system for mole balance.

If the gas phase concentration of the diffusing substance is measured by a sensor that gives an output signal proportional to the concentration, then Equation (3-2) can be written in terms of the saturation signal, S^{sat} and the steady-state signal, S^{ss} from the sensor to obtain the following equation:

$$k_s A(S^{sat} - S^{ss}) = QS^{ss} \qquad (3-3)$$

For the system shown in Figure 3-1, a new steady-state at the same experimental conditions (i.e. fixed rotational speed, N, fixed solids volume fraction, η and presence or

absence of baffles) can be obtained by changing the gas flow rate, Q. Consider any two steady-states such as shown in Figure 3-2.
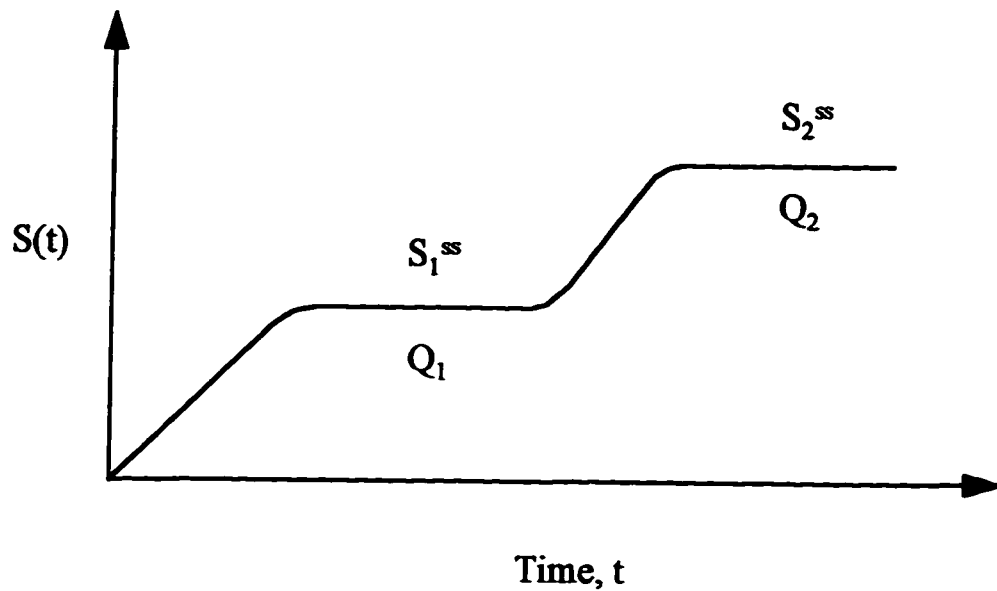
Figure 3-2. Steady-states for the system at different gas flow rates.

The following equations can be written for the two steady-states in terms of the sensor signals:

$$k_s A(S^{sat} - S_1^{ss}) = Q_1 S_1^{ss} \qquad (3\text{-}4)$$

$$k_s A(S^{sat} - S_2^{ss}) = Q_2 S_2^{ss} \qquad (3\text{-}5)$$

where subscript 1 denotes the signal and gas flow rate for the first steady-state and subscript 2 denotes the signal and gas flow rate for the second steady-state. From

Equations (3-4) and (3-5), the saturation signal, S^{sat} can be eliminated to obtain the following expression for evaluating the volumetric mass transfer coefficient, k_sA :

$$k_sA = \left[\frac{S_1^{ss}Q_1 - S_2^{ss}Q_2}{S_2^{ss} - S_1^{ss}} \right] \qquad (3-6)$$

By evaluating the data in a piecewise manner, the sensor signal can be used to obtain k_sA without detailed calibration or measurement of the response to the saturated concentration. Also when the data is analyzed piecewise, the steady-state(s) where there was drift in the instrument reading can be ignored so that there is less error in the experimentally determined value of k_sA.

3.1.2 Steady-state slope method

For developing the expression for the steady-state slope method, Equation (3-3) can be rearranged to obtain:

$$S^{ss} = \frac{S^{sat}k_sA}{(Q + k_sA)} \qquad (3-7)$$

$$\frac{1}{S^{ss}} = \frac{1}{S^{sat}} + \left[\frac{1}{S^{sat}k_sA} \right]Q \qquad (3-8)$$

From Equation (3-8) it can be seen that linear regression of the data when plotted as $1/S^{ss}$ versus Q for an experimental condition (i.e. fixed rotational speed, N, fixed solids volume fraction, η and presence or absence of baffles) will give an intercept, b equal to $\dfrac{1}{S^{sat}}$ and a slope, m equal to $\dfrac{1}{S^{sat}k_sA}$. Volumetric mass transfer coefficient, k_sA by the slope method can be evaluated from the following expression:

$$k_sA = \frac{b}{m} \qquad (3\text{-}9)$$

The only disadvantage of this approach is the possibility of drift in the sensor signal with time. Computation of k_sA by the slope method will provide a cross-check for the values obtained by the piecewise method and also verify if significant drift in the sensor signal occurred with time.

Evaluation of k_sA using the piecewise or slope method is independent of the gas flow rate, Q, when the drum wall velocity is the dominant velocity in the system. Equation (3-3) can only be used to analyze a series of steady-states if k_sA is independent of the gas flow rate. This approximation will be satisfied if the particle motion is greater than the axial gas velocity. For every experimental condition, the ratio of drum wall velocity, V_w (calculated by Equation (3-15)) to the superficial axial gas velocity,u has to be greater than unity in order to satify the approximation mentioned above.

3.2 Computation of residence time distribution (RTD) of the gas in the drum and the average residence time, τ

The RTD function, E(t), for a positive step input with constant rate of tracer addition to the feed initiated at time, t=0 is given by Fogler (1992) as:

$$E(t) = \frac{d}{dt}\left[\frac{C(t)}{C_f - C_i}\right]$$
(3-10)

where C(t) is the tracer concentration in the drum, C_i is the initial tracer concentration in the drum before the step change and C_f is the steady-state tracer concentration in the drum.

Concentration of the tracer can be detected by a sensor and Equation (3-10) can be rewritten in terms of the sensor signal to obtain:

$$E(t) = \frac{d}{dt}\left[\frac{S(t)}{S_f - S_i}\right]$$
(3-11)

where S(t) is the tracer signal after the step change, S_i is the initial tracer signal before the step change and S_f is the steady-state tracer signal. Using forward, central and backward

difference approximations as shown in Appendix A, $\dfrac{dS(t)}{dt}$ can be calculated from the experimental data, S(t).

E(t) function for a perfectly mixed CSTR is given by Fogler (1992):

$$E(t) = \frac{1}{\tau} e^{-\frac{t}{\tau}} \tag{3-12}$$

where τ is the average residence time of the gas. The predicted value of the average residence time, τ_{pred} is given by:

$$\tau_{pred} = \frac{V[1-(1-\varepsilon)\eta]}{Q} \tag{3-13}$$

where V is the volume of the drum and Q is the volumetric flow rate of the gas.

From Equations (3-11) and (3-12) the following equation is derived (Appendix A) which can be used for evaluating the average residence time, τ:

$$S(t) = S_f - (S_f - S_i)e^{-\frac{t}{\tau}} \tag{3-14}$$

3.3 Derivation of equation for evaluating surface particle velocity, V_s in the active-layer region of the rolling bed

Consider the cross-section of the drum as shown in Figure 3-3. The velocity profiles in the upper active layer zone, V_a and in the lower bulk flow zone, V_b are

assumed to be linear. The surface particle velocity in the active-layer is denoted as V_s and the drum wall velocity is denoted as V_W. Other quantities that are shown in Figure 3- 3 are : drum length, L, drum radius, R, active layer depth, h_a, total bed depth, h, rotational speed, N and angular velocity, ω. There is a no slip condition at z=0. The drum wall velocity is defined as:

$$V_W = R\omega = \frac{2\pi RN}{60} \tag{3-15}$$
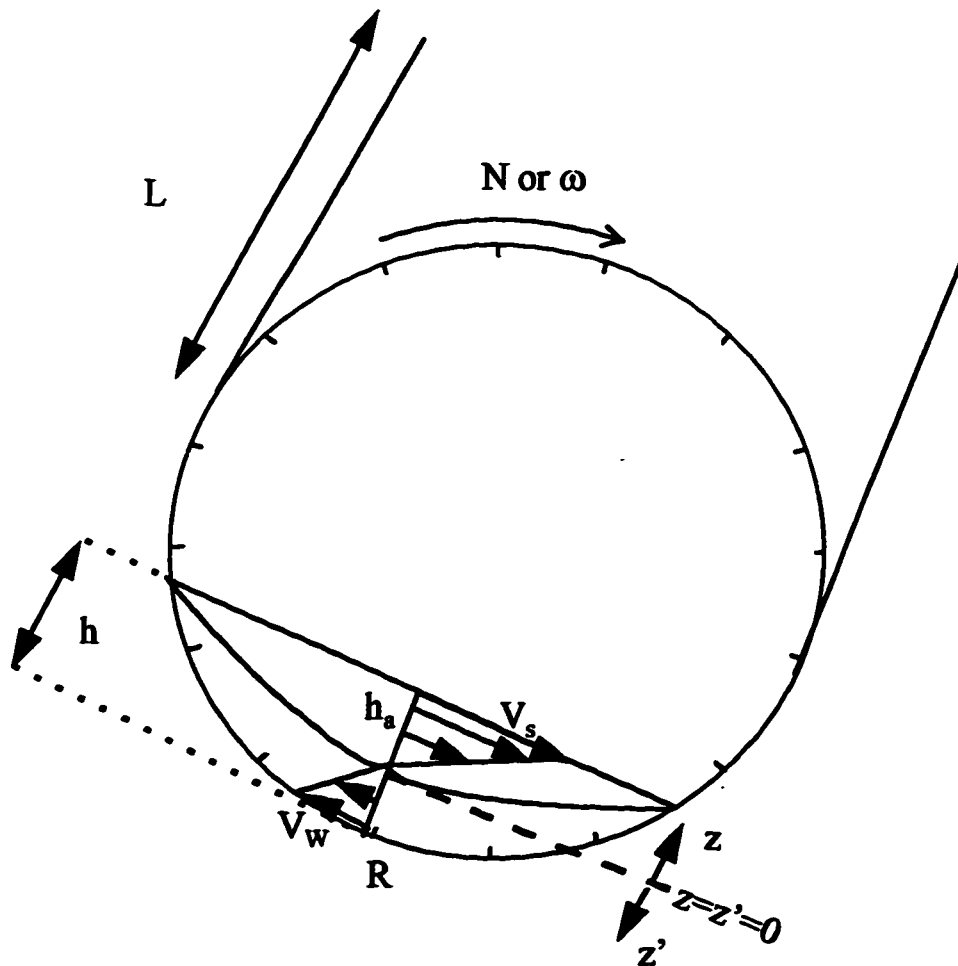
Figure 3-3. Velocity profiles in the active and bulk region of the rolling bed.

By applying the following boundary conditions: at $z=0, V_a (0)=0$ and at $z=h_a$, $V_a(h_a)=V_s$, the linear velocity profile in the active region, $V_a(z)$ is given by:

$$V_a(z) = \frac{V_s z}{h_a} \tag{3-16}$$

Similarly, by applying the following boundary conditions: at $z'=0$, $V_b(0)=0$ and at $z'=h-h_a$, $V_b(h-h_a)=V_W$, the linear velocity profile in the bulk region, $V_b(z')$ is given by:

$$V_b(z') = \frac{V_W z'}{(h-h_a)} \tag{3-17}$$

The volumetric flow of solids to the active layer region, Q_{top} is given by:

$$Q_{top} = \int_0^{h-h_a} \frac{L.V_W z' \, dz'}{(h-h_a)} = \frac{L.V_W(h-h_a)}{2} \tag{3-18}$$

The volumetric flow of solids to the bottom, bulk region, Q_{bulk} is given by:

$$Q_{bulk} = \int_0^{h_a} \frac{L.V_s z \, dz}{h_a} = \frac{LV_s h_a}{2} \tag{3-19}$$

By equating Equations (3-18) and (3-19) the following expression for V_s is obtained:

$$V_s = V_W \left[\frac{h}{h_a} - 1 \right]$$

(3-20)

Substituting for V_W in the above equation, the following expression for evaluating, V_s is obtained:

$$V_s = \frac{2\pi RN}{60} \left[\frac{h}{h_a} - 1 \right]$$

(3-21)

4. MATERIALS AND EXPERIMENTAL METHODS

This section describes the experimental technique, apparatus and procedure used for the measurement of mass transfer coefficients and the criteria used for the selection of the solid phase and hydrocarbon for the experiments. Some preliminary experiments had to be done to determine (i) constant-rate drying period of the solids and (ii) residence time distribution of the gas. The experimental apparatus and procedure for these preliminary experiments are also mentioned in this section.

4.1 Experimental Technique for the measurement of mass transfer coefficients

The experimental method used for gas-solid mass transfer measurements in the past in packed and fluidized systems involved evaporation of n-decane from the surface of Celite catalyst carriers (Wilkins and Thodos, 1969). The concentration of n-decane in air was measured by a hydrocarbon analyzer. These experiments were conducted during the constant rate of evaporation period to avoid internal resistances to mass transfer. A similar technique was used in the current experiments. A volatile hydrocarbon was evaporated into dry air from the surface of the porous solid and concentration of the hydrocarbon in the gas phase was detected by a mass spectrometer. The current experiments were also done during the constant-rate drying period of the solids saturated with the hydrocarbon.

4.2   Selection of solid phase and hydrocarbon for the mass transfer study

For the mass transfer experiments, a solid phase which is porous and capable of absorbing large quantities of hydrocarbon was required. Also the solid particles would be essentially spherical and about 2-4 mm in diameter. To avoid the problem of controlling the particle size, the particles should be low dusting and high mechanical strength. These specifications were met by Alumina S-201, 5X8 mesh catalyst carriers manufactured by LaRoche Chemical Industries Inc., Baton Rouge. This catalyst carrier has a bulk density of 737-769 kg/m^3. The pore volume is 0.46 cc/g (vacuum dried solids). The particle size is between 2.4 and 4 mm in diameter.

The hydrocarbon to be used in the experiments should absorb in the porous matrix of the solid in large quantities such that the solid is saturated. Also the hydrocarbon should be relatively cheap and non-toxic. A low vapour pressure hydrocarbon is desirable so that the evaporation rate is low and there is no wet-bulb temperature effect. Thus the particle surface temperature will be the dry bulb temperature of the gas (i.e. close to room temperature). These desirable properties of the hydrocarbon were satisfied by n-decane, 99+% (Sigma, St. Louis). The density of n-decane is 0.73 g/ml. The vapour pressure of n-decane at ambient temperature was measured by Wilkins and Thodos (1969). The experimental values they obtained were 126.5 Pa and 169.3 Pa at 20 °C and 24 °C respectively. For the hydrocarbon concentration in the gas phase to be measured by a mass spectrometer, the mass spectrum of the hydrocarbon should be readily available and the

ions formed should be easily detectable. The mass spectrum of n-decane was readily available and the strongest signal is at mass-to-charge ratio (m/e) of 43 (Stenhagen et al., 1969). The next most intense peak is at m/e ratio of 57 followed by the peak at m/e ratio of 41.

4.3 Experimental apparatus and procedure for the determination of the constant-rate drying period of the solids and F_E^{max}

When a porous solid is dried, the moisture content decreases with time. Most of the moisture that is removed comes from the interior of the solid. The moisture content, X (dry basis) is plotted as a function of time, t (Perry and Green, 1984) as shown in Figure 4-1.
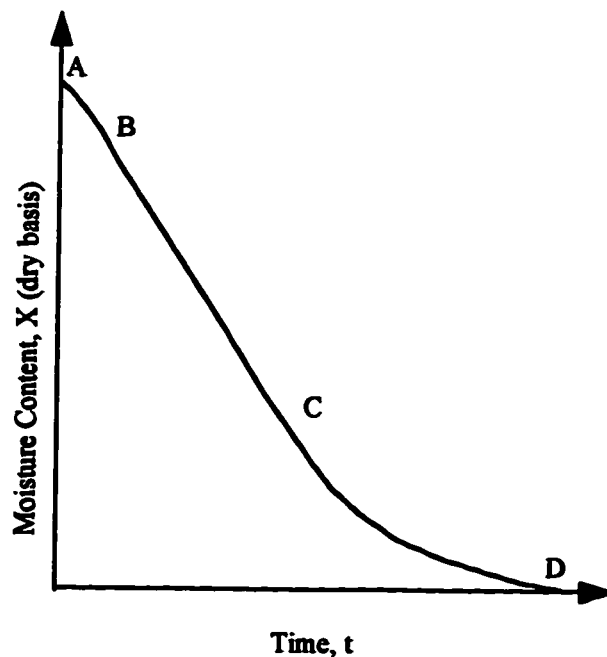
Figure 4-1. Drying curve of a solid.

There are three distinct sections on the curve shown in the figure. Section AB is the initial transient. Section BC represents the constant-rate period and the curved section CD represents the falling-rate period. During the constant-rate period, the moisture movement within the solid is rapid enough to maintain saturated conditions at the surface. As a result, drying is independent of the moisture content and the drying rate is constant. Drying during this period is controlled by external resistances to mass transfer. The falling-rate period begins at the critical moisture content where the constant-rate ends. As the moisture content falls below this critical value, the drying rate decreases. This is due to unsaturated conditions at the surface of the solid. The drying process is controlled by the internal as well as external mass transfer resistances. The principle of constant-rate drying also applies to the evaporation of hydrocarbons from the surface of a porous solid. For mass transfer experiments, it is desirable to operate in the constant-rate drying period of the solid so that the internal mass transfer resistances are absent.

The fraction evaporated, F_E was defined as the mass of hydrocarbon evaporated divided by the initial mass of hydrocarbon. To ensure constant drying conditions prevail, the upper limit of F_E needs to be determined for the particular porous solids (saturated with hydrocarbon) used in the mass transfer experiments. The fraction of total hydrocarbon that is evaporated during the constant rate period is denoted by F_E and the following equation is used for calculating its maximum value:

$$F_E^{max} = \frac{\text{Mass of hydrocarbon evapourated in the constant drying period}}{\text{Total mass of hydrocarbon present in saturated solids}} \quad (4\text{-}1)$$

A wind tunnel type tray dryer as shown in Figure 4-2 was used for obtaining the experimental data. The sample tray was loaded with solids (vacuum dried and saturated with n-decane or just vacuum dried) and placed over a digital balance (1364 MP, Sartorius, Germany) in the drying chamber. The cross-section of the air duct is 0.12m x 0.12m, of the drying chamber is 0.185m x 0.15m and of the sample tray is 0.125m x 0.16m. The gate was left open to allow ambient air into the duct. A blower supplied the duct air to the drying chamber. Air temperature and velocity in the duct was measured by a namometer.

The air temperature was in the range 24.6-25.7 °C and the air velocity in the duct was 1.0 m/s for the experiments. The air velocity in the drying chamber was 0.52 m/s. The weight of the tray and the solids was recorded with time (every 10-15 minutes). The blower fan was turned off when recording the weight to avoid error due to fluctuations in the reading caused by turbulence. The weight of the tray was recorded at the end of the experiment. From these weight measurements and the vacuum-dry weight of the solids, the mass of n-decane present in the saturated solids as a function of time was evaluated. Thus necessary data was collected to determine the constant-rate drying period as well as the value of F_E^{max} (Equation 4-1). Observations such as condensation and color change of the solids were also made. The solids that were used in the experiments were unsieved S-201 Alumina catalyst carriers (5X8 mesh).

1. Blower
2. Sample Tray
3. Digital Balance
4. Drying Chamber
5. Air Duct
6. Namometer
7. Gate
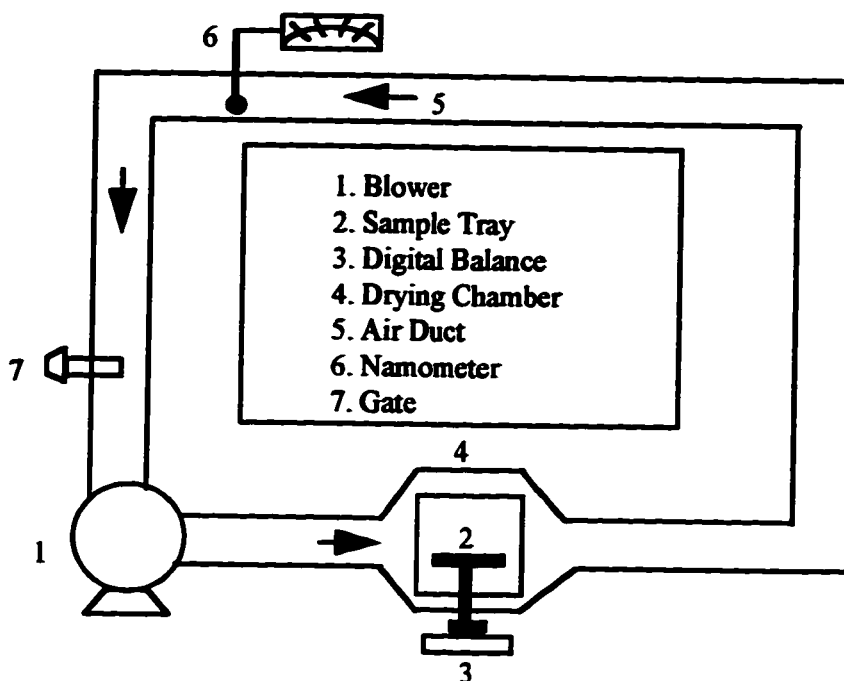
Figure 4-2. Tray Drying Equipment.

The procedure used for preparation of solids was as follows: the alumina beads (~ 50 g) were vacuum dried at 200 °C and 6.5 kPa for about 1.5 hours. The solids were cooled in a dessicator for about half an hour. The vacuum dried solids were saturated in 50 mL of n-decane for about 24 hours at room temperature (21-22 °C). The saturated solids were recovered by filtration and then wiped dry to remove any free surface liquid from the beads. Since ambient air was used in these experiments, the adsorption of water from the air onto vacuum-dried solids was also determined. For this experiment, the solids

were prepared according to the procedure outlined above except that the solids were not saturated with n-decane.

4.4   Rotating drum mass transfer experimental apparatus and procedure

Schematic diagram of the equipment used in the rotating drum experiments is shown in Figure 4-3. The drum reactor was made of plexiglas which enabled the cross-section of the drum to be viewed from the two ends. The mouths of the drum at the two ends were sealed by rubber stoppers. The drum length was 0.308 m and the diameter was 0.29 m. Volume of the drum was 20 L. Two types of internals were used in the drum. For measurement of mass transfer coefficient in the presence of baffles, a stainless steel cage with eight baffles was inserted in the drum. The width of the baffles was 10% of the drum diameter. For measurement of mass transfer coefficients in the absence of baffles, a stainless steel cage with sixteen thin rods (2.3 mm diameter) was inserted. This was done to prevent the solids from slipping and to ensure the solids motion was in the rolling mode.

The drum was placed on two rollers which were rotated, through a chain and gears, by means of a variable speed motor. Building air was introduced in the experimental set up through a valve and pressure regulator. The air was then passed through a coalescing filter (A2651 82-700BX, Balston Inc., Haverhill) to remove entrained hydrocarbons. Next the air was passed through a Drierite Gas Purifier (L68GP, W.A.

Hammond Drierite Co., Xenia) where the drierite bed and molecular sieves removed the moisture present in the air. Flow rate of dry air into the drum was regulated by a flow meter (UFC 3020 or UFC 1200A ,Unit Instruments Inc., Orange) and controller (URS-100,Unit Instruments Inc., Orange).

1. Air supply valve	5. Flow meter	9. Mass spectrometer
2. Pressure regulator	6. Controller	10. Computer
3. Coalescing filter	7. Rotary drum	11. Motor
4. Gas Purifier	8. Glass trap	12. Roller
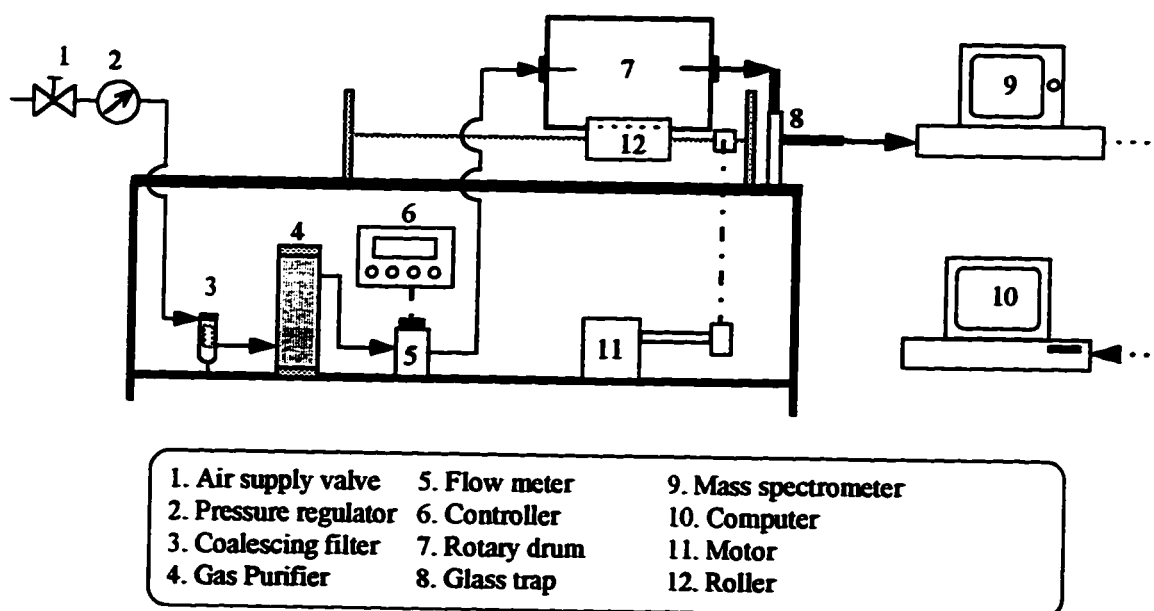
Figure 4-3. Schematic Diagram of the Equipment for Rotating Drum Experiments.

Gas stream exiting the drum was passed through a glass trap to capture any entrained solids before entering the mass spectrometer (Dycor Quadrupole Gas Analyzer M200ED , Ametek, Pittsburgh). The n-decane signal (at m/e ratio of 43) with time generated by the mass spectrometer sensor was recorded on a computer (Personal Computer XT, IBM, Toronto).

Two flow meters were used in the experiments. For flow rates between 1-6 litres per minute, model UFC 1200A was used and for flow rates between 6-20 litres per minute, model UFC 3020 was used. These flow meters were calibrated for building air at ambient temperature and pressure. The calibrations were done using a Bell Prover Meter (American Meter Co., Philadelphia). The calibration curves for these flow meters are shown in Appendix B.

To prevent the n-decane from condensing, the sampling capillary (Chromatographic Specialities, Brockville, deactivated fused silica, 4m, 0.25 mm ID) was heated to temperatures above ambient. The different components before the drum entrance were connected by Poly-Flo (Imperial Eastman, Chicago) tubing. However, the components after the drum exit were connected by Nylo-Seal (Imperial Eastman, Chicago) and glass tubing to ensure negligible amount of n-decane was adsorbed from the gas stream exiting the drum.

Absolute calibration of the mass spectrometer could not be done due to lack of appropriate internal standard. Argon is a suitable internal standard as it is cheap. However, this standard could not be used as its peak at m/e ratio of 40 overlapped with that of n-decane (at m/e ratio of 41). Also the signal produced by the mass spectrometer drifted with time due to room temperature fluctuations and inherent drift in the instrument reading. As a result, constant correction in the signal due to drift was required. This

problem could not be resolved due to lack of internal standard. The interpretation of the data (Section 3.1.1) was designed to compensate for the drift in the signal.

The material that was loaded in the drum consisted of unsieved S-201 alumina catalyst carrier (5X8 mesh) particles saturated with n-decane. Preparation of the saturated solids was done in ~700 g batches (based on untreated S-201 weight). The untreated solids were vacuum dried at 250 °C and 6.5 kPa for about eight hours. The vacuum dried solids were cooled overnight in a dessicator. The cooled solids were then saturated in 700 mL of n-decane for about twent-four hours at room temperature (21-22 °C). The saturated solids were recovered by decantation and filtration. The saturated solids were wiped dry using absorbant wipers to remove the free surface liquid. The solids were reused after an experiment by saturating them under the same experimental conditions as mentioned above. The weight of solids was recorded using a digital balance (PC2000, Mettler, Nanikon). For all the batches of solids used in the experiments (after saturating or resaturating) the following mass ratios were obtained:

$$\frac{\text{Mass of n}-\text{decane adsorbed}}{\text{Mass of vacuum}-\text{dried (VD) solids}} = 0.345 - 0.347$$

$$\frac{\text{Mass of n}-\text{decane adsorbed}}{\text{Mass of saturated solids}} = 0.256 - 0.258$$

The bulk density of the saturated solids was measured in a 100 ml volumetric cylinder having a diameter of 2.5 cm. The bulk density of the saturated solids was in the range 985-1005 kg/m^3.

The drum operating conditions were: rotational speed, N: 0.09 to 2.0 rpm and solids volume fraction of saturated solids, η: 0.043 to 0.25. Dry air flow rates in the 1-20 L/min range were used in the study. The drum was operating at room temperature and pressure. Dry air supplied to the drum was at room temperature which was in the range 21.5 to 23.8 °C. The atmospheric pressure varied in the range 689.3 mmHg to 718.3 mmHg.

The experimental procedure was as follows: the weight of the saturated solids was measured and the solids were loaded in the drum. The solids bed temperature at the start of the experiment was recorded. Dry air flow rate was set using the flow meter and controller. After the air was introduced in the drum, in as minimum time as possible, the drum rotation and recording of the n-decane signal from the mass spectrometer were initiated. The n-decane signal was recorded at 30 second intervals. For the same experimental conditions (i.e. fixed rotational speed, N, fixed solids volume fraction, η and presence or absence of baffles) after a steady-state was reached, the air flow rate was changed. At every experimental condition, a series of step up or down in flow rate was done and the corresponding transients and steady-states were recorded. This was done to

confirm the steady-states that were obtained as the sensor signal sometimes drifted with time. A sample of the raw data is shown in the Results and Discussion chapter.

During the entire experimental run, drum rotational speed, air flow, room temperature and atmospheric pressure were measured. Drum rotational speed was measured by placing a mark on the drum and measuring the time required for one revolution. Atmospheric pressure was measured by a mercury barometer and the temperature was measured by a thermometer. At the end of the experiment, weight of the solids in the drum was measured to ensure that the experiment was conducted during the constant-rate drying period of the solids. The solids bed temperature was also measured at the end of the experiment to check if the solids had heated up or cooled down significantly compared to room temperature.

During the experiment, physical observations regarding dusting, color change of the solids and condensation of liquid in the drum or tubing were made. Also detailed observations of the particle motion were made. In the presence of baffles, showering patterns/frequencies, types of particle motion and surface particle velocity observations were made. For the rolling bed case (no baffles), more detailed observations were made. The quantities that were measured while the drum was in motion are shown in Figure 4-4.

These quantities were: active bed depth, h_a, total bed depth, h, dynamic angle of repose, θ, and chord length, L_c. The dynamic angle of repose was measured with a long

arm protractor by viewing the bed through the plexiglas end of the drum. Similarly, the chord length of the solids bed was measured by a metric scale. For measuring the active layer and total bed depths, a millimeter scale was pasted across the center of the plexiglas end of the drum. As the drum rotated, h_a and h were measured by viewing the bed from the end where the millimeter scale was pasted. The depths were measured at the point of maximum thickness of the rolling bed. Qualitative observations about the surface particle velocity, V_s were also made.
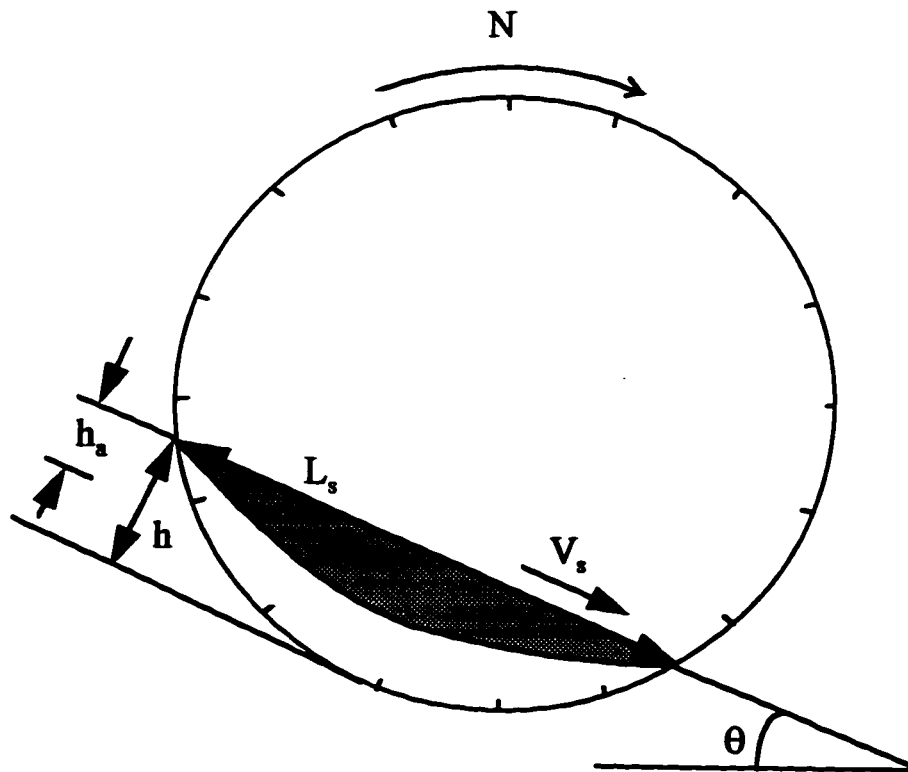
Figure 4-4. Quantities measured quantitatively or qualitatively for rolling bed experiments.

4.5   Experimental equipment and procedure for the determination of the residence time distribution of the gas

To establish whether the gas phase in the drum was well-mixed, the residence time distribution was measured. In this experiment, a positive-step input using Argon (Ar) as the tracer was done by switching the feed to the drum from air (Ar =0.934 mole%) to Calibration gas (Ar =2.01%). The equipment used in the experiment is shown in Figure 4-3. When the air was to be switched, the calibration gas cylinder (Praxair, Mississauga) was connected to the flow meter and controller. The solids used in the experiment were not vacuum dried and were not saturated with n-decane. The drum was operating at 2.27 rpm with a solids volume fraction of 0.10. The gas flow rate was 5.63 L/min. Sixteen thin rods (2.3 mm diameter) were placed along the drum wall to ensure the solids bed was in the rolling mode. These conditions were chosen because the solids mixing would be low and gas bypassing the drum would be high.

During bypassing, a part of the total gas flow rate that enters the drum, exits without mixing with the solids and gas in the drum. Bypassing may occur at high gas flow rates. The argon gas phase concentration in the exit gas stream with time was detected by a mass spectrometer. The Ar signal at m/e ratio of 40 with time (before and after the step input) was recorded on the computer at 30 second intervals until steady-state in the drum was reached. The raw data of this experiment are shown in Appendix A.

5. RESULTS AND DISCUSSION

5.1 Constant-rate drying period of solids

Three experimental runs (CD#1, CD#2 and CD#3) were conducted in the tray dryer (Figure 4-2). From the experimental data, values of F_E^{max} were calculated. Of these three runs, the first two were conducted using vacuum-dried solids that were saturated with n-decane and the third run was done using vacuum-dried solids. As mentioned in section 4.3, ambient air was used in the experiment so the adsorption of moisture from air onto vacuum-dried solids was determined from CD#3 run. From the experimental data (Appendix C), the decane content, X (dry basis) as a function of time, t was obtained for CD#1 and CD#2 runs.

Figure 5-1 shows the plot obtained from the experimental data of CD#1 run. The shape of the drying curve is similar to the one shown in Figure 4-1. It can be seen that the constant-rate period lasts till approximately 50 minutes from the start of the experiment after which the falling-rate period begins. During the constant-rate period, the decane content, X linearly decreased with time. A similar trend was noticed for CD#2 run and the constant-rate period lasted till 50 minutes as well. The drying curve for that run is given in Appendix C. During these experiments (CD#1 and CD#2) there was no condensation of liquid on the sample tray. The solids saturated with n-decane were of beige color at the

start of the experiment. As the experiment proceeded, the color of the solid beads turned lighter (approaching white) indicating that the n-decane was being evaporated from the surface of the porous solids. Figure 5-2 shows the moisture adsorbed by the vacuum-dried solids (CD#3 run) as a function of time.
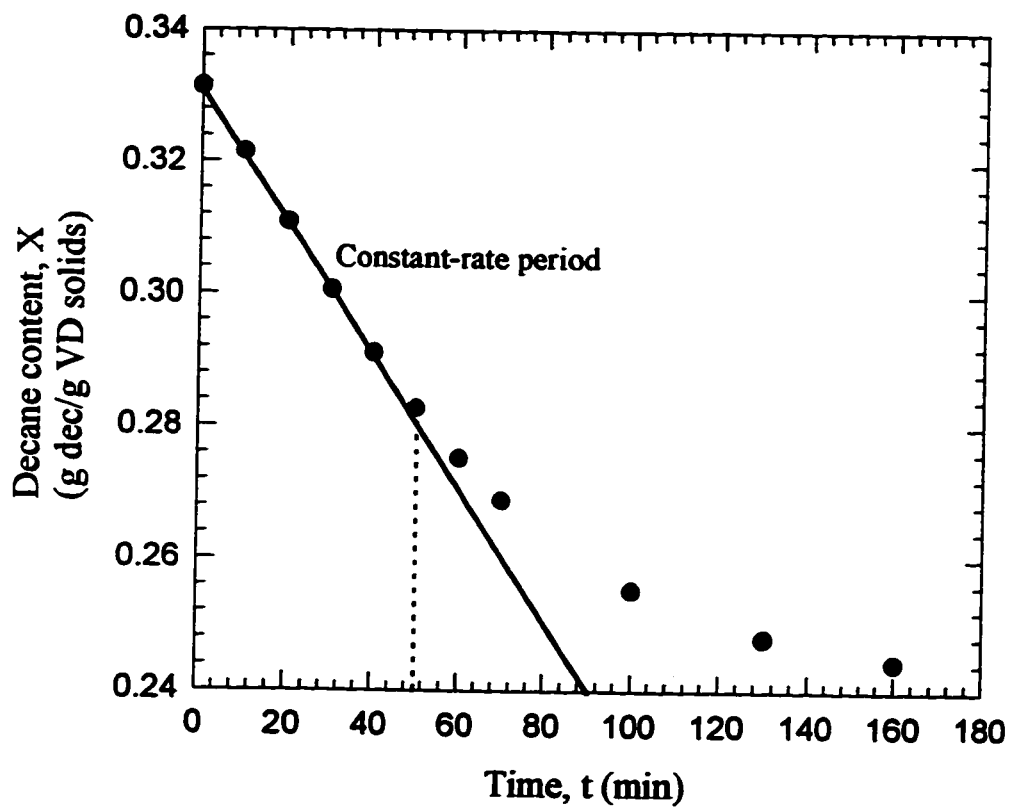
Figure 5-1. Drying curve of Alumina S-201 solids saturated with n-decane.

To ensure that constant drying conditions prevailed during the mass transfer experiments, the value of F_E^{max} using Equation (4-1) was calculated. Two estimates of
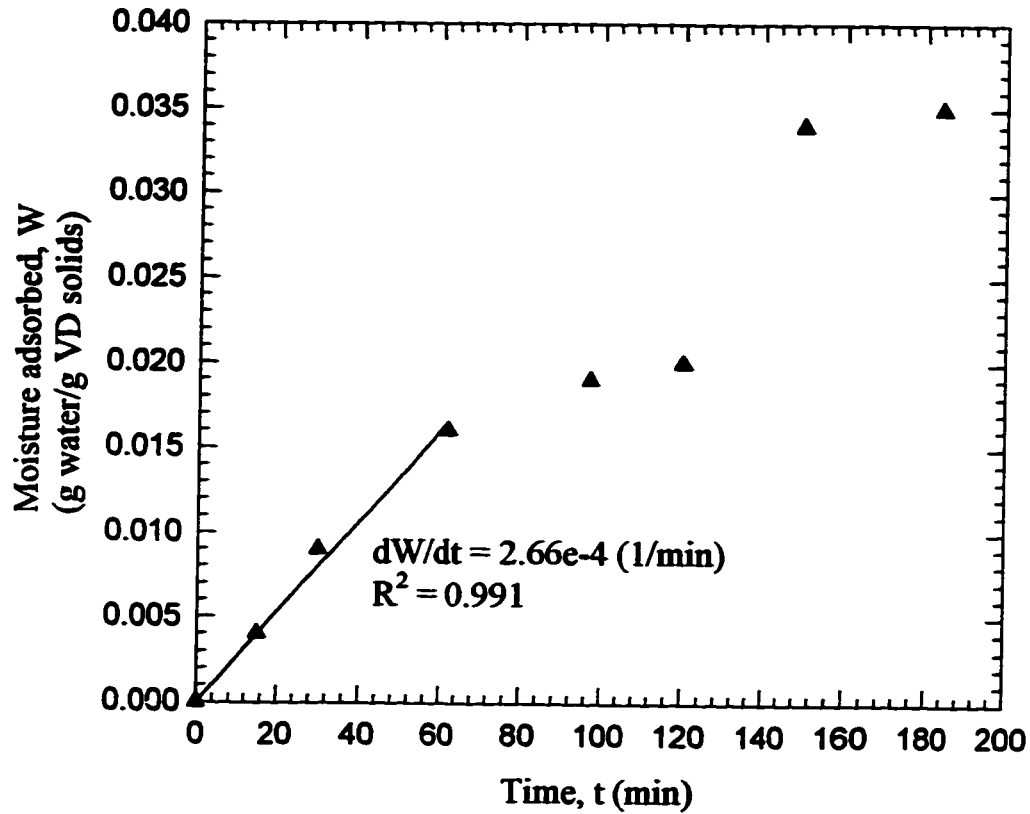
Figure 5-2. Moisture adsorption curve for vacuum-dried S-201 solids.

F_E^{max} were calculated, one ignoring the water adsorption and one corrected for the water

adsorption. The true value of F_E^{max} would lie between these two values. The calculations

used in estimating F_E^{max} are given in Appendix C. The true value of F_E^{max} lies in the

following range:

$$0.154 \leq F_E^{max} \leq 0.194 \qquad (5\text{-}1)$$

The value of F_E for the mass transfer experiments should be lower than the range shown in Equation (5-1) if constant drying conditions were to prevail during the experiment. For the mass transfer experiments, the value of F_E ranged from 0.004816 to 0.0921. Hence the mass transfer experiments were conducted in the constant-rate drying period of the solids.

5.2   Residence time distribution of the gas in the drum

The residence time distribution of the gas phase was measured by a positive step input as described in Section 4.5. The drum was operating at 2.27 rpm and solids volume fraction of 0.10. The gas flow rate was 5.63 L/min. The solids bed motion was in the rolling mode. These experimental conditions were chosen as they would mimic some of the problems like gas bypassing the drum and low solids mixing, that might occur during the mass transfer experiments. When a part of the gas that enters the drum exits without mixing with the gas present in the drum, then bypassing is said to occur. Bypassing may occur at high gas flow rates and could result in the artificial lowering of the n-decane signal from the mass spectrometer sensor. The residence time distribution of the gas at higher flow rates (> 6 L/min) could not be measured as the transient data were very few.

The raw data and sample calculations for this experiment are given in Appendix A. The residence time distribution function, E(t) was calculated using Equation (3-11). Figure 5-3 shows the E(t) function obtained from the step tracer experiment. The experimental E(t) curve was also fitted to the E(t) function for a perfectly mixed CSTR given by Equation (3-12). The average residence time, τ obtained from this curve fit was compared with τ_{pred} calculated using Equation (3-13). From Figure 5-3 it can be seen that there is a large amount of scatter in the experimental E(t) data. This could be due to the numerical approximations that were used in calculating the derivative, dS/dt in Equation (3-11). As a result of this scatter, the average residence time, τ was greater than the value of τ_{pred}.

The problem of scatter in the E(t) data was avoided by curve fitting the original signal, S(t) to Equation (3-14) which is repeated below:

$$S(t) = S_f - (S_f - S_i)e^{-\frac{t}{\tau}} \qquad (5-2)$$

Figure 5-4 shows the original signal and the curve fit to Equation (5-2). From the curve fit, the average residence time, τ was found to be 3.35 min which is in close agreement with the predicted value of 3.34 min. Therefore there were no dead zones in the drum or bypassing of gas from the drum. Also the gas phase was well mixed as the original signal fitted well to the exponential decay expected for a CSTR.
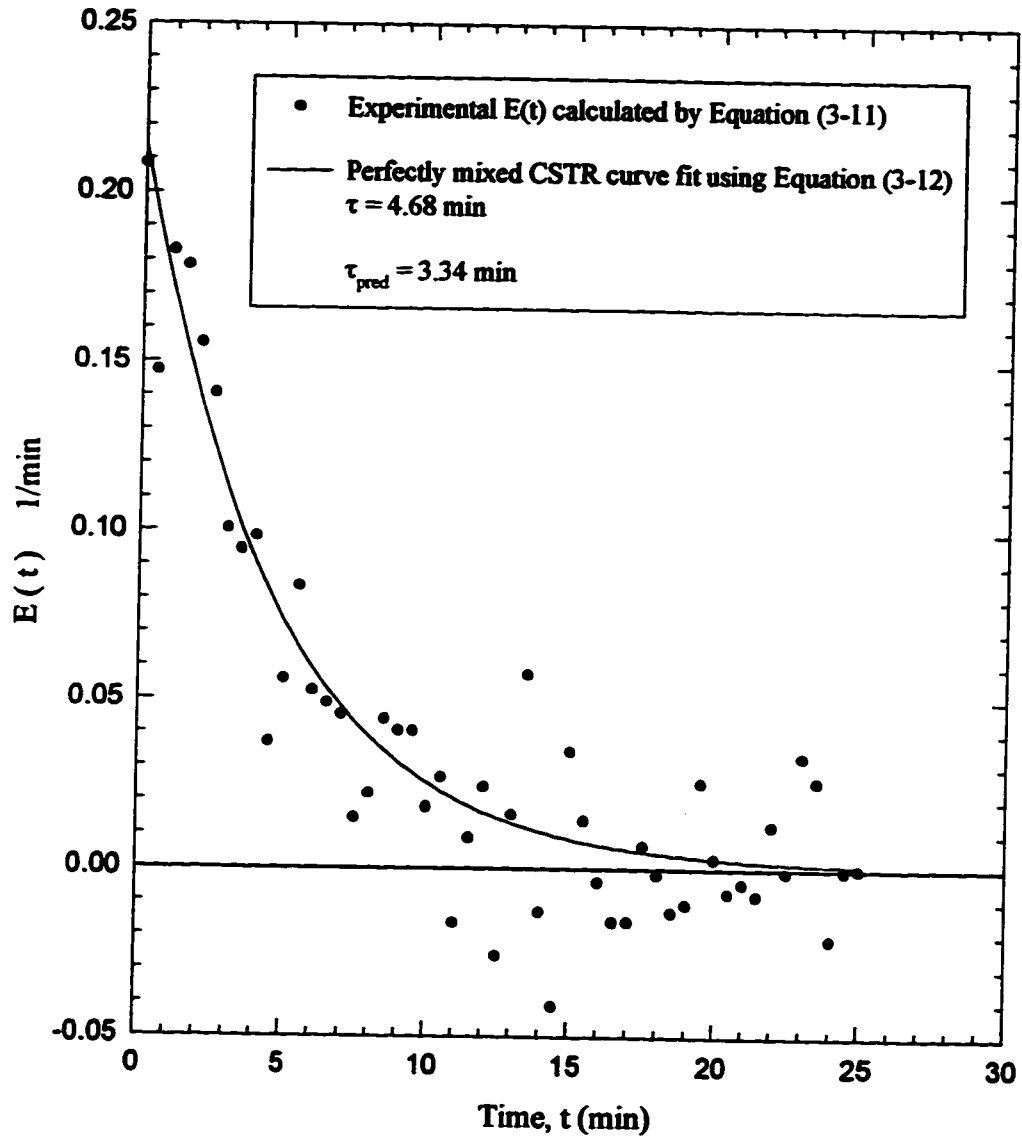
Figure 5-3. Residence time distribution function, E(t) from the step tracer experiment.
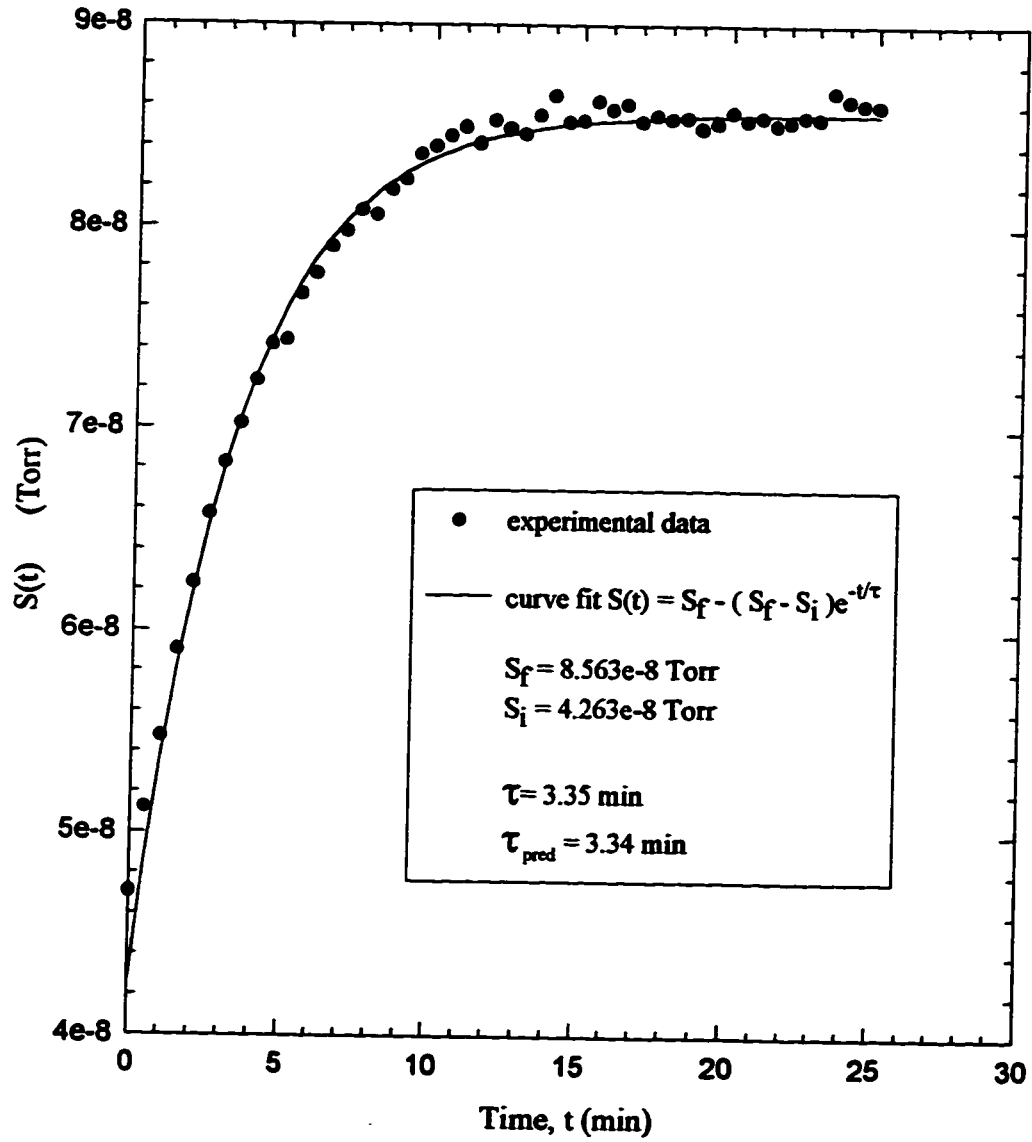
Figure 5-4. Tracer signal S(t) fitted to an exponential fit for a CSTR.

5.3 Particle motion observations in the presence and absence of baffles

As mentioned in Section 4.4, a number of qualitative and quantitative particle motion observations were made during the mass transfer experiments. The following sections describe observations of the particle motion in the rotating drum, with and without baffles.

5.3.1 Particle motion in the presence of baffles

In the presence of baffles, showering patterns/frequencies, types of particle motion and surface particle velocity observations were made for drum rotational speeds in the range 0.09 to 2.0 rpm. The particle motion was studied at solids volume fraction of 0.043 and 0.086. Figure 5-5 shows the particle motion observed at solids volume fraction, η of 0.043.

From Figure 5-5 it can be seen that baffles A, B and C were not overloaded with solids. As the drum rotated, the top layer of solids present on baffle A showered onto baffle B. Similarly top layers of particles from baffle B showered onto baffle C. Thus particle mixing was high in the presence of baffles. Two regimes of particle motion were observed with rotational speed, N. At rotational speeds less than 0.5 rpm, the solids stayed on the baffles for a longer period of time. The frequency of showering from baffle A to B and baffle B to C was low hence the bed renewal was slow.
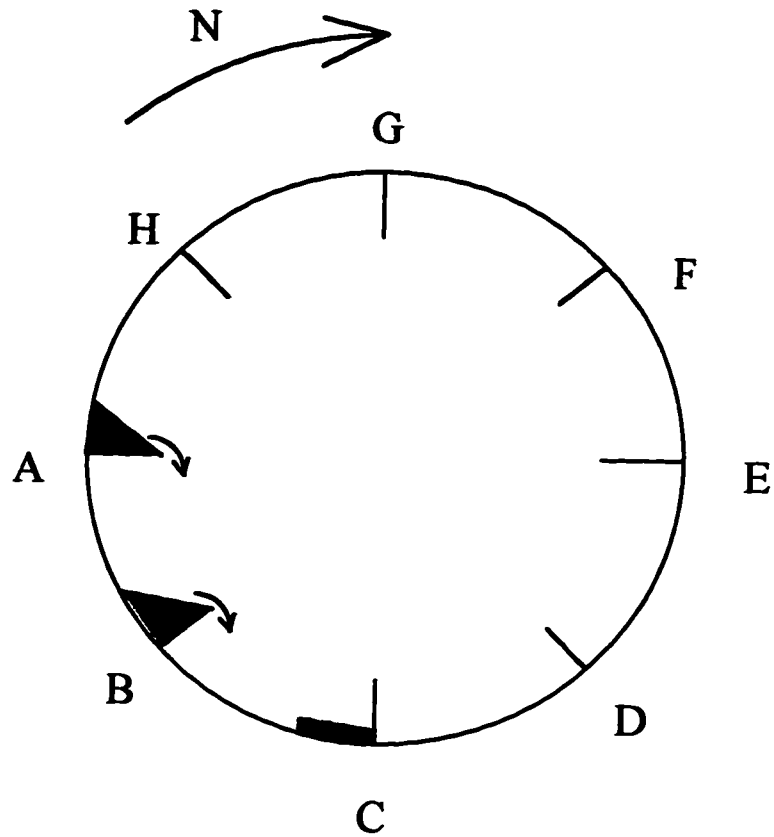
Figure 5-5. Particle motion in the presence of eight baffles for η=0.043 and rotational speed from 0.09 to 2.0 rpm.

The showering pattern was like flow over a weir. At rotational speeds larger than 0.5 rpm, the showering frequency markedly increased with rotational speed. Therefore the bed renewal was faster. The particle velocities were high due to the free fall that occurred

during showering. The motion of the particles was complex, therefore the area available for mass transfer, A, could not be estimated.

Figure 5-6 shows the particle motion that was observed when the solids volume fraction, η was doubled to 0.086.
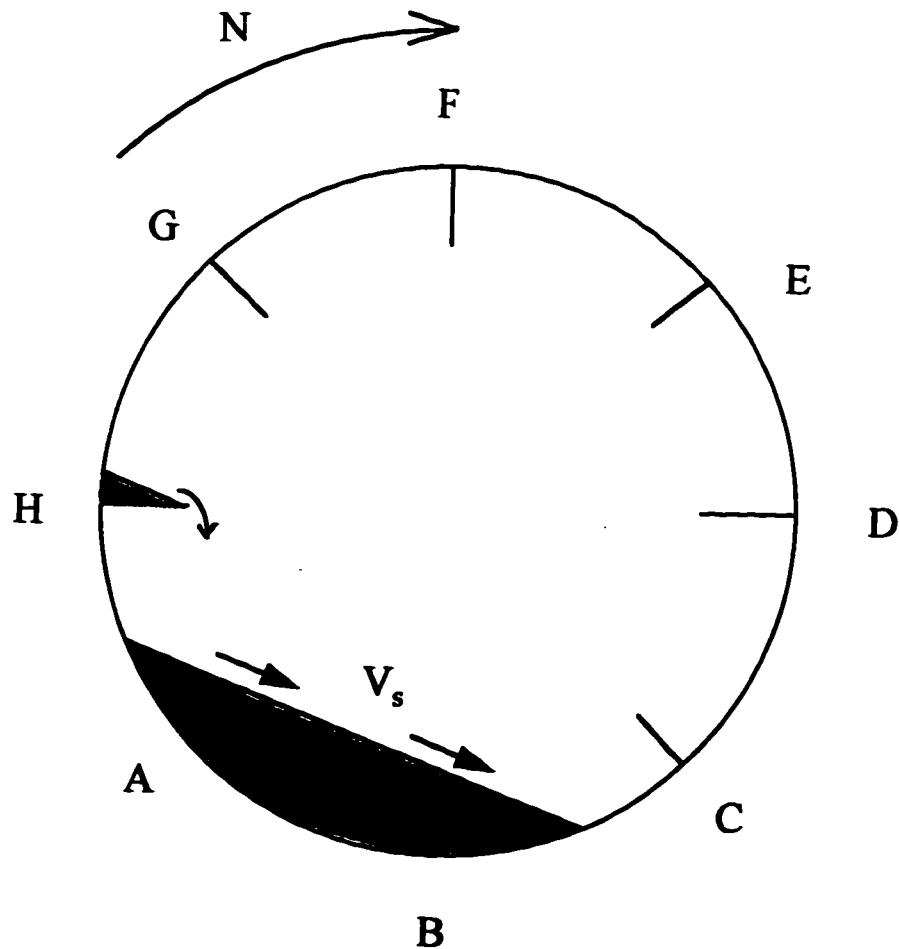
Figure 5-6. Particle motion in the presence of eight baffles for η =0.086 and rotational speed from 0.30 to 2.0 rpm.

From Figure 5-6 it can be seen that the baffles were overloaded and baffle B was completely buried. As the drum rotated, two types of particle motion were observed. Showering occurred from baffle H to A, while rolling of particles was observed from baffle A towards baffle C. During showering, top layers of particles on baffle H showered onto baffle A. The showering pattern was like flow over a weir. The solids bed between baffles A, B and C was inclined. As showering occurred, simultaneously a thin top layer of particles rolled down the inclined surface. The surface particle velocity along the inclined surface is denoted as V_s in Figure 5-6. Both the showering frequency and the surface particle velocity were visually observed to increase with rotational speed in the range 0.3 to 2.0 rpm. The particle velocities were also high in this case due to the free fall involved during showering. Solids bed renewal also occurred due to showering and rolling. Gas-solid contacting may not be more efficient than at solids volume fraction of 0.043 because the baffles were overloaded. As a result, the excess solids formed a bed at the bottom of the drum which effectively did not contact the gas. Due to the complex particle motion, area available for mass transfer, A could not be estimated.

5.3.2   Particle motion in the absence of baffles

In the absence of baffles, the solids bed motion was in the rolling mode. This was due to the sixteen thin rods that were inserted along the drum wall to prevent the solids from slipping in the drum. Since the particle motion in the absence of baffles is relatively less complex than with baffles, detailed observations (qualitative and

quantitative) were made. The particle motion observations were done in the following range of rotational speed, N : 0.29 to 2.0 rpm and solids volume fraction, η : 0.043 to 0.25.

Figure 5-7 is a schematic diagram of the particle motion that was observed. As the drum rotated, a thin top layer of particles in the active layer region rolled down the inclined bed surface. The surface particle velocity, V_s was visually noticed to increase with the drum rotational speed. Segregation of solid particles or bed loosening was not observed. The solids bed was inclined at the dynamic angle of repose, θ. Surface renewal occurred as the solids that rolled down were brought back to the surface by the drum rotation. The active layer region was crescent shaped as also observed by Henein et al.(1983a). The lower plug flow zone was also crescent shaped. Particles that rolled down often collided with other particles. These collisions promoted mixing in the active layer region. The particles in the bottom, bulk flow region had no relative motion among them, hence there was no mixing in this region of the solids bed. The particles along the bottom wall of the drum moved in the opposite direction than the rolling particles.

In Figure 5-7, the thickness of the active layer region is denoted as h_a and the total bed depth as h. The chord length of the top planar surface is denoted as L_s. The quantities that were measured quantitatively were h_a, h, L_s and θ. Table 5-1 shows the results that were obtained at solids volume fraction of 0.043 and varying rotational speed. The solids bed was shallow at this solids volume fraction.
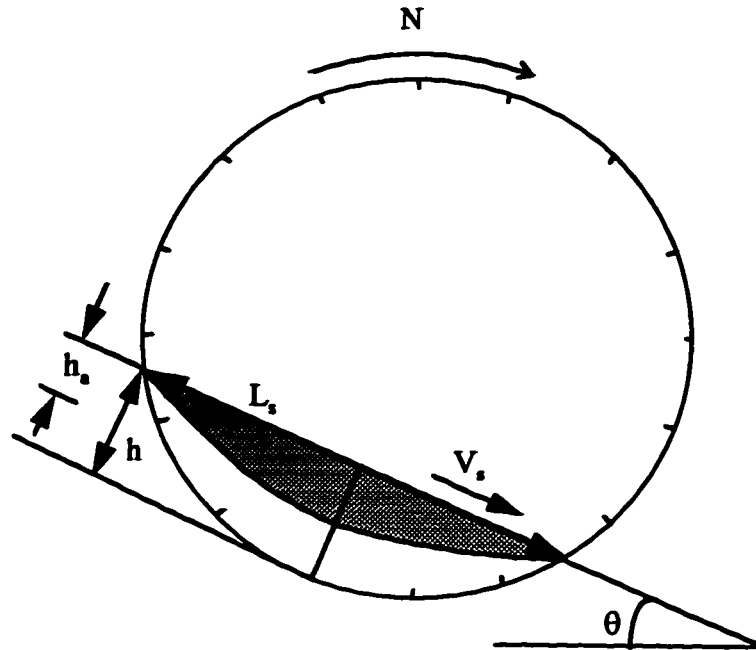
Figure 5-7. Particle motion in the absence of baffles.

From the measurements shown in Table 5-1, it can be concluded that at a fixed holdup and varying rotational speed, the total bed depth, chord length and dynamic angle of repose were almost constant. The dynamic angle of repose was about 28 °. The thickness of the active layer region, h_a increased with rotational speed such that the fraction of bed in active motion (h_a/h) increased from 23.5 % to 44.9 %. This indicates that overall solids mixing increased with rotational speed as both the surface particle velocity and fraction of bed in active motion increased. The experimentally measured chord length was close to the theoretical value (0.164 m) which confirmed that the solids bed had not loosened. The theoretical value is the geometric chord length and the

calculation of this value is shown in Appendix E. Particle segregation was not observed when the solids bed was viewed through the plexiglas end.

Table 5-1.   Measurements of active layer depth, total bed depth, chord length and dynamic angle of repose at different rotational speeds and solids volume fraction of 0.043.

N (rpm)	h_a (m)	h (m)	h_a/h (%)	L_a (m)	θ (°)
0.291	6.17e-3	0.0262	23.5	0.160	28.0
0.576	6.77e-3	0.0267	25.4	0.160	27.5
1.213	8.00e-3	0.0265	30.2	0.160	28.5
1.657	1.00e-2	0.0267	37.5	0.155	28.0
1.967	1.18e-2	0.0263	44.9	0.160	28.5

Table 5-2 shows the results that were obtained at a fixed rotational speed of 1.1 rpm and varying solids volume fraction from 0.043 to 0.25. From the measurements shown in Table 5-2, it can be concluded that the dynamic angle of repose was almost constant at 28 °. The chord length increased with the solids volume fraction. The solids bed did not loosen up as the experimentally measured values of the chord length were close to the theoretical values. The active-layer depth increased with η, however the fraction of bed in active motion (h_a/h) decreased from 30.2 % to 19.4 %. The surface particle velocity did not visually seem to change with holdup. Particle segregation was not observed when the solids bed was viewed through the plexiglas end. The bed behavior was

more defined at solids volume fraction greater than 0.043 as the solids bed was not shallow. The rolling motion of the particles was also smoother (less collisions) at the solids volume fraction was increased.

Table 5-2.   Measurements of active layer depth, total bed depth, chord length and dynamic angle of repose at different solids volume fraction and rotational speed of 1.1 rpm.

η	h_a (m)	h (m)	h_a/h (%)	L_s (m)	* L_s (m) theoretical	θ (°)
0.043	0.00800	0.0265	30.2	0.160	0.164	28.5
0.086	0.01163	0.0423	27.4	0.195	0.201	27.5
0.172	0.01300	0.0669	19.4	0.240	0.243	28.0
0.25	0.01719	0.0865	19.8	0.262	0.265	27.5

* theoretical chord length is the geometric value (calculation shown in Appendix E)

Henein et al.(1983 a) found that the dynamic angle of repose was not affected by bed depth or rotational speed. This was also observed in the current experimental study. For a spherical particle of 4.9 mm diameter, Henein et al. found the dynamic angle of repose to be 30.2 °. This is in close agreement with the value of 28 ° obtained in the current experiments. Also there was agreement with their observation of increase in active-layer depth with increase in percent fill or increase in rotational speed. They had observed that for a particle size of 4.3 mm diameter, at a rotational speed greater than 2.0 rpm and at a bed depth of 0.065 m, the fraction of bed in active motion was 15.4 %. In the present experiment for the same range of particle size, at 1.1 rpm and bed depth of 0.067

m, the fraction of bed in active motion was 19.4 %. Henein et al. (1983 a) had also observed that for shallow beds at rotational speeds less than 2.0 rpm, the active layer occupied upto one-third of the total bed depth. In the present experiment, a similar trend was observed at solids volume fraction of 0.043 (shallow bed).

Woodle and Munro (1993) had also observed that the active layer depth, h_a increased with the solids volume fraction. They had assumed the active layer to be of a finite thickness as shown in Figure 2-3b.

Boateng and Barr (1996) concluded from their experimental study that the thin active-layer was crescent shaped and typically 4 % of the chord length. In the current study, at constant drum rotational speed, the active layer thickness, h_a varied from 4.9 % to 6.5 % of the chord length for solids volume fraction ranging from 0.043 to 0.25. At fixed solids volume fraction of 0.043, h_a varied from 3.8 % at 0.29 rpm to 7.2 % at 2.0 rpm.

In Section 2.1, the surface particle velocity results of Mu and Perlmutter (1980 b) and Lebas et al.(1995) were mentioned. From the linear regression of their data, the dependency of surface particle velocity, V_s was obtained. Equation (2-3) indicates that $V_s \propto N^{0.674}$ and Equation (2-4) indicates that $V_s \propto N^{0.583}$. Tscheng and Watkinson (1979) found that $V_s \propto N^{0.5}$.

From the experimental measurements of h_a and h for solids volume fraction varying from 0.043 to 0.25 and rotational speed varying from 0.29 to 2.0 rpm, the surface particle velocity, V_s was estimated using Equations (2-2) and (3-21). The sample calculations are shown in Appendix E. It is important to note that the surface velocity calculations depend on the accuracy of the total bed depth, h and active layer depth, h_a measurements. Since these quantities were measured visually, the precision of the measurement is about one particle diameter(2.4 to 4.0 mm). Also error in the measurements made at solids volume fraction of 0.043 will be high as the solids bed was quite shallow and most of it was in active motion.

In Figure 5-8, the surface particle velocity calculated using Equation (2-2) is plotted as a function of rotational speed. Linear regression of the data on a logarithmic plot gave the following regression line:

$$V_s = 0.0567N^{0.548}$$

(5-3)

From Equation (5-3) it can be seen that $V_s \propto N^{0.548}$ which is in close agreement with the trends observed in the literature.

In Figure 5-9, the surface particle velocity, V_s calculated using Equation (3-21) is plotted as a function of rotational speed for solids volume fraction of 0.043. Linear regression of the data shown in Figure 5-9 on a logarithmic plot gave the following regression line:

$$V_s = 0.0313N^{0.538} \tag{5-4}$$

From Equation (5-4) it can be concluded that $V_s \propto N^{0.538}$ which is in close agreement with the trends observed by Tscheng and Watkinson (1979), Mu and Perlmutter (1980 b) and Lebas et. al (1995).
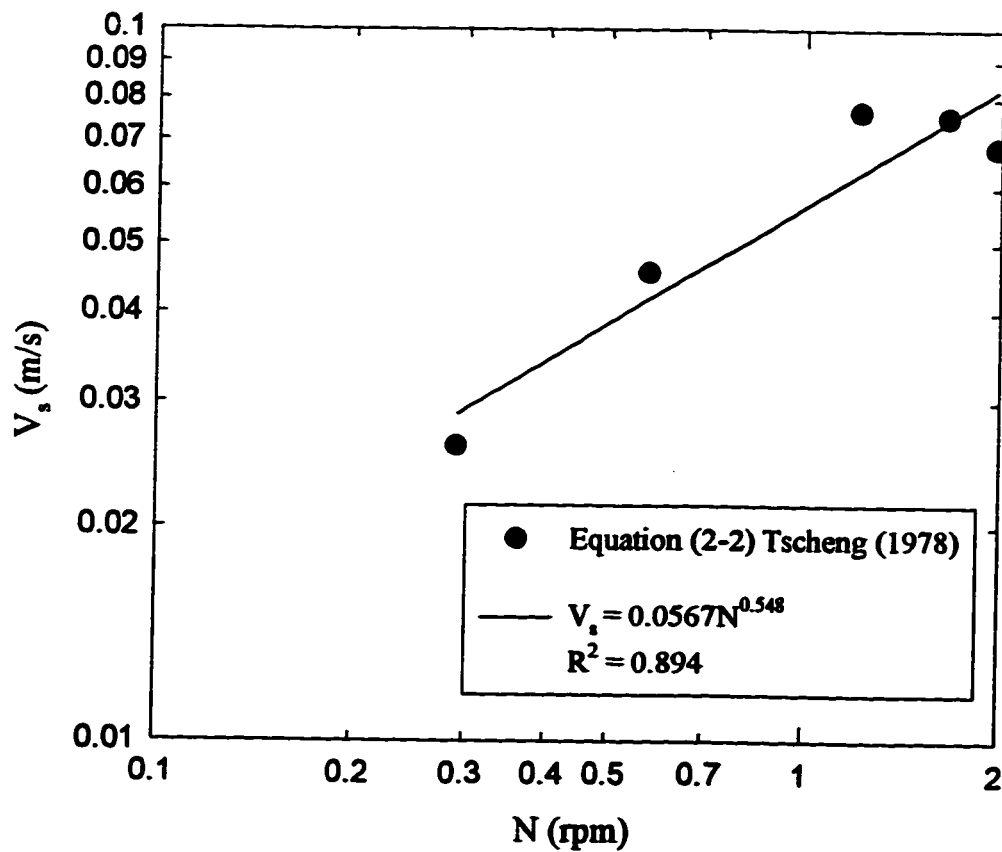
Figure 5-8. Surface particle velocity as a function of rotational speed for $\eta=0.043$. Surface velocity calculated using Equation (2-2).
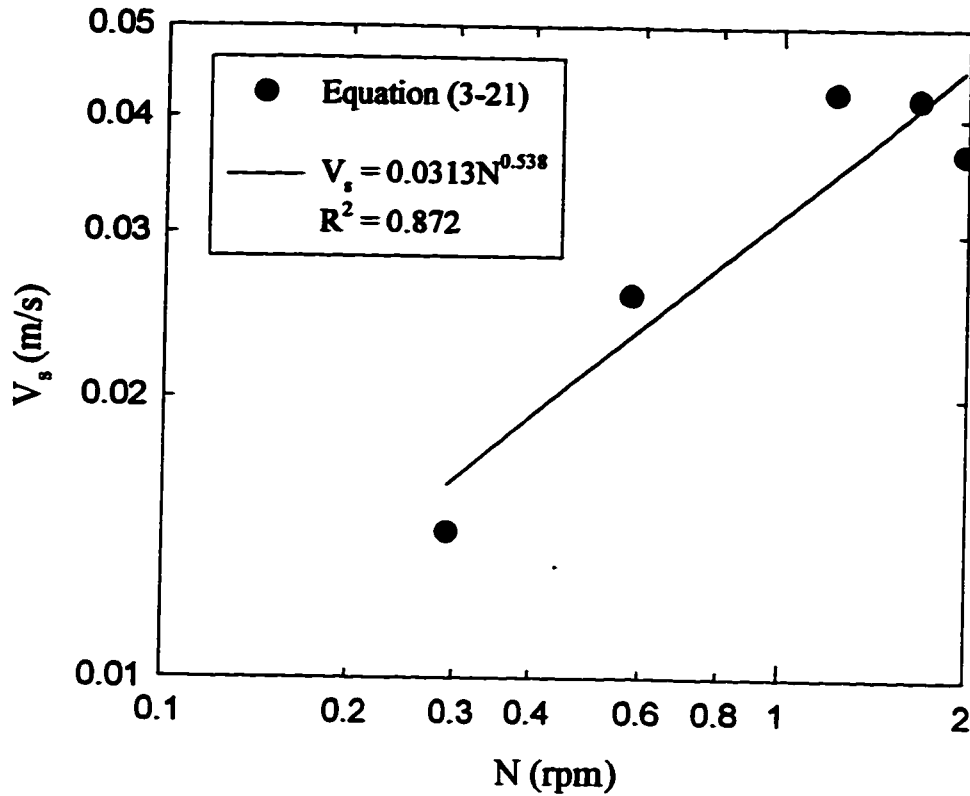
Figure 5-9. Surface particle velocity as a function of rotational speed for η=0.043. Surface velocity calculated using Equation (3-21).

In Figure 5-10, surface particle velocities calculated from Equations (2-2) and (3-21) using experimental measurements at rotational speed of 1.1 rpm are plotted as a function of the solids volume fraction.
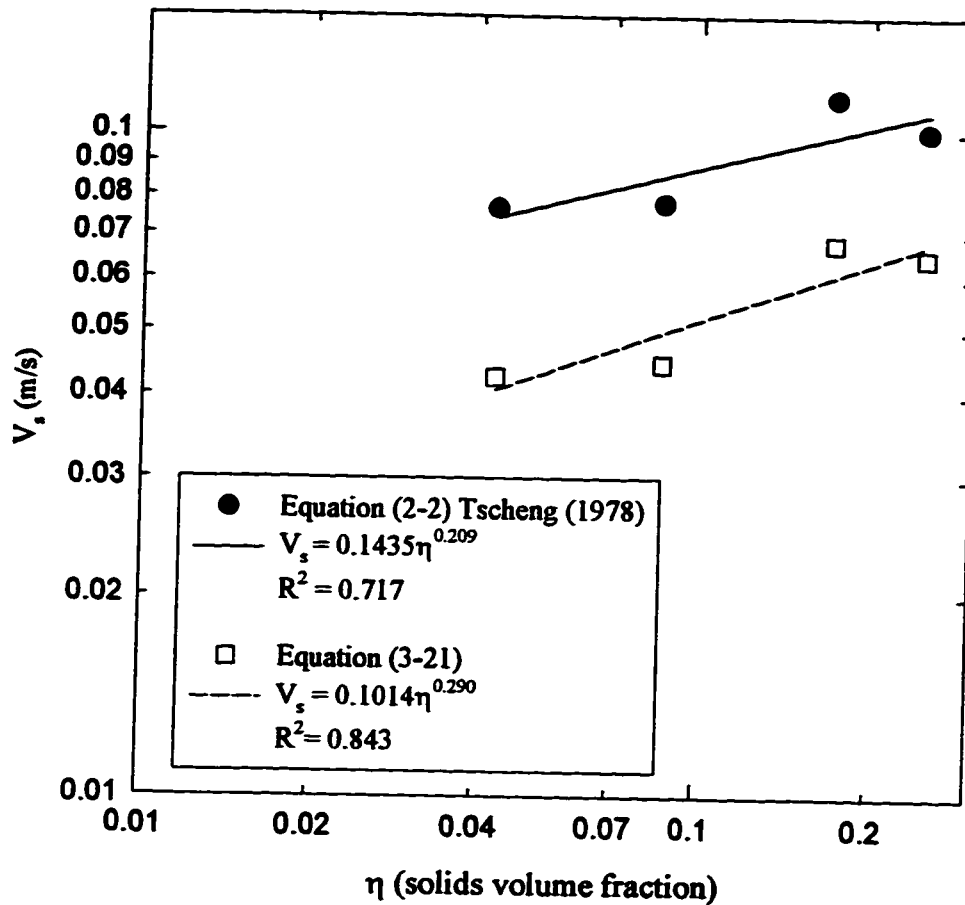
Figure 5-10. Surface particle velocity as a function of solids volume fraction for N=1.1 rpm. Surface velocity calculated using Equations (2-2) and (3-21).

Linear regression of the data (Equation (2-2)) shown in Figure 5-10 on a logarithmic plot gave the following regression line:

$$V_s = 0.1435\eta^{0.209} \tag{5-5}$$

Linear regression of the data (Equation (3-21)) shown in Figure 5-10 on a logarithmic plot gave the following regression line:

$$V_s = 0.1014\eta^{0.290} \tag{5-6}$$

From Equations (5-5) and (5-6) it can be concluded that the surface particle velocity increases with increasing solids volume fraction, η in the drum. However, in the current experimental study the surface particle velocity, as observed visually, did not seem to increase with increasing solids volume fraction. A possible reason for this discrepancy is that in the current experiments, the surface particle velocity was observed visually and is therefore subject to a higher degree of error compared to other methods such as photography.

5.4 Computation of volumetric mass transfer coefficient, k_sA from the raw data

As mentioned in Section 3.1, the steady-state piecewise and steady-state slope methods were used in the evaluation of k_sA from the raw data. A sample of the raw data is shown in Figure 5-11. It can be seen from Figure 5-11 that a series of step up and down in gas flow rates were done to confirm the steady-states that were obtained. The notation 100 %(2), 60 %(2) and 25 %(2) means that the gas flow rate was set to 100 %, 60 % and 25 % for the second time within the same experiment to confirm the steady-states that were obtained. The raw data for this rolling bed experiment were good as there was almost no drift evident in the sensor signal with time.

Equation (3-6) used for the computation of the volumetric mass transfer coefficient, k_sA by the piecewise method is repeated below:

$$k_sA = \left[\frac{S_1^{ss}Q_1 - S_2^{ss}Q_2}{S_2^{ss} - S_1^{ss}} \right] \qquad (5-7)$$
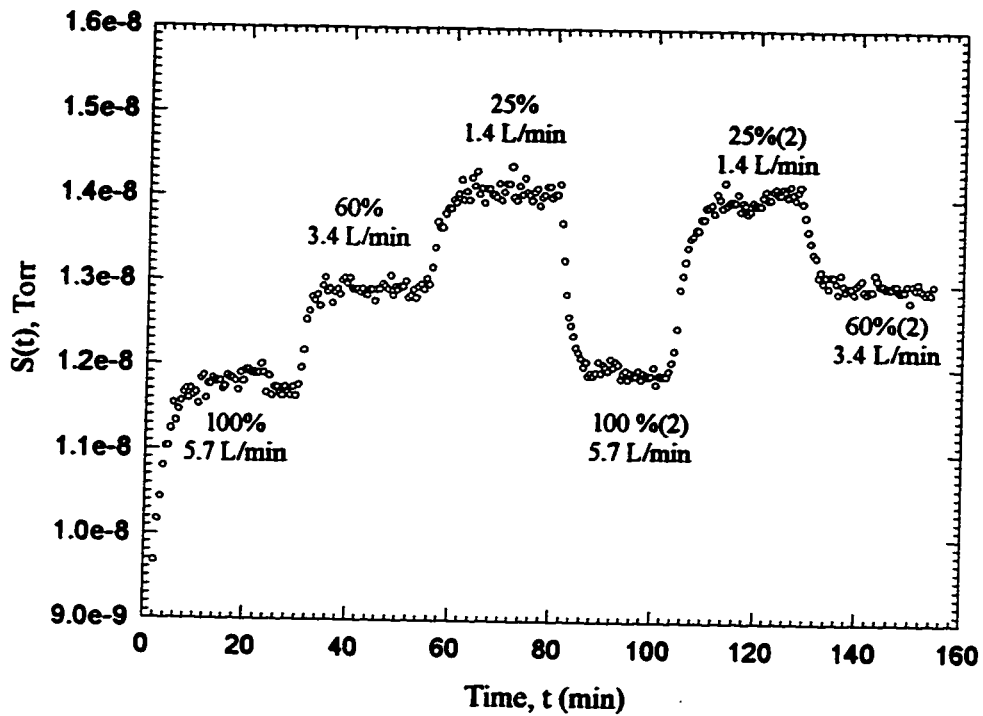
Figure 5-11. Sensor signal for rolling bed experiment at rotational speed of 1.21 rpm and solids volume fraction of 0.043.

Equation (3-9) was used in the computation of the volumetric mass transfer coefficient, k_sA by the slope method. Evaluation of k_sA using these two methods required that the drum wall velocity (Equation (3-15)) be the dominant velocity in the system so that k_sA value is independent of the gas flow rate. For every mass transfer experiment, the

ratio of the drum wall velocity to the maximum superficial gas velocity, V_w/u was calculated. The ratio V_w/u must be greater than unity to satisfy the assumption that k_cA is independent of the gas flow rate. To verify if the mass transfer experiment was conducted during the constant-rate drying period of the saturated solids, the experimental value of F_E was evaluated using Equation (4-1). The experimental F_E value has to be lower than F_E^{max} defined as Equation (5-1) for constant drying conditions to prevail during the mass transfer experiments. A sample calculation that shows how the values of k_cA, V_w/u and F_E were evaluated is shown in Appendix D.

For the experimental raw data shown in Figure 5-11, the computed values of k_cA using the two methods are given in Table 5-3. For this rolling bed experiment, the value of F_E was 0.0233 which is lower than F_E^{max}. Therefore the experiment was conducted during the constant-rate drying period of the solids. The ratio V_w/u was 12.0 which indicates that the drum wall velocity is the dominant velocity. Hence the k_cA values were essentially independent of the gas flow rate.

In Section 3.1.1 it was mentioned that evaluation of k_cA piecewise using Equation (5-7) requires two steady-state sensor signals (S_1^{ss}, S_2^{ss}) and two gas flow rates (Q_1 and Q_2). As shown in Table 5-3, for the piecewise method calculations, six segments were considered. From sensor signals and air flow rates at 100 % flow (1.1788e-8 Torr, 5.7 L/min) and 60% flow (1.2911e-8 Torr, 3.4 L/min) the value of k_cA using Equation (5-7) was 20.58 L/min. The average of the k_cA values from the six segments was 21.76 L/min.

The value of k_sA obtained by the slope method was 21.72 L/min. The R^2 value of the plot of $1/S^{ss}$ versus Q from which the k_sA value was obtained was 0.99. The high R^2 value suggests that the linear fit is good and the data are not scattered. The values of k_sA obtained by the two methods are quite close which indicates that there was insignificant amount of drift in the sensor signal with time.

Table 5-3. Computed values of k_sA for the rolling bed experiment at rotational speed of 1.21 rpm and solids volume fraction of 0.043.

Flow (%)	Q (L/min)	S^{ss} (Torr)	Piece	k_sA(L/min) piece method	k_sA (L/min) by slope method
100	5.700	1.1788e-8	100% to 60%	20.58	21.72
60	3.414	1.2911e-8	60% to 25%	20.80	
25	1.413	1.4074e-8	25% to 100%(2)	22.24	R^2= 0.99
100(2)	5.697	1.1916e-8	100%(2) to 25%(2)	22.87	
25(2)	1.413	1.4017e-8	25%(2) to 60%(2)	23.35	
60(2)	3.413	1.2970e-8	100% to 25%	20.69	
				Avg. 21.76	

Normally any two consecutive steady-states were used in the evaluation of k_sA by the piecewise method. However, in the absence of any drift in the signal, longer steps can be taken in the calculation using Equation (5-7) such as the piece from 100 % gas flow to 25 % gas flow in Figure 5-11. From Figure 5-11, it can be seen that the steady-states obtained for the same gas flow rate (e.g. 100 % and 100 %(2)) are essentially the same. This indicated that the sensor signal was relatively drift free during that period so longer steps could be taken.

The utility of taking longer steps in the absence of drift is important in cases where the sensor signals corresponding to two consecutive steady-states are quite close. From Equation (5-7) it can be seen that if the magnitude of the two sensor signals is close, then the magnitude of the denominator will be small, resulting in a larger variability in the computed value of k_sA. This problem can be avoided by using steady-states that are not consecutive and the magnitude of the steady-state signals is not close. However, it is important that the period between the two non-consecutive steady-states is drift free to avoid any errors due to drift in the computed value of k_sA. During some mass transfer experiments, there was significant drift in the sensor signal with time such as shown in Figure 5-12.
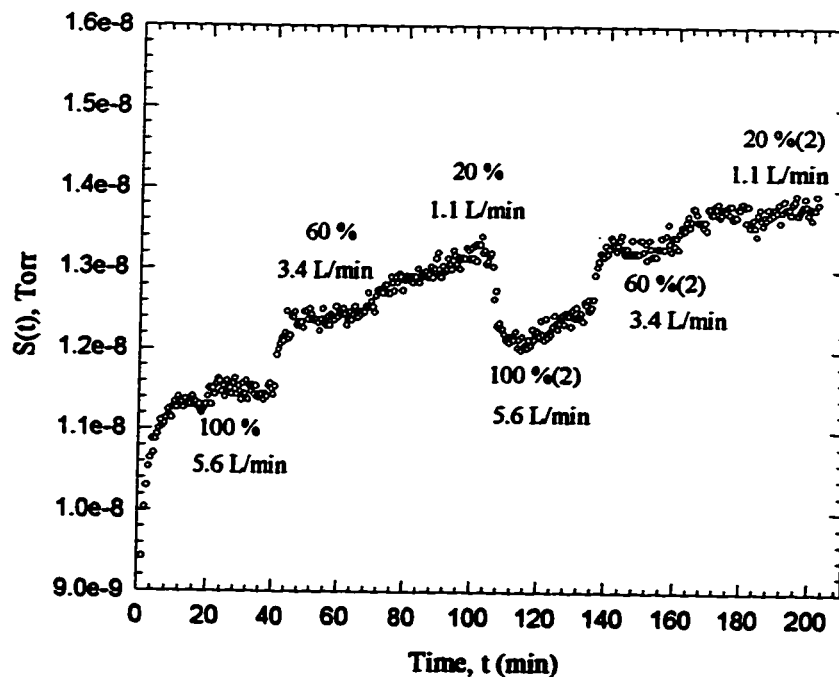
Figure 5-12. Sensor signal for experiment in the presence of baffles at rotational speed of 1.01 rpm and solids volume fraction of 0.086.

The value of k_sA obtained by the slope method was 33.5 L/min. The R^2 value of the linear plot was 0.68 indicating that the linear fit is not good and the data are scattered. The k_sA values from the piecewise method ranged from 23.2 L/min to 72.5 L/min. Thus the data set was rejected as no definite steady-states were achieved due to significant drift.

In Section 5.2, results of the residence time distribution of the air in the drum at an air flow rate of 5.63 L/min were presented. For some of the mass transfer experiments higher air flow rates (6-19 L/min) were used to prevent the air from becoming saturated with n-decane. This also prevented the liquid from condensing in the drum or tubing. Bypassing of the gas from the drum is more likely to occur at high gas flow rates. However, the residence time distribution of the gas at higher flow rates could not be measured as very few transient data would be available from the step tracer experiment.

It was hypothesized that if bypassing of the gas from the drum occurred, then k_sA would increase with increase with gas flow rate, Q. This is because when bypassing occurs, the steady-state signal would artificially be lowered as a part of the total gas flow rate entering the drum would exit without mixing with drum contents. From Equation (5-7) it can be seen that when the steady-state signal is artificially lowered, the denominator becomes very small, causing an artificial increase in the value of k_sA. Also at high Q, the magnitude of the signal will be small which will result in a larger variability in the computed value of k_sA. If gas bypassing occurred then k_sA values obtained from the piecewise method using steady-states at low Q would consistently be lower than the values obtained using steady-states at high Q.

An example of the raw data where bypassing occurred is shown in Figure 5-13. The values of k_sA from the raw data in Figure 5-13 are given in Table 5-4. It is evident that the k_sA values calculated using the steady-state signals at Q values of 18.9 L/min are higher than at the other air flow rates. Therefore the value of k_sA is biased with gas flow rate, Q. For an experiment where bias was evident, the average value of k_sA by piecewise method was calculated by excluding k_sA values obtained using flow rate(s) where bypassing occurred. The calculation of k_sA by slope method was done by ignoring the steady-states corresponding to the flow rate(s) where bypassing occurred. For the raw data in Figure 5-13, the average k_sA value was 57.2 L/min.
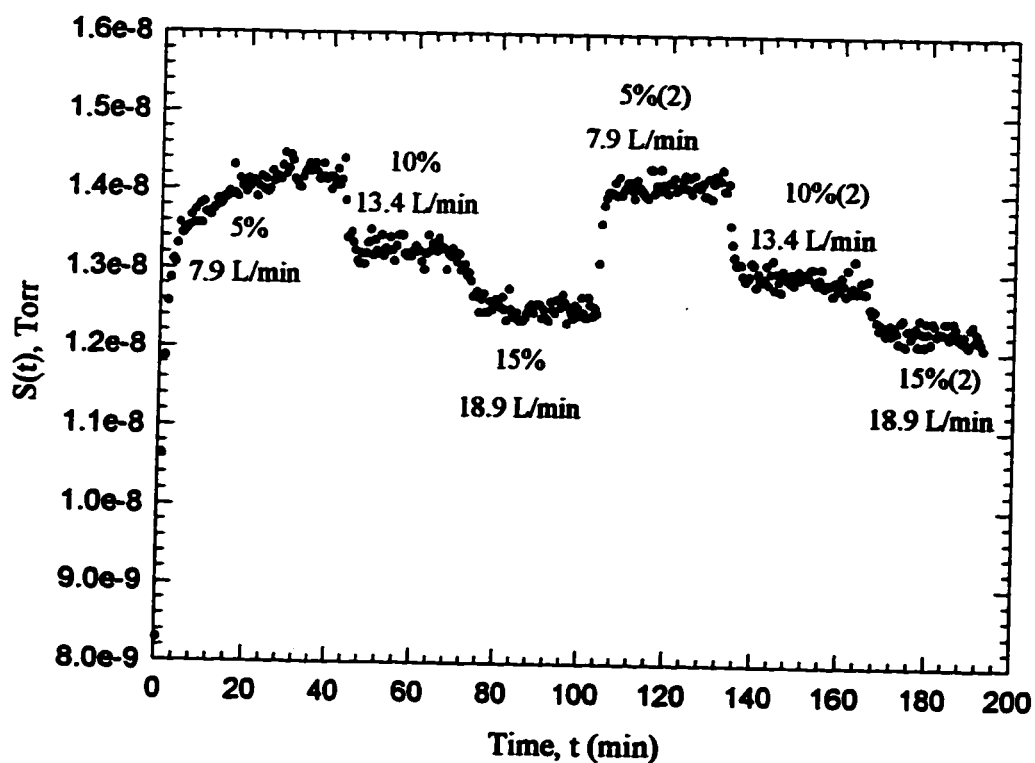
Figure 5-13. Sensor signal for mass transfer experiment in the presence of baffles at rotational speed of 1.33 rpm and solids volume fraction of 0.086.

Table 5-4. Computed values of k_tA obtained in the presence of baffles at rotational speed of 1.33 rpm and solids volume fraction of 0.086.

Flow (%)	Q(L/min)	S^m (Torr)	Piece	k_tA(L/min) piece method	k_tA(L/min) by slope method
5	7.925	1.4212e-8	5% to 10%	63.84	56.6
10	13.389	1.3207e-8	10% to 15%	86.11 *	R^2= 0.958
15	18.857*	1.2519e-8*	5% to 15%	72.91*	
5(2)	7.932	1.4116e-8	15% to 5%(2)	77.71*	
10(2)	13.405	1.2914e-8	5%(2) to 10%(2)	50.86	
15(2)	18.874*	1.2265e-8*	10%(2) to15%(2)	89.95*	
				Avg. 57.2	

* quantities ignored due to bypassing of air from the drum.

Upon analyzing the data for experiments where high gas flow rates were used, bypassing of gas from the drum was found to occur at air flow rates greater than 15 L/min on the basis of bias of the k_tA values with Q.

The results of the mass transfer experiments in the presence and absence of baffles are presented in the next section. During these mass transfer experiments, there was negligible dusting of solids and there was no condensation of liquid in the drum or tubing. In the figures only the average of the k_tA values obtained by the piecewise method are reported as this method of computation reduced the error due to drift in the sensor signal. The 95 % confidence error bars for the average value are also plotted. The ratio of the drum wall velocity to the superficial gas velocity, V_w/u for the mass transfer experiments varied from 1.8 to 20.4. Thus the value of k_tA evaluated from the raw data is essentially

independent of the gas flow rate, Q, provided that there was no bypassing of gas from the drum.

5.5   Gas-solid volumetric mass transfer coefficient, k_sA in the presence of baffles

Raw data for the mass transfer experiments in the presence of eight baffles are given in Appendix D. The volumetric mass transfer coefficient, k_sA was calculated from the raw data as mentioned in Sections 3.1 and 5.4. In the presence of baffles, at constant solids volume fraction of 0.043, the drum rotational speed was varied from 0.09 to 2.0 rpm. Figure 5-14 shows the average value of k_sA obtained by the piecewise method plotted as a function of the drum rotational speed. The 95 % confidence error bars are also plotted.

From Figure 5-14 it is evident that the volumetric mass transfer coefficient, k_sA linearly increased with increasing drum rotational speed. These experimental results are expected from the particle motion observations mentioned in Section 5.3.1. The particle mixing increased with increasing drum rotational speed due to increase in the showering frequency. As a result, the bed renewal was faster when the drum rotational speed was increased.

As mentioned in Section 5.4, during the mass transfer experiments the drum wall velocity was the dominant velocity. Therefore the particle velocity was more important

than the superficial gas velocity. The values of $k_s A$ were essentially independent of the gas flow rates used in the experiments. The experimental data seems scattered but the variation as indicated by the error bars is about 20 % to 30 %. The scatter in data is comparable with the scatter evident in the mass transfer data for packed beds (Petrovic and Thodos, 1968). The particle motion due to showering is quite complex. Therefore the area available for mass transfer could not be estimated.
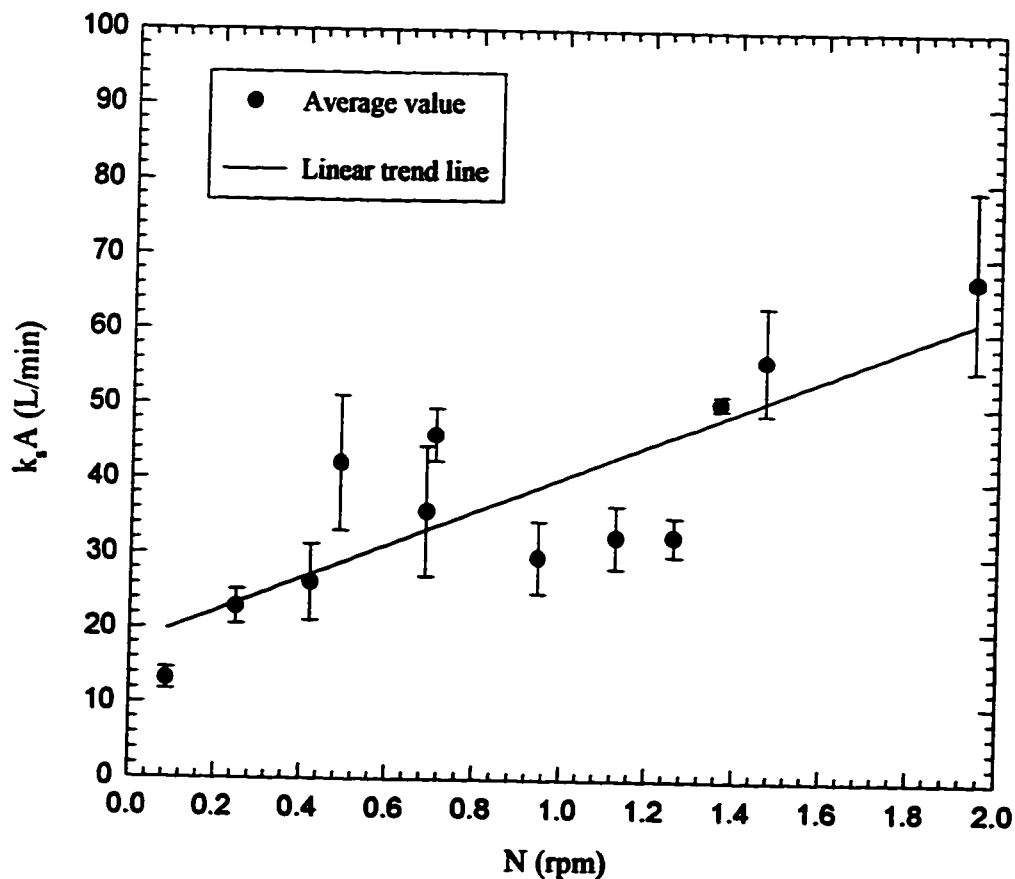
Figure 5-14. Volumetric mass transfer coefficient in the presence of baffles at solids volume fraction of 0.043 and varying rotational speed.

Figure 5-15 shows the volumetric mass transfer coefficient, k_sA obtained in the presence of baffles when the solids volume fraction was doubled to 0.086. The drum rotational speed was varied from 0.38 to 1.90 rpm. In Figure 5-15 average of the k_sA values obtained by the piecewise method is plotted with the 95% confidence error bars. For some mass transfer experiments, only point estimates of k_sA were available due to bypassing of gas from the drum.
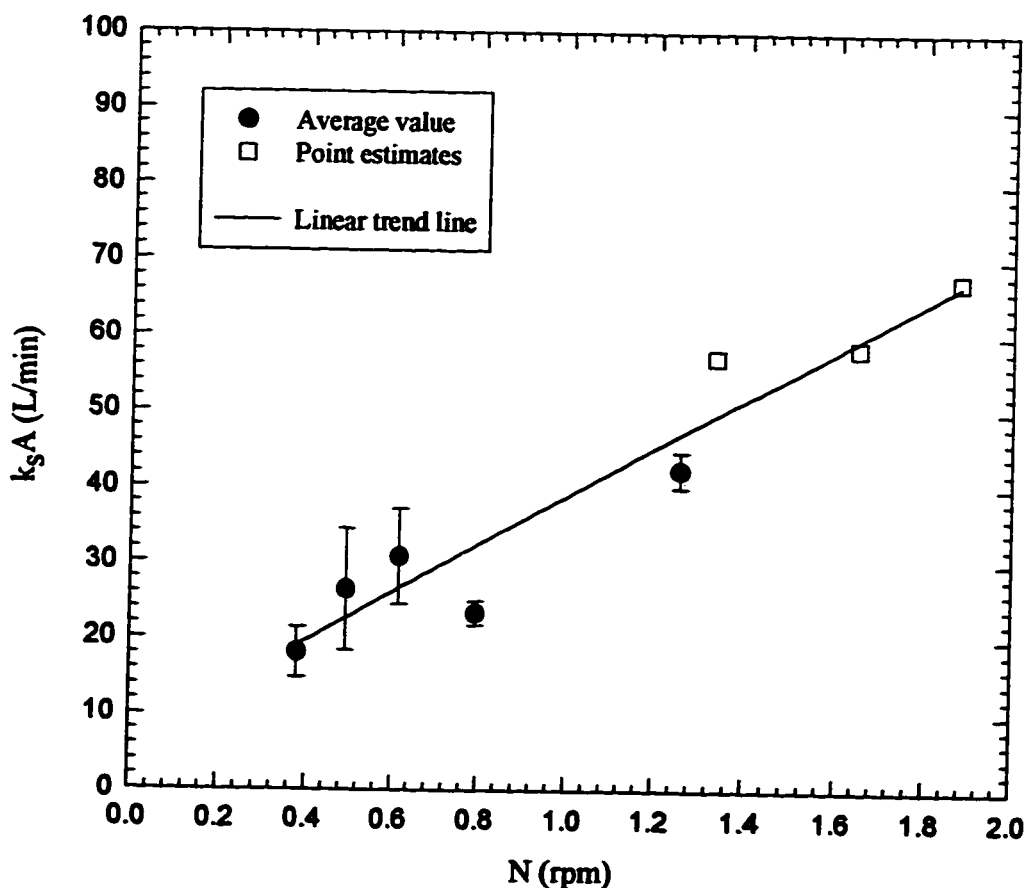
Figure 5-15. Volumetric mass transfer coefficient in the presence of baffles for solids volume fraction of 0.086 and varying drum rotational speed.

It is evident from Figure 5-15, that the volumetric mass transfer coefficient linearly increased with increasing drum rotational speed. The particle motion observations presented in Section 5.3.1 support this trend as the bed renewal was faster with increasing rotational speed due to increase in the showering frequency and surface particle velocity.

The drum wall velocity was the dominant velocity in the experiment, therefore k_cA is essentially independent of the gas flow rate. The variation in the value of k_cA obtained is shown by the error bars in the range 14 % to 35 %. This variation in mass transfer data is comparable with the mass transfer data in packed beds (Petrovic and Thodos, 1968). The particle motion is quite complex as both showering and rolling of particles had occurred. Due to this reason, the area for mass transfer could not be estimated.

The volumetric mass transfer coefficient obtained in the presence of baffles at solids volume fractions of 0.043 and 0.086 are plotted as a function of drum rotational speed in Figure 5-16. From the figure it is evident that the volumetric mass transfer coefficient is independent of the solids volume fraction within experimental error. Although the particle motion observed at these two holdups was different, the mass transfer coefficients are essentially the same.
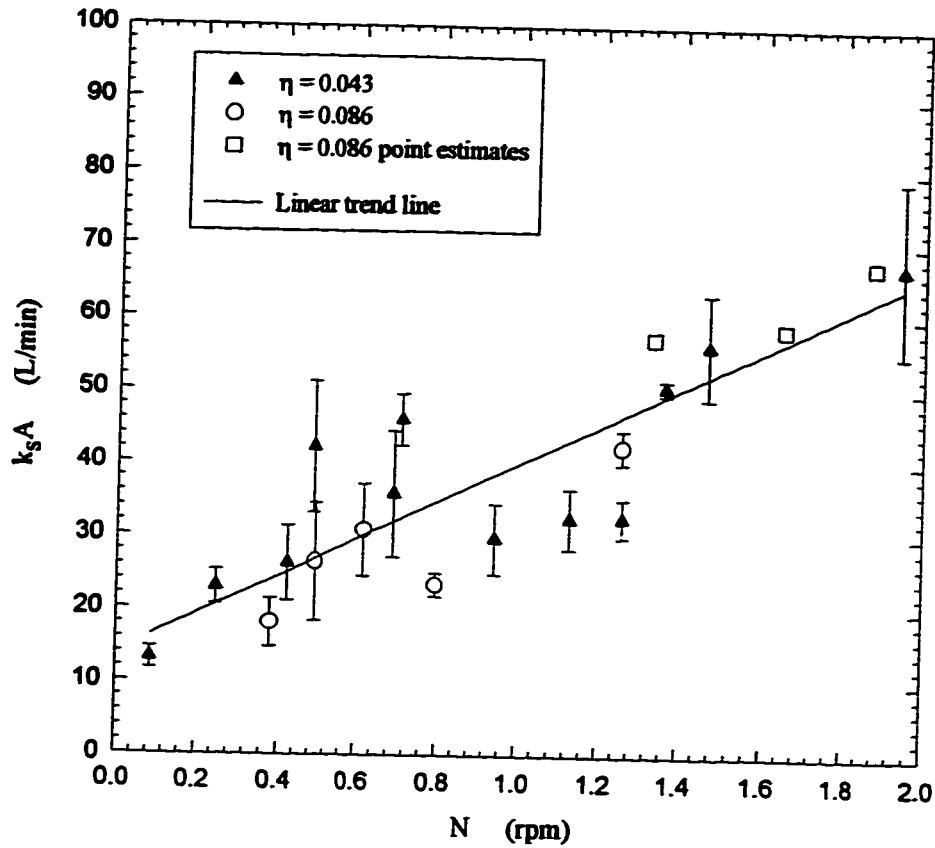
Figure 5-16. Volumetric mass transfer coefficient in the presence of baffles at solids volume fraction of 0.043 and 0.086 as a function of drum rotational speed.

Current experimental findings are consistent with the experimental study by Friedman and Marshall (1949). As mentioned in Section 2.5.2, they found that the volumetric heat transfer coefficient, Ua was independent of the solids volume fraction after a critical value of 0.030 was reached. Increasing solids volume fraction above 0.030 caused the flights to be fully loaded. The excess solids formed a bed at the bottom of the

drum which did not effectively contact the air. In the current experiments, similar solids motion was observed at solids volume fraction of 0.086. The baffles were overloaded and the excess solids formed a rolling bed. Only the particles that were showering effectively contacted the air. Therefore, by doubling the solids volume fraction, the number of particles that effectively contacted the air did not increase by a large amount. As a result the volumetric mass transfer coefficient was independent of the solids volume fraction.

As mentioned in Chapter 1, gas-solid mass transfer is important in solid-state fermentation systems. Information about gas-solid mass transfer or oxygen transfer in solid-state fermentation processes is unavailable in the literature, therefore, the results from this study cannot be compared to prior work.

Mass transfer coefficients obtained from the current experiments can be compared with gas-liquid mass transfer coefficients in liquid state fermentation, $k_L a$ for a low viscosity liquid in a sparged and agitated fermentor. Yegneswaran et al.(1990) used the following values of $k_L a$ for carbon-dioxide to fit their experimental data obtained at typical fermentor operating conditions: 1.67 min^{-1} in a 2 L fermentor and 0.417 min^{-1} in a 20 L fermentor. From these mass transfer coefficients, the mass transfer coefficients for oxygen were calculated by correcting for the difference in the diffusivities oxygen and carbon-dioxide in water. The sample calculations are shown in Appendix G. The corresponding mass transfer coefficients obtained from the carbon-dioxide mass transfer

coefficient of Yegneswaran et al.(1990) are: 1.96 min^{-1} in the 2 L fermentor and 0.490 min^{-1} in a 20 L fermentor.

In the current experiments, the volumetric mass transfer coefficients, k_sA for the baffled case and at a solids volume fraction of 0.043 varied from 13.22 L/min to 67.01 L/min. By taking into account the volume of the solids bed, these k_sA values can be converted to mass transfer coefficients as defined in fermentation, k_sa using the following equation:

$$k_sa = \frac{k_sA}{V \cdot \eta}$$

(5-8)

where η is the solids volume fraction and V is the drum volume.

A sample calculation for evaluating k_sa is given in Appendix G. The corresponding k_sa values at solids volume fraction of 0.043 are in the range 15.37 min^{-1} to 77.92 min^{-1}. In the presence of baffles and at a solids volume fraction of 0.086, the k_sA values ranged from 18.12 L/min to 67.35 L/min. The corresponding k_sa values by taking into account the solids bed volume are in the range 10.53 min^{-1} to 39.16 min^{-1}.

The current mass transfer coefficients were found using n-decane as a model compound. The mass transfer coefficients, k_sa, for oxygen in a rotating drum were calculated from the n-decane mass transfer coefficients. This was done by correcting for the difference in the gas phase diffusivities of n-decane and oxygen. A sample calculation

is given in Appendix G to show how k_sa values for oxygen transfer in a rotating drum were obtained.

The mass transfer coefficients, k_sa for oxygen in a rotating drum at solids volume fraction of 0.043 varied from 36.2 min^{-1} to 183.5 min^{-1}. At solids volume fraction of 0.086, the mass transfer coefficients varied from 24.8 min^{-1} to 92.2 min^{-1}.

It can be observed that the mass transfer coefficients, k_sa for oxygen obtained from the current rotating drum experiments are approximately one to two orders of magnitude higher than the gas-liquid oxygen mass transfer coefficients, k_La for a typical agitated liquid fermentor. The maximum oxygen flux would be proportional to these mass transfer coeffcients, therefore, oxygen transfer to the microorganisms is more efficient in solid-state fermentation systems than liquid fermentation systems. Consequently, solid-state fermentation in a rotating drum might be an attractive option for some cultures as opposed to liquid fermentation in an agitated fermentor.

As mass transfer area could not be estimated, mass transfer coefficient, k_s could not be decoupled from the volumetric mass transfer coefficient, k_sA. Also variables such as particle size, drum size, gas properties and diffusivity were not changed in the current experiments. Consequently, a generalized correlation for Sherwood number for mass transfer in a rotating drum could not be obtained. Experiments which investigate the

effect of increasing the drum size on the volumetric mass transfer coefficient would be useful for scale-up purposes.

5.6   Gas-solid volumetric mass transfer coefficient, k_sA in the absence of baffles

Raw data for the mass transfer experiments in the absence of baffles are given in Appendix D. In all cases the bed motion was in the rolling mode. Experimentally determined values of k_sA by the piecewise method are also given in Appendix D. For the rolling bed experiments at constant solids volume fraction of 0.043, the drum rotational speed was varied from 0.29 to 2.0 rpm. The volumetric mass transfer coefficient, k_sA as a function of drum rotational speed is shown in Figure 5-17.

In this figure, the average of the k_sA values obtained by the piecewise method are plotted along with the 95 % confidence error bars. Figure 5-17 indicates that the volumetric mass transfer coefficient linearly increased with increasing drum rotational speed. The error bars indicate that the variation in the k_sA value is up to 36 % which is comparable to the variation in the mass transfer data for packed beds (Petrovic and Thodos, 1968). The drum wall velocity was the dominant velocity therefore k_sA values were independent of the gas flow rate.

In Section 5.3.2 particle motion in the absence of baffles was described. The fraction of bed in active motion had increased with increasing drum rotational speed. Also

the surface particle velocity was visually observed to increase with the drum rotational speed. From these particle motion observations it is evident that the solids mixing increased with increasing drum rotational speed. This suggests that the volumetric mass transfer coefficient should increase at higher rotational speeds due to better solids mixing.
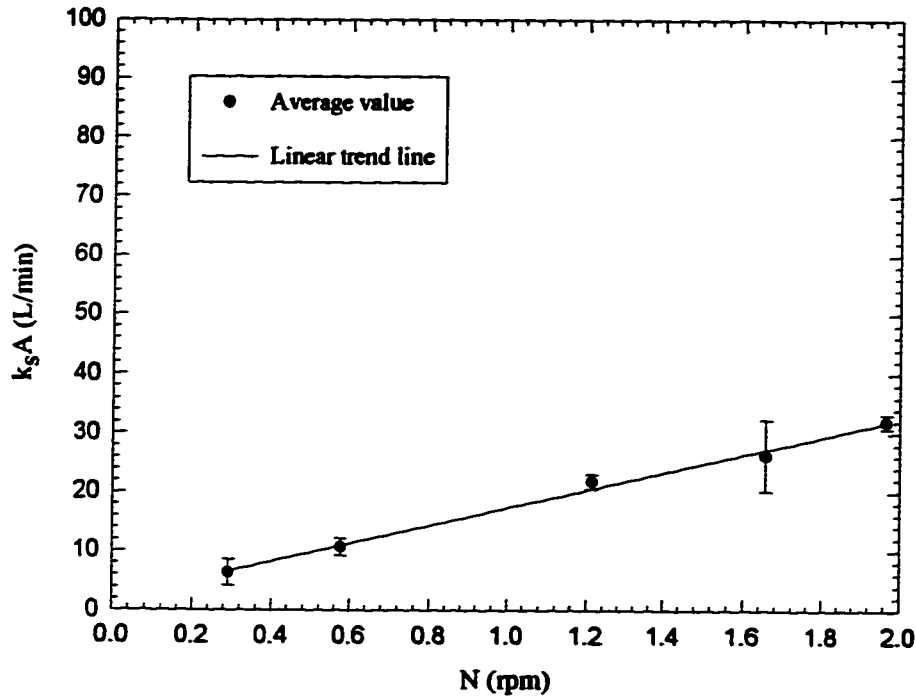
Figure 5-17. Volumetric mass transfer coefficient for the rolling bed at solids volume fraction of 0.043 and varying drum rotational speed.

The volumetric mass transfer coefficient, k_sA in the absence of baffles at solids volume fraction of 0.043 and varying drum rotational speed ranged from 6.35 L/min to 32.03 L/min. As mentioned in Section 5.5, k_sA values can be converted to k_sa values by

taking into account the solids bed volume. The corresponding $k_a a$ values are in the range 7.38 min^{-1} to 37.24 min^{-1}.

From the experimental $k_a a$ values for n-decane, the corresponding $k_a a$ values for oxygen were calculated by correcting for the difference in the gas phase diffusivities of n-decane and oxygen. A sample calculation is given in Appendix G to show how $k_a a$ values for oxygen were evaluated. At solids volume fraction of 0.043, the mass transfer coefficient for oxygen obtained in a rotating drum without baffles are in the range 17.38 min^{-1} to 87.7 min^{-1}.

The current $k_a a$ values for oxygen are roughly one to two orders of magnitude higher than the $k_L a$ values for oxygen (1.96 min^{-1} and 0.490 min^{-1}) obtained from the experimental data of Yegneswaran et al.(1990) for sparged, agitated tanks. Therefore, oxygen transfer to microorganisms in solid state fermentation in 20 L rotating drums is better than in liquid state fermentation.

To investigate the dependency of volumetric mass transfer coefficient, $k_a A$ on solids volume fraction, another set of rolling bed experiments were done where the drum rotational speed was held constant at 1.1 rpm and the solids volume fraction was varied from 0.043 to 0.25. The average of the $k_a A$ values along with the 95 % confidence error bars is plotted as a function of the solids volume fraction in Figure 5-18. From the figure it can be seen that the value of $k_a A$ increased with increasing solids volume fraction. From

the particle motion observations in Section 5.3.2, it is important to note that the fraction of the bed in active motion had decreased with η but the chord length had increased with η. The surface particle velocity did not visually seem to be affected by the solids volume fraction in the drum based on visual observation. Mass transfer would depend on the velocity of the solids with respect to the gas phase, so that constant velocity would suggest a constant value of k_s.
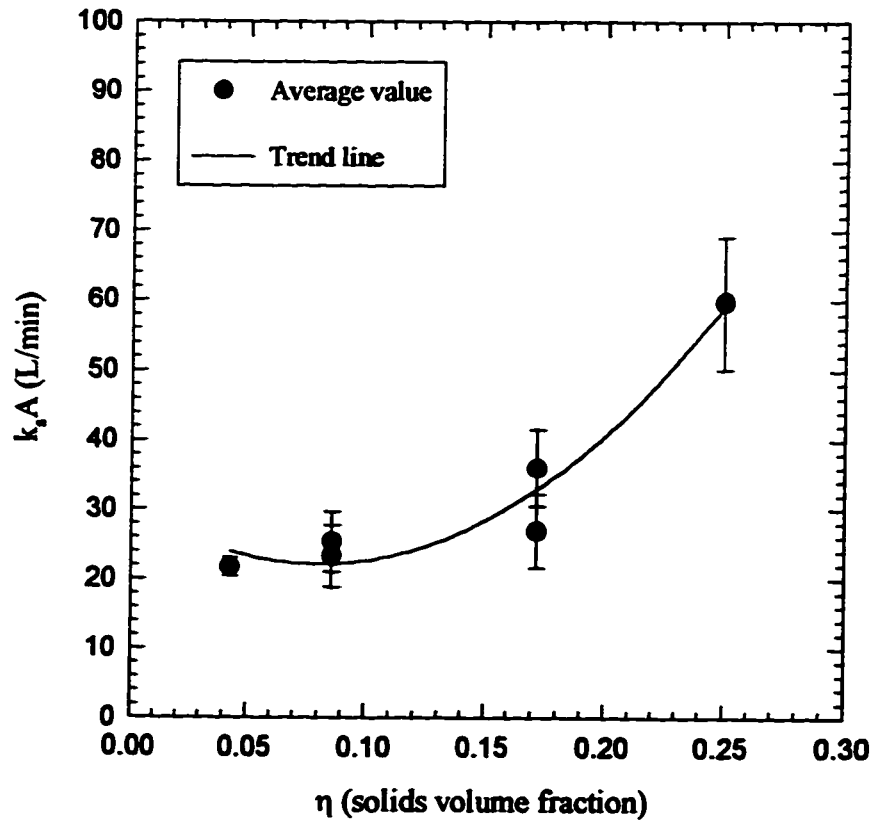
Figure 5-18. Volumetric mass transfer coefficient at rotational speed of 1.1 rpm and varying solids volume fraction.

These observations suggest that there may be an increase in the mass transfer area with increasing η which resulted in the overall increase of the volumetric mass transfer coefficient, k_cA. The mass transfer area in a rolling bed could not be estimated directly. However, the volumetric mass transfer coefficient was normalized on the basis of the volume of bed renewed. These results are presented in Section 5.8.

5.7   Comparison of volumetric mass transfer coefficient in the presence and absence of baffles

The volumetric mass transfer coefficient, k_cA with and without baffles in the drum are plotted as a function of drum rotational speed in Figure 5-19. This figure contains the k_cA values for the rolling bed at solids volume fraction of 0.043 and k_cA values in the presence of baffles at solids volume fractions of 0.043 and 0.086.

From Figure 5-19 it is evident that volumetric mass transfer coefficients in the presence of baffles are higher than for the rolling bed case in the 0.09 to 2.0 rpm range. These results can be explained through particle motion observations. In the presence of baffles, the particle velocity was high relative to the air velocity due to the free fall involved during showering. As a result, the solids mixing was high and the particles effectively contacted the air. The particle velocity in the rolling bed was lower, resulting in comparatively low solids mixing. Due to better mixing and effective gas-solid contacting, the volumetric mass transfer coefficients for the baffled case were higher.

The current experimental results compare well with the experimental results of Friedman and Marshall (1949). They had observed that the volumetric heat transfer coefficient, Ua increased as the number of flights in the drum was increased from zero to eight. These results are consistent with the present results as there was an increase in the volumetric mass transfer coefficient as the baffles were increased from zero (rolling bed) to eight.
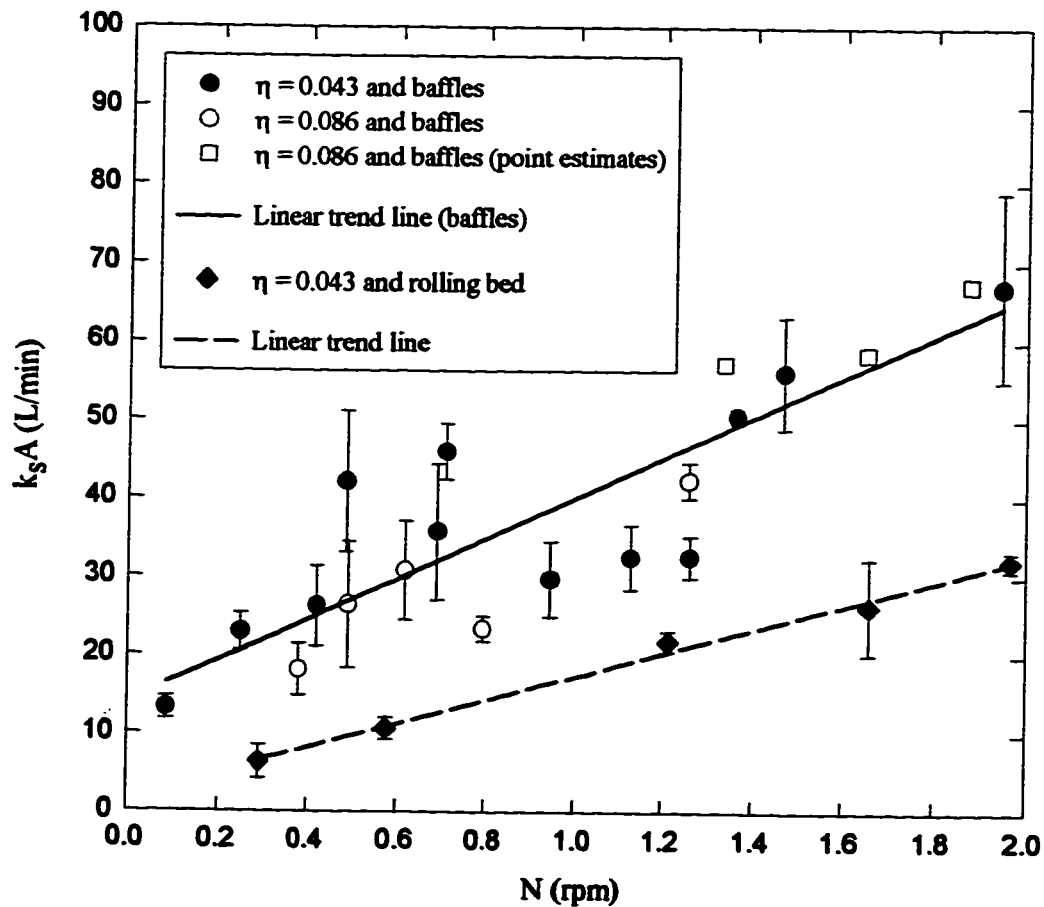
Figure 5-19. Volumetric mass transfer coefficient in the presence and absence of baffles for varying drum rotational speed.

5.8 Normalized mass transfer coefficient, k_s' for the rolling bed

The volumetric mass transfer coefficients, k_sA, for the rolling bed at varying drum rotational speed and solids volume fraction were presented in Section 5.6. To obtain the mass transfer coefficient, k_s, the area available for mass transfer needs to be estimated. In the literature, the heat transfer area in a rolling bed was assumed to be the chord length times the kiln length (Section 2.5.4). However, as stated by Tscheng and Watkinson (1979) the true contact area would be larger due to the rolling motion of the particles. Also the particles gave a rough surface with more area than the plane of the bed surface.

In the present study, mass transfer area could not be estimated as the dependency of the area on some important length and velocity scales that changed with the experimental condition was not known. In the experiments, the active layer depth, h_a and particle velocity, V_s changed with the drum rotational speed. Also as the solids volume fraction was varied both h_a and chord length, L_s had changed. As the mass transfer area, A could not be estimated, the mass transfer coefficient, k_s could not be decoupled from the volumetric mass transfer coefficient, k_sA.

However, the volumetric mass transfer coefficients for the rolling bed were normalized on the basis of the volume of bed renewed by drum rotation following the surface renewal approach to gas-liquid mass transfer. Figure 5-20 shows the schematic

diagram of the solids bed and the parameters used in the calculation of the volume of bed renewed. The volume of bed renewed was assumed to be equal to the cross-sectional area of the active bed, S_A times the drum length, L.

The cross-sectional area of the active bed was evaluated from the experimental measurements of total bed depth, h and active layer depth, h_a. This method of normalization is sensitive to the accuracy of the measurements of h_a and h. The accuracy of the measurements particularly at solids volume fraction of 0.043 is not very good as the solids bed was shallow and about 1/3 of the total bed was in active motion.
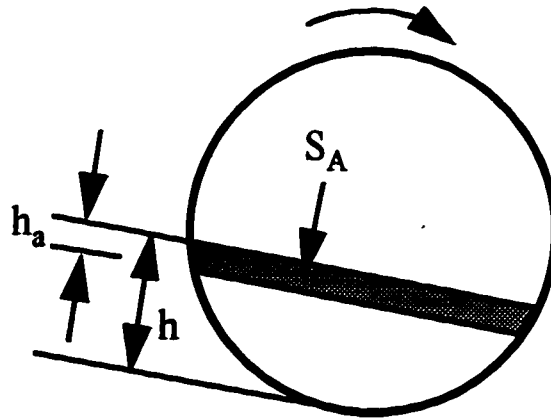
Figure 5-20. Schematic diagram of the rolling bed with the cross-sectional area of the active bed, S_A.

The calculated values of the cross-sectional area of the active bed, S_A are given in Appendix E for the rolling bed experiments. A sample calculation is given in Appendix E

to show how S_A was evaluated. For calculating S_A it was assumed that the active-layer was of finite thickness, h_a (Figure 2-3b). The normalized mass transfer coefficient, k_s' for the rolling bed was calculated using the following equation:

$$k_s' = \frac{k_s A}{60000 \cdot S_A \cdot L}$$

(5-9)

The conversion factor of 60000 arises because the reported $k_s A$ values are in L/min. The calculated values of k_s' are given in Appendix F with a sample calculation to show how k_s' was evaluated. In Figure 5-21, the normalized mass transfer coefficient, k_s' at solids volume fraction of 0.043 is plotted as a function of drum rotational speed.

Linear regression of the data in Figure 5-21 on a logarithmic plot gave the following regression line:

$$k_s' = 0.733 N^{0.560}$$

(5-10)

From Figure 5-21 it can be seen that the normalized mass transfer coefficient increased with increasing drum rotational speed. These results can be expected as the particle mixing increased with rotational speed due to increase in both the surface particle velocity and the fraction of bed in active motion (h_a/h).
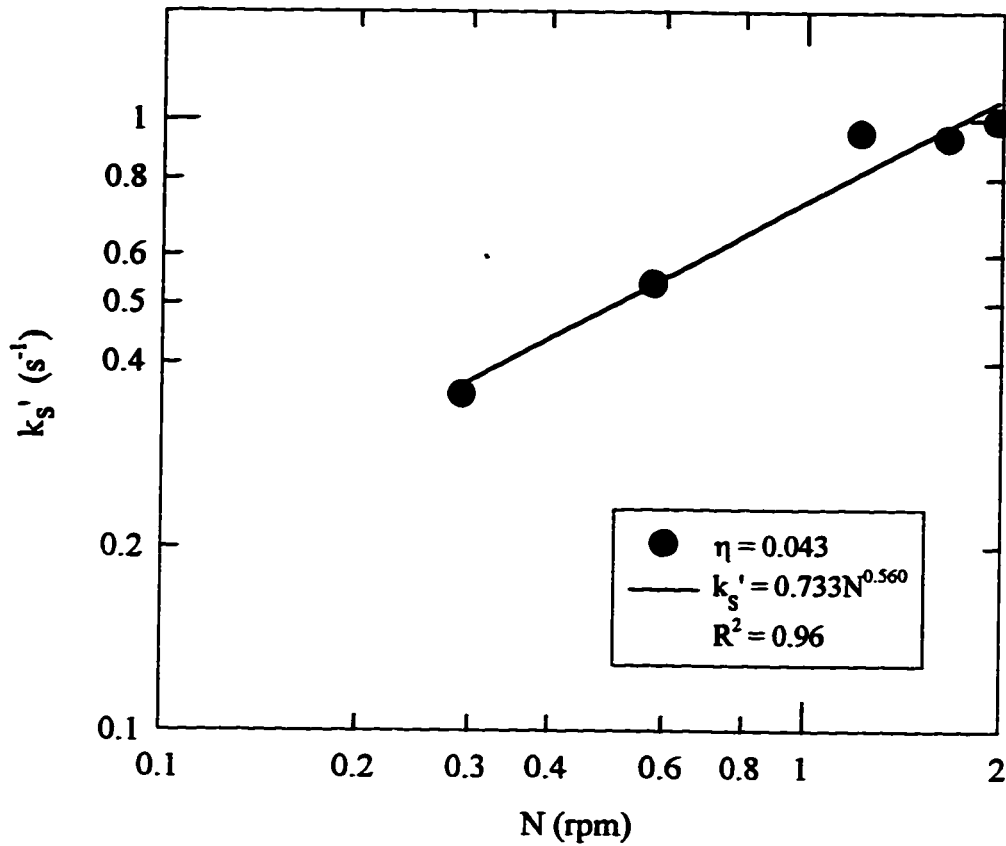
Figure 5-21. Normalized mass transfer coefficient for the rolling bed as a function of drum rotational speed and solids volume fraction of 0.043.

In Figure 5-22, the normalized mass transfer coefficient, k_s' at rotational speed of 1.1 rpm and varying solids volume fraction are presented. It is evident from Figure 5-22 that the value of k_s' decreased sharply as solids volume fraction was increased from 0.043 to 0.086. The decrease in k_s' value could be due to the difference in the bed motion as the

holdup was increased. At solids volume fraction of 0.043, the solids bed was quite shallow and approximately 1/3 of the total bed was in active motion. As the solids volume was increased to 0.086, the fraction of bed in active motion declined to 27.4 %. Thus the k_s' value was higher at the lower holdup due to high solids mixing.
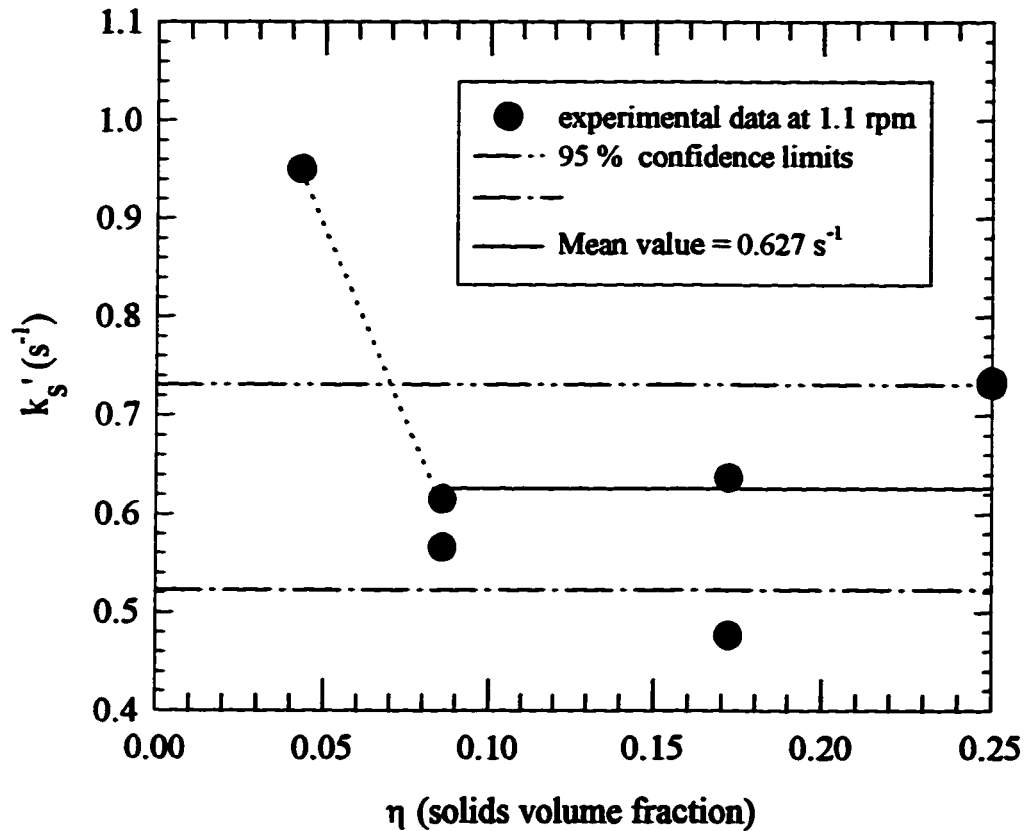
Figure 5-22. Normalized mass transfer coefficient at 1.1 rpm and varying solids volume fraction.

Increase in solids volume fraction from 0.086 to 0.25 did not significantly change the k_s' value. The mean value of k_s' for solids volume fraction in the range 0.086 to 0.25 was 0.627 s^{-1}. The 95 % confidence limits (calculation in Appendix F) of the mean value are also shown in Figure 5-22. Since the experimental data (except one point) lie within the confidence interval, it can be concluded that statistically the k_s' value did not change for solids volume fraction in the range 0.086 to 0.25.

The relative error between the experimental k_s' values and the mean value for solids volume fraction in the range 0.086 to 0.25 were calculated (Appendix F) and the results are shown in Figure 5-23. It can be seen from Figure 5-23 that the relative errors are distributed about the mean value (0.627 s^{-1}).

The data obtained from the current experiments were not enough to obtain a generalized correlation of k_s' with drum rotational speed, N and solids volume fraction, η. The dominant characteristic length for this system and mass transfer area could not be estimated from the results of the current rolling bed experiments.

Also many experimental variables such as drum size, particle size, gas properties and diffusivity were held constant in the current experiments. Consequently, no generalized correlation was obtained for the Sherwood number for mass transfer in a rolling bed.
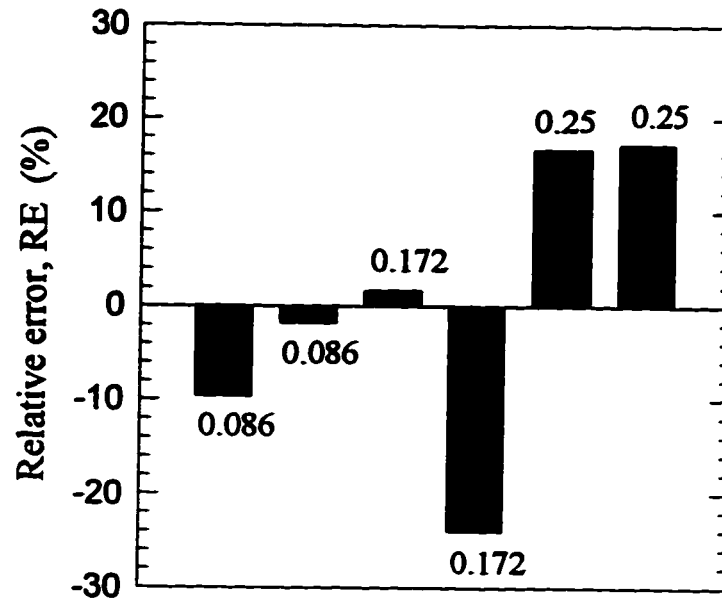
Figure 5-23. Relative error of the k_c' values at varying solids volume fraction.

5.9   Comparison of rolling bed mass transfer results with heat and mass transfer studies in the literature

In Section 2.0, the literature studies on heat and/or mass transfer in fluidized beds, fixed beds, moving beds, rolling bed and for a single sphere were reviewed. The results from some of these studies are compared with the current rolling bed mass

transfer results in this section. Heat transfer results should be useful due to the analogy between heat and mass transfer.

Ranz and Marshall (1952) had measured gas-solid mass transfer coefficients by studying evaporation of water drops. From Equation (2-22) it can be concluded that:

$$k_s \propto U_o^{0.5} \tag{5-11}$$

where k_s is the mass transfer coefficient and U_o is the relative velocity of the sphere through the fluid. This relative velocity can be approximated by the particle velocity if it is the dominant velocity in the system.

In the current experiments, the drum velocity is the dominant velocity compared to the superficial gas velocity, u. From Equation (5-10) it can be seen that:

$$k_s^{'} \propto N^{0.560} \tag{5-12}$$

Thus the dependency of the mass transfer coefficient on the dominant velocity is comparable to the results of Ranz and Marshall (1952).

Tscheng and Watkinson (1979) measured gas-solid heat transfer coefficient in a rolling bed. They conducted the experiments in the similar operating ranges of rotational speed (0.4 to 6.0 rpm) and solids volume fraction (0.065 to 0.170) as in the present study. However, their experiments were conducted at air velocities about 2 to 3 orders of magnitude larger than in the present experiments. The correlation they obtained is repeated below:

$$Nu_{gs} = 0.46 Re_g^{0.535} Re_\omega^{0.104} \eta^{-0.341} \tag{5-13}$$

From Equation (5-13) it can be concluded that:

$$h_{gs} \propto N^{0.104} u^{0.535} \eta^{-0.341} \tag{5-14}$$

It is evident from the above equation that the effect of drum rotational speed, N on the heat transfer coefficient, h_{gs} was lower than the effect of superficial gas velocity, u. This was because much higher gas velocities were used in their experiments. Also they observed a slight negative effect of increasing solids volume fraction, η on the heat transfer coefficient. This is consistent with the present experimental finding as the value of k_s' had decreased when the solids volume fraction was increased from 0.043 to 0.086.

Mu and Perlmutter (1981) had used Equation (2-29) to evaluate the gas-solid heat transfer coefficient, h_{gs}. From Equation (2-29) it can be seen that:

$$h_{gs} \propto \left[u^2 + V_s^2 \right]^{0.4} \tag{5-15}$$

If the particle velocity, V_s is larger than the superficial gas velocity, u then Equation (5-15) can be rewritten as:

$$h_{gs} \propto V_s^{0.8} \tag{5-16}$$

The normalized mass transfer coefficient, k_s' for the rolling bed at solids volume fraction of 0.043 and varying drum rotational speed were plotted as a function of the

surface particle velocity, V_s to see if a similar dependency as in Equation (5-16) was obtained. Figure 5-24 shows the plot of k_s' versus surface particle velocity calculated using Equation (2-2). Linear regression of the data in Figure 5-24 on a logarithmic plot gave the following regression line:

$$k_s' = 11.86V_s^{0.971} \qquad (5-17)$$
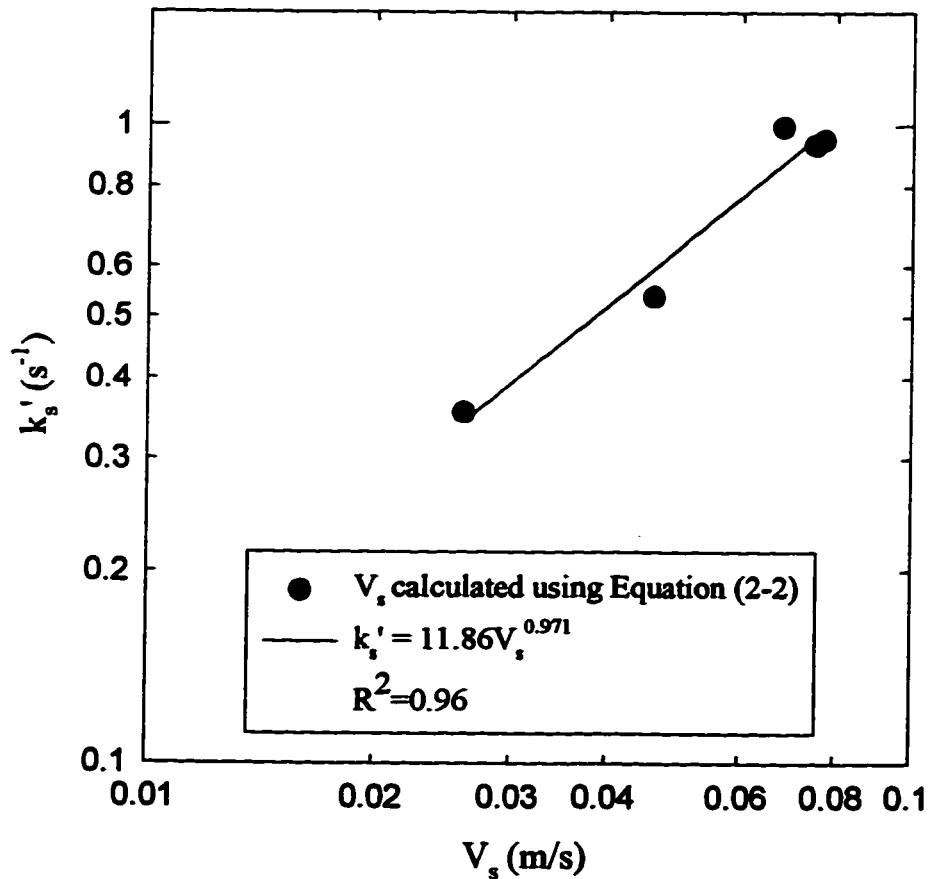
Figure 5-24. Normalized mass transfer coefficient at η=0.043 plotted as a function of surface particle velocity calculated using Equation (2-2).

Comparison of Equation (5-17) with (5-16) indicates that the dependency of heat

or mass transfer coefficient on the surface particle velocity is roughly of the same order.

Figure 5-25 shows the plot of normalized mass transfer coefficient at solids volume

fraction of 0.043 with varying surface particle velocity calculated using Equation (3-21).
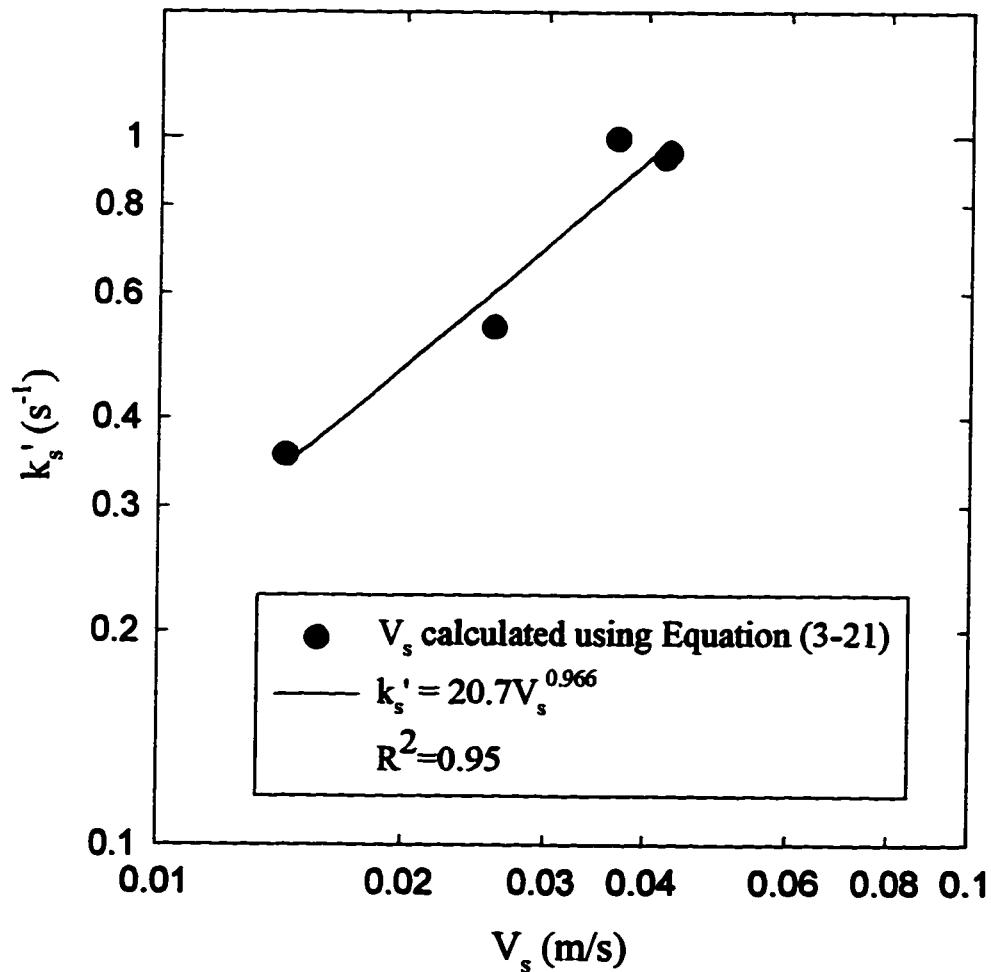
Figure 5-25. Normalized mass transfer coefficient at η=0.043 plotted as a function of
surface particle velocity calculated using Equation (3-21).

Linear regression of the data shown in Figure 5-25 on a logarithmic plot gave the following regression line:

$$k_s^{'} = 20.7 V_s^{0.966} \qquad (5\text{-}18)$$

Comparing Equation (5-18) with Equation (5-16) suggests that the dependency of heat or mass transfer coefficient on the surface particle velocity is roughly of the same order.

A study of convective gas-solid heat transfer in a counter-current moving bed was conducted by Akiyama et al.(1993). From Equation (2-16) it can be concluded that:

$$h_{gs} \propto u^{0.5} \qquad (5\text{-}19)$$

In the current rolling bed experiments, the dominant velocity is the drum velocity as opposed to the superficial gas velocity. The dependence of $k_s^{'}$ on rotational speed was shown in Equation (5-12) which is comparable to the Akiyama et al. results.

5.10   Implications for solid-state fermentation

In Chapter 1, it was mentioned that gas-solid mass transfer is important in solid-state fermentation. Solid-state fermentation is a developing technology and has a number of advantages over liquid state (submerged) fermentation. The main advantage is the ease of oxygen transfer to the microorganisms (Habib and Dale, 1986).

In Sections 5.5 and 5.6, the rotating drum values of $k_s a$ for oxygen in the presence and absence of baffles were compared with $k_L a$ values for oxygen in a typical liquid fermentor. It was found that the gas-solid mass transfer coefficients, $k_s a$ were approximately one to two orders of magnitude higher than the $k_L a$ values. Assuming that the driving force is the same for the gas-solid and gas-liquid systems, then the oxygen transfer rate in gas-solid systems is higher. Therefore, from the present study it can be concluded that the problem of oxygen transfer to the microorganisms in liquid fermentation systems can be overcome by use of alternative methods like solid-state fermentation carried out in a rotating drum fermentor.

Although rotating drums can be used to eliminate oxygen transfer limitations, there are other problems that are encountered in solid-state fermentation. The most serious problem is heat build up due to the metabolic heat generated by the microorganisms (de Reu et al., 1993). Heat removal is essential for maintaining high yields of product. Consequently, heat transfer is important in rotary drum solid-state fermentors. The temperature rise in the fermentor can be controlled by periodic drum rotation, gas temperature, gas flow rate and length of rotation period.

Other problems encountered in rotating drum fermentors are aggregation of the solids into balls (clumping) and growth retardation as a result of particle attrition (Lonsane et al., 1985). Therefore, solids mixing and movement of solid fibrous material is

of some concern in rotating drum fermentors. As well, fungal mycelium can be destroyed due to tumbling of the solids. The shear forces that damage the mycelium may further increase in the presence of baffles due to the lifting and dropping of solids (Fung and Mitchell, 1995).

6. CONCLUSIONS

1. The effect of drum rotational speed on the volumetric mass transfer coefficient, k_sA in the presence of baffles was studied in the range 0.09 to 2.0 rpm and solids volume fraction in the range 0.043 to 0.086. The volumetric mass transfer coefficient linearly increased with the drum rotational speed from 13.22 L/min at 0.09 rpm to 67.01 L/min at 2.0 rpm. These results are expected as solids mixing increased with increasing rotational speed of the drum.

2. The volumetric mass transfer coefficient in the presence of baffles was independent of the solids volume fraction, η although two types of solids motion were observed. At solids volume fraction of 0.043, the baffles were not overloaded with solids. With increasing drum rotational speed, the showering frequency increased. Thus solids mixing increased with the drum rotational speed. At a solids volume fraction of 0.086, the baffles were overloaded and one baffle was completely buried. Both showering and rolling motion of particles were observed. The showering frequency and rolling particle velocity increased with the drum rotational speed. Even for this case the solids mixing increased with increasing drum rotational speed. Due to the complexity of the particle motion the mass transfer area, A, could not be estimated at both holdups.

3. The effect of drum rotational speed on the volumetric mass transfer coefficient, k_sA in the absence of baffles was investigated in the range 0.29 to 2.0 rpm at a solids

volume fraction of 0.043. In the absence of baffles, the solids bed was in the rolling mode. The volumetric mass transfer coefficient linearly increased with the drum rotational speed from 6.35 L/min at 0.29 rpm to 32.03 L/min at 2.0 rpm. These results were consistent with the particle motion that was observed in the rolling bed. The solids mixing increased with increasing drum rotational speed which resulted in higher mass transfer coefficients. The volumetric mass transfer coefficients in the presence of baffles were higher than for the rolling bed in the range of rotational speed mentioned above. This was expected as solids mixing was higher in the presence of baffles due to showering of particles.

4.   The effect of solids volume fraction on the volumetric mass transfer coefficient for the rolling bed was studied at 1.1 rpm. The volumetric mass transfer coefficient, k_sA increased with the solids volume fraction from 21.76 L/min at solids volume fraction of 0.043 to 59.95 L/min at solids volume fraction of 0.25.

5.   Particle motion for the rolling bed was simpler than in the presence of baffles, therefore detailed bed motion observations were made which included total bed depth, h and active layer depth, h_a. At constant solids volume fraction of 0.043 and varying rotational speed in the range 0.29 to 2.0 rpm, the fraction of bed in active motion (h_a/h) increased from 23.5 % to 44.9 %. At a constant rotational speed of 1.1 rpm and varying solids volume fraction in the range 0.043 to 0.25, the fraction of bed in active motion (h_a/h) decreased from 30.2 % to 19.4 %. From the experimentally measured values of h

and h_a at solids volume fraction of 0.043, the surface particle velocity was calculated to obtain the following expression:

$$V_s \propto N^{0.538-0.548}$$

The above result compared well with the results of Tscheng and Watkinson (1979), Mu and Perlmutter (1980 b) and Lebas et al.(1995). At a fixed rotational speed of 1.1 rpm and solids volume fraction varying from 0.043 to 0.25, the surface particle velocity was calculated and the following expression:

$$V_s \propto \eta^{0.209-0.290}$$

6.   For the rolling bed, the exact area available for mass transfer could not be estimated. The mass transfer area is assumed to be influenced by the active layer depth, h_a, the chord length, L_s and the surface particle velocity, V_s. The dependency of mass transfer area on these parameters could not be estimated from the results of the current experiments. However, the volumetric mass transfer coefficient, $k_s A$ for the rolling bed was normalized by volume of bed renewed due to drum rotation.

7.   The normalized mass transfer coefficient, k_s' for the rolling bed at a solids volume fraction of 0.043 varied from 0.355 s^{-1} at 0.29 rpm to 0.994 s^{-1} at 2.0 rpm. The normalized mass transfer coefficient at solids volume fraction of 0.043 were correlated with the drum rotational speed by the following expression:

$$k_s^{'} = 0.733N^{0.560}$$

8.   The normalized mass transfer coefficients, $k_s^{'}$ for the rolling bed at a fixed rotational speed of 1.1 rpm and solids volume fraction varying from 0.043 to 0.25 were also calculated. The value of $k_s^{'}$ was 0.950 s^{-1} at solids volume fraction of 0.043. The $k_s^{'}$ value decreased sharply to 0.566 s^{-1} as the solids volume fraction was increased to 0.086. This could be due to the difference in the solids bed motion at the two holdups. At solids volume fraction of 0.043, the bed was quite shallow and about 1/3 of the total bed was in active motion. At the higher holdup, the solids bed was not shallow and the fraction of bed in active motion declined to 27 %. Vigorous solids mixing at the lower holdup had increased the $k_s^{'}$ value. As the solids volume fraction was further increased from 0.086 to 0.25, the value of $k_s^{'}$ was essentially constant. The mean value of $k_s^{'}$ was 0.627 s^{-1} for solids volume fraction in the range 0.086 to 0.25.

9.   The trends in the normalized mass transfer coefficient, $k_s^{'}$ for the rolling bed at constant holdup and varying drum rotational speed were consistent with the prior results of Ranz and Marshall (1952), Tscheng and Watkinson (1979), Mu and Perlmutter (1981).

10.   The gas-solid mass transfer coefficients, $k_s a$ for oxygen in a rotating drum in the presence and absence of baffles were estimated to be one to two orders of magnitude higher than the gas-liquid mass transfer coefficients, $k_L a$ for oxygen in a typical low agitation liquid fermentor. If it is assumed that the driving forces are the same for the gas-

solid and gas-liquid systems, then oxygen transfer is higher in the gas-solid systems. Therefore, solid-state fermentation in a rotating drum fermentor offers better oxygen transfer to the microorganisms as compared to liquid fermentation systems.

7. RECOMMENDATIONS

1.   Current experiments were conducted for one drum size. The effect of scale-up on the gas-solid mass transfer coefficient needs to be investigated by conducting experiments in a larger drum.

2.   The mass transfer area, A in the presence or absence of baffles could not be estimated in the present study. Specially designed experiments are needed to study the effect of rotational speed and holdup on the mass transfer area.

3.   Rolling bed mass transfer experiments need to be conducted where variables such as gas properties, diffusivity and particle diameter are varied to establish a generalized correlation for Sherwood number for mass transfer in a rolling bed.

4.   The problem of drift in the mass spectrometer signal can be avoided by using other instruments such as a gas chromatograph for measuring mass transfer coefficients.

REFERENCES

Akiyama, T., Takahashi, R. and Yagi, J., 1993, Measurements of heat transfer coefficients between gas and particles for a single sphere and for moving beds. *ISIJ International*, **33(6)**, 703-710.

Asea, P.E.A., Kucey, R.M.N. and Stewart, J.W.B., 1988, Inorganic phosphate solubilization by two *Penicillium* species in solution culture and soil. *Soil Biology and Biochemistry*, **20(4)**, 459-464.

Barr, P.V., Brimacombe, J.K., and Watkinson, A.P., 1989a, A heat transfer model for the rotary kiln: Part I: Pilot kiln trials. *Metallurgical Transactions B*, **20**, 391-402.

Barr, P.V., Brimacombe, J.K., and Watkinson, A.P., 1989b, A heat transfer model for the rotary kiln: Part II: Development of the cross-section model. *Metallurgical Transactions B*, **20**, 391-402.

Berry, D.F, Tomkinson, R.A., Hetzel, G.M., Mullins, D.E., and Young, R.W., 1993, Application of solid state fermentation techniques to dispose of Chlorpyrifos and Metolachlor, *Waste Management*, **13**, 271-277.

Brimacombe, J.K. and Watkinson, A.P.,1978a, Heat transfer in a direct-fired rotary kiln: 1. Pilot plant and experimentation. *Metallurgical Transactions B,***9**, 201-208.

Brimacombe, J.K. and Watkinson, A.P.,1978b, Heat transfer in a direct-fired rotary kiln:II. Heat flow results and their interpretation. *Metallurgical Transactions B,***9**, 209-219.

.

Cannel, E. and Moo-Young, M., 1980a, Solid-state fermentation systems, *Process Biochemistry*, **15(5)**, 2-7.

Carley-Macauly, K.W. and Donald, M.B., 1964, The mixing of solids in tumbling mixers-II. *Chemical Engineering Science*, **19**, 191-199.

Chang, Y.M., 1994, Heat and mass transfer between gas and solid particles in transverse bed of aerated rotary kiln incinerator. *Journal of Chemical Engineering of Japan*, **27(4)**, 443-448.

Dwivedi, P.N. and Upadhyay, S.N., 1977, Particle-fluid mass transfer in fixed and fluidized beds. *Industrial and Engineering Chemistry, Process Design and Development*, **16(2)**, 157-165.

Cannel, E. and Moo-Young, M., 1980b, Solid-state fermentation systems, *Process Biochemistry*, **15(6)**, 24-28.

Ferron, J.R. and Singh, D.K., 1991, Rotary kiln transport processes. *Journal of the American Institute of Chemical Engineers*, **37(5)**, 747-758.

Fogler, H.S., "Elements of Chemical Reaction Engineering", PTR Prentice-Hall Inc., 2nd ed., 1992.

Friedman, S.J., and Marshall, W.R., 1949, Studies in rotary drying Part II- Heat and mass transfer. Chemical Engineering Progress, **45(9)**, 573-588.

Fung, C.J. and Mitchell, D.A., 1995, Baffles increase performance of solid-state fermentation in rotating drum bioreactors. *Biotechnology techniques*, **9(4)**, 295-298.

Henein, H., Brimacombe, J.K. and Watkinson, A.P., 1983a, Experimental study of transverse bed motion in rotary kilns. *Metallurgical Transactions B*, **14B**, 191-205.

Henein, H., Brimacombe, J.K. and Watkinson, A.P., 1983b, The modeling of transverse solids motion in rotary kilns. *Metallurgical Transactions B*, **14B**, 191-205.

Hirosue, H. and Shinohara, J., 1976, Volumetric heat transfer coefficient in rotary dryers and coolers. *Heat transfer-Japanese Research*, **5(4)**, 59-66.

Hogg, R. and Fuerstenau, D.W., 1972, Transverse mixing in rotating cylinders, *Powder Technology*, **6**, 139-148.

Kumar, H.B. and Sublette, K.L., 1993, Effect of high voidage on mass transfer coefficient in a fluidized bed. *Chemical Engineering Communications*, **121**, 157-163.

Kunii, D. and Levenspiel, O., "Fluidization Engineering", John Wiley & Sons, Inc., New York, 1969.

Kunii, D. and Levenspiel, O., "Fluidization Engineering", John Wiley & Sons, Inc., New York, 1977.

Larroche, C. and Gros, J.B., 1989, Strategies for spore production by *Penicillium roqueforttii* using solid state fermentation techniques, *Process Biochemistry*, **24**, 97-103.

Lebas, E., Hanrot, F., Ablitzer, D. and Houzelot, J.L., 1995, Experimental study of residence time, particle movement and bed depth profile in rotary kilns. *Canadian Journal of Chemical Engineering*, **73**, 173-179.

Lehmberg, K., Hehl, M. and Schugerl, K., 1977, Transverse mixing and heat transfer in horizontal rotary drum reactors. *Powder Technology*, **18**, 149-163.

Lonsane, B.K., Ghildyal, N.P., Budiatman, S. and Ramakrishna, S.V., 1985,Engineering aspects of solid state fermentation. *Enzyme and Microbial Technology*, **7**, 258-265.

Mehrotra, S.P. and Brimacombe, J.K., 1990, Kinetics of gasification of coal char with CO_2 in a rotary reactor. *Ironmaking and Steelmaking*, **17(2)**, 93-104.

Mu, J. and Perlmutter, D.D., 1980a, The mixing of granular solids in a rotary cylineder. *Journal of the American Institute of Chemical Engineers*, **26(6)**, 928-934.

Mu, J. and Perlmutter, D.D., 1980b, The mixing of granular solids in a rotary cylinder. Part 2. Experiment results and parameter estimation. *Institution of Chemical Engineers Symposium Series No. 59*, 5:7/1-5:7/20.

Mu, J. and Perlmutter, D.D., 1981, A simulation study of rotary reactor performance, *Chemical Engineering Communications*, **9**, 101-120.

Nigam, P., and Singh, D., 1994, Solid-state (substrate) fermentation systems and their applications in biotechnology. *Journal of Basic Microbiology*, **6**, 405-423.

Owens, W.D., Silcox, G.D., Lighty, J., Deng, X.A., Pershing, D.W., Cundy, V.A., Leger, C.B., and Jakway, A.L., 1992, The desorption of toluene from a montmorillonite clay adsorbent in a rotary kiln environment, *Journal of Air Waste Management Association*, **42**, 681-690.

Oyama, Y., 1980, Particle motion in a horizontal rotating cylinder, *International Chemical Engineering*, **20(1)**, 36-55.

Perry, R.H. and Green, D., "Perry's Chemical Engineers' Handbook", 6th ed., Mc-Graw Hill Inc., New York, 1984.

Perron, J. and Bui, R.T., 1990, Rotary Cylinders: solid transport prediction by dimensional and rheological analysis. *Canadian Journal of Chemical Engineering,* **68,** 61-68.

Perron, J. and Bui, R.T., 1992, Rotary Cylinders: Transverse bed motion prediction by rheological analysis, *Canadian Journal of Chemical Engineering,* **70,** 223-231.

Petrovic, L.J. and Thodos, G., 1968, Mass transfer in the flow of gases through packed beds. *Industrial & Engineering Chemistry Fundamentals,* **7(2),** 274-280.

Rajagopalan, S. and Modak, J.M., 1994, Heat and mass transfer simulation studies for solid-state fermentation processes, *Chemical Engineering Science,* **49(3),** 2187-2193.

Ranz, W.E. and Marshall, W.R., 1952a, Evaporation from drops. *Chemical Engineering Science,* **48(3),** 141-146.

Ranz, W.E. and Marshall, W.R., 1952b, Evaporation from drops. *Chemical Engineering Science,* **48(4),** 173-179.

Rao, S.J., Bhatia, S.K. and Khakar, D.V., 1991, Axial transport of granular solids in rotating cylinders. Part 2: Experiments in a non-flow system. *Powder Technology,* **67,** 153-162.

Richardson, J.F. and Szekely, T., 1961, Mass transfer in a fluidized bed. *Transactions of the Institution of Chemical Engineers,* **39,** 212-222.

Rutgers, R., 1965, Longitudinal mixing of granular material flowing through a rotating cylinder- Part I. Descriptive and theoretical. *Chemical Engineering Science*, **20**, 1079-1087.

Saeman, W.C., 1951, Passage of solids through rotary kilns. *Chemical Engineering Progress*, **47(10)**, 508-574.

Saeman, W.C. and Mitchell, T.R., 1954, Analysis of rotary dryer and cooler performance. *Chemical Engineering Progress*, **50(9)**, 467-475.

Schofield, F.R. and Gilkin, P.G., 1962, Rotary driers and coolers for granular fertilizers. *Transactions of the Institution of Chemical Engineers*, **40**, 183-190.

Sherritt, R.G., Caple, R., Behie, L.A. and Mehrotra, A.K., 1993, Movement of solids through flighted rotating drums. Part I. Model formulation. *Canadian Journal of Chemical Engineering*, **71**, 337-346.

Sherritt, R.G., Behie, L.A., and Mehrotra, A.K., The movement of solids in flighted rotating drums, "Mixed-Flow Hydrodynamics-Advances in Engineering Fluid Mechanics Series", Cheremisinoff, N.P., ed., Gulf Publishing Company, Houston, 1996, 421-440.

Sherwood, T.K., Pigford, R.L. and Wilke, C.R., "Mass Transfer", McGraw-Hill Inc., New York, 1975.

Sissom, L.E. and Jackson, T.W., 1967, Heat exchange in fluid-particle moving beds. *Journal of Heat Transfer*, **89**, 1-6.

Smith, R.S., 1992, Legume inoculant formulation and application. *Canadian Journal of Microbiology*, **38**, 485-492.

Somasegaran, P., 1985, Inoculant production with diluted cultures of Rhizobium spp. and autoclaved peat: Evaluation of diluents, *Rhizobium* spp., peats, sterility requirements, storage and plant effectiveness. *Applied and Environmental Microbiology*, **50(2)**, 398-405.

Stenhagen, E., Abrahamsson, S. and McLafferty, F.W., "Atlas of mass spectral data", vol.2, Interscience Publishers, New York, 1969.

Treybal, R.E., "Mass-Transfer Operations", 3 rd ed., McGraw-Hill Inc., 1980.

Tscheng, S.H., "Convective Heat Transfer in a Rotary Kiln", Ph.D. Thesis, University of British Columbia, Vancouver, B.C., Canada, 1978.

Tscheng, S.H. and Watkinson, A.P., 1979, Convective heat transfer in a rotary kiln. *Canadian Journal of Chemical Engineering*, **57**, 433-443.

Wakao, N. and Funazkri, T., 1978, Effect of fluid dispersion coefficients on particle-to-fluid mass transfer coefficients in packed beds. *Chemical Engineering Science*, **33**, 1375-1384.

Wei, G.C., 1983, Beta SiC powders produced by carbothermic reduction of silica in a high-temperature rotary furnace, *Communications of the American Ceramic Society*, **66**, 111-113.

Wes, G.W.J., Drinkenburg, A.A.H. and Stermerding, S., 1976, Solids mixing and residence time distribution in a horizontal rotary drum reactor. *Powder Technology*, **13**, 177-184.

Wilkins, G.S. and Thodos, G., 1969, Mass transfer driving forces in packed and fluidized Beds, *Journal of the American Institute of Chemical Engineers*, **15(1)**, 47-50.

Woodle, G.R. and Munro, J.M., 1993, Particle motion and mixing in a rotary kiln. *Powder Technology*, **76**, 241-245.

Yegneswaran, P.K., Gray, M.R. and Thompson, B.G., 1990, Kinetics of CO2 hydration in fermentors: pH and pressure effects. *Biotechnology and Bioengineering*, **36**, 92-96.

Yoon, P. and Thodos, G., 1972, Mass transfer in the flow of gases through shallow fluidized beds. *Chemical Engineering Science*, **27**, 1549-1554.

APPENDIX A

This appendix contains the raw data from the positive step tracer experiment which were used to calculate the residence time distribution function, $E(t)$ and the average residence time, τ of the gas phase. Equations used in the evaluation of $E(t)$ and τ are stated in the appendix and the derivation of Equation (3-14) is shown. Also sample calculation for the evaluation of $\dfrac{dS}{dt}$ using the forward, backward and central difference approximations is shown.
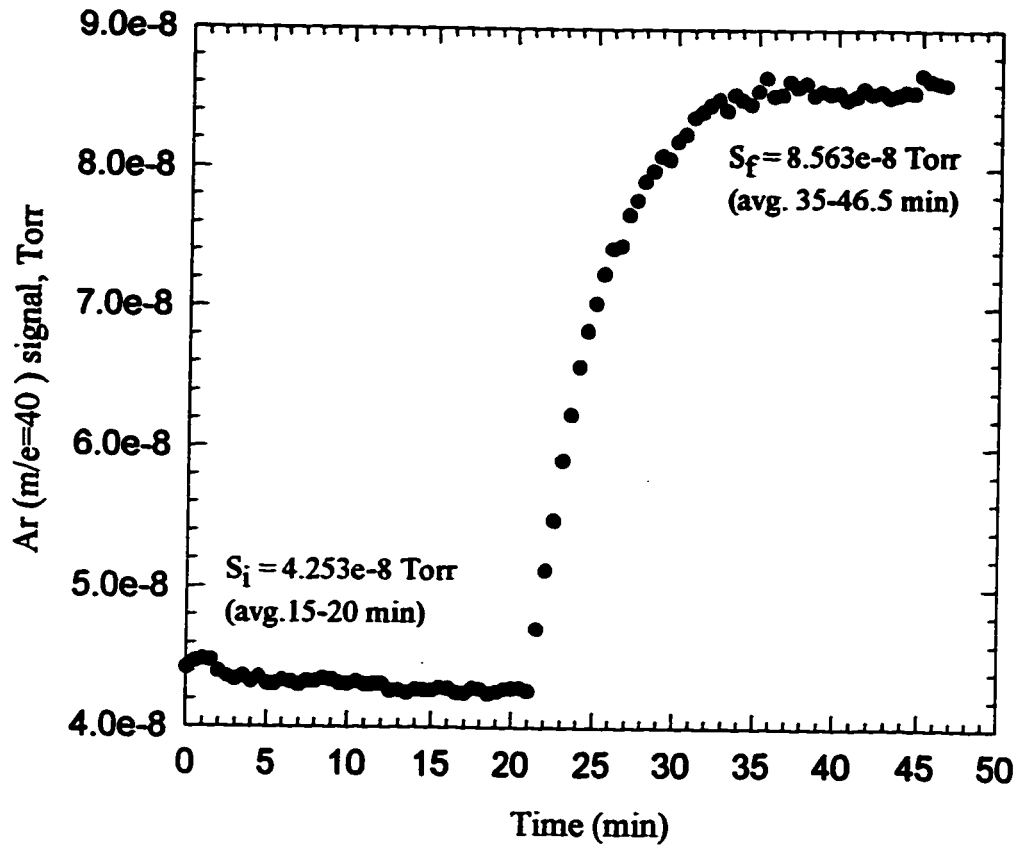
Figure A-1. Raw data for the step tracer experiment.

Positive Step: switched from Air (Ar = 0.934%) to Calgas (Ar = 2.01%)

Experimental Conditions: Used unsaturated S-201, 5X8 mesh and drum with no baffles.

Used 16 rods (2.3 mm diameter) to ensure solids bed motion was in the rolling mode.

$\eta = 0.10$

N = 2.27 rpm

Q = 5.63 L/min

$V = 20$ L

$\varepsilon = 0.4$ (void fraction in packed beds, Perry and Green, 1984)

Calculation of τ_{pred}: $\quad \tau_{pred} = \dfrac{V[1-(1-\varepsilon)\eta]}{Q} = 3.34$ min

S_i was obtained by averaging the signal from $t = 15$ min to $t = 20$ min

S_f was obtained by averaging the signal from $t = 35$ to $t = 46.5$ min

Calculation of dS/dt and E (t) from the experimental data

$$E(t) = \frac{d[S(t)]}{dt} \frac{1}{(S_f - S_i)} \tag{A-1}$$

$S_f = 8.563$ E-08 Torr

$S_i = 4.263$ E-08 Torr

$S_f - S_i = 4.3$ E-08 Torr

$h = 0.5$ min as data collected every 30 seconds

To calculate dS/dt, the forward, central and backward difference approximations are used (Gerald and Wheatley, 1989). The experimental data (S(t) and t) and computed values of dS(t)/dt and E(t) are shown in table A-1. For these calculations, t=0 min is the time at which the feed is switched to Calgas ie. at 21.5 min after start of the experiment.

Table A-1. Raw data and computed values of dS/dt and E(t).

Orig. Time (min)	Orig. signal (Torr)	Orig.Time (min)	Orig. signal (Torr)	Time, t (min)	S(t) (Torr)	dS(t)/dt (Torr/min)	E(t) 1/min
0.0	4.4166E-08	25.5	7.2366E-08	0.0	4.7066E-08	8.9680E-09	0.2086
0.5	4.4633E-08	26.0	7.4166E-08	0.5	5.1233E-08	6.3320E-09	0.1473
1.0	4.4800E-08	26.5	7.4366E-08	1.0	5.4766E-08	7.8555E-09	0.1827
1.5	4.4733E-08	27.0	7.6633E-08	1.5	5.9033E-08	7.6727E-09	0.1784
2.0	4.3900E-08	27.5	7.7666E-08	2.0	6.2333E-08	6.6833E-09	0.1554
2.5	4.3566E-08	28.0	7.9000E-08	2.5	6.5733E-08	6.0440E-09	0.1406
3.0	4.3366E-08	28.5	7.9766E-08	3.0	6.8266E-08	4.3278E-09	0.1006
3.5	4.3600E-08	29.0	8.0833E-08	3.5	7.0233E-08	4.0612E-09	0.0944
4.0	4.3233E-08	29.5	8.0600E-08	4.0	7.2366E-08	4.2273E-09	0.0983
4.5	4.3533E-08	30.0	8.1866E-08	4.5	7.4166E-08	1.6000E-09	0.0372
5.0	4.3100E-08	30.5	8.2366E-08	5.0	7.4366E-08	2.4060E-09	0.056
5.5	4.3033E-08	31.0	8.3600E-08	5.5	7.6633E-08	3.5943E-09	0.0836
6.0	4.3300E-08	31.5	8.4000E-08	6.0	7.7666E-08	2.2560E-09	0.0525
6.5	4.3233E-08	32.0	8.4500E-08	6.5	7.9000E-08	2.1000E-09	0.0488
7.0	4.3000E-08	32.5	8.4933E-08	7.0	7.9766E-08	1.9550E-09	0.0455
7.5	4.3266E-08	33.0	8.4133E-08	7.5	8.0833E-08	6.3433E-10	0.0148
8.0	4.3233E-08	33.5	8.5266E-08	8.0	8.0600E-08	9.4400E-10	0.022
8.5	4.3433E-08	34.0	8.4866E-08	8.5	8.1866E-08	1.8935E-09	0.044
9.0	4.3366E-08	34.5	8.4600E-08	9.0	8.2366E-08	1.7453E-09	0.0406
9.5	4.3100E-08	35.0	8.5533E-08	9.5	8.3600E-08	1.7397E-09	0.0405
10.0	4.3066E-08	35.5	8.6500E-08	10.0	8.4000E-08	7.7217E-10	0.018
10.5	4.3233E-08	36.0	8.5200E-08	10.5	8.4500E-08	1.1552E-09	0.0269
11.0	4.3033E-08	36.5	8.5266E-08	11.0	8.4933E-08	-7.0033E-10	-0.0163
11.5	4.3033E-08	37.0	8.6233E-08	11.5	8.4133E-08	3.8300E-10	0.0089
12.0	4.3100E-08	37.5	8.5833E-08	12.0	8.5266E-08	1.0328E-09	0.024
12.5	4.2566E-08	38.0	8.6100E-08	12.5	8.4866E-08	-1.1213E-09	-0.0261
13.0	4.2600E-08	38.5	8.5233E-08	13.0	8.4600E-08	6.8367E-10	0.0159
13.5	4.2433E-08	39.0	8.5533E-08	13.5	8.5533E-08	2.4777E-09	0.0576
14.0	4.2666E-08	39.5	8.5366E-08	14.0	8.6500E-08	-5.5500E-10	-0.0129
14.5	4.2666E-08	40.0	8.5433E-08	14.5	8.5200E-08	-1.7620E-09	-0.041
15.0	4.2600E-08	40.5	8.4900E-08	15.0	8.5266E-08	1.4885E-09	0.0346
15.5	4.2833E-08	41.0	8.5133E-08	15.5	8.6233E-08	6.0600E-10	0.0141
16.0	4.2766E-08	41.5	8.5700E-08	16.0	8.5833E-08	-1.7183E-10	-0.004
16.5	4.2433E-08	42.0	8.5300E-08	16.5	8.6100E-08	-6.8333E-10	-0.0159
17.0	4.2433E-08	42.5	8.5466E-08	17.0	8.5233E-08	-6.7817E-10	-0.0158
17.5	4.2766E-08	43.0	8.5100E-08	17.5	8.5533E-08	2.8850E-10	0.0067
18.0	4.2733E-08	43.5	8.5233E-08	18.0	8.5366E-08	-7.7833E-11	-0.0018
18.5	4.2400E-08	44.0	8.5500E-08	18.5	8.5433E-08	-5.5467E-10	-0.0129
19.0	4.2500E-08	44.5	8.5400E-08	19.0	8.4900E-08	-4.5567E-10	-0.0106
19.5	4.2733E-08	45.0	8.6700E-08	19.5	8.5133E-08	1.0888E-09	0.0253
20.0	4.2766E-08	45.5	8.6300E-08	20.0	8.5700E-08	1.2833E-10	0.003
20.5	4.2833E-08	46.0	8.6100E-08	20.5	8.5300E-08	-3.0650E-10	-0.0071
21.0	4.2600E-08	46.5	8.6033E-08	21.0	8.5466E-08	-1.8883E-10	-0.0044
21.5	4.7066E-08			21.5	8.5100E-08	-3.4400E-10	-0.008
22.0	5.1233E-08			22.0	8.5233E-08	5.4433E-10	0.0127
22.5	5.4766E-08			22.5	8.5500E-08	-4.4000E-11	-0.001
23.0	5.9033E-08			23.0	8.5400E-08	1.4222E-09	0.0331
23.5	6.2333E-08			23.5	8.6700E-08	1.1000E-09	0.0256
24.0	6.5733E-08			24.0	8.6300E-08	-9.0550E-10	-0.0211
24.5	6.8266E-08			24.5	8.6100E-08	-2.6700E-10	-0.0062
25.0	7.0233E-08			25.0	8.6033E-08	-1.0000E-12	0

3 Point Forward Difference: $S'(t_i) = \dfrac{-S(t_{i+2}) + 4S(t_{i+1}) - 3S(t_i)}{2h}$ (A-2)

$\dfrac{dS(t = 0\,min)}{dt} = \dfrac{[-5.4766E - 08 + 4(5.1233E - 08) - 3(4.7066E - 8)]\,Torr}{2(0.5\,min)}$

$= 8.968E - 09\,Torr\,/\,min$

$E(t = 0\,min) = \dfrac{dS(t = 0\,min)}{dt}\dfrac{1}{S_f - S_i} = \dfrac{8.968E - 09\,Torr\,/\,min}{4.3E - 08\,Torr} = 0.2085\,1\,/\,min$

4 Point Central Difference: $S'(t_i) = \dfrac{-S(t_{i+2}) + 8S(t_{i+1}) - 8S(t_{i-1}) + S(t_{i-2})}{12h}$ (A-3)

$E(t = 1\,min) = \dfrac{7.8555E - 09\,Torr\,/\,min}{4.3E - 08\,Torr} = 0.1827\,1\,/\,min$

2 Point Central Difference: $S'(t_i) = \dfrac{S(t_{i+1}) - S(t_{i-1})}{2h}$ (A-4)

$E(t = 24.5\,min) = \dfrac{-2.67E - 10\,Torr\,/\,min}{4.3E - 08\,Torr} = -0.006211\,/\,min$

3 Point Backward Difference: $S'(t_i) = \dfrac{3S(t_i) - 4S(t_{i-1}) + S(t_{i-2})}{2h}$ (A-5)

$E(t = 25\,min) = \dfrac{-1.0E - 12\,Torr\,/\,min}{4.3E - 08\,Torr} = 2.325E - 05\,1\,/\,min$

Derivation of Equation (3-14)

Equation (3-14) is derived from Equations (3-11) and (3-12) which are repeated here:

$$E(t) = \frac{d}{dt}\left[\frac{S(t)}{S_f - S_i}\right] \tag{A-6}$$

$$E(t) = \frac{1}{\tau}e^{-\frac{t}{\tau}} \tag{A-7}$$

$$\frac{dS(t)}{dt}\left[\frac{1}{S_f - S_i}\right] = \frac{1}{\tau}e^{-\frac{t}{\tau}}$$

$$dS(t) = (S_f - S_i)ae^{-at}dt \quad \text{where} \quad a = \frac{1}{\tau}$$

$$\int_{S_i}^{S(t)} dS = (S_f - S_i)a\int_0^t e^{-at}dt$$

$$S(t) - S_i = (S_f - S_i)a\left[\frac{-1}{a}e^{-at} + \frac{1}{a}\right]$$

$$S(t) = S_i + (S_f - S_i) - (S_f - S_i)e^{-at}$$

$$S(t) = S_f - (S_f - S_i)e^{-\frac{t}{\tau}} \qquad \text{Equation (3-14) or (A-8)}$$

From a curve fit of the experimental data (S(t) and t) to Equation (A-8), the average residence time, τ can be evaluated.

Reference: Gerald, C.F. and Wheatley P.O., "Applied Numerical Analysis", 4 th ed., Addison-Wesley Publishing Company, Don Mills, 1989.

APPENDIX B

This appendix contains the calibration curves of the two flow meters used in the experiments. Also the equation used for converting flow rate from standard litres per minute to litres per minute is also given.

.
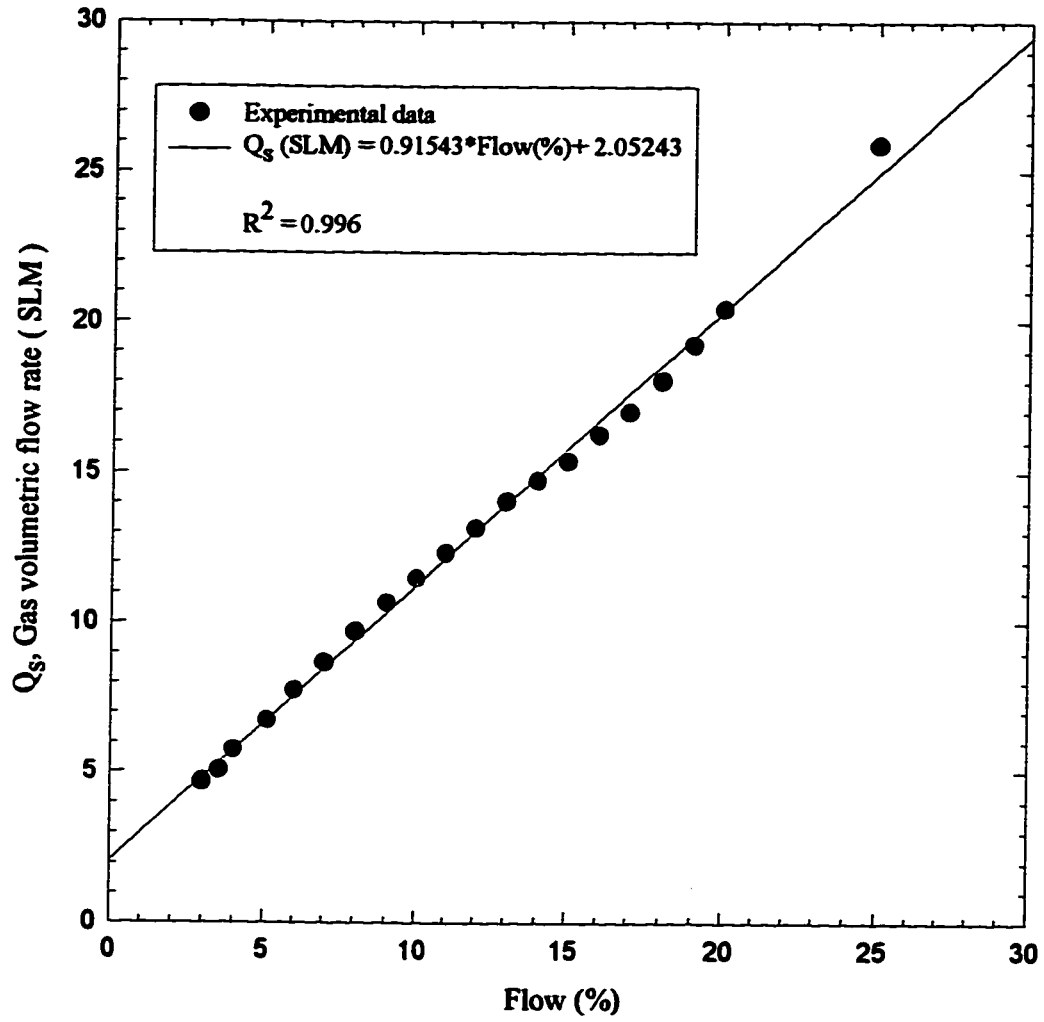
Figure B-1. Calibration curve for the UFC 3020 flow meter (0-100 SLM range)
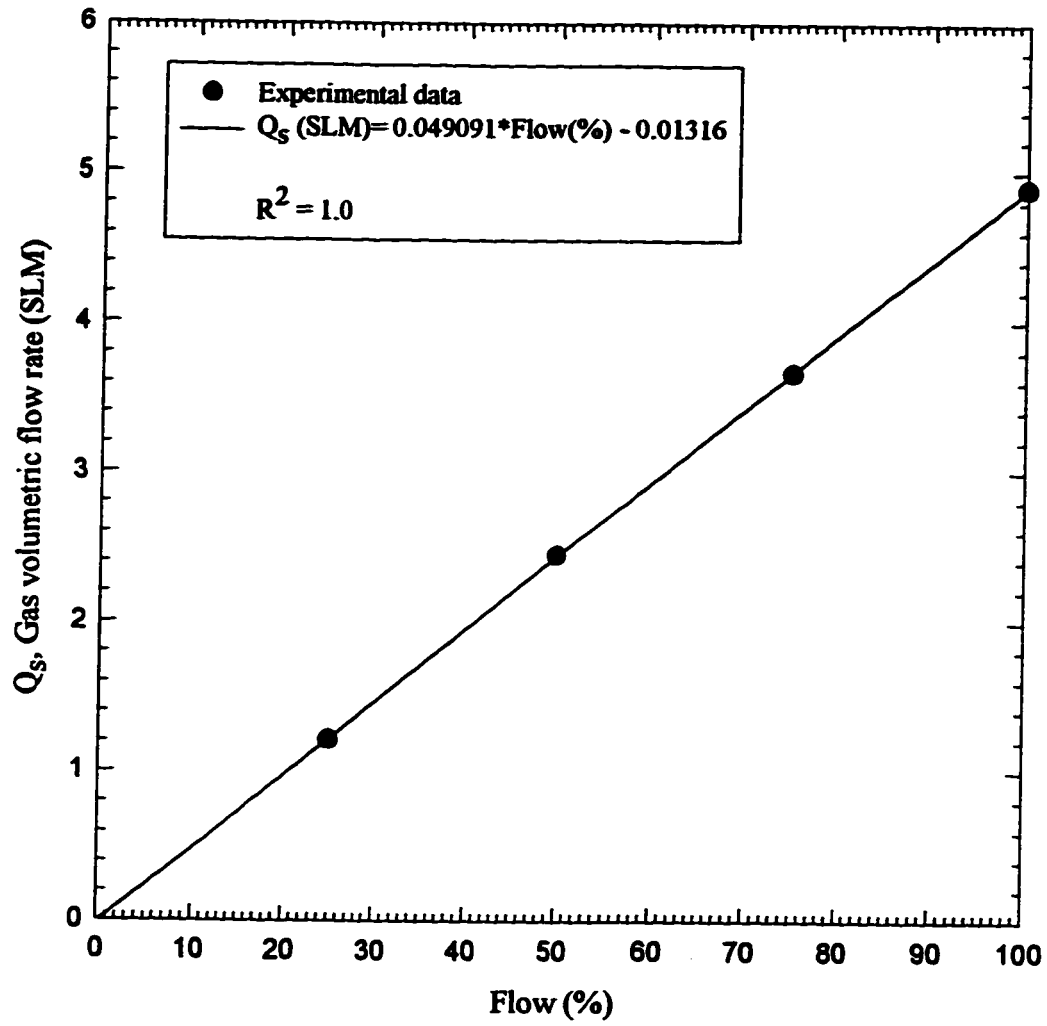
Figure B-2. Calibration curve for the UFC 1200A flow meter (0-5 SLM range).

The equation for converting the gas flow rate from standard litres per minute (SLM) to litres per min was :

$$Q = \frac{P_s Q_s T}{T_s P}$$ (B-1)

where

P_s standard atmospheric pressure, 760 mm Hg

Q_s standard gas volumetric flow rate, SLM (calculated for the experimentally

       measured Flow (%) value from the calibration graphs B-1 or B-2)

T room temperature, K

P room pressure, mmHg

T_s standard temperature, 273 K

Q gas volumetric flow rate, L/min

Equation B-1 can be rewritten as:

$$Q = \frac{760 Q_s T}{273 P}$$ (B-2)

Equation (B-2) was used for gas flow rate unit conversion.

APPENDIX C

This appendix contains the raw data of the experiments from which the constant-rate drying period of the solids was determined. Calculations are also given to show how the values of F_E^{max} (Equation 4-1) were determined.

As mentioned in Section 4.3, vacuum-dried solids that were saturated with n-decane were used in the tray drying experiment for determining the constant-rate period. There were two experiments done (CD#1 and CD#2) to check the reproducibility . Since ambient air was used in these experiments, another run (CD#3) was done to account for the adsorption of water from air onto the vacuum-dried solids. The raw data, graphs and calculations of F_E^{max} from these 3 experiments are given below.

Table C-1. Experimental data for CD#1 run at room temperature of 24.6 °C.

Time (min)	m_{tot} (g)	m_d (g)	X(g dec/ g VD solids)	DE (g dec eva/g VD solids)
0	145.16	14.622	0.331	0.000
10	144.72	14.182	0.321	0.009973
20	144.25	13.712	0.311	0.020627
30	143.80	13.262	0.301	0.030826
40	143.38	12.842	0.291	0.040346
50	143.01	12.472	0.283	0.048733
60	142.68	12.142	0.275	0.056213
70	142.40	11.862	0.269	0.062559
100	141.80	11.262	0.255	0.076159
130	141.48	10.942	0.248	0.083413
160	141.32	10.782	0.244	0.087039

m_t = mass of tray = 86.42 g

m_b = mass of vacuum-dried solids= 44.118 g

m_d= mass of decane present in saturated solids = m_{tot} - m_b - m_t

m_{tot} = mass of tray plus saturated solids.

$X = m_d / m_b$ = decane content (dry basis)

DE = decane evaporated (dry basis)
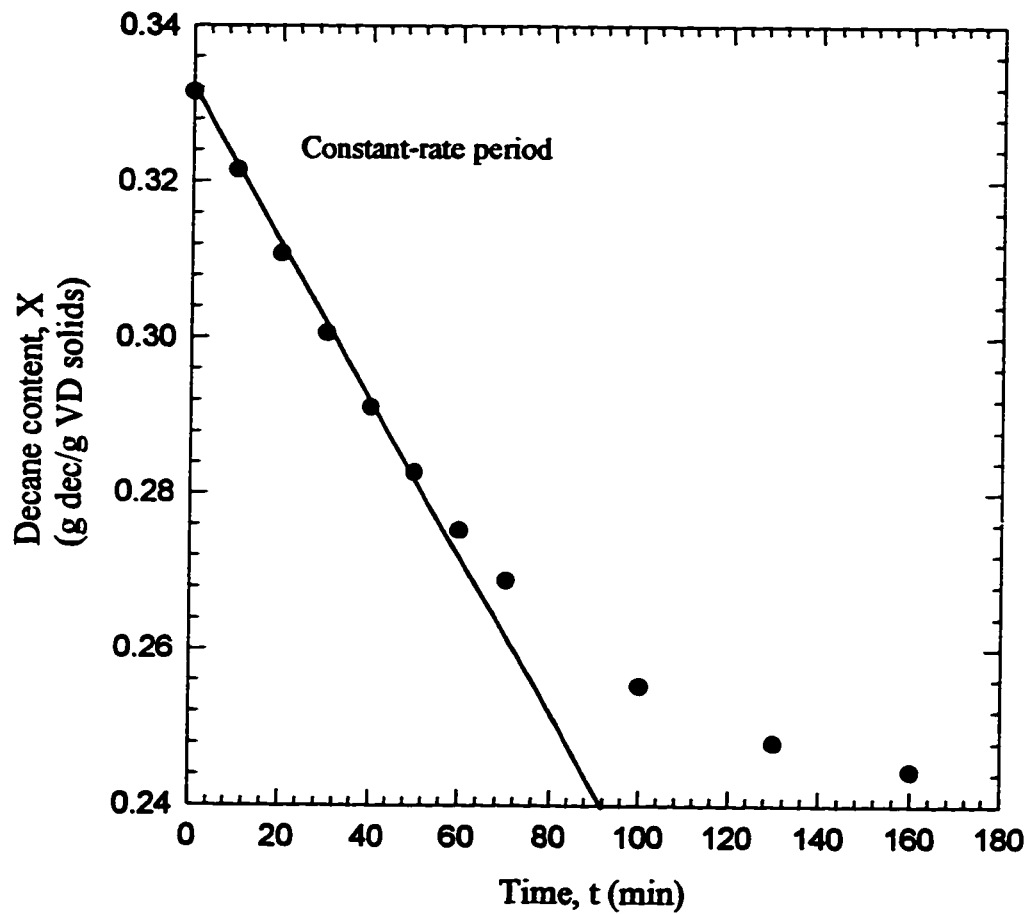
Figure C-1. Decane content as a function of time for CD#1 run.

Table C-2. Experimental data for CD#2 run at room temperature of 25.4 °C.

Time (min)	m_{tot} (g)	m_d (g)	X(g dec/ g VD solids)	DE (g dec eva/g VD solids)
0	145.27	14.755	0.335	0.000000
10	144.81	14.295	0.324	0.010432
20	144.30	13.785	0.313	0.021998
30	143.83	13.315	0.302	0.032657
40	143.41	12.895	0.292	0.042182
50	143.02	12.505	0.284	0.051026
60	142.69	12.175	0.276	0.058510
80	142.19	11.675	0.265	0.069849
100	141.84	11.325	0.257	0.077787
130	141.52	11.005	0.250	0.085044
160	141.20	10.685	0.242	0.092301

m_t = mass of tray = 86.42 g

m_b = mass of vacuum-dried solids= 44.095 g

m_d= mass of decane present in saturated solids = m_{tot} - m_b - m_t

m_{tot} = mass of tray plus saturated solids.

X = m_d / m_b = decane content (dry basis)

DE = decane evaporated (dry basis)
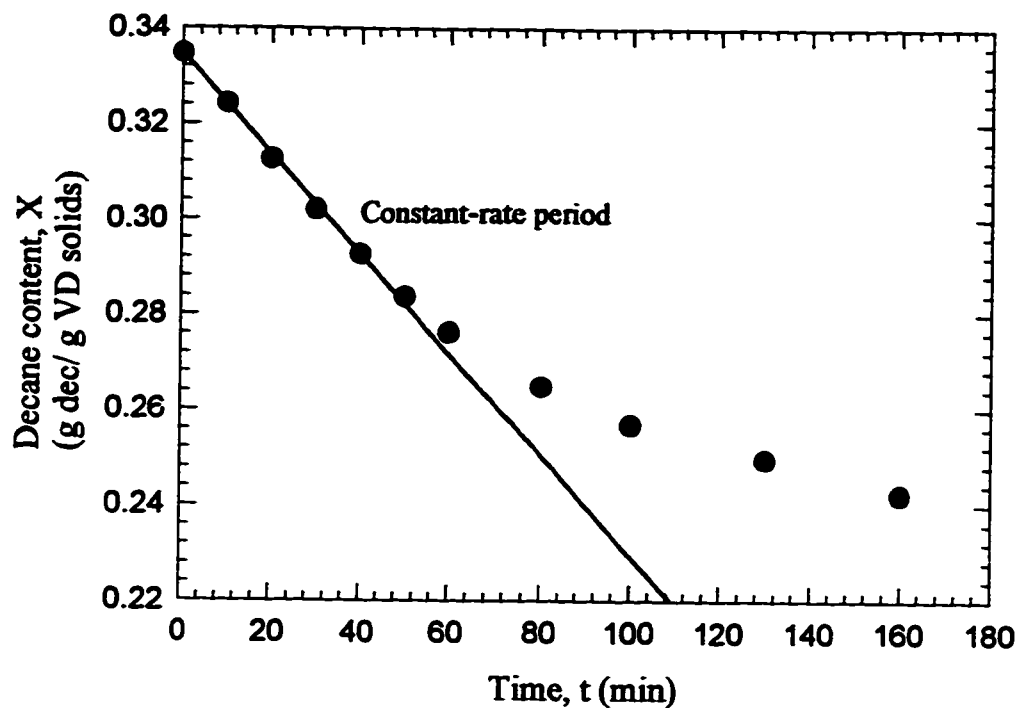
Figure C-2. Decane content as a function of time for CD#2 run.

Table C-3. Experimental data for CD#3 run at room temperature of 25.7 °C.

Time (min)	*m_{tot} (g)	m_w (g)	W(g water/ g VD solids)
0.00	136.49	-0.006	0.000
15.00	136.72	0.224	0.004
30.00	136.93	0.434	0.009
61.41	137.30	0.804	0.016
97.00	137.45	0.954	0.019
120.00	137.50	1.004	0.020
150.00	138.22	1.724	0.034
184.03	138.26	1.764	0.035

m_t = mass of tray = 86.47 g

*m_{tot} = mass of tray plus vacuum-dried solids

m_w = moisture adsorbed = m_{tot} - m_t - m_b

m_b = mass of vacuum-dried solids = 50.026 g

W = moisture adsorbed (dry basis) = m_w/m_b

dW/dt = 2.66e-4 (1/min)
R^2 = 0.991
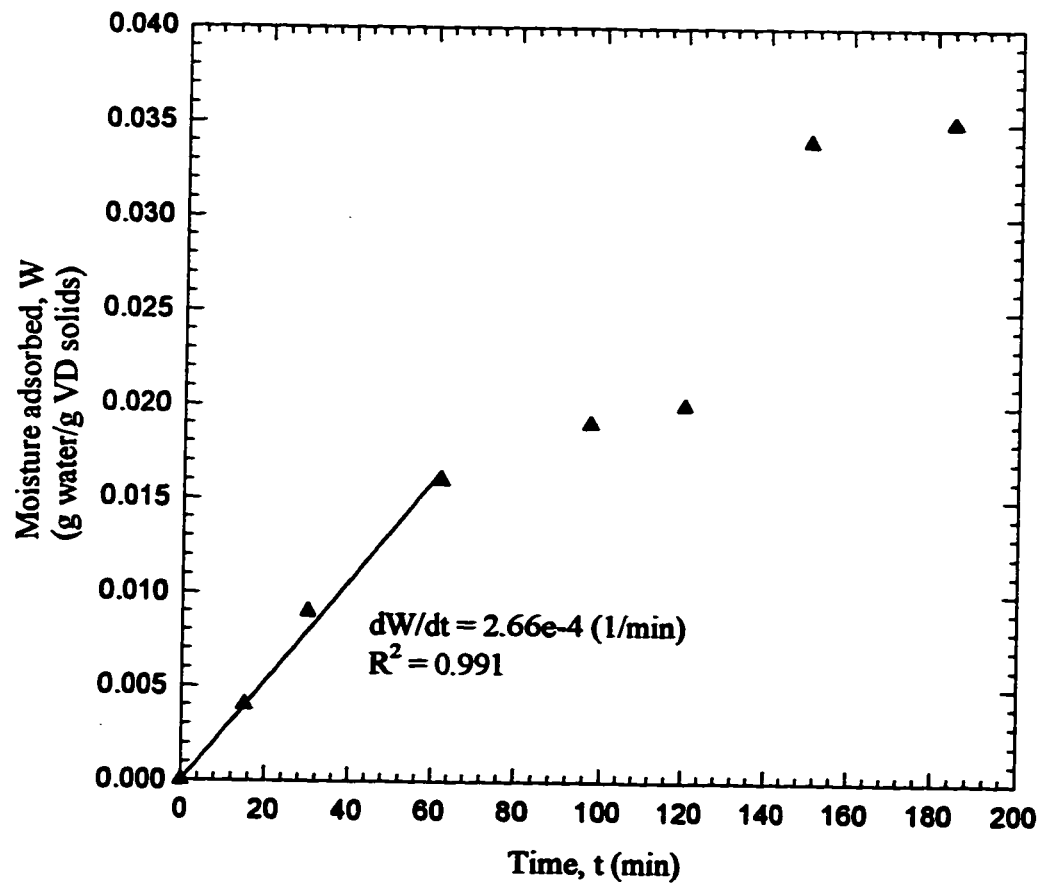
Figure C-3. Moisture Adsorbed as a function of time for CD#3 run.

Computation of F_E^{max} (Equation 4-1) for CD#1 and CD#2 runs.

dt = constant-rate period, min

m_b = mass of vacuum-dried solids, g

m_d = mass of n-decane in saturated solids, g

DE = decane evaporated (dry basis), g dec eva/ g VD solids

dDE/dt = slope of decane evaporated, DE versus time, t curve in the constant-rate region.

dW/dt = slope of moisture adsorbed, W versus time, t curve in the constant-rate region.

From Figures C-1 and C-2 it can be seen that the constant-rate period is till approximately

50 minutes from the start of the experiments, so dt = 50 min. Figure C-4 shows the DE

versus t plot for CD#1 run and the dDE/dt value in the constant-rate region.
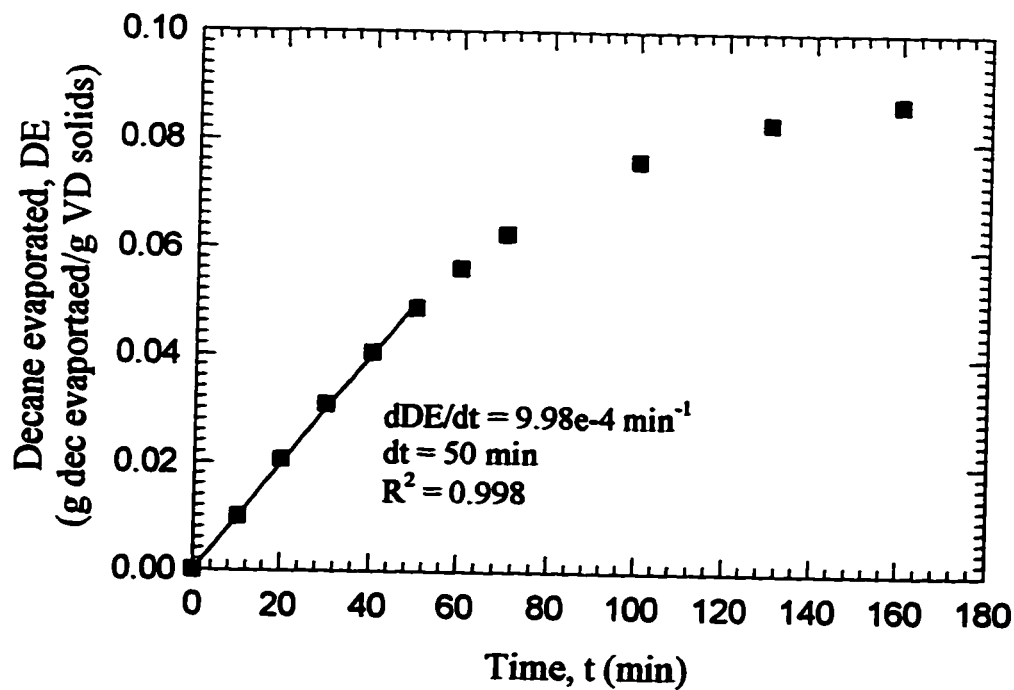
Figure C-4. Decane evaporated as a function of time for CD#1 run.

Figure C-5 shows the DE versus t plot for CD#2 run and the dDE/dt value in the constant-rate region.

dDE/dt = 0.001048 min^{-1}
dt = 50 min
R^2= 0.998
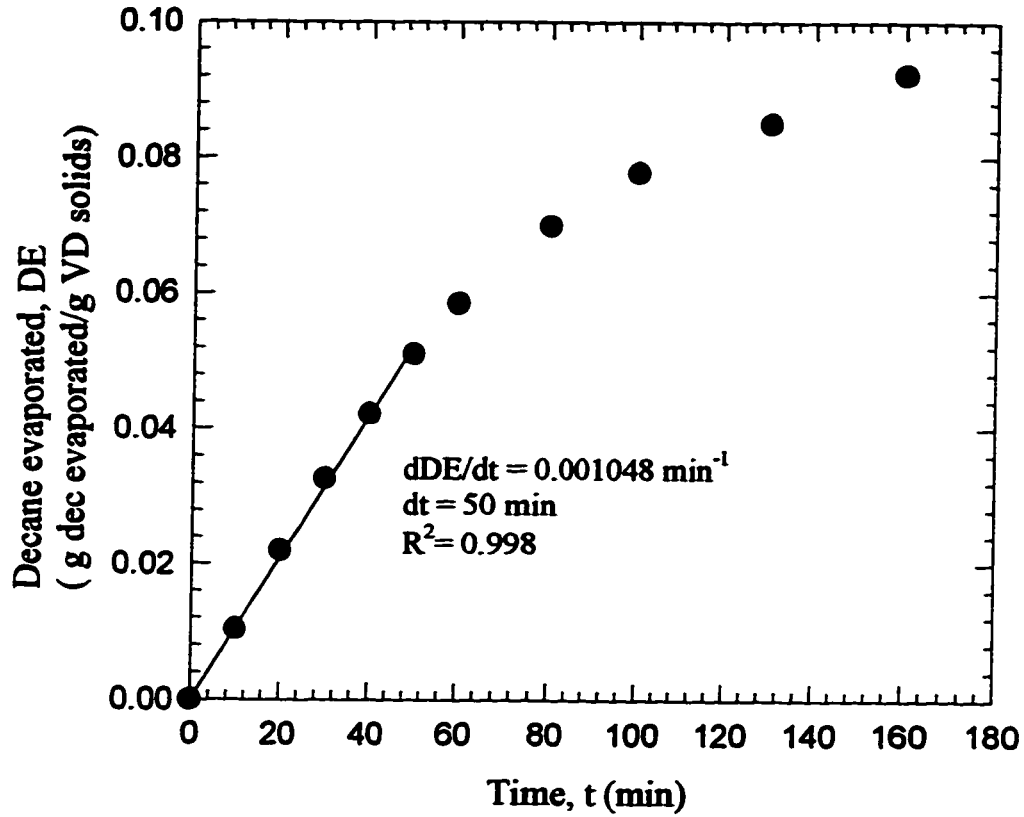
Figure C-5. Decane evaporated as a function of time for CD#2 run.

Calculation of F_E^{max} (ignoring water adsorption)

CD#1 run: $F_E^{max} = \left[\dfrac{dDE}{dt}\right] dt \dfrac{m_b}{m_d} = 9.98e - 4(50)\left[\dfrac{44.118}{14.622}\right]\dfrac{g \ dec \ eva}{g \ total \ dec}$

$$F_E^{max} = 0.151$$

CD#2 run:
$$F_E^{max} = \left[\frac{dDE}{dt}\right]dt\frac{m_b}{m_d} = 1.048e - 3(50)\left[\frac{44.095}{14.755}\right]\frac{g \text{ dec eva}}{g \text{ total dec}}$$

$$F_E^{max} = 0.157$$

Average:
$$F_E^{max} = \frac{0.157 + 0.151}{2} = 0.154$$

Calculation of F_E^{max} (correcting for water adsorption)

DE_c = corrected value of decane evaporated during constant-rate period,

g dec evaporated/ g VD solids.

$$DE_c = \frac{dDE}{dt}dt + \frac{dW}{dt}dt$$

$$F_E^{max} = DE_c\frac{m_b}{m_d}$$

CD#1 run:
$$DE_c = [9.98e - 4(50) + 2.66e - 4(50)] = 0.0632\frac{g \text{ dec eva}}{g \text{ VD solids}}$$

$$F_E^{max} = 0.0632\left[\frac{44.118}{14.622}\right]\frac{g \text{ dec eva}}{g \text{ total dec}}$$

$$F_E^{max} = 0.191$$

CD#2 run: $\quad DE_c = \left[1.048e-3(50)+2.66e-4(50)\right] = 0.0657\dfrac{g\ dec\ eva}{g\ VD\ solids}$

$$F_E^{max} = 0.0657\left[\dfrac{44.095}{14.755}\right]\dfrac{g\ dec\ eva}{g\ total\ dec}$$

$$F_E^{max} = 0.196$$

Average: $\quad F_E^{max} = \dfrac{0.191+0.196}{2} = 0.194$

Overall result: $0.154 \leq F_E^{max} \leq 0.194$

Mass transfer experiments:

Range of F_E was from 0.004816 to 0.0921. Therefore the mass transfer experiments were conducted during constant-rate drying period of the solids.

APPENDIX D

This appendix contains the raw data for the mass transfer experiments and the values of k_cA obtained by the slope and piecewise methods. Calculated values of the ratio of the drum wall velocity to the maximum superficial gas velocity, V_W/u and F_E are also given. A sample calculation is provided to show how to obtain the values of k_cA (by the two methods) and the values of V_W/u and F_E.

RD Ex# 42   No baffles (rolling bed) η =4.3%, N= 0.576 rpm
T=22 ^{O}C, P=710 mmHg, Bed T=22.6 ^{O}C
5slm@60%, 40%, 20%, Q= 1.121-3.392 L/min
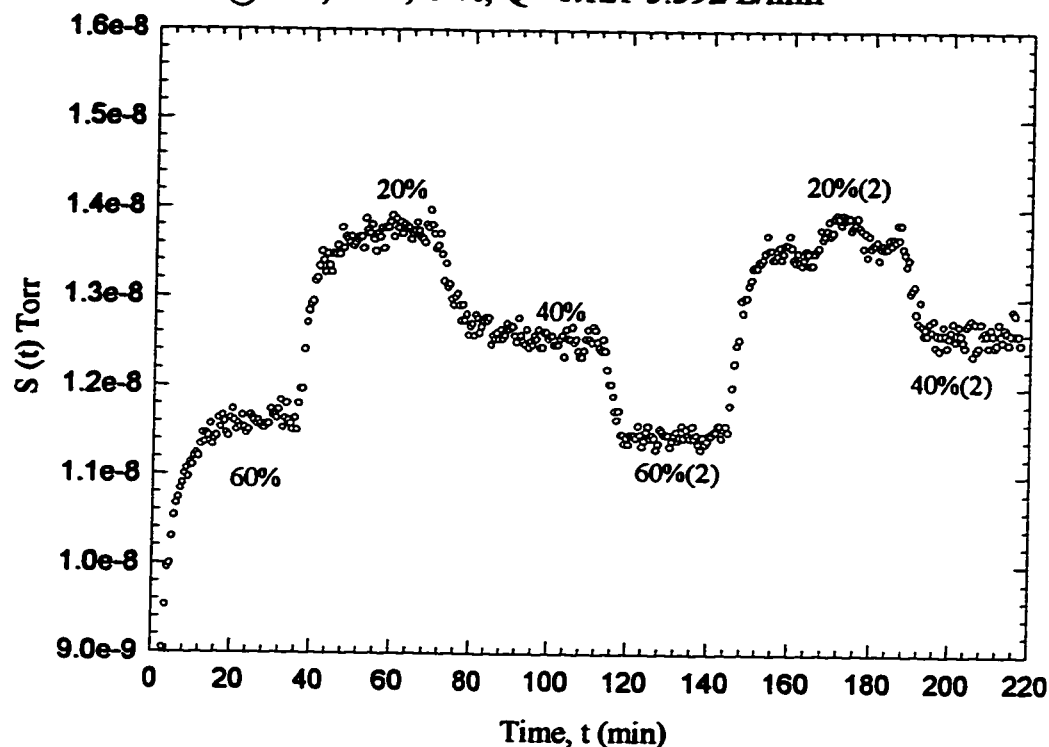
| Solids (@start) | 854.34 g | Bulk density | 997.7 kg/m^3 |
| Solids (@end | 849.90 g | F_E | 0.0203 |

No condensation and no dusting in the drum.
Ratio of drum wall velocity to maximum superficial gas velocity, V_w/u = 10.22

Flow (%)	Q(L/min)	S* (Torr)	Piece	k$_e$A(L/min) piece method	k$_e$A(L/min) by slope method
60	3.392	1.1601e-8	60% to 20%	11.26	b= 65967328.079
20	1.121	1.3735e-8	20% to 40%	10.46	m= 6109154.86
40	2.255	1.2510e-8	40% to 60%(2)	10.14	R^2= 0.996
60(2)	3.392	1.1459e-8		Avg.= 10.62	k$_e$A=b/m = 10.80
20(2)	1.121	1.3715e-8			
40(2)	2.255	1.2604e-8			

Note: 60(2) means that the flow rate was set at 60% for the second time to confirm the steady-state that was achieved. This notation will be used when the same flow rate is set again within the same experiment.

Sample Calculation for obtaining the values of k_sA, V_W/u and F_E.

For this sample calculation, the raw data from RD Ex# 42 (no baffles, $\eta=0.043$, N=0.576 rpm) will be used. The flow meter used in this experiment was UFC 1200A(0-5 SLM range). The calibration graph (Figure B-2) for this flow meter is shown in Appendix B. The curve equation is as follows:

$$Q_s = -0.01316 + 0.049091 * Flow(\%)$$

For calculation of k_sA using **piecewise method**, consider the piece when air flow rate was stepped down from 60% flow (steady-state values:Q_1, S^{ss}_1) to 20% flow (steady-state values: Q_2, S^{ss}_2) . The air flow rates for these steady-states were calculated using Equation (B-2):

$$Q(L / min) = \frac{760Q_sT}{273P}$$

<u>Steady-state 1</u>

At 60% flow, $Q_s = 60(0.049091) - 0.01316 = 2.932$ SLM

T= 295.15 K   P= 710mmHg

$Q = \frac{760 * 2.932 * 295.15}{710 * 273} = 3.392$ L / min i.e $Q_1 = 3.392$ L / min

<u>Steady-state 2</u>

At 20% flow, $Q_s = 20(0.049091) - 0.01316 = 0.969$ SLM

$$Q = \frac{760 * 0.969 * 295.15}{710 * 273} = 1.121 \quad L / min \quad i.e \quad Q_2 = 1.121 \, L / min$$

To obtain the steady-state signals, S^{ss}_1 and S^{ss}_2, S(t) readings were averaged after steady-state was reached.

S^{ss}_1(average of S(t) values from t=21 min to t=36 min) = 1.1601e-8 Torr

S^{ss}_2(average of S(t) values from t=55 min to t=80 min) = 1.3735e-8 Torr

Calculation of k_sA by piecewise method was done using Equation (3-6) which is repeated below:

$$k_sA = \left[\frac{S^{ss}_1 Q_1 - S^{ss}_2 Q_2}{S^{ss}_2 - S^{ss}_1} \right]$$

$$k_sA = \left[\frac{1.1601e - 8 * 3.392 - 1.3735e - 8 * 1.121}{1.3735e - 8 - 1.1601e - 8} \right] = 11.26 \quad L / min$$

Similarily k_sA values for two other pieces (20% to 40% and 40% to 60%(2)) were calculated and the values obtained were 10.46 L/min and 10.14 L/min respectively. The average value of k_sA from the 3 pieces was 10.62 L/min. Last two pieces ie 60% to 20%(2) and 20%(2) to 40%(2) were ignored due to drift in the signal, S(t).

For calculation of k_sA using the **slope method**, graph of $1/S^{ss}$ versus Q was drawn. In order to do this the values of S^{ss} and Q for every steady-state were calculated as described in the procedure for the piecewise method. The linear regression was done to obtain the slope,m and the intercept, b. The graph created from the experimental data is shown below.

RD Ex#42 No baffles (rolling bed) η=4.3%, N=0.576 rpm
T=22 °C, P=710mmHg, BedT=22.6 °C
5slm@60,40,20%, Q=1.121-3.392 L/min
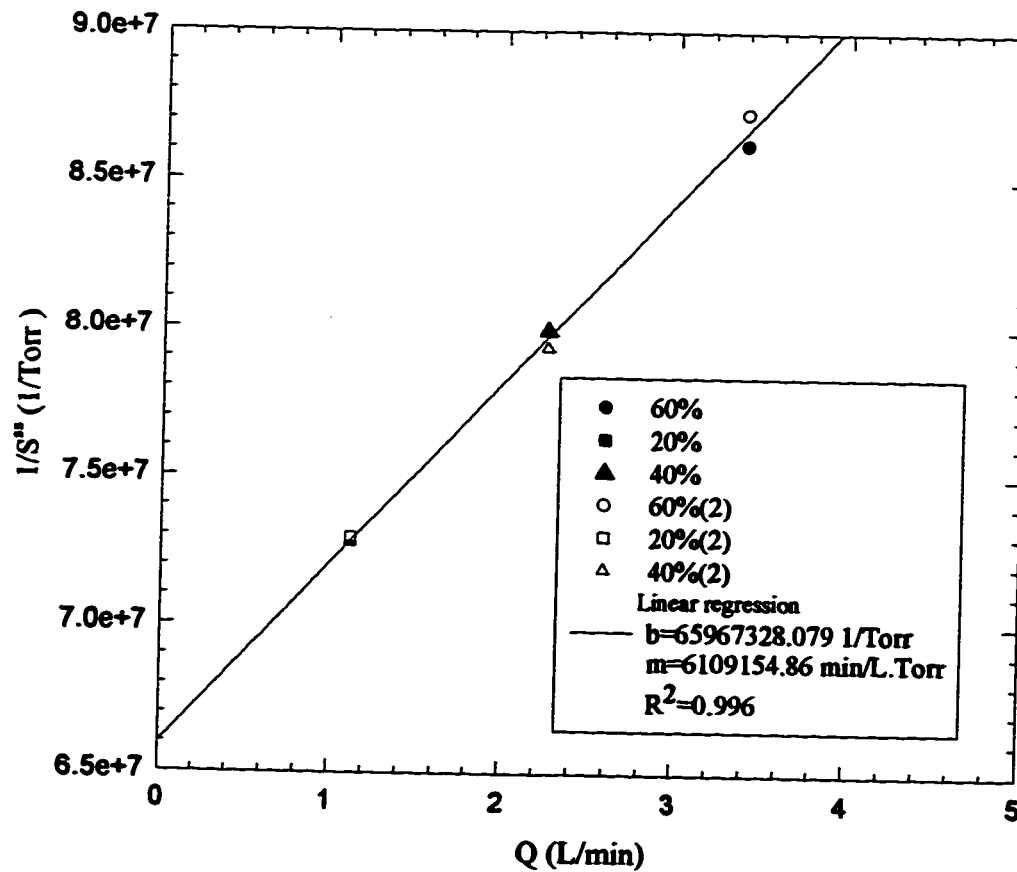
From Equation (3-9) k_sA was calculated by the slope method:

$$k_s A = \frac{b}{m} = \frac{65967328.079}{6109154.86} = 10.8 \quad L / min$$

Comparison with the slope method:

This data set was relatively good as there was little drift in the sensor signal with time. The values of $k_s A$ using the two methods agreed well within the experimental error.

$$\% \ Error = \left[\frac{k_s A \ (piecewise) - k_s A(slope)}{k_s A(piecewise)} \right]$$

$$\% \ Error = \left[\frac{10.62 - 10.80}{10.62} \right] = -1.69 \ \%$$

Calculation of the ratio of drum wall velocity to superficial gas velocity, V_W/u

The drum wall velocity was calculated using Equation (3-15) which is repeated as follows:

$$V_W = \frac{2\pi RN}{60} = \frac{2\pi(0.145m)0.576}{60s} = 8.746e - 3 \quad m / s$$

The superficial air velocity was calculated at maximum flow rate (Q=3.392 L/min) used in the experiment as it would give the lower limit of the ratio, V_W/u. The equation used for calculating the velocity, u is:

$$u = \frac{Q}{1000 * A_c * 60} \quad \text{where} \quad A_c = \pi R^2 = \pi (0.145 \text{ m})^2 = 6.605e-2 \quad \text{m}^2$$

$$u = \frac{3.392 \text{ m}^3}{1000 * 60 \text{ s} * 6.605e-2 \quad \text{m}^2} = 8.559e-4 \quad \text{m/s}$$

$$\frac{V_W}{u} = \frac{8.746e-3 \text{ m/s}}{8.559e-4 \text{ m/s}} = 10.2$$

Therefore in this experiment, the ratio V_W/u would at least be 10.2 ensuring that the drum wall velocity is the dominant velocity in the system

.

Calculation of F_E using Equation (4-1) :

The following ratio (Section 4.4) was used to find the amount of n-decane in the saturated solids:

$$\frac{\text{Mass of n} - \text{decane adsorbed}}{\text{Mass of saturated solids}} = 0.256$$

$$F_E = \frac{854.3 \text{ g} - 849.9 \text{ g}}{0.256 * 854.3 \text{ g}} = 0.0203$$

Note: the value of F_E obtained from the mass transfer experiment (0.0203) was lower than the range of F_E^{max} obtained from the constant-rate drying study ($0.154 \leq F_E^{max} \leq 0.194$). Thus the mass transfer experiment was conducted during the constant-rate drying conditions.

RD EX#45 No baffles (rolling bed) η=4.3% N=1.657 rpm
T=22.8 °C, P=707.1 mmHg, Bed T=22.4 °C
5slm@100%,60%,20%, Q= 1.126-5.709 L/min
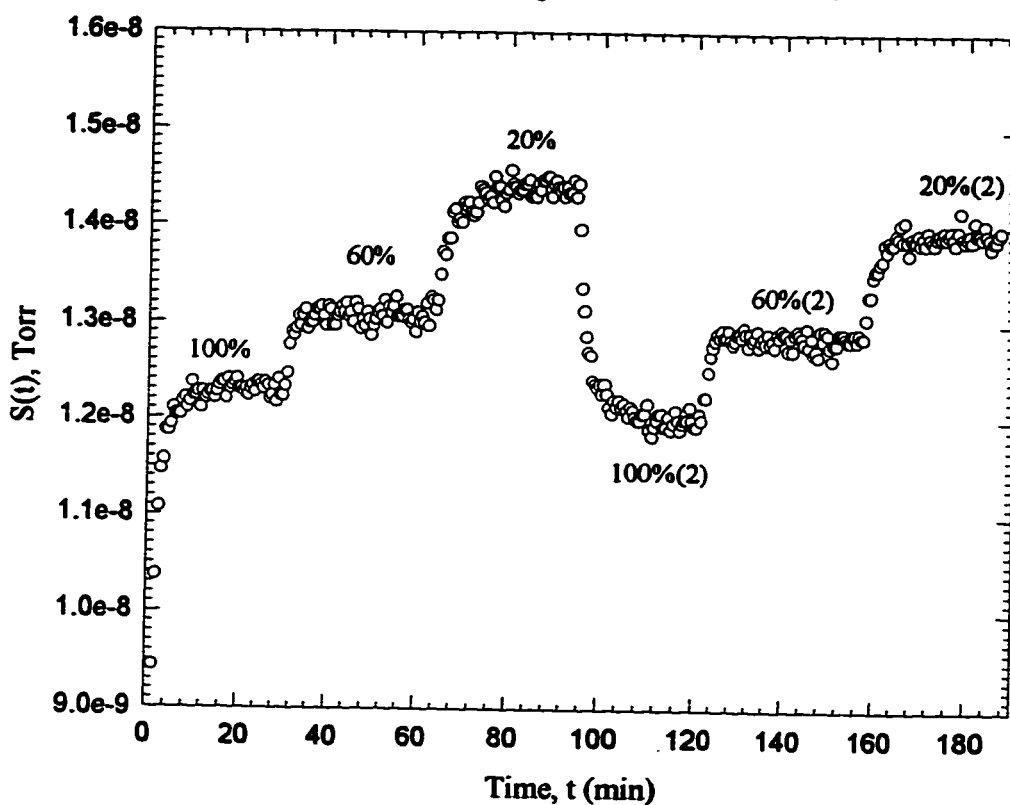
Solids (@start)   857.97 g   **Bulk density**   1003 kg/m³
Solids(@end)   not available F_E not available
No condensation and no dusting in the drum.
Ratio of drum wall velocity to maximum superficial gas velocity, V_w/u = 17.5

Flow (%)	Q (L/min)	S** (Torr)	Piece	k_eA(L/min) piece method	k_eA(L/min) by slope method
100	5.698	1.2308e-8	100% to 60%	33.0	b= 67989815.367
60	3.414	1.3080e-8	60% to 20%	21.56	m= 2554359.23
20	1.126	1.4399e-8	100%(2) to 60%(2)	28.89	R^2= 0.95
100(2)	5.709	1.1990e-8	60%(2) to 20%(2)	26.06	k_eA=b/m = 26.62
60(2)	3.416	1.2841e-8	20% to 100%(2)	21.68	
20(2)	1.129	1.3921e-8		Avg. 26.24	

RD EX#46 No baffles(rolling bed) η=4.3%, N=1.967 rpm
T=22.9 °C, P=695.05mmHg, BedT=22.6 °C
5slm@100%,60%,20%, Q=1.148-5.808 L/min
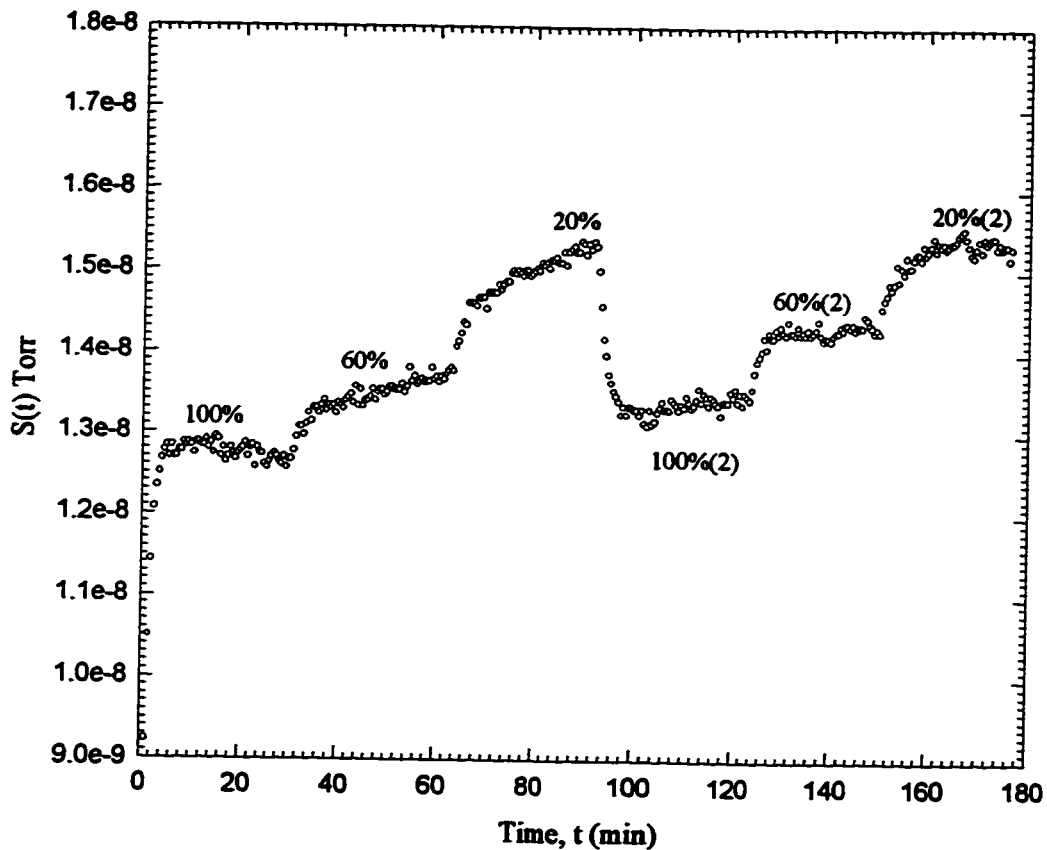
| Solids (@start) | 856.75 g | Bulk density | 990.37 kg/m³ |
| Solids(@end) | 851.25 g | F_E | 0.02508 |

No condensation and no dusting in the drum.
Ratio of drum wall velocity to maximum superficial gas velocity, $V_w/u = 20.4$

Flow (%)	Q (L/min)	S^{ss} (Torr)	Piece	k_sA(L/min) piece method	k_sA(L/min) by slope method
100	5.793	1.2701e-8	20% to 100%(2)	32.69	b= 62719369.2
60	3.474	1.3671e-8	100%(2) to 60%(2)	31.05	m= 2419467.29
20	1.148	1.528e-8	60%(2) to 20%(2)	32.54	R²= 0.891
100(2)	5.808	1.3431e-8	100%(2) to 20%(2)	31.83	k_sA=b/m = 25.92
60(2)	3.479	1.4337e-8			
20(2)	1.150	1.5328e-8		Avg. 32.03	

RD Ex#47 No baffles (rolling bed) η=4.3%,N=0.291 rpm
T=22.9 °C, Bed T=22.6 °C, P=718.3 mmHg
5slm@60%,40%,20%, Q=1.111-3.362 L/min
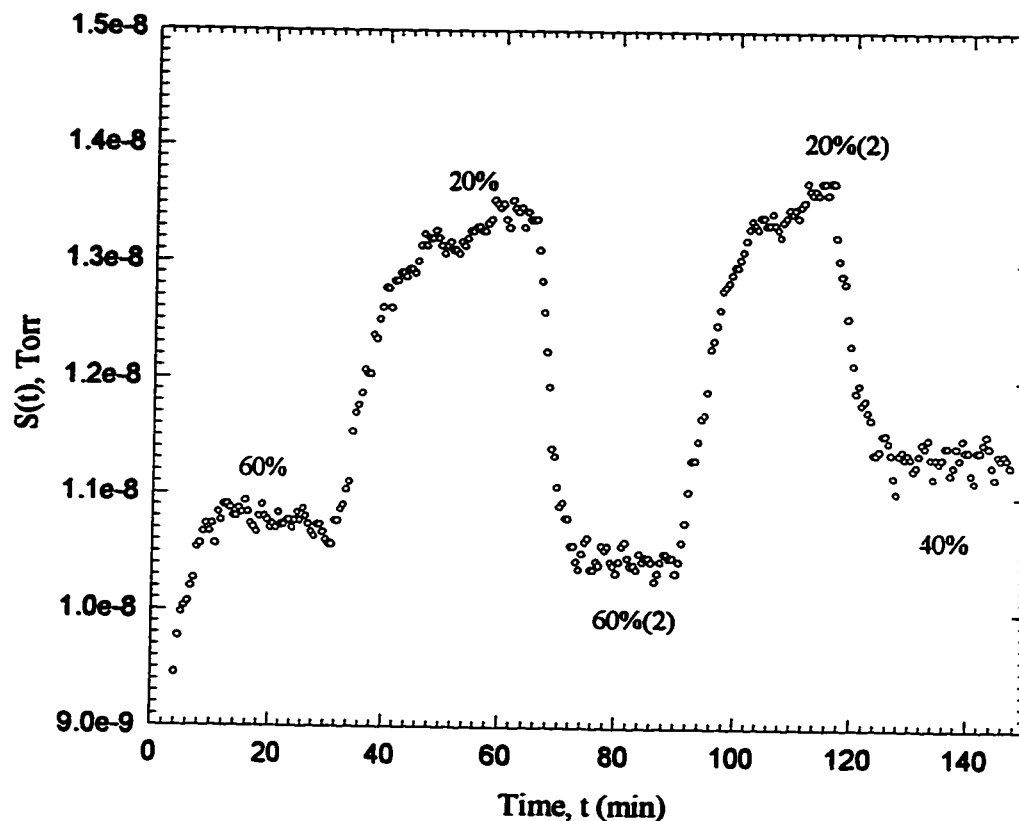
Solids (@start)	856.42 g	Bulk density	999.31 kg/m^3
Solids(@end)	853.41 g	F_E	0.0137

No condensation and no dusting in the drum.
Ratio of drum wall velocity to maximum superficial gas velocity, V_W/u = 5.2

Flow (%)	Q (L/min)	S$^{\infty}$ (Torr)	Piece	k_sA(L/min) piece method	k_sA(L/min) by slope method
60	3.359	1.0725e-8	60% to 20%	7.819	b= 64619048.078
20	1.111	1.3423e-8	20% to 60%(2)	6.734	m= 9129961.66
60(2)	3.362	1.0436e-8	60%(2) to 20%(2)	6.298	R^2= 0.965
20(2)	1.112	1.3605e-8	20%(2) to 40%	4.556	k_sA=b/m = 7.077
40	2.237	1.1352e-8			
				Avg. 6.352	

RD Ex#54 No baffles(rolling bed) η=4.3% N=1.213 rpm
T=22.6 $^{\circ}$C, P=707.0mmHg, Bed T=22.5 $^{\circ}$C
5slm@100%,60%,25%, Q=1.413-5.700 L/min

Solids (@start)	856.40 g	Bulk density	1003.6 kg/m^3
Solids(@end)	851.27 g	F_E	0.0233

No condensation and no dusting in the drum.
Ratio of drum wall velocity to maximum superficial gas velocity, V_W/u = 12.0

Flow (%)	Q (L/min)	S^{ss} (Torr)	Piece	k_aA(L/min) piece method	k_aA(L/min) by slope method
100	5.700	1.1788e-8	100% to 60%	20.58	b= 66825884.5
60	3.414	1.2911e-8	60% to 25%	20.80	m= 3076939.51
25	1.413	1.4074e-8	25% to 100%(2)	22.24	R^2= 0.99
100(2)	5.697	1.1916e-8	100%(2) to 25%(2)	22.87	k_aA=b/m = 21.72
25(2)	1.413	1.4017e-8	25%(2) to 60%(2)	23.35	
60(2)	3.413	1.2970e-8	100% to 25%	20.69	
				Avg. 21.76	

RD EX#48 No baffles(rolling bed) η= 8.6%, N=1.120 rpm
T=22.8 oC, P=708.22 mmHg, Bed T=22.4 oC
5slm@100%,20%,60%, Q=5.707-1.129 L/min

Solids (@start)	1714.07 g		Bulk density	1001 kg/m³
Solids(@end)	1709.41 g		F_E	0.01062

No condensation and no dusting in the drum.
Ratio of drum wall velocity to maximum superficial gas velocity, $V_w/u = 11.8$

Flow (%)	Q (L/min)	S** (Torr)	Piece	k_aA(L/min) piece method	k_aA(L/min) by slope method
100	5.707	1.2182e-8	100% to 60%	20.52	b= 67307017.85
60	3.416	1.3348e-8	60% to 20%	27.01	m= 2610051.39
20	1.129	1.4433e-8	100% to 20%	23.65	R²= 0.959
100(2)	5.675	1.2070e-8	20% to 100%(2)	22.09	k_aA=b/m = 25.79
20(2)	1.222	1.3268e-8			
				Avg. 23.32	

RD EX#50 No baffles(rolling bed) η=8.6% N=1.111rpm
T=22.9 °C, BedT=22.6 °C, P=711mmHg
5slm@100%,20%,60%, Q= 1.123-5.674 L/min
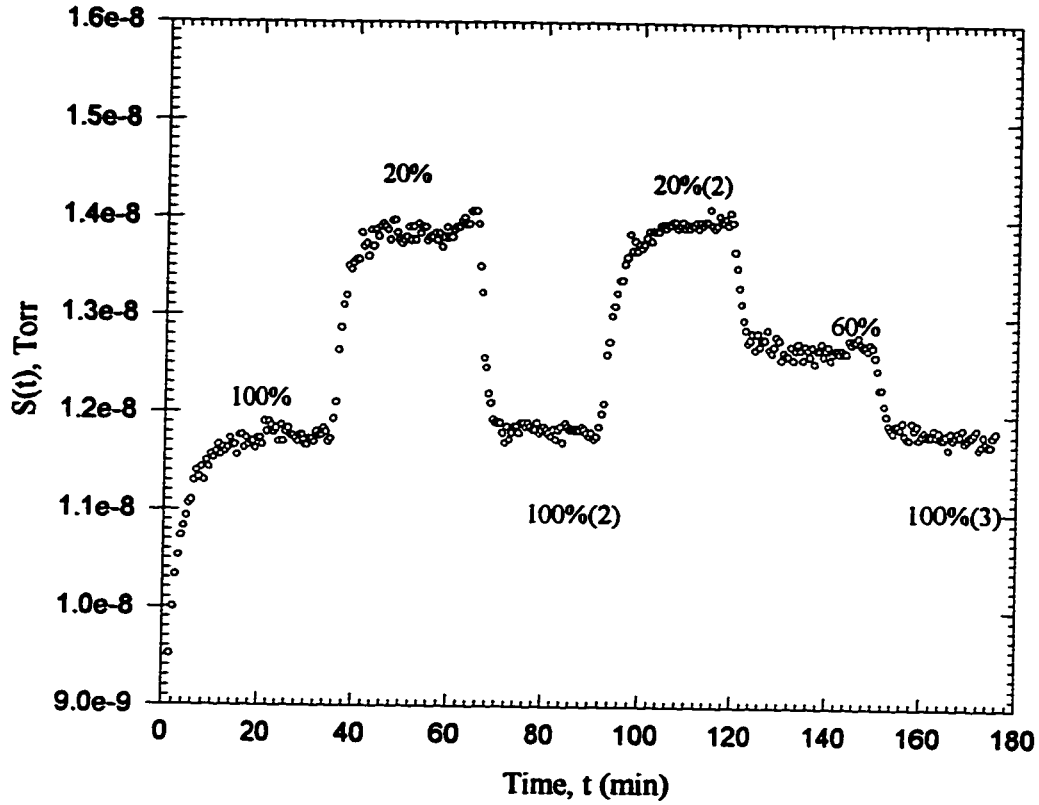
Solids (@start)	1713.96 g	Bulk density	995.13 kg/m³
Solids(@end)	1707.79 g	F_E	0.014062

No condensation and no dusting in the drum.
Ratio of drum wall velocity to maximum superficial gas velocity, V_W/u = 11.8

Flow (%)	Q (L/min)	S* (Torr)	Piece	k_tA(L/min) piece method	k_tA(L/min) by slope method
100	5.670	1.1767e-8	100% to 20%	24.32	b= 68823828.89
20	1.123	1.3870e-8	20% to 100%(2)	25.18	m= 2830442.45
100(2)	5.674	1.1824e-8	100%(2) to 20%(2)	24.16	R^2= 0.997
20(2)	1.123	1.3952e-8	20%(2) to 60%	21.46	k_tA=b/m = 24.32
60	3.396	1.2676e-8	60% to 100%(3)	33.35	
100(3)	5.672	1.1786e-8	20%(2) to 100%(3)	23.63	
				Avg. 25.35	

RD EX#49 No baffles(rolling bed) η=17.2% N= 1.059 rpm
T=23.0 °C, P=714.5 mmHg, Bed T=22.7 °C
5slm@100%,20%, Q=1.117-5.647 L/min

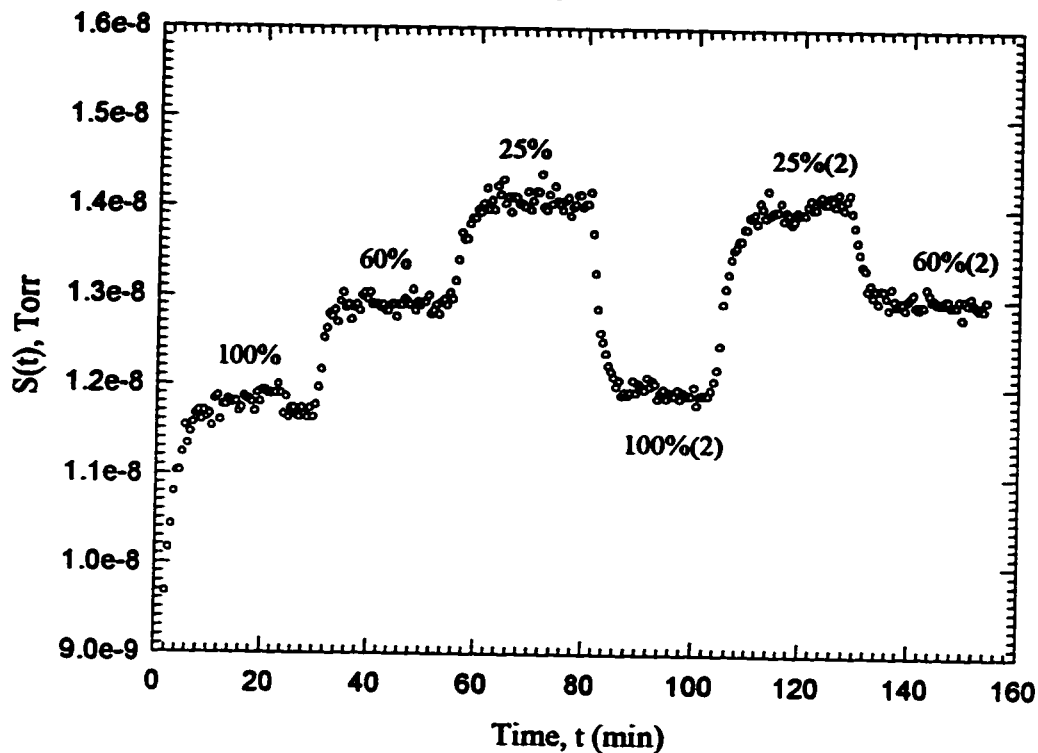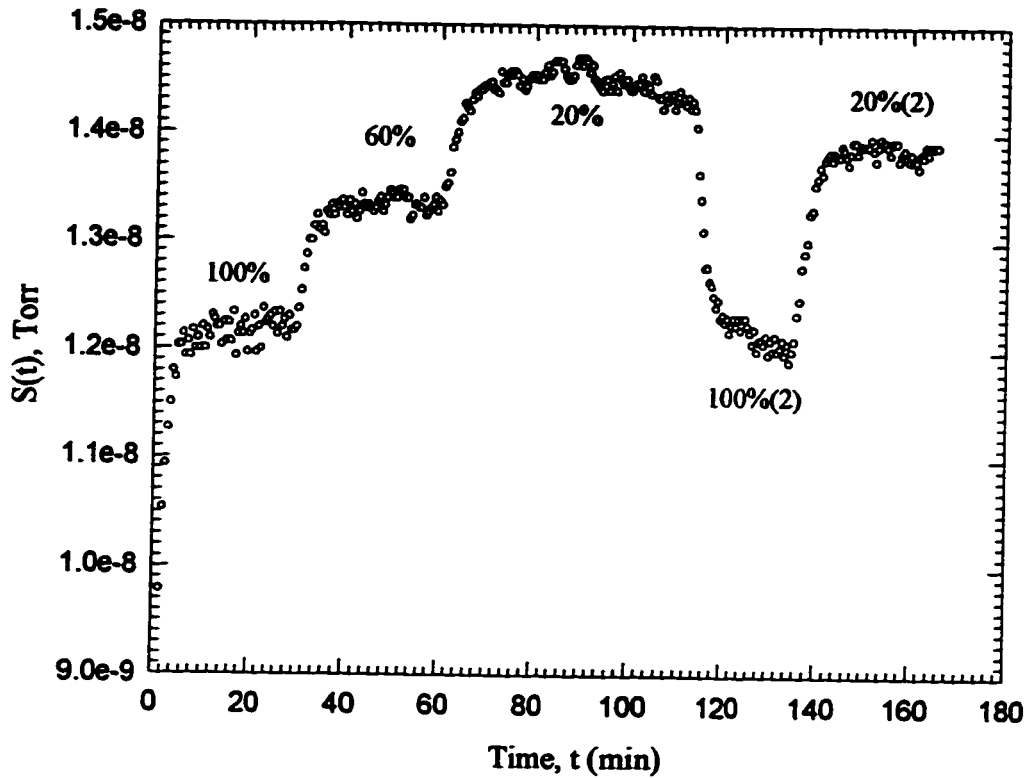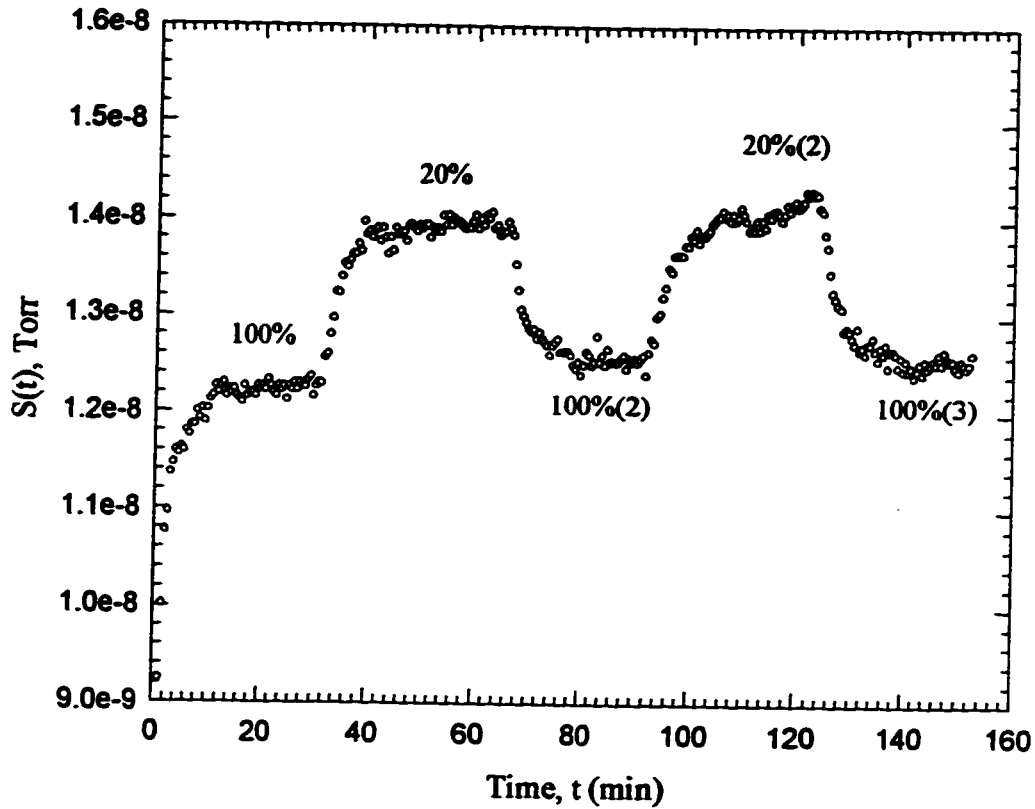Solids (@start)   3425.99 g   Bulk density   999.61 kg/m³
Solids(@end)   3419.63 g F_E 0.00722
No condensation and no dusting in the drum.
Ratio of drum wall velocity to maximum superficial gas velocity, V_w/u = 11.3

Flow (%)	Q (L/min)	S^{ss} (Torr)	Piece	k_sA(L/min) piece method	k_sA(L/min) by slope method
100	5.642	1.2257e-8	100% to 20%	31.90	b= 69166518.38
20	1.117	1.3937e-8	20% to 100%(2)	40.40	m= 1976212.7
100(2)	5.647	1.2566e-8	100%(2) to 20%(2)	36.32	R^2= 0.972
20(2)	1.118	1.4086e-8	20%(2) to 100%(3)	35.41	k_sA=b/m = 34.99
100(3)	5.647	1.2532e-8			
				Avg. 36.01	

RD Ex#51 No baffles(rolling bed) η=17.2% N=1.104 rpm
T=22.8 °C, P=708.1 mmHg, Bed T=22.6 °C
5slm@100%,60%,20%, Q=1.126-5.697 L/min

Solids (@start)	3429.51 g	Bulk density	996.56 kg/m³
Solids(@end)	3424.09 g	F_E	0.00617

No condensation and no dusting in the drum.
Ratio of drum wall velocity to maximum superficial gas velocity, V_W/u = 11.7

Flow (%)	Q (L/min)	S^{ss} (Torr)	Piece	k_aA(L/min) piece method	k_aA(L/min) by slope method
100	5.688	1.1577e-8	100% to 60%	22.88	b= 68876624.804
60	3.408	1.2581e-8	60% to 20%	25.61	m= 2584635.80
20	1.126	1.3655e-8	100%(2) to 60%(2)	30.02	R²= 0.841
100(2)	5.697	1.2363e-8	60%(2) to 20%(2)	29.27	k_aA=b/m = 26.65
60(2)	3.412	1.3208e-8			
20(2)	1.127	1.4201e-8			
				Avg. 26.95	

RD Ex#52 No baffles(rolling bed) η=25% N=1.068 rpm
T=22.7 °C, P=708mmHg, Bed T=22.8 °C
5slm@100%,60%,20%, Q= 1.127-5.694 L/min

Solids (@start)	4965.48 g	Bulk density	993.17 kg/m³
Solids(@end)	4958.55 g	F_E	0.0055

No condensation and no dusting in the drum.
Ratio of drum wall velocity to maximum superficial gas velocity, V_W/u = 11.3

Flow (%)	Q (L/min)	S∞ (Torr)	Piece	k_aA(L/min) piece method	k_aA(L/min) by slope method
100	5.694	1.2925e-8	100% to 60%	52.58	b= 70960054.83
60	3.407	1.3453e-8	100% to 20%	67.04	m= 1138580.52
20	1.127	1.3791e-8	20% to 100%(2)	60.53	R^2= 0.979
100(2)	5.694	1.2840e-8	100%(2) to 20%(2)	58.47	k_aA=b/m = 62.32
20(2)	1.127	1.3824e-8			
60(2)	3.409	1.3401e-8			
				Avg. 59.66	

RD EX#53 No baffles(rolling bed) η= 25%, N=1.054 rpm
T=22.5 °C, P=714.5mmHg, Bed T=22.3 °C
5slm@100%,20%, Q=1.114-5.651 L/min

Solids (@start)   4958.55 g   Bulk density   998.53 kg/m^3
Solids(@end)   4952.58 g F_E 0.004816
No condensation and no dusting in the drum.
Ratio of drum wall velocity to maximum superficial gas velocity, V_W/u = 11.2

Flow (%)	Q (L/min)	S^{ss} (Torr)	Piece	k_eA(L/min) piece method	k_eA(L/min) by slope method
100	5.694	1.2037e-8	20% to 100%(2)	65.38	b= 74024833.49
20	3.407	1.3196e-8	100%(2) to 20%(2)	54.52	m= 1242534.62
100(2)	1.127	1.2358e-8			R^2= 0.819
20(2)	5.694	1.3328e-8		Avg. 59.95	k_eA=b/m = 59.57
100(3)	1.127	1.2645e-8			

RD Ex#14 8 baffles, η=4.3%, N=0.0873 rpm
T=22.2 ^{o}C, P=711.1mmHg, Bed T=22.8 ^{o}C
5SLM @50%, 35%, 20%, Q= 1.119-2.821 L/min
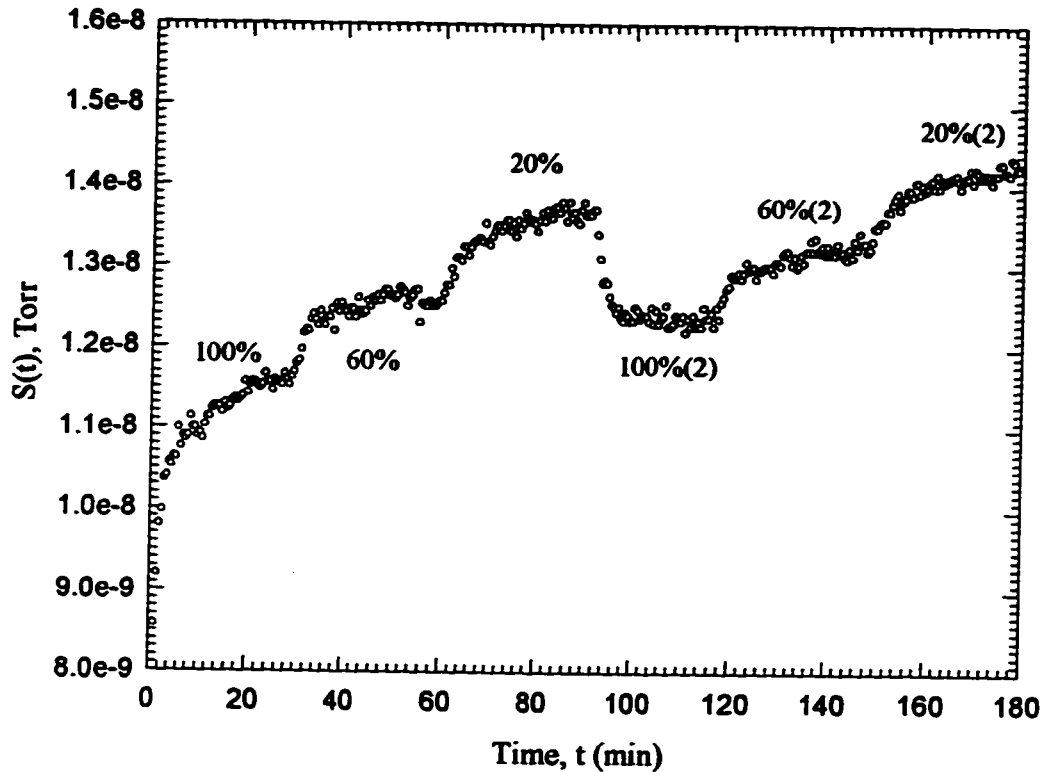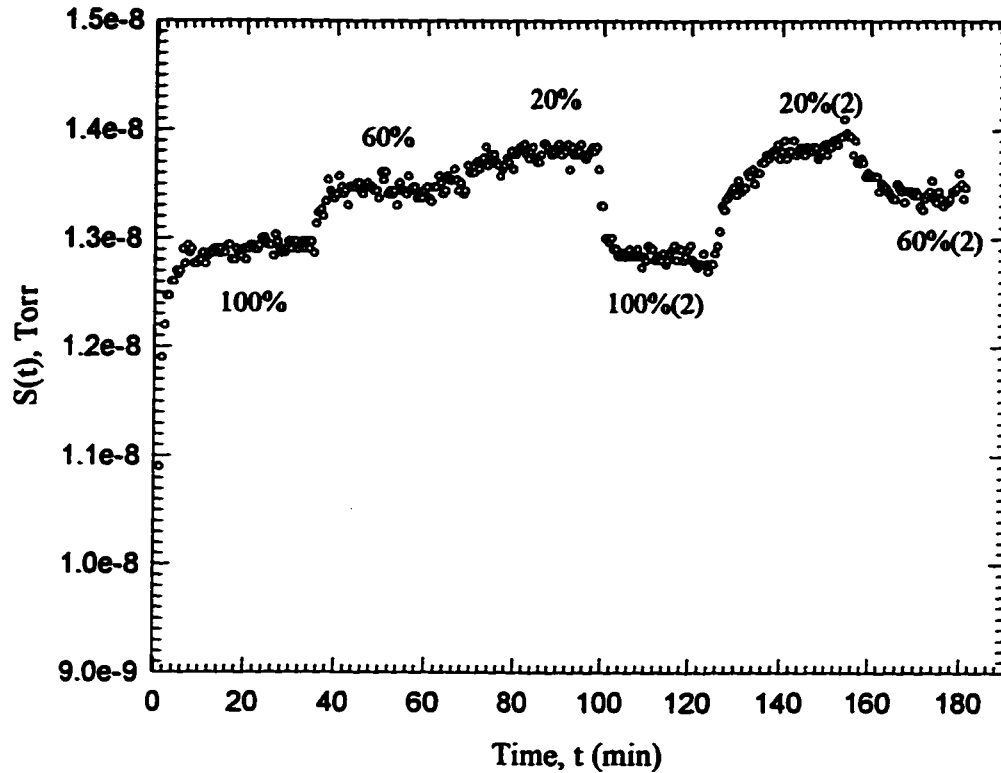

Solids (@start)   855.48 g   Bulk density 992.4 kg/m^3
Solids (@end   852.20 g F_E 0.01498
No condensation and no dusting in the drum.
Ratio of drum wall velocity to maximum superficial gas velocity, V_W/u = 1.86

Flow (%)	Q(L/min)	S^{ss} (Torr)	Piece	k_sA(L/min) by piece method	k_sA(L/min) by slope method
50	2.821	1.0796e-8	50% to 20%	12.90	b= 75784610.80
20	1.119	1.2107e-8	20% to 50%(2)	15.22	m= 5986765.15
35	1.970	1.1421e-8	50% to 35%	12.73	R^2= 0.881
50(2)	2.821	1.0965e-8	20% to 35%	13.05	k_sA=b/m = 12.66
20(2)	1.120	1.2366e-8	50%(2) to 20%(2)	12.19	
35(2)	1.972	1.1036e-8		Avg. 13.218	

RD Ex#13 8 baffles, η =4.3%, N=0.25 rpm
T=21.5 $^{\circ}$C, P=711.5mmHg, bed T= 21.9 $^{\circ}$C
5 slm@20%,50%, 75%, Q=1.116 - 4.229 L/min

Solids (@start)	853.25 g	Bulk density	987.4 kg/m^3
Solids (@end	849.19 g	F_E	0.01859

No condensation and no dusting in the drum.
Ratio of drum wall velocity to maximum superficial gas velocity, V_W/u = 3.52

Flow (%)	Q(L/min)	S^{ss} (Torr)	Piece	k_sA(L/min) piece method	k_sA(L/min) by slope method
75	4.229	1.1195e-8	75% to 20%	22.66	b= 76773542.27
50	2.813	1.1889e-8	75% to 50%	20.03	m= 2889543
20	1.116	1.2661e-8	20% to 75%(2)	24.08	R^2= 0.96
75(2)	4.228	1.1269e-8	50% to 20%	25.02	k_sA=b/m = 26.7
50(2)	2.812	1.1694e-8	50% to 75%(2)	22.91	
20(2)	1.116	1.2334e-8			
				Avg. 22.94	

RD Ex#17 8baffles, η=4.3%, N=1.127rpm
T=21.9 °C, P=717.6 mmHg, Bed T=21.9 °C
5slm@100%,50%,20%, Q=1.108-5.615 L/min
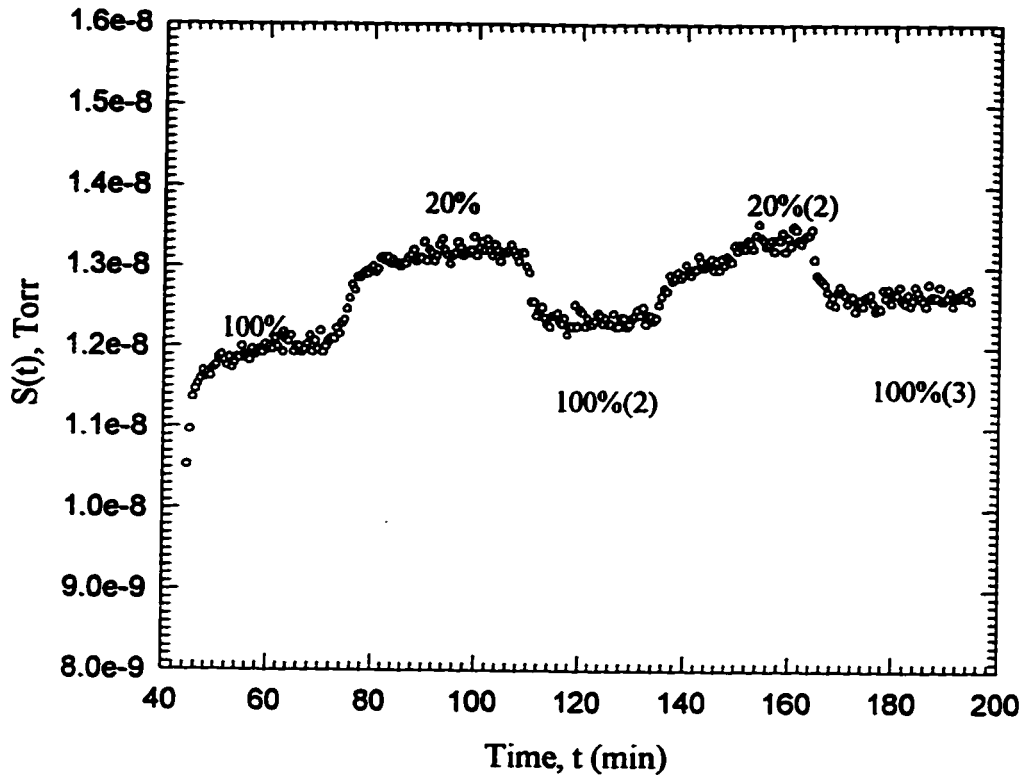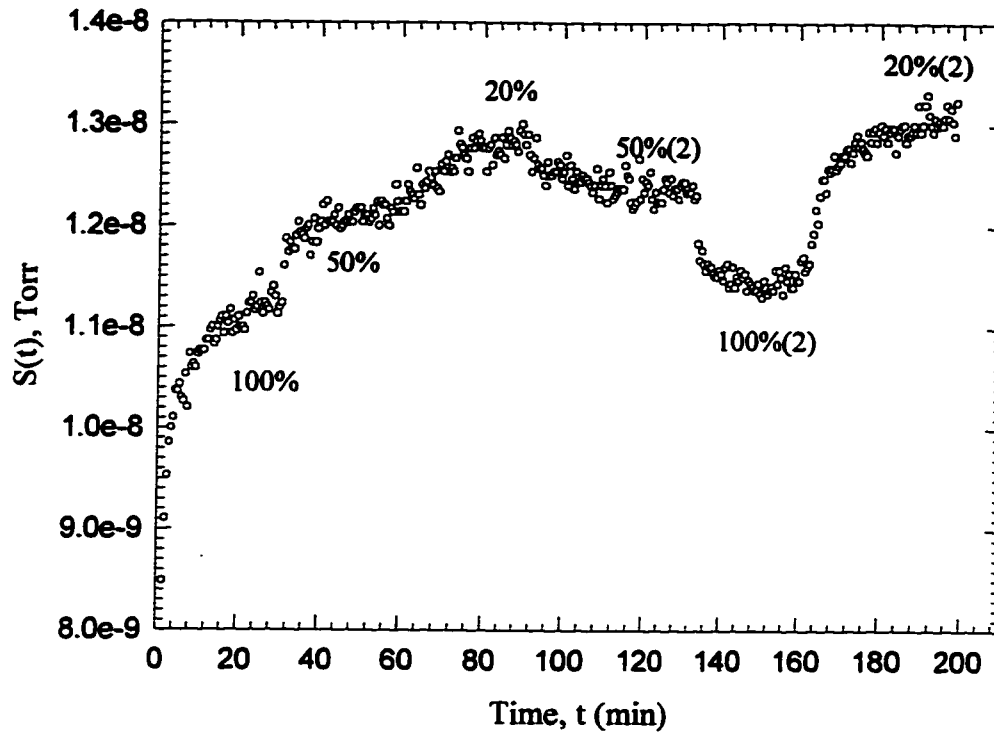

Solids (@start)   855.50 g   Bulk density   993.08 kg/m^3
Solids (@end   849.40 g F_E 0.02785
No condensation and no dusting in the drum.
Ratio of drum wall velocity to maximum superficial gas velocity, V_W/u = 12.0

Flow (%)	Q(L/min)	S^{ss} (Torr)	Piece	k$_s$A(L/min) piece method	k$_s$A(L/min) by slope method
100	5.606	1.1200e-8	100% to 50%	31.64	b= 74991112.08
50	2.793	1.2115e-8	50% to 20%	29.54	m= 2375553.086
20	1.108	1.2781e-8	100% to 20%	30.75	R^2= 0.96
50(2)	2.796	1.2348e-8	20% to 100%(2)	38.12	k$_s$A=b/m = 31.57
100(2)	5.615	1.1464e-8	100%(2) to 75%(2)	32.14	
20(2)	1.111	1.3017e-8		Avg.32.44	

Rd Ex#21 8 baffles, η=4.3%, N=1.468rpm
T=22.7 $^{\circ}$C, P=691.6 mmHg, Bed T=23.1 $^{\circ}$C
5slm@ 100%, 80%, 60%, 40%Q=2.322 - 5.825 L/min
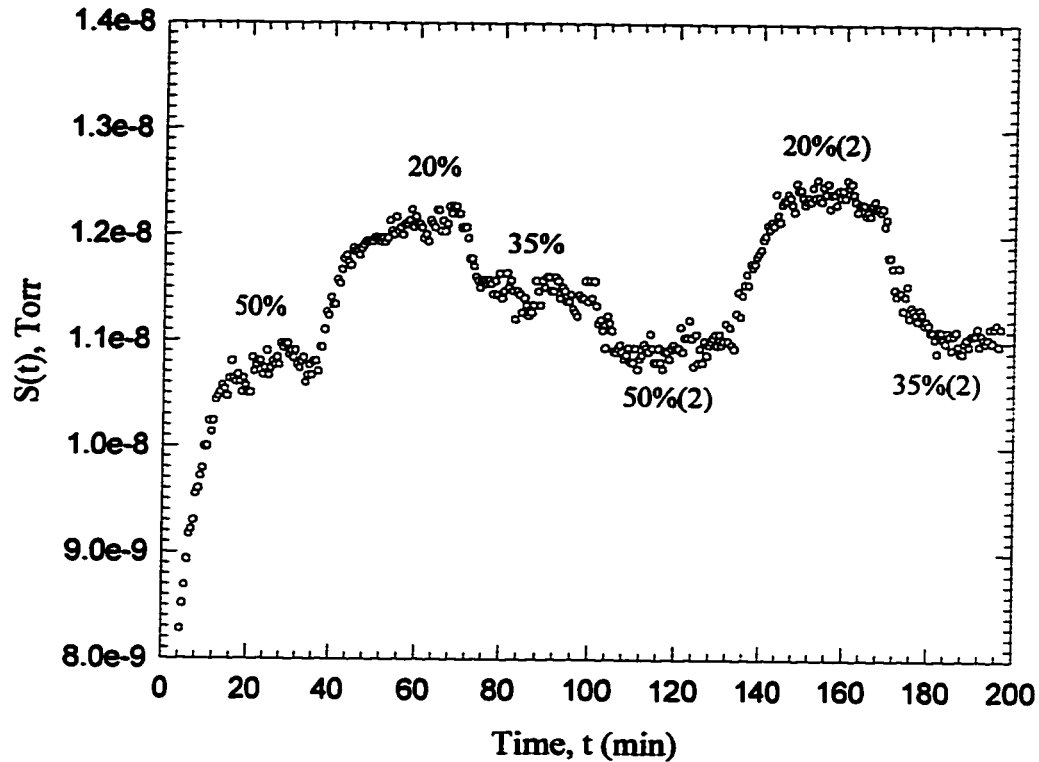

Solids (@start)   856.77 g   Bulk density   992.7 kg/m^3
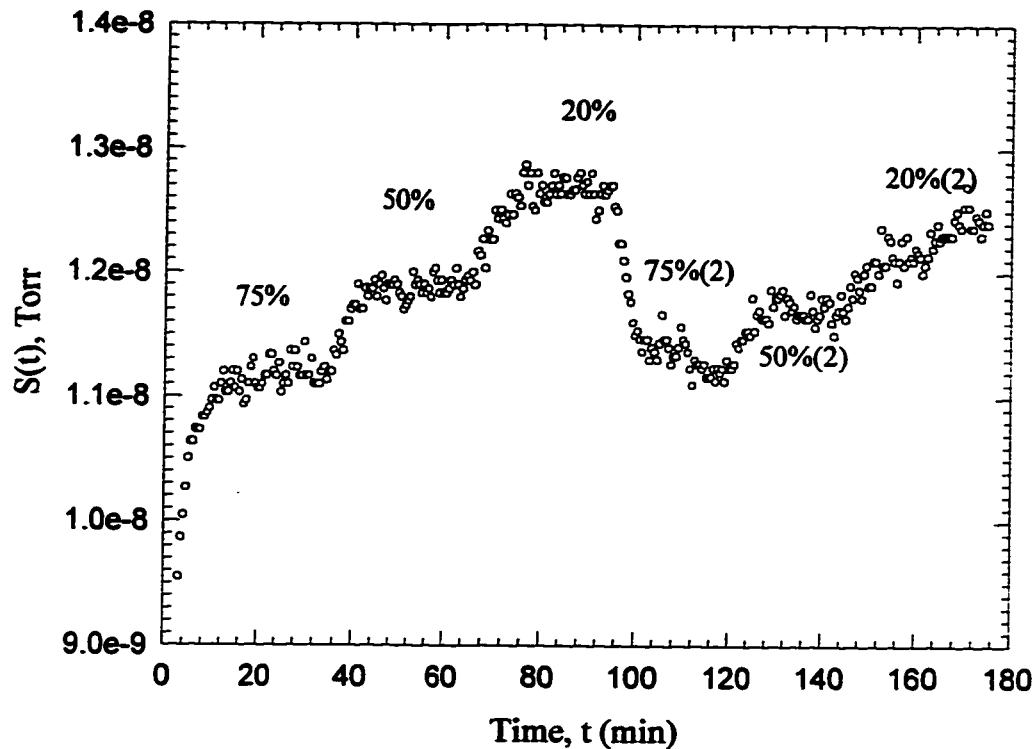Solids (@end   847.44 g F_E 0.04254
No condensation and no dusting in the drum.
Ratio of drum wall velocity to maximum superficial gas velocity, $V_W/u = 15.1$

Flow (%)	Q(L/min)	S^{ss} (Torr)	Piece	$k_s A$(L/min) piece method	$k_s A$(L/min) by slope method
100	5.818	1.3454e-8	60% to100%(2)	58.69	b= 64259264.49
80	4.651	1.3882e-8	100%(2) to 40%	53.00	m= 1572262.66
60	3.485	1.4310e-8	40% to 80%(2)	56.72	R^2= 0.925
100(2)	5.825	1.3791e-8			k_sA=b/m = 40.87
60(2)	3.493	1.4292e-8		Avg.56.14	
40	2.323	1.4664e-8			
80(2)	4.663	1.4105e-8			
40(2)	2.322	1.4827e-8			

RD Ex#26 8 baffles, η=4.3%, N=0.944 rpm
T=23.6 °C, P=713.53 mmHg, BedT=23.6 °C
5slm@100%, 60%, 25% Q=1.404-5.666 L/min

Solids (@start)	854.61 g	Bulk density	998.5 kg/m³
Solids (@end	845.50 g	F_E	0.04164

No condensation and no dusting in the drum.
Ratio of drum wall velocity to maximum superficial gas velocity, V_W/u = 10.0

Flow (%)	Q(L/min)	S^{ss} (Torr)	Piece	k_rA(L/min) piece method	k_rA(L/min) by slope method
100	5.666	1.2704e-8	100%(3) to 25%(3)	30.22	b= 68052132.63
60	3.393	1.2915e-8	25%(2) to 100%(3)	28.336	m= 2157326.02
25	1.405	1.3811e-8	60%(2) to 25%(2)	26.55	R^2= 0.905
100(2)	5.666	1.2229e-8	60%(3) to 25%(3)	33.57	k_rA=b/m = 31.54
60(2)	3.392	1.3346e-8		Avg.29.67	
25(2)	1.404	1.4295e-8			
100(3)	5.664	1.2504e-8			
60(3)	3.397	1.3423e-8			
25(3)	1.406	1.4187e-8			

RD EX#25 8 baffles, η=4.3%, N=1.26 rpm
T=23.3 °C, P=700.15 mmHg, Bed T=23.8 °C
5slm@100%, 60%, 25% Q=1.430-5.77 L/min
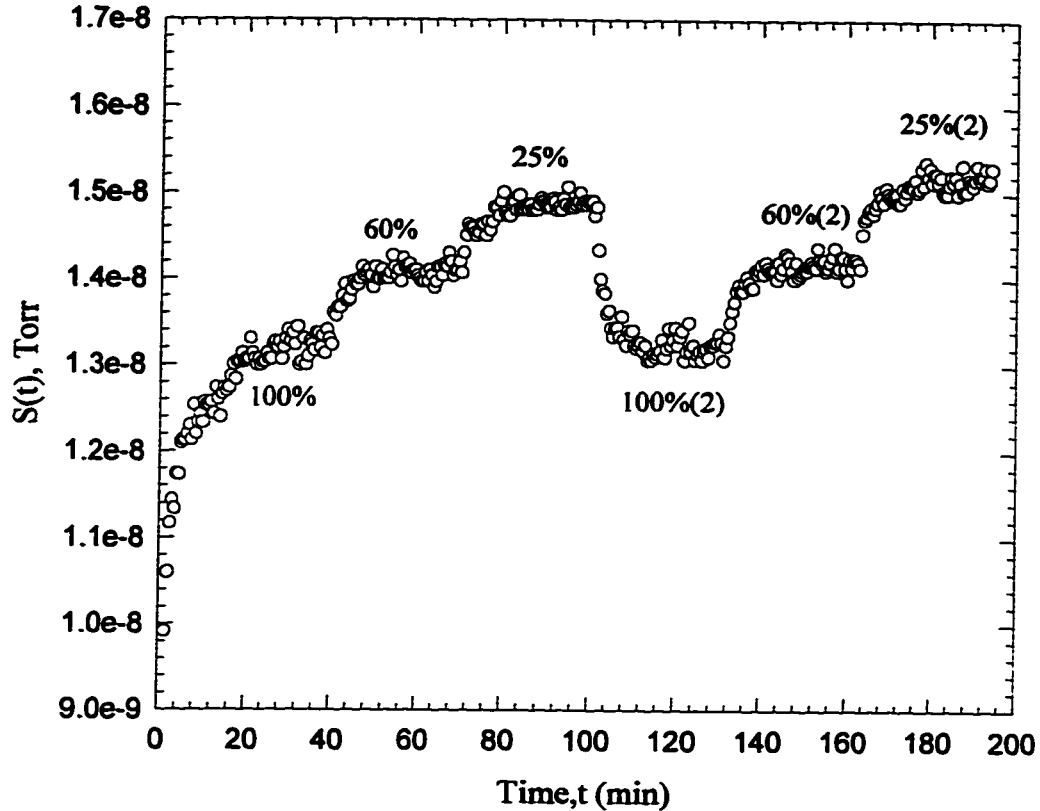
Solids (@start)	858.73 g	Bulk density	998.2 kg/m^3
Solids (@end	850.96 g	F_E	0.03534

No condensation and no dusting in the drum.
Ratio of drum wall velocity to maximum superficial gas velocity, V_W/u = 13.2

Flow (%)	Q(L/min)	S^{ss} (Torr)	Piece	k$_s$A(L/min) piece method	k$_s$A(L/min) by slope method
100	5.77	1.3223e-8	100% to60%	32.20	b= 63620944.36
60	3.454	1.4082e-8	60% to 25%	34.60	m= 2080149.847
25	1.43	1.4873e-8	100% to 25%	33.35	R^2= 0.988
100(2)	5.765	1.3227e-8	25% to 100%(2)	33.41	k$_s$A=b/m = 30.58
60(2)	3.454	1.4167e-8	100%(2) to 60%(2)	29.064	
25(2)	1.431	1.5161e-8		Avg. 32.52	

RD Ex#27 8 baffles, η= 4.3%, N=0.421 rpm
T=23.8 °C, P=710.24 mmHg, Bed T=23.3 °C
5slm@ 100%, 60%, 25% Q=1.412-5.706 L/min
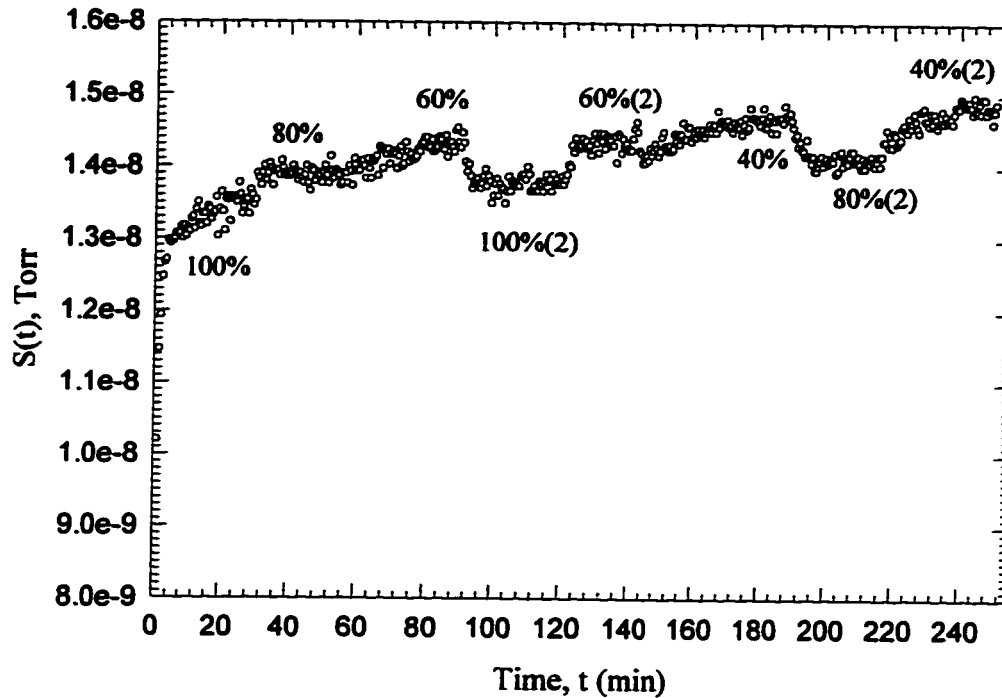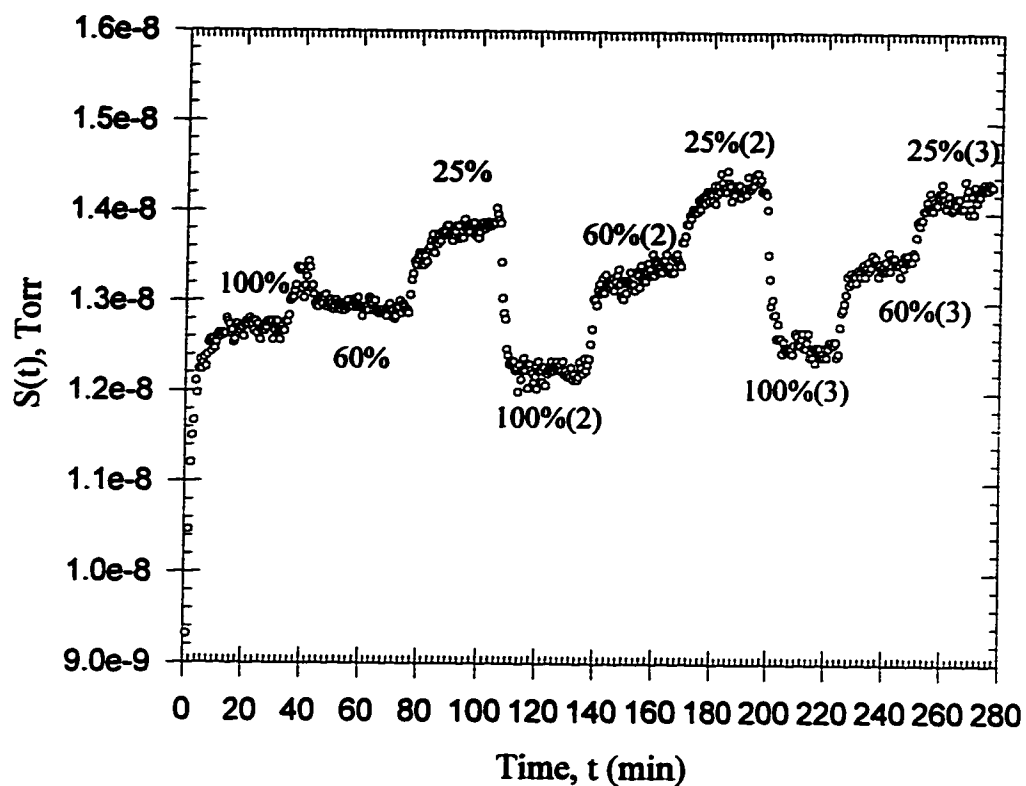

Solids (@start)   855.10 g   Bulk density   992.5 kg/m^3
Solids (@end   847.46 g F_E 0.03490
No condensation and no dusting in the drum.
Ratio of drum wall velocity to maximum superficial gas velocity, V_W/u = 4.44

Flow (%)	Q(L/min)	S^{ss} (Torr)	Piece	k_tA(L/min) piece method	k_tA(L/min) by slope method
100	5.690	1.1849e-8	100% to 25%	22.70	b= 68103035.97
60	3.413	1.2841e-8	25% to 100%(2)	26.59	m= 2702879.88
25	1.412	1.3951e-8	25%(2) to 60%(3)	31.76	R^2= 0.981
100(2)	5.706	1.2095e-8	60% to 25%	21.74	k_tA=b/m = 25.2
60(3)	3.409	1.3057e-8	100%(2) to 25%(2)	28.30	
25(2)	1.412	1.3844e-8		Avg.26.218	

RD Ex#28 8 baffles, η=4.3%, N=0.688 rpm
T=23.5 C, P=709.4 mmHg, Bed T=23.2 $^{\circ}$C
5slm@100%, 60%, 25% Q=1.412-5.695L/min

Solids (@start)	860.45 g	Bulk density 1005 kg/m^3
Solids (@end	853.64 g	F_E 0.03092

No condensation and no dusting in the drum.
Ratio of drum wall velocity to maximum superficial gas velocity, V_W/u = 7.3

Flow (%)	Q(L/min)	S^{ss} (Torr)	Piece	k$_g$A(L/min) piece method	k$_g$A(L/min) by slope method
100	5.695	1.2770e-8	100% to 25%	43.23	b= 69139031.16
60	3.415	1.3669e-8	25%(2) to 100%(2)	36.08	m= 1767911.36
25	1.412	1.3996e-8	25% to 100%(2)	32.91	R^2= 0.870
100(2)	5.693	1.2444e-8	60%(2) to 25%(2)	30.73	k$_g$A=b/m = 39.1
60(2)	3.414	1.3052e-8			
25(2)	1.412	1.3865e-8		Avg.35.74	

RD Ex#22 8 baffles, η=4.3%, N=0.707 rpm
T=22.7 °CP=691.3mmHg, Bed T=23.2 °C,
5slm@100%,70%,30% Q=1.738-5.834 L/min

| Solids (@start) | 858.04 g | Bulk density | 997.2 kg/m^3 |
| Solids (@end | 850.23 g | F_E | 0.03556 |

No condensation and no dusting in the drum.
Ratio of drum wall velocity to maximum superficial gas velocity, V_W/u = 7.3

Flow (%)	Q(L/min)	S^{ss} (Torr)	Piece	k$_t$A(L/min) piece method	k$_t$A(L/min) by slope method
100	5.824	1.3095e-8	70% to 30%	48.77	b= 66058494.87
70	4.073	1.3865e-8	30% to 100%(2)	46.61	m= 1635267.02
30	1.738	1.4506e-8	100%(2) to 30%(2)	44.64	R^2= 0.951
100(2)	5.830	1.3374e-8	70% to 100%(2)	43.78	k$_t$A=b/m = 40.4
70(2)	3.706	1.3720e-8			
30(2)	1.741	1.4553e-8		Avg.45.95	

RD Ex#41 8 baffles, η=4.3%, N=1.946rpm
T=22.3 °C, P=706.8mmHg, BedT=22.4 °C
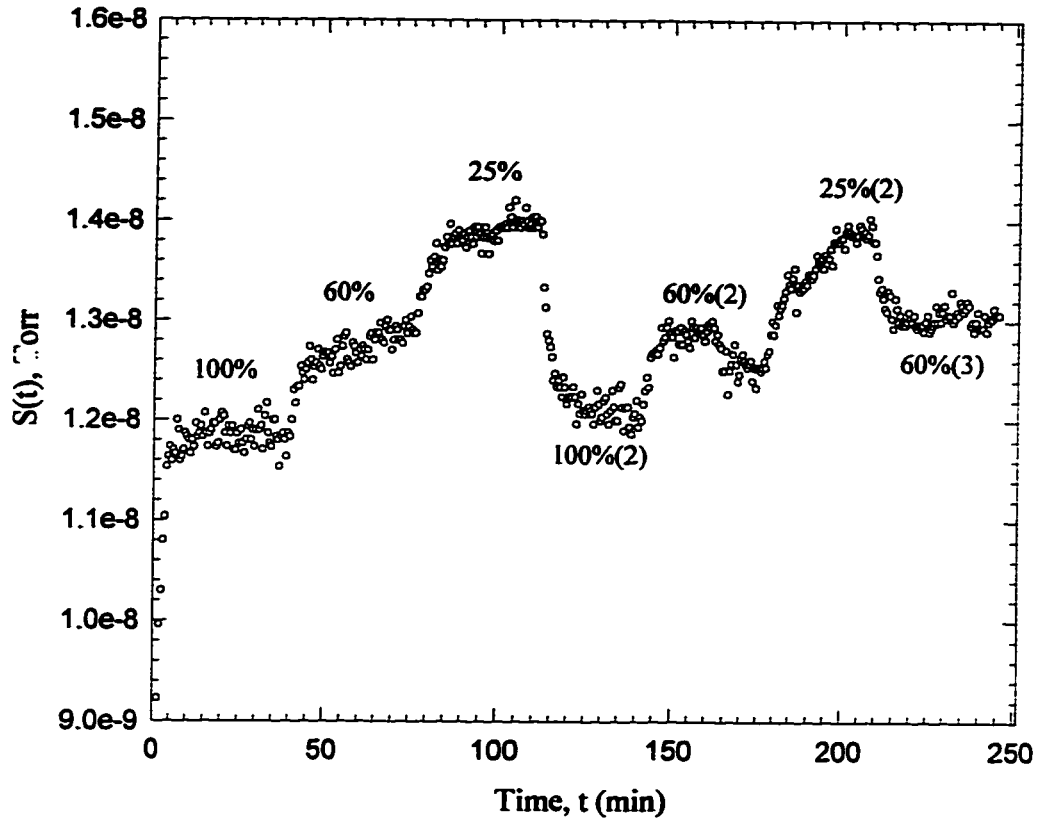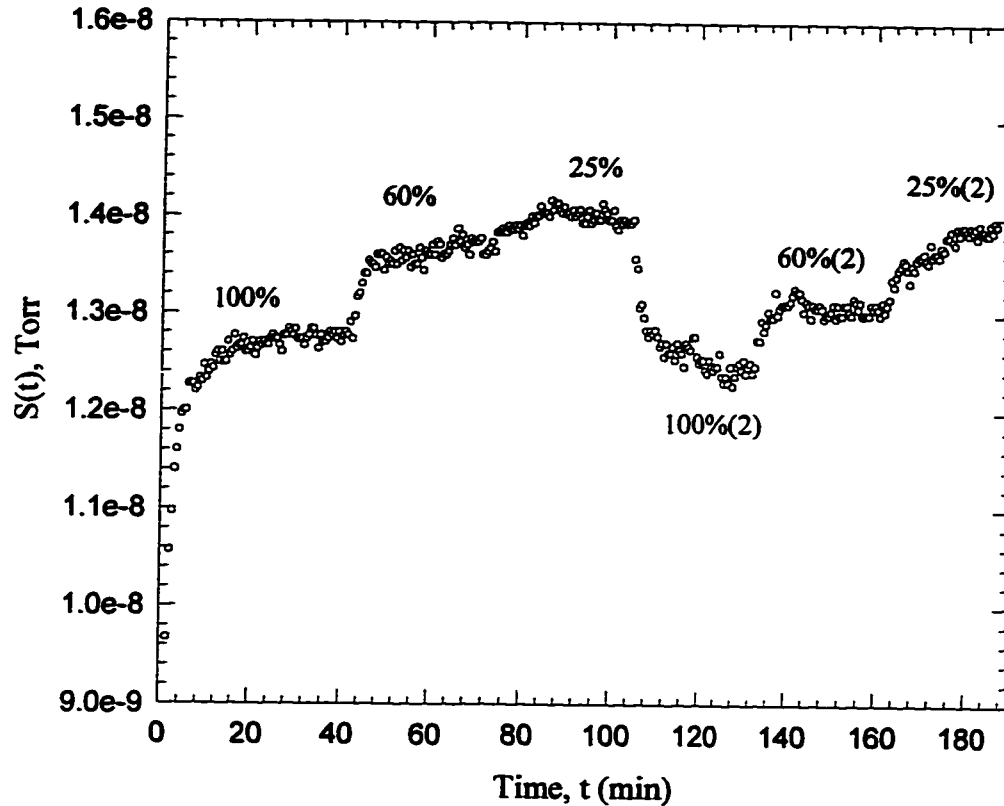100slm@10%,7%,4%, Q=6.643-13.036L/min

Solids (@start)   858.05 g   Bulk density 1001 kg/m^3
Solids (@end   846.43 g F_E 0.0529
No condensation and no dusting in the drum.
Ratio of drum wall velocity to maximum superficial gas velocity, $V_W/u = 9.0$

Flow (%)	Q(L/min)	S^{ss} (Torr)	Piece	k_sA(L/min) piece method	k_sA(L/min) by slope method
10	13.036	1.1463e-8	4% to 10%(2)	63.30	b= 71952916.81
4	6.643	1.2504e-8	10% to 4%	63.75	m= 1202574.8
7	9.832	1.1884e-8	10%(2) to 7%	77.41	R^2= 0.965
10(2)	13.035	1.1457e-8	4% to 7%	54.48	k_sA=b/m = 59.83
4(2)	6.651	1.2629e-8	7% to 10%(2)	76.11	
7(2)	9.848	1.1782e-8		Avg. 67.01	

RD EX# 23 8 baffles, η=4.3%, N=1.363 rpm
T=23.5 °C, P=692.6 mmHg, Bed T=23.2 °C
100slm@4%, 7%, 10%, 15% Q=6.805 - 18.809 L/min
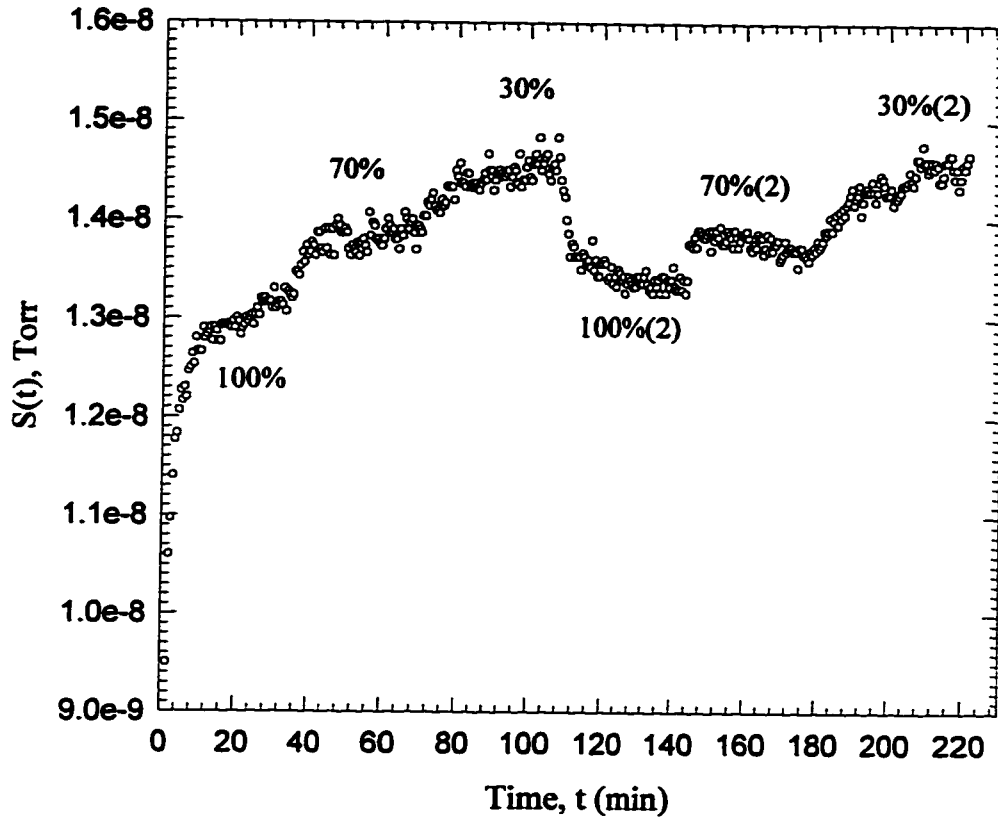

Solids (@start)   856.40 g   Bulk density   995.8 kg/m³
Solids (@end   836.21 g F_E 0.09209
No condensation and no dusting in the drum.
Ratio of drum wall velocity to maximum superficial gas velocity, $V_W/u = 6.1$

Flow (%)	Q(L/min)	S^{ss} (Torr)	Piece	k_sA(L/min) piece method	k_sA(L/min) by slope method
4	6.805	1.3548e-8	4% to 15%*	58.35 *	b= 64943194.2
10	13.345	1.1941e-8	15% * to 4%(2)	67.23 *	m= 1415475.08
*15	18.777*	1.1445e-8*	10% to 4%(2)	50.86	R²= 0.98
4(2)	6.819	1.3292e-8	4% to 10%	50.11	k_sA=b/m = 45.88
10(2)	13.368	1.1932e-8	4%(2) to 15%(2)*	58.52 *	
*15(2)	18.809*	1.2131e-8*	4%(2) to 10%(2)	50.64	
7	10.082	1.2587e-8		Avg. 50.54	

Note: * means that air was bypassing the drum at that Flow(%). k_sA values (piecewise and slope methods)
were calculated by excluding the values marked by * due to bypassing of gas.

RD Ex#11 8 baffles, η=4.3%, N=0.487 rpm
T=22.2 $^\circ$C, P=713.05mmHg, BedT=22.4 $^\circ$C
100slm@3%,5%, 7%, 10%, 15% Q=7.642-18.187 L/min
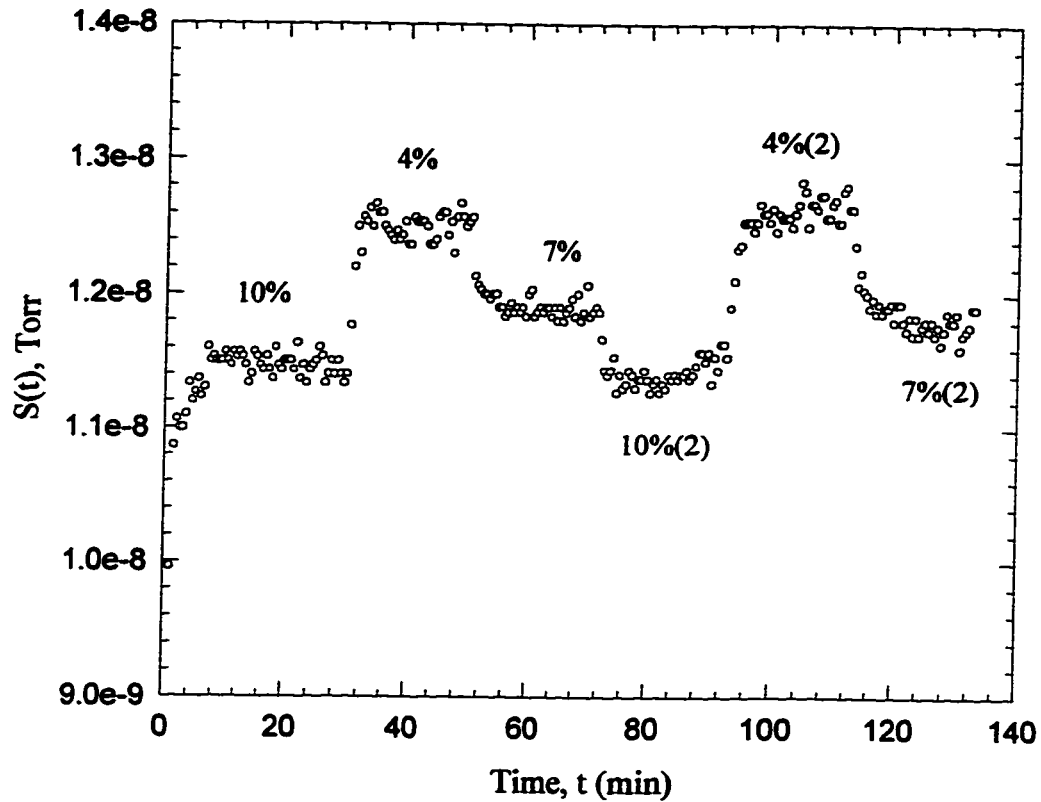

Solids (@start)   863.67 g   Bulk density   998.5 kg/m^3
Solids (@end   846.04 g F_E 0.07984

No condensation and no dusting in the drum.

Ratio of drum wall velocity to maximum superficial gas velocity, V_W/u = 2.2

Flow (%)	Q(L/min)	S^{ss} (Torr)	Piece	k_sA(L/min) piece method	k_sA(L/min) by slope method
3	5.531	1.1877e-8	10% to 15%*	78.05 *	b= 75227636.7
5	7.644	1.1383e-8	15% * to 5%(2)	65.38 *	m= 1834348
10	12.921	1.0282e-8	10% to 3%(2)	48.23	R^2= 0.933
*15	18.187*	9.6521e-9*	15%* to 3%(2)	54.25*	k_sA=b/m =41.01
5(2)	7.642	1.1046e-8	3%(2) to 10%(2)	40.88	
3(2)	5.528	1.1696e-8	5%(2) to 10%(2)	48.02	
10(2)	12.91	1.0091e-8	5%(2) to 3%(2)	30.40	
			3% to 5%	43.15	
				Avg. 42.14	

Note: * means that air was bypassing the drum at that Flow(%). k_sA values (piecewise and slope methods) were calculated by excluding the values marked by * due to bypassing of gas.

RD EX#29 8 baffles, η=8.6%, N= 0.38 rpm
T=23.3 °C, Bed T=22.8 °C, P=710.3 mmHg
5 slm@100%,60%,25%, Q=1.409-5.69 L/min
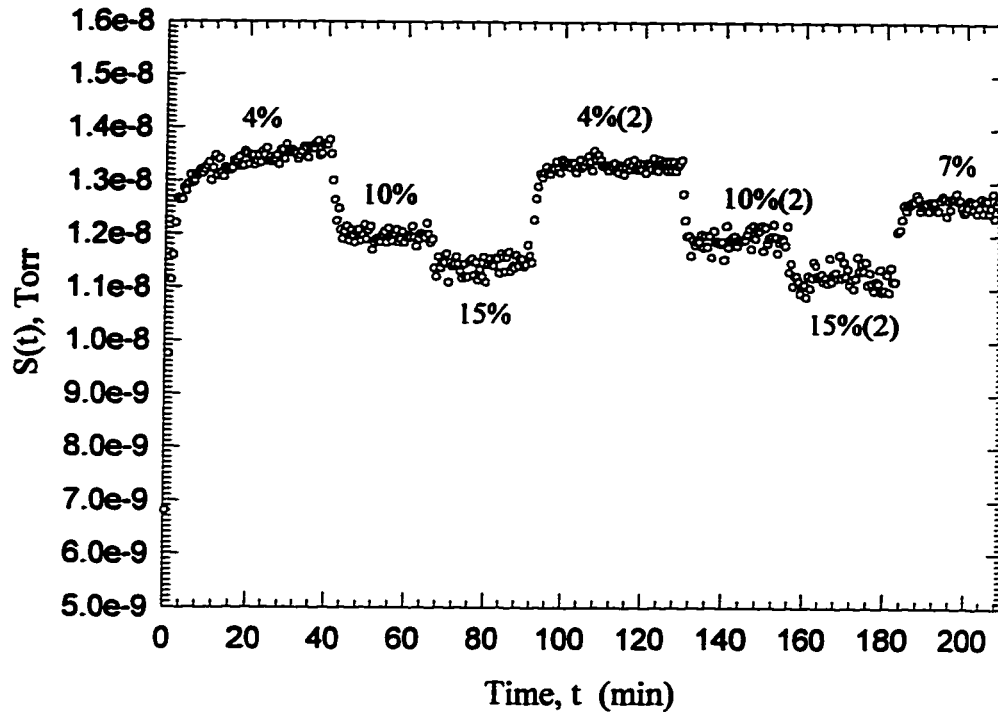

Solids (@start)   1713.47 g   Bulk density   996.2 kg/m³
Solids (@end   1706.64 g F_E 0.01557
No condensation and no dusting in the drum.
Ratio of drum wall velocity to maximum superficial gas velocity, V_W/u = 4.0

Flow (%)	Q(L/min)	S$^{\infty}$ (Torr)	Piece	k_sA(L/min) piece method	k_sA(L/min) by slope method
100	5.674	1.1847e-8	100% to 60%	19.50	b=66389478.59
60	3.406	1.3020e-8	60% to 25%	16.84	m= 2945524.64
25	1.411	1.4443e-8	100% to 25%	18.01	R²= 0.956
100(2)	5.690	1.2272e-8			k_sA=b/m = 22.54
60(2)	3.403	1.3031e-8		Avg. 18.12	
25(2)	1.409	1.3995e-8			

RD Ex# 30 8 baffles, η=8.6%, N=0.794 rpm
T=23.2 °C, P=711.6 mmHg, Bed T=22.9°C
5slm@ 100%, 60%, 30% Q=1.689-5.681 L/min

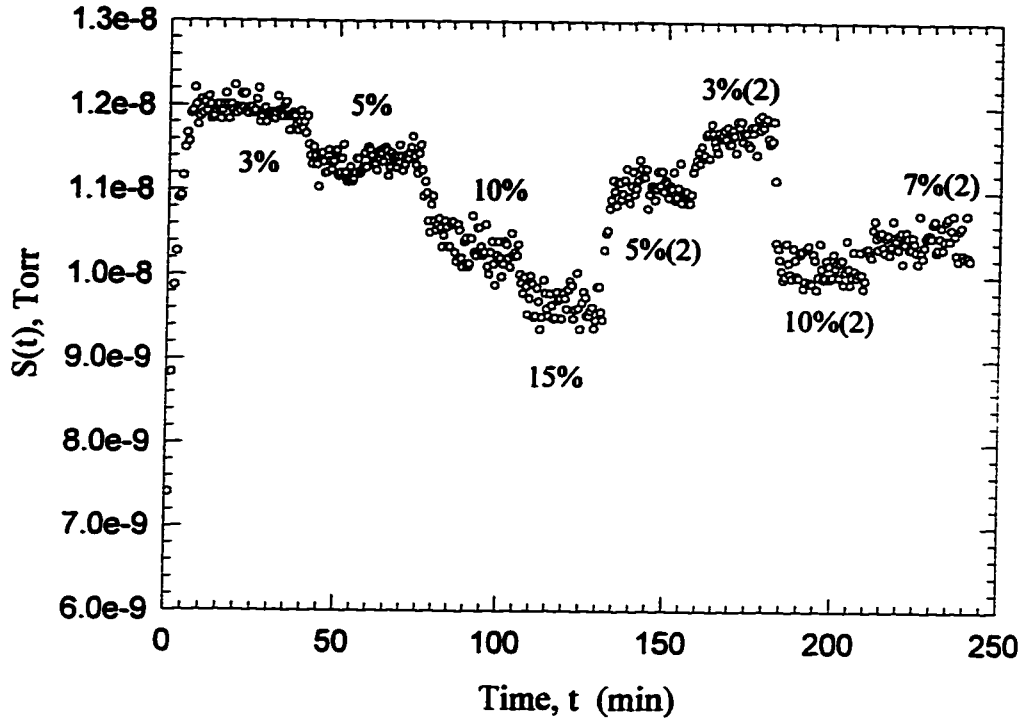| Solids (@start)	1712.66 g	Bulk density	993.6 kg/m^3
Solids (@end	1706.05 g	F_E	0.01371

No condensation and no dusting in the drum.
Ratio of drum wall velocity to maximum superficial gas velocity, V_w/u = 8.4

Flow (%)	Q(L/min)	S^{ss} (Torr)	Piece	k_sA(L/min) piece method	k_sA(L/min) by slope method
100	5.667	1.2725e-8	100% to 30%	21.57	b=62766649.92
60	3.394	1.388e-8	100%(2) to 30%(2)	25.04	m= 2711952.19
30	1.689	1.4901e-8	100% to 60%	21.65	R^2= 0.995
100(2)	5.681	1.2856e-8	60%(2) to 30%(2)	26.87	k_sA=b/m = 23.14
60(2)	3.401	1.3940e-8	30% to 100%(2)	23.41	
30(2)	1.694	1.4773e-8	60% to 30%	21.49	
			30% to 60%(2)	23.14	
			100%(2) to 60%(2)	23.64	
				Avg. 23.35	

RD EX#36 8 baffles, η=8.6%, N= 0.492 rpm
T=23.0 °C, P=693.6 mmHg, Bed T=22.8 °C
5slm @100,60,40%, Q = 2.316-5.820 L/min

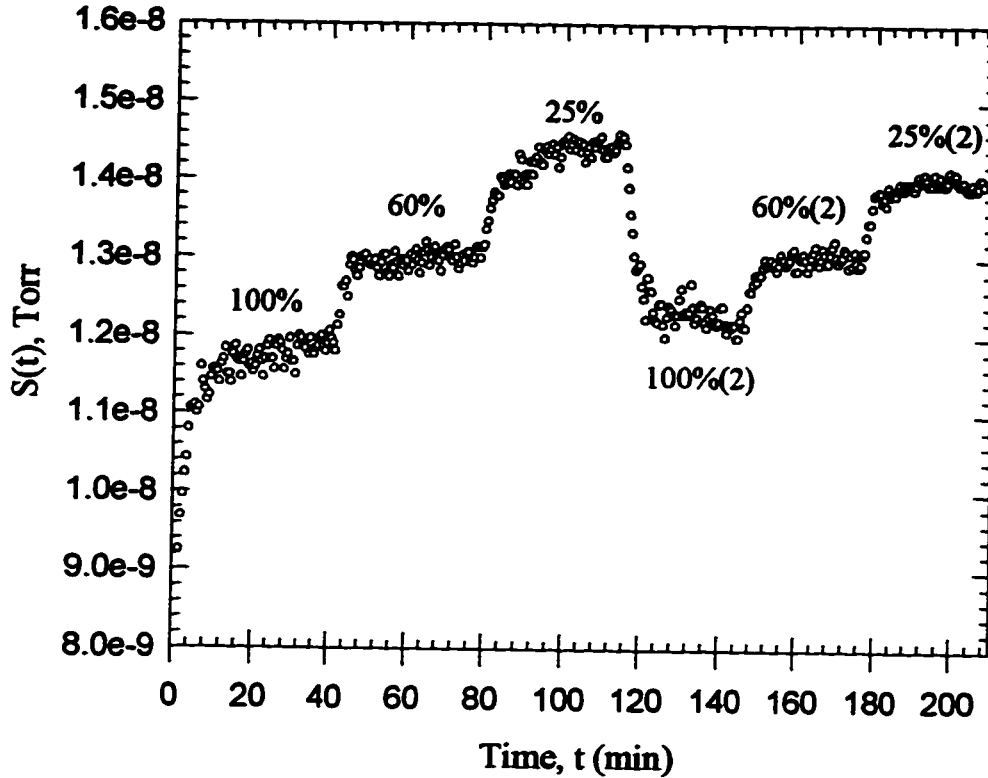| Solids (@start)	1711.25 g	Bulk density	993.4 kg/m³
Solids (@end	1703.18 g	F_E	0.0184

No condensation and no dusting in the drum.
Ratio of drum wall velocity to maximum superficial gas velocity, V_W/u = 5.1

Flow (%)	Q(L/min)	S* (Torr)	Piece	k_sA(L/min) piece method	k_sA(L/min) by slope method
100	5.82	1.3293e-8	100% to 40%	24.84	b=61523780.72
60	3.486	1.4615e-8	100%(2) to 40%(2)	31.05	m= 2277860.93
40	2.316	1.5008e-8	100% to 60%	19.982	R²= 0.972
100(2)	5.816	1.3408e-8	100%(2) to 60%(2)	29.70	k_sA=b/m = 27.0
60(2)	3.482	1.4351e-8		Avg. 26.39	
40(2)	2.317	1.4814e-8			

RD EX#40 8baffles, η=8.6%, N=0.616rpm
T=22.2 °C, P=714.9mmHg, BedT=22.3 °C
5slm@100%, 60%, 20%, Q=1.114-5.629L/min
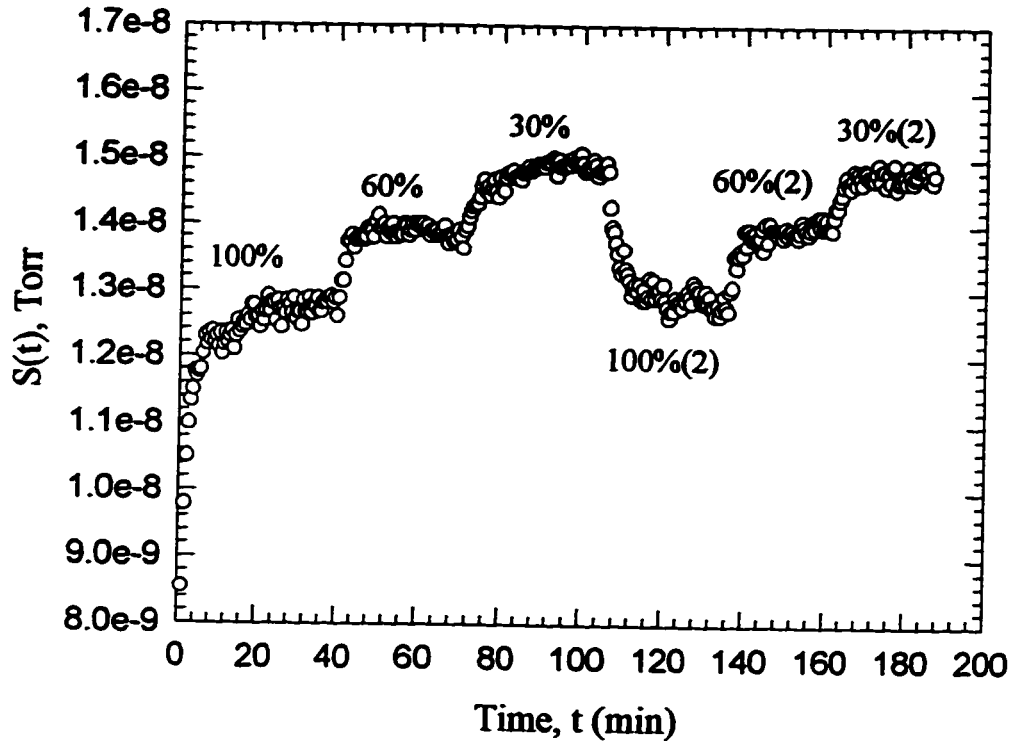

Solids (@start)   1708.86 g   Bulk density   995.6 kg/m³
Solids (@end   1703.02 g F_E 0.01335
No condensation and no dusting in the drum.
Ratio of drum wall velocity to maximum superficial gas velocity, V_W/u = 6.6

Flow (%)	Q(L/min)	S* (Torr)	Piece	k_sA(L/min) piece method	k_sA(L/min) by slope method
100	5.629	1.2037e-8	20% to 100%(2)	32.88	b=72362218.48
60	3.370	1.2568e-8	100%(2) to 60%(2)	25.64	m= 2078085.69
20	1.114	1.3308e-8	60%(2) to 20%(2)	34.70	R²= 0.971
100(2)	5.628	1.1748e-8	100%(2) to 20%(2)	29.86	k_sA=b/m = 34.82
60(2)	3.371	1.2662e-8		Avg. 30.77	
20(2)	1.114	1.3460e-8			

RD Ex#35 8 baffles, η=8.6%, N=1.257 rpm
T=23.3 $^{\circ}$C, P=691.3 mmHg, Bed T=22.9 $^{\circ}$C
5slm@100%, 80%, 60%, Q=3.498-5.846 L/min
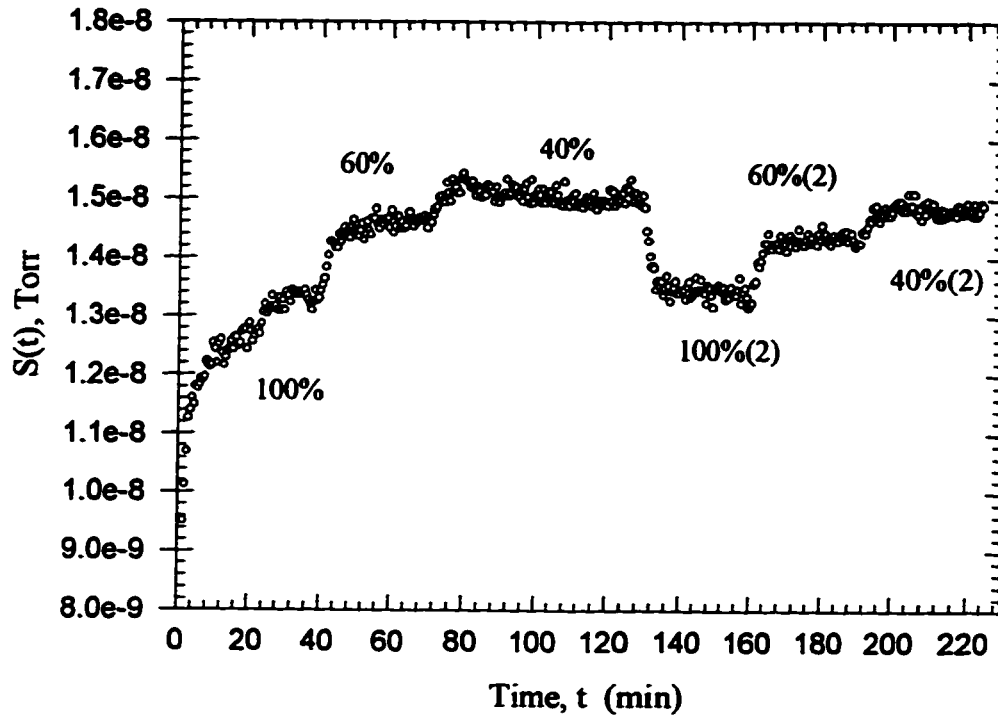

Solids (@start)   1713.78 g   Bulk density   995.7 kg/m^3
Solids (@end   1705.12 g F_E 0.019739
No condensation and no dusting in the drum.
Ratio of drum wall velocity to maximum superficial gas velocity, V_W/u = 12.9

Flow (%)	Q(L/min)	S$^\infty$ (Torr)	Piece	k$_a$A(L/min) piece method	k$_a$A(L/min) by slope method
100	5.826	1.4371e-8	100%(2) to 80%(2)	41.39	b=57269304.12
80	4.667	1.4885e-8	80%(2) to 60%(2)	43.26	m= 1789621.83
60	3.498	1.5531e-8	100%(2) to 60%(2)	42.33	R^2= 0.56
100(2)	5.846	1.5198e-8			k$_a$A=b/m = 32.0
80(2)	4.670	1.5586e-8		Avg. 42.33	
60(2)	3.503	1.5975e-8			

RD EX#34 8 baffles, η=8.6%, N=1.333 rpm
T=23.0 °C, P=689.3mmHg, Bed T=23.0 °C
100slm@5%, 10%, 15%, Q=7.925-18.874 L/min

Solids (@start)	1710.1 g		Bulk density	985.6 kg/m³
Solids (@end	1689.83 g		F_E	0.0463

No condensation and no dusting in the drum.

Ratio of drum wall velocity to maximum superficial gas velocity, V_w/u = 6.0

Flow (%)	Q(L/min)	S* (Torr)	Piece	k_aA(L/min) piece method	k_aA(L/min) by slope method
5	7.925	1.4212e-8	5% to 10%	63.84	b= 61935187.8
10	13.389	1.3207e-8	10% to 15%*	86.11 *	m=1093439.9
*15	18.857*	1.2519e-8*	5% to 15%*	72.91*	R²= 0.958
5(2)	7.932	1.4116e-8	15%* to 5%(2)	77.71*	k_aA=b/m = 56.6
10(2)	13.405	1.2914e-8	5%(2) to 10%(2)	50.86	
*15(2)	18.874*	1.2265e-8*	10%(2) to 15%(2)*	89.95*	
				Avg. 57.2	

Note: * means that air was bypassing the drum at that Flow(%). k_aA values (piece and slope method) were calculated by excluding the values marked by * due to bypassing of gas.

RD Ex#32 8 baffles, η=8.6%, N=1.876 rpm
T=23.4 °C, P=698.3 mmHg, Bed T=22.7 °C
100 slm@ 4%,85,12%,15%, Q=6.749-18.655 L/min

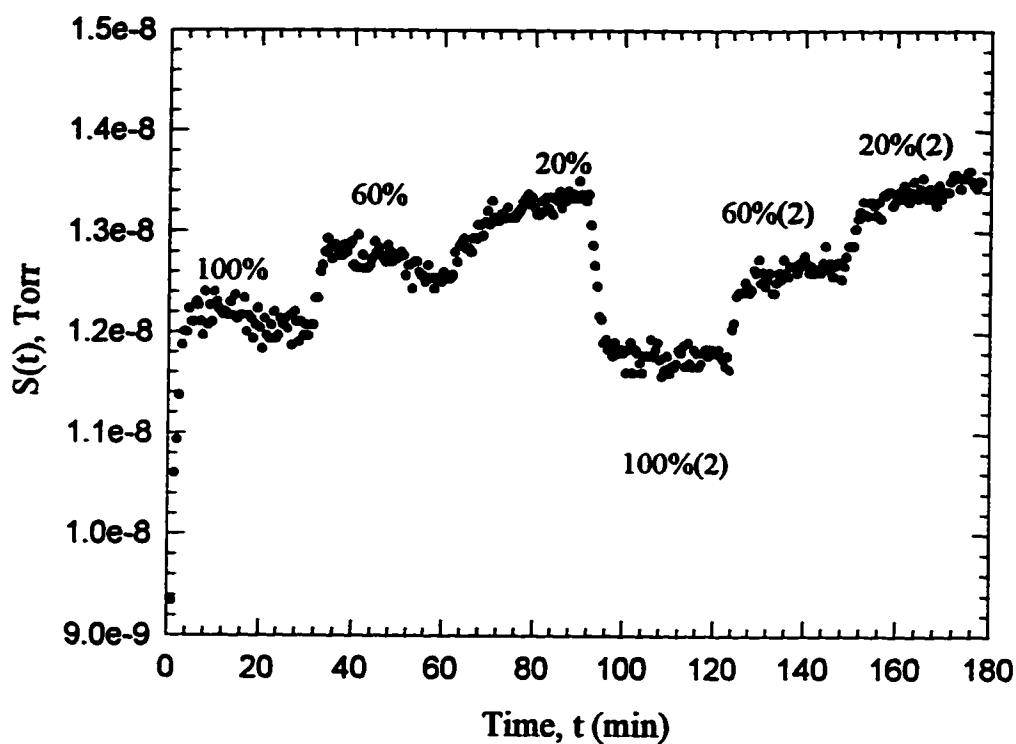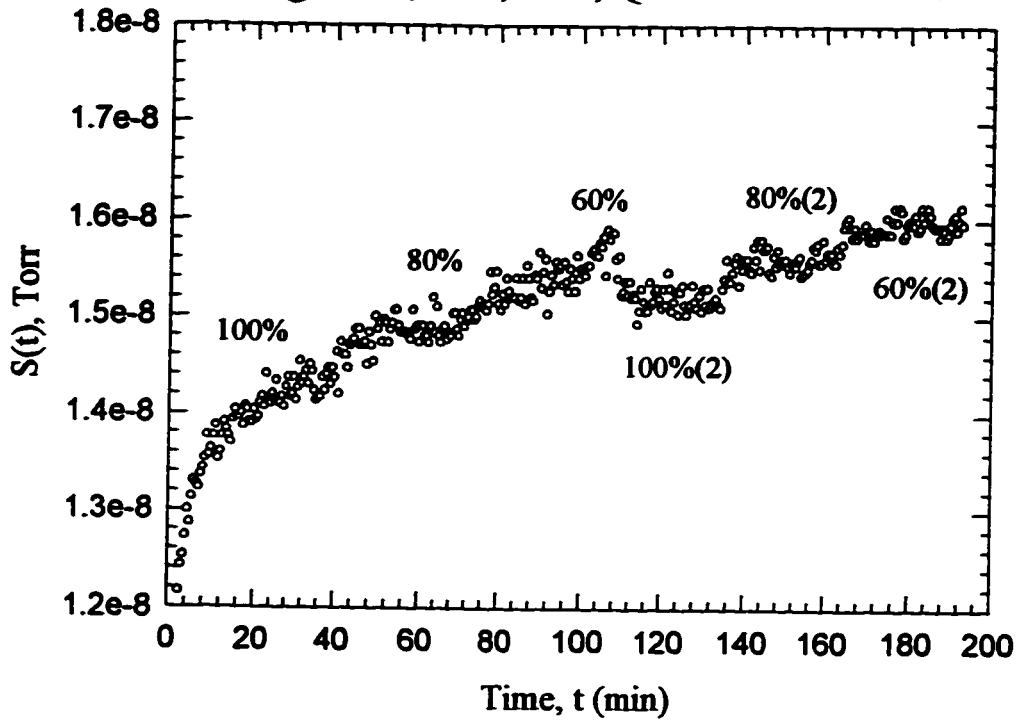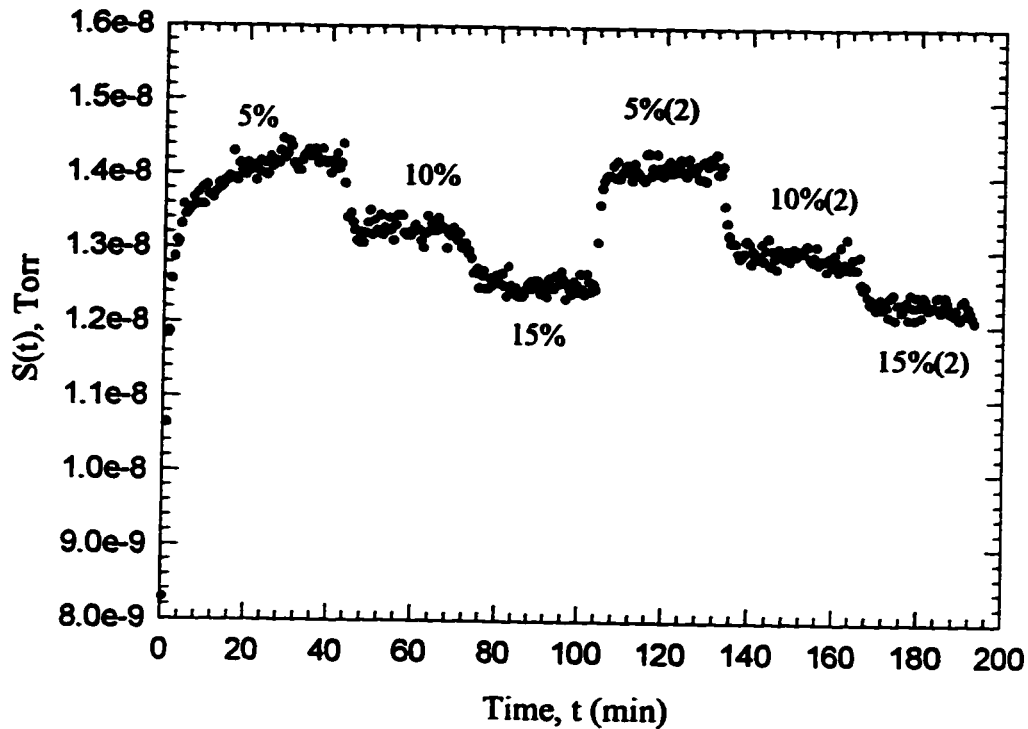Solids (@start)   1713.47 g   Bulk density   986.7 kg/m³
Solids (@end   1689. g   F$_E$ 0.05622
No condensation and no dusting in the drum.
Ratio of drum wall velocity to maximum superficial gas velocity,$_w$Xu = 10.2

Flow (%)	Q(L/min)	S$^{\infty}$ (Torr)	Piece	k$_a$A(L/min) piece method	k$_a$A(L/min) by slope method
4	6.749	1.4594e-8	8%(2) to 15%*	73.29*	b= 63188318.8
8	11.075	1.3789e-8	15%(2)* to 8%(3)	86.09 *	m=790907.4
*12	15.410*	1.3336e-8*	8% (2)to 12%(2)*	58.37*	R²= 0.897
8(2)	11.079	1.4054e-8	8%(3) to 12%(3)*	84.57*	k$_a$A=b/m = 79.9
*15	18.655*	1.2896e-8*	4% to 8%	67.35	
*12(2)	15.410*	1.3229e-8*		Point estimate	
*15(2)	18.643*	1.2897e-8*		67.35	
8(3)	11.071	1.3859e-8			
*12(3)	15.399*	1.3259e-8*			

Note: * means that air was bypassing the drum at that Flow(%). k$_a$A values (piecewise and slope method) were calculated by excluding the values marked by * due to bypassing of gas.

RD Ex#33 8 baffles, η=8.6%, N=1.649 rpm
T=23.2 °C, P=688.3mmHg, Bed T=22.9 °C
100slm@5%, 10%, 15%, Q=7.935-18.921 L/min

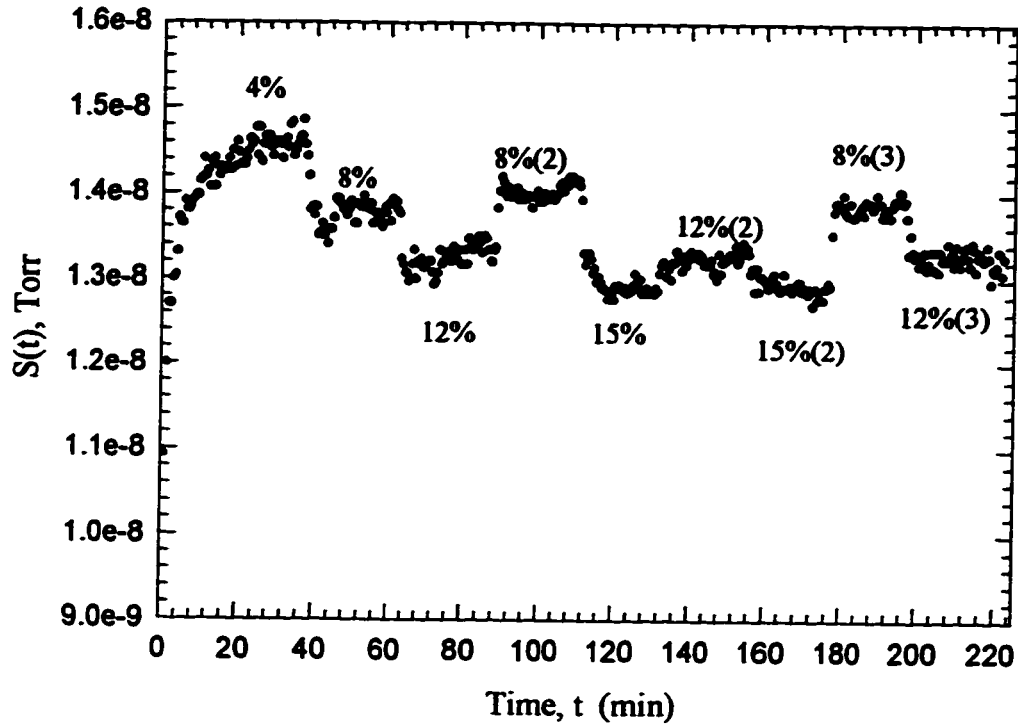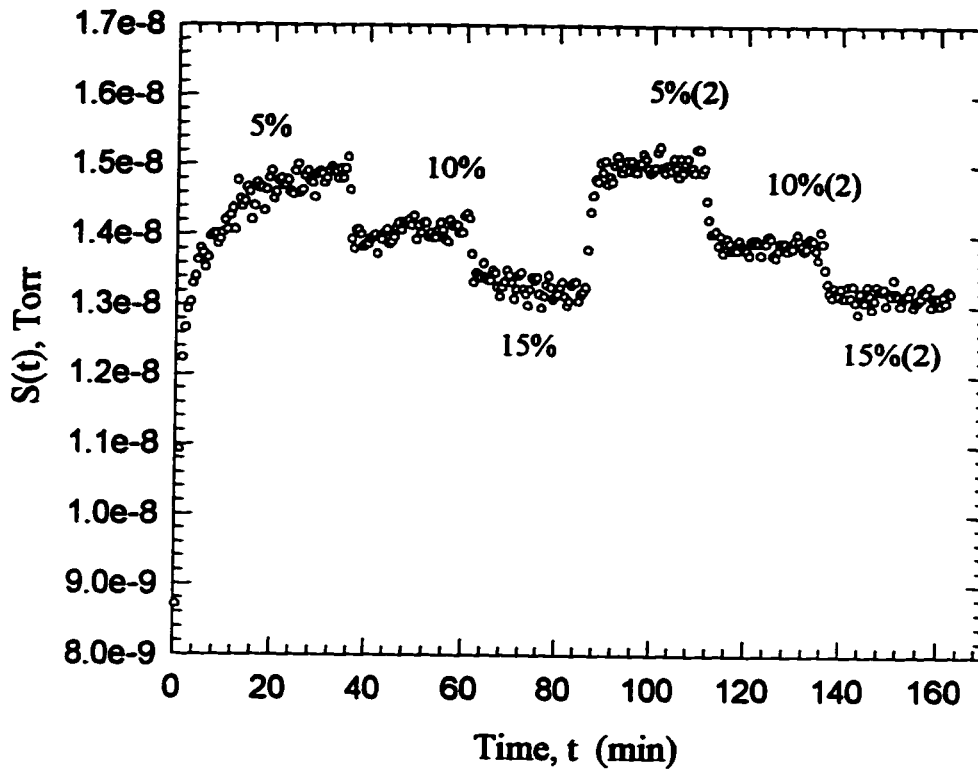|				
Solids (@start)	1710.02 g	Bulk density	992.2 kg/m^3	
Solids (@end	1692.06 g	F_E	0.0409	

No condensation and no dusting in the drum.

Ratio of drum wall velocity to maximum superficial gas velocity, V_w/u = 8.9

Flow (%)	Q(L/min)	S$^{\infty}$ (Torr)	Piece	k_eA(L/min) piece method	k_eA(L/min) by slope method
5	7.938	1.4801e-8	10% to 15%*	70.62*	b= 60603950.2
10	13.414	1.4085e-8	5% to 15%*	83.85 *	m=814784.2
*15	18.899*	1.3222e-8*	15%* to 5%(2)	72.60*	R^2= 0.95
5(2)	7.935	1.5022e-8	5% to 15%(2)*	80.38*	k_eA=b/m = 74.4
10(2)	13.434	1.3874e-8	10%(2) to 15%(2)*	88.30*	
*15(2)	18.921*	1.3164e-8*	5%(2) to 10%(2)	58.52	
				Point estimate	
				58.52	

Note: * means that air was bypassing the drum at that Flow(%). k_eA values (piecewise and slope method) were calculated by excluding the values marked by * due to bypassing of gas.

APPENDIX E

This appendix contains the values of cross-sectional area of the active bed, S_A, central angle, β, chord length (geometric), L, and surface particle velocity, V_s. Sample calculations are included to show how the above quantities were evaluated.

Calculation of the central angle, β and chord length, L_s (geometric).

Consider the following Figure E-1 :
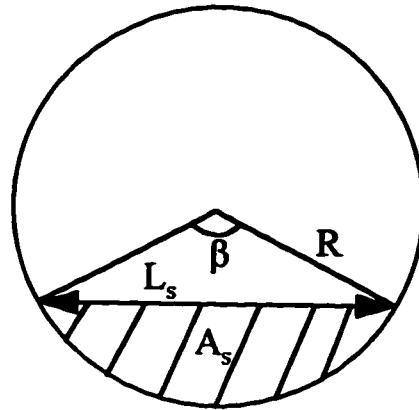
Figure E-1. Circle segments.

where: R radius, m

A. segment area, m^2

L_s chord length, m

β central angle, rad

The equation that relates the solids volume fraction, η to the area of the segment, A. was derived as follows:

$$\frac{V_{bed}}{V} = \frac{A_s L}{A_c L} \tag{E-1}$$

where L is the drum length, V_{bed} is the solids bed volume, A_c is the cross-sectional area and V is the drum volume. From Equation (E-1) the following equations can be derived:

$$A_s = A_c \eta \qquad \text{(E-2)}$$

$$\frac{A_s}{R^2} = \pi \eta \qquad \text{(E-3)}$$

In Table 1-19a (Perry and Green, 1984) for values of A_s/R^2, the corresponding values of β and L_s/R are given. The values of A_s/R^2 using Equation (E-3) were calculated for the range of η in the present study. Then by interpolation, the corresponding values of L_s/R and β were calculated. From L_s/R and R, the geometric chord length, L_s was calculated.

Example: At η=0.043, $\dfrac{A_s}{R^2} = \pi \eta = \pi(0.043) = 0.1350885$

From Table 1-19a, the following values were obtained for interpolation:

A_s/R^2	β (rad)	L_s/R
0.1298199	1.18682	1.11839
0.1353483	1.20428	1.13281

By interpolation: β= 1.203457 rad

$$L_s/R = 1.132132$$

$$L_s = 1.132132 * 0.145m = 0.1642 \text{ m}$$

The values of β and L_s (geometric) for the different values of η are shown in Table E-1 below.

Table E-1. Calculated values of β and L_s as a function of η.

η	β (rad)	L_s (m)
0.043	1.2034	0.1642
0.086	1.5398	0.2019
0.172	1.9930	0.2435
0.250	2.3099	0.2653

Calculation of the cross-sectional area of the active bed, S_A.

Consider the following Figure E-2:
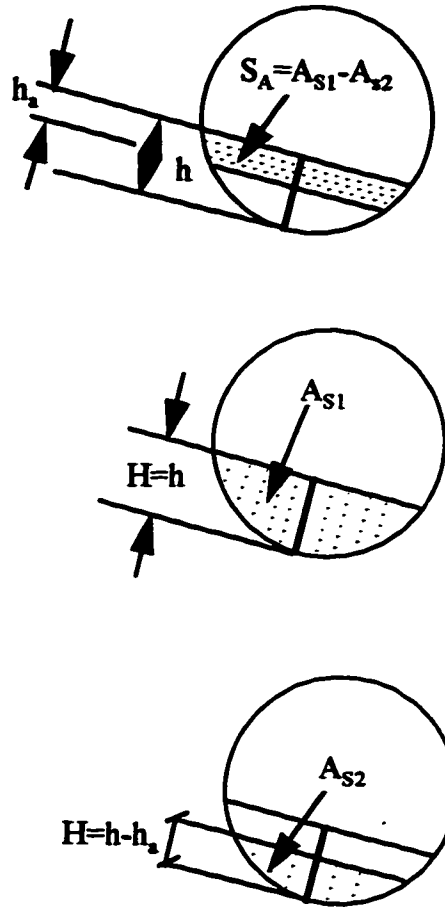
Figure E-2. Circle segment for calculating S_A.

where: R   radius, m

   A_{S1}, A_{S2} segment areas, m^2

   h   total bed depth, m

h_a active bed depth, m

H   height, m

From the experimentally measured values of h_a and h, the value of H/R was calculated. In Table 1-19a. Circular segments (Perry and Green, 1984), for values of H/R, the corresponding values of A_s/R^2 are given. For the experimental values of H/R, the values of A_{s1}/R^2 and A_{s2}/R^2 were found by interpolation.

Example: Rolling bed experiment at N=0.291 rpm, η=0.043

        h_a = 6.17e-3 m   h = 0.0262 m   R= 0.145 m

@H/R= h/R = 0.1806896 the following values were obtained from Table1-19a for interpolation to obtain the value of A_{s1}/R^2 :

H/R	A_{s1}/R^2
0.175874	0.1353483
0.180848	0.1410188

By interpolation: A_{s1}/R^2 = 0.14083828

@H/R= (h-h_a)/R = 0.1381379 the following values were obtained from Table 1-19a for interpolation to obtain the value of A_{s2}/R^2:

H/R	A_{S2}/R^2
0.133975	0.0905860
0.138371	0.0950155

By interpolation: $A_{S2}/R^2 = 0.09478065$

$$S_A = \left[\frac{A_{S1}}{R^2} - \frac{A_{S2}}{R^2} \right] R^2 = 9.684e - 4 \ m^2$$

The calculated values of S_A at different N and η are given in Table E-2 below.

Table E-2. Calculated values of the cross-sectional area of the active bed, S_A.

N (rpm)	η	S_A (m^2)
0.291	0.043	9.684e-4
0.576	0.043	1.067e-3
1.213	0.043	*1.239e-3
1.657	0.043	1.522e-3
1.967	0.043	1.743e-3
1.115	0.086	2.229e-3
1.082	0.172	3.059e-3
1.061	0.250	4.415e-3

* used this S_A value at N=1.1 and 1.2 rpm as the value of S_A did not significantly change in that range of drum rotational speed.

Calculation of Surface Particle velocity, V_s using Equations (3-21) and (2-2).

The two equations used for calculating V_s are repeated below:

$$V_s = \frac{2\pi RN}{60}\left[\frac{h}{h_a} - 1\right]$$ (3-21)

$$V_s = \frac{\pi N}{120 h_a}\left[L_s^2 - 8Rh_a \cos\left(\frac{\beta}{2}\right)\right]$$ (2-2)

In the calculations, experimentally measured values of N, h_a and h were used. The values of β and L_s (goemetric) were obtained from circular segments (Table E-1). The geometric chord length of the solids bed was used in in the calculation as it was very close to the experimentally measured value.

Sample Calculation: N= 0.291 rpm h_a= 6.17e-3 m, h=0.0262 m L_s=0.1642 m

β= 1.2034 rad R=0.145 m

Using Equation (3-21):

$$V_s \frac{2\pi(0.145)(0.291)}{60}\left[\frac{0.0262}{6.17e-3} - 1\right]$$

V_s = 0.014344 m/s

Using Equation (2-2):

$$V_s = \frac{\pi(0.291)}{120(6.17e-3)}\left[(0.1642)^2 - 8(0.145)(6.17e-3)\cos\left(\frac{1.2034}{2}\right)\right]$$

$$V_s = 0.02601 \text{ m/s}$$

The values of V_s for $\eta=0.043$ and varying N are shown in Table E-3 below.

Table E-3. Calculated values of V_s using Equations (3-21) and (2-2) for $\eta=0.043$ and varying drum rotational speed.

N (rpm)	V_s (Equation 3-21) m/s	V_s (Equation 2-2) m/s
0.291	0.014344	0.02601
0.576	0.025748	0.04563
1.213	0.042593	0.07666
1.657	0.042018	0.07547
1.967	0.036702	0.06801

The values of V_s for N =1.1 rpm and varying solids volume fraction are shown in Table E-4.

Table E-4. Calculated values of V_s using Equations (3-21) and (2-2) for N=1.1 rpm and varying solids volume fraction.

η	V_s (Equation 3-21) m/s	V_s (Equation 2-2) m/s
0.043	0.04259	0.0766
0.086	0.04465	0.0780
0.172	0.06812	0.1131
0.250	0.06496	0.1007

APPENDIX F

This appendix contains the normalized mass transfer coefficient, k_s' for the rolling bed mass transfer experiments. A sample calculation is also included to show how k_s' was evaluated. Also calculations of the 95% confidence interval for the mean k_s' value and relative error for the k_s' values at varying solids volume fraction are presented.

Calculation of normalized mass transfer coefficient, k_s' for the rolling bed experiments

The normalized mass transfer coefficient, k_s' was calculated using Equation (5-9) which is repeated below.

$$k_s' = \frac{k_s A}{60000 \cdot S_A \cdot L} \qquad (F\text{-}1)$$

where S_A is the cross-sectional area of the active bed, L is the length of the drum and $k_s A$ is the volumetric mass transfer coefficient. The calculated values of S_A are given in Appendix E (Table E-2) and the $k_s A$ values for the rolling bed experiments are given in Appendix D.

In Table F-1 the k_s' values for the rolling bed experiments at solids volume fraction of 0.043 and varying drum rotational speed are presented.

Table F-1. Calculated k_s' values for the rolling bed at $\eta = 0.043$ and varying drum rotational speed.

N (rpm)	$k_s A$ (L/min)	S_A (m^2)	Volume of bed renewed $S_A \cdot L$ (m^3)	k_s' (s^{-1})
0.291	6.352	9.684e-4	2.983e-4	0.355
0.576	10.62	1.067e-3	3.286e-4	0.539
1.213	21.76	1.239e-3	3.816e-4	0.950
1.657	26.24	1.522e-3	4.688e-4	0.933
1.967	32.03	1.743e-3	5.368e-4	0.994

Sample Calculation for obtaining k_s' at: N=0.291 rpm and η=0.043

$$k_s' = \frac{k_s A}{60000 \cdot S_A \cdot L}$$

$$k_s' = \frac{6.352}{60000 * 9.684e-4 * 0.308 \ s}$$

$$k_s' = 0.355 \ s^{-1}$$

In Table F-2, the k_s' values for the rolling bed at drum rotational speed of 1.1 rpm and varying solids volume fraction are presented.

Table F-2. Calculated k_s' values for the rolling bed at N=1.1 rpm and varying solids volume fraction.

η	$k_s A$ (L/min)	S_A (m^2)	Volume of bed renewed $S_A \cdot L$ (m^3)	k_s' (s^{-1})
0.043	21.76	1.239e-3	3.816e-4	0.950
0.086	23.32	2.229e-3	6.865e-4	0.566
0.086	25.35	2.229e-3	6.865e-4	0.615
0.172	36.01	3.059e-3	9.422e-4	0.637
0.172	26.95	3.059e-3	9.422e-4	0.477
0.250	59.66	4.415e-3	1.360e-3	0.731
0.250	59.95	4.415e-3	1.360e-3	0.735

Calculation of 95 % confidence interval for the mean k_s' value for η varying from 0.086 to 0.25

The following equation (Miller et al., 1990) was used to calculate the 95% confidence interval for the mean k_s' value:

$$x_m - t_{\frac{\alpha}{2}} \cdot \frac{s}{\sqrt{n}} < k_s' < x_m + t_{\frac{\alpha}{2}} \cdot \frac{s}{\sqrt{n}} \qquad \text{(F-2)}$$

where n is the sample size, x_m is the sample mean, s is the sample standard deviation and $t_{\alpha/2}$ is a t-distribution constant. The sample mean, x_m was calculated from the k_s' values listed in Table F-2 for for η varying from 0.086 to 0.25.

$$x_m = \frac{[0.566 + 0.615 + 0.637 + 0.477 + 0.731 + 0.735]}{6} = 0.627 \text{ s}^{-1}$$

In Equation (F-2) the value of $t_{\alpha/2}$ was found from Table 4 (Miller et al., 1990) at n=6 and (n-1) degrees of freedom. The value of $t_{\alpha/2}$ obtained was 2.571.

The sample standard deviation, s was calculated from the sample variance, s^2 (Miller et al., 1990) which is defined as:

$$s^2 = \frac{\sum_{i=1}^{n} [k_{s,i}' - x_m]^2}{n-1} \qquad \text{(F-3)}$$

where $k_{s,i}'$ are the individual k_s' values used in the calculation of x_m.

The calculated value of $s^2 = 9.7984e\text{-}3$ s^{-2} from which the standard deviation, s obtained was:

$$s = 9.899e\text{-}2 \; s^{-1}$$

Using Equation (F-2) the 95% confidence interval is:

$$0.627 - 2.571 * \frac{9.899e-2}{\sqrt{6}} < k_s' < 0.627 + 2.571 * \frac{9.899e-2}{\sqrt{6}}$$

$$0.523 \quad s^{-1} < k_s' < 0.731 \quad s^{-1}$$

Calculation of the relative error, RE for k_s' values obtained for solids volume fraction varying from 0.086 to 0.25

The mean of the k_s' values, x_m obtained was : 0.627 s^{-1}

The relative error of the individual k_s' values from the mean value, x_m was calculated using the following equation:

$$RE = \left[\frac{k_{s,i}' - x_m}{x_m} \right] * 100 \tag{F-4}$$

where $k_{s,i}'$ are the individual k_s' values used in the calculation of x_m.

The calculated values of relative error of the k_s' values obtained at drum rotational speed of 1.1 rpm and solids volume fraction varying from 0.086 to 0.25 are given in Table F-3.

Table F-3. Calculated values of relative error at $x_m = 0.627 \ s^{-1}$.

η	RE (%)	$k_s' \ (s^{-1})$
0.086	-9.73	0.566
0.086	-1.91	0.615
0.172	+1.59	0.637
0.172	-23.9	0.477
0.25	+16.6	0.731
0.25	+17.2	0.735

Reference: Miller, J.R., Freund, J.E. and Johnson, R., "Probability and Statistics for

Engineers", 4 th ed., Prentice Hall, New Jersey, 1990.

APPENDIX G

This appendix contains the values of the gas phase diffusivities of oxygen and n-decane and liquid phase diffusivities of oxygen and carbon-dioxide. The calculation of the diffusivity of n-decane in air is also shown. A sample calculation is also given to show how the mass transfer coefficient defined in fermentation, k_La, was obtained from the volumetric mass transfer coefficient, k_LA. Calculation of the conversion of the gas phase n-decane mass transfer coefficient to gas phase oxygen mass transfer coefficient is shown. Also sample calculation of the conversion of the liquid phase carbon-dioxide mass transfer coefficient to the liquid phase oxygen mass transfer coefficient is given.

.

Calculation of $k_s a$ value for n-decane from the experimentally measured gas-solid mass transfer coefficient, $k_s A$ for n-decane

The $k_s A$ values can be converted to $k_s a$ values using Equation (5-8) which is repeated below:

$$k_s a = \frac{k_s A}{V \cdot \eta} \qquad \text{(G-1)}$$

where V is the drum volume and η is the solids volume fraction.

Example: V =20 L, η = 0.043, $k_s A$ = 13.22 L/min at N=0.0873 rpm and in the presence of baffles

From Equation (G-1): $\qquad k_s a = \dfrac{13.22 \text{ L} / \text{min}}{20 \text{ L} \cdot 0.043} = 15.37 \text{ min}^{-1}$

Calculation of the gas phase diffusivity of n-decane in air

The following expression was used to evaluate the diffusivity, D_{AB} for non-polar gas pairs (Hines and Maddox, 1985):

$$D_{AB} = \frac{1.858 \times 10^{-27} T^{\frac{3}{2}}}{P \sigma_{AB}^2 \Omega_D} \left[\frac{1}{M_A} + \frac{1}{M_B} \right]^{0.5} \qquad \text{(G-2)}$$

where:

T $\qquad$ = absolute temperature, K

P $\qquad$ = absolute pressure, atm

σ_{AB} $\qquad$ = collision diameter, m

Ω_D = collision integral

M_A = molecular weight of A, kg/kmol

M_B = molecular weight of B, kg/kmol

$$\sigma_{AB} = \frac{\sigma_A + \sigma_B}{2} \qquad\qquad (G-3)$$

where value of σ_A and σ_B are found tabulated in Treybal (1980) or calculated from the following equation (Treybal, 1980):

$$\sigma = 1.18\upsilon^{\frac{1}{3}} \qquad\qquad (G-4)$$

where υ is the molal volume of the liquid at normal boiling point, m^3/kmol.

The value of the collision integral, Ω_D are a function of $\left(\dfrac{\varepsilon}{k}\right)_{AB} \cdot T$ which are given in Table 2-4 (Hines and Maddox, 1985).

The value of $\left(\dfrac{\varepsilon}{k}\right)_{AB}$ is calculated using:

$$\left(\frac{\varepsilon}{k}\right)_{AB} = \left[\left(\frac{\varepsilon}{k}\right)_A \cdot \left(\frac{\varepsilon}{k}\right)_B\right]^{0.5} \qquad\qquad (G-5)$$

The value of $\left(\dfrac{\varepsilon}{k}\right)$ are tabulated (Treybal, 1980) or calculated using the following expression:

$$\left(\frac{\varepsilon}{k}\right) = 1.21T_b \qquad\qquad (G-6)$$

where T_b is the normal boiling point, K.

Subscripts:

A = component A (air)

B = component B (n-decane)

Calculation of D_{AB} for n-decane in air:

<u>Properties of air (Component A) from Treybal (1980):</u>

$$M_A = 29.0 \text{ g/mol}, \ \sigma_A = 0.3711 \text{ nm} = 3.711e\text{-}10 \text{ m}, \ \left(\frac{\varepsilon}{k}\right)_A = 78.6 \text{ K}$$

<u>Properties of n-decane (Component B) :</u>

Estimation of σ_B and $\left(\dfrac{\varepsilon}{k}\right)_B$ using Equations (G-4) and (G-6).

From Treybal (1980): $\upsilon_B = \dfrac{14.8(10) + 22(3.7)}{1000} = 0.2294 \text{ m}^3 \text{ / kmol.}$

$$\sigma_B = 1.18(0.2294)^{\frac{1}{3}} = 7.223 \text{ nm} = 7.223e-10 \text{ m}$$

$T_b = 174.1 \ ^\circ\text{C}$ for n-decane from Dean (1992).

$$\left(\frac{\varepsilon}{k}\right)_B = 1.21(174.1 + 273.15) = 541.17 \text{ K}$$

Estimation of $\left(\dfrac{\varepsilon}{k}\right)_{AB}$ and σ_{AB} using Equations (G-3) and (G-5):

$$\sigma_{AB} = \frac{3.711e-10 + 7.223e-10}{2} = 5.46e - 10 \text{ m}$$

$$\left(\frac{\varepsilon}{k}\right)_{AB} = \sqrt{78.6 * 541.17} = 206.24 \text{ K}$$

Mass transfer experiments were conducted at temperatures in the range 21.5 °C to 23.8 °C and pressure in the range 689.3 mmHg to 718.3 mmHg. To calculate the diffusivity, the average temperature and pressure during the mass transfer experiments were used.

$T = (22.7 + 273.15)K = 295.85 \, K$

$P = 703.8 \, mmHg / 760 \, mm \, Hg = 0.926 \, atm$

The value of the collision integral, Ω_D was found for:

$$\left(\frac{\varepsilon}{k}\right)_{AB} T = \frac{295.85}{206.24} = 1.4345$$

From Table 2-4 (Hines and Maddox, 1985) the value of Ω_D was found to be 1.221.

The gas phase diffusivity of n-decane in air was calculated using Equation (G-2):

$$D_{AB} = \frac{1.858 \times 10^{-27} (295.85)^{\frac{3}{2}}}{0.926 \cdot (5.46 \times 10^{-10})^2 (1.221)} \left[\frac{1}{29} + \frac{1}{142.3}\right]^{0.5}$$

The gas phase diffusivity, D_{AB} for n-decane is 5.7e-6 m^2/s.

Conversion of gas-solid n-decane mass transfer coefficient, $(k_s a)_{n-dec}$ to gas-solid oxygen mass transfer coefficient, $(k_s a)_{O_2}$

From Equation (2-22) for gas-solid systems it can be noted that:

$$Sh \propto Sc^{\frac{1}{3}} \tag{G-7}$$

Using Equations (2-10) and (2-13), Equation (G-7) can be rewritten as:

$$k_s \propto D_{AB}^{2/3} \quad \text{or} \quad k_s a \propto D_{AB}^{2/3} \tag{G-8}$$

In the current mass transfer experiments, n-decane was used as a model compound to obtain gas-solid mass transfer coefficient in a rotating drum. To convert these mass transfer coefficients for n-decane, $(k_s a)_{n-dec}$ to mass transfer coefficients for oxygen, $(k_s a)_{O_2}$ a correction has to be made for the difference in the diffusivities of n-decane and oxygen in air. The following equation can be derived from Equation (G-8) which is used to calculate $(k_s a)_{O_2}$:

$$(k_s a)_{O_2} = (k_s a)_{n-dec} \cdot \left[\frac{(D_{AB})_{O_2}}{(D_{AB})_{n-dec}} \right]^{\frac{2}{3}} \tag{G-9}$$

Example: $k_s A = 13.22$ L/min, $k_s a = 15.37$ min^{-1}, N=0.0873 rpm, $\eta = 0.043$

From Table 5-47(Bolz and Tuve, 1984) the diffusivity of oxygen in air at 25 °C and 1 atm pressure was found to be: $(D_{AB})_{O_2} = 2.06$ e-5 m^2/s

Using Equation (G-9): $(k_s a)_{O_2} = 15.37 \left[\frac{2.06e-5}{5.7e-6} \right]^{\frac{2}{3}}$

$$(k_s a)_{O_2} = 36.2 \text{ min}^{-1}.$$

Table G-1. Calculated values of the gas-solid oxygen mass transfer coefficient, $(k_s a)_{O_2}$

$(k_s a)_{n-dec}$, min^{-1}	$(k_s a)_{O_2}$, min^{-1}
7.38	17.38
10.53	24.8
15.37	36.2
37.24	87.7
39.16	92.2
77.92	183.5

Conversion of gas-liquid carbon-dioxide mass transfer coefficient, $(k_L a)_{CO_2}$ to gas-liquid oxygen mass transfer coefficient, $(k_L a)_{O_2}$

For mass transfer from a sphere in liquid phase the dependency of Sherwood number on Schmidt number is given by (Geankoplis, 1993):

$$Sh \propto Sc^{\frac{1}{3}} \tag{G-10}$$

From Equation (G-10) it can be observed that:

$$k_L \propto D_{AB}^{2/3} \qquad \text{or} \qquad k_L a \propto D_{AB}^{2/3} \tag{G-11}$$

Yegneswaran et al. (1990) used the following values of the gas-liquid CO_2 mass transfer coefficient, $(k_L a)_{CO_2}$ at ~ 25 °C to fit their experimental data : 1.67 min^{-1} in a 2L

fermentor and 0.417 min^{-1} in a 20 L fermentor. To convert the $(k_La)_{CO_2}$ values to gas-liquid oxygen mass transfer coefficient, $(k_La)_{O_2}$ a correction for the difference in the diffusivities of oxygen and carbon-dioxide was made.

From Equation (G-11) it can be noted that:

$$(k_La)_{O_2} = (k_La)_{CO_2} \cdot \left[\frac{(D_{AB})_{O_2}}{(D_{AB})_{CO_2}} \right]^{\frac{2}{3}} \tag{G-12}$$

From Table 3-319 (Perry and Green, 1984) the diffusivities of oxygen and carbon-dioxide in water at 25 °C and 1 atm pressure are found to be:

$$(D_{AB})_{O_2} = 2.5 \text{ e-9 m}^2/\text{s}.$$

$$(D_{AB})_{CO_2} = 1.96\text{e-9 m}^2/\text{s}.$$

The $(k_La)_{CO_2}$ value is converted to $(k_La)_{O_2}$ using equation (G-12).

Example: At $(k_La)_{CO_2} = 1.67$ min^{-1}.

$$(k_La)_{O_2} = 1.67 \left[\frac{2.5e - 9}{1.96e - 9} \right]^{\frac{2}{3}}$$

$$(k_La)_{O_2} = 1.964 \text{ min}^{-1}.$$

At $(k_La)_{CO_2} = 0.417$ min^{-1}.

$$(k_La)_{O_2} = 0.490 \text{ min}^{-1}.$$

References:

Bolz, R.E. and Tuve, G.L., "CRC Handbook of Tables for Applied engineering science",

    2 nd ed., CRC Press Inc., Boca Raton, 1984.

Dean, J.A., "Lange's Handbook of Chemistry", 14 th ed., Mc-Graw Hill, New York,

    1992.

Geankoplis, C.J., "Transport Processes and Unit Operations", 3 rd ed., PTR Prentice Hall,

    New Jersey, 1993.

Hines, A.L. and Maddox, R.N., "Mass Transfer Fundamentals and Applications",

    Prentice-Hall, Inc., Englewood Cliffs, 1985.